# Stony Brook University

# Molecular Mechanism of Rhodopsin Photoactivation

A Dissertation Presented

by

**Shivani Ahuja**

To

The Graduate School

In Partial Fulfillment of the

Requirements

for the Degree of

**Doctor of Philosophy**

in

**Physics**

Stony Brook University

**December 2008**

**Stony Brook University**

The Graduate School

**Shivani Ahuja**

We, the dissertation committee for the above candidate for the
Doctor of Philosophy degree, hereby recommend
acceptance of this dissertation.

**Dr. Steven O. Smith** - Dissertation Advisor
Professor, Biochemistry and Cell Biology

**Dr. Harold J. Metcalf -** Chairperson of Defense
Professor, Physics and Astronomy

**Dr. George F. Sterman**
Professor, Physics and Astronomy

**Dr. Chris J. Jacobsen**
Professor, Physics and Astronomy

**Dr. Thomas P. Sakmar**
Professor, Molecular Biology and Biochemistry, Rockefeller University

This dissertation is accepted by the Graduate School

Lawrence Martin
Dean of the Graduate School

# Abstract of the Dissertation

## Molecular Mechanism of Rhodopsin Photoactivation

by

**Shivani Ahuja**

**Doctor of Philosophy**

in

**Physics**

Stony Brook University

2008

Rhodopsin is the visual photoreceptor responsible for black and white vision in low light that is found in the rod cells of the human retina. It is a 40 kDa eukaryotic membrane protein that belongs to the large, pharmaceutically important family of G protein-coupled receptors (GPCRs). These receptors have a common architecture consisting of seven transmembrane helices. Activation of rhodopsin by light is initiated by isomerization of its photoreactive 11-*cis* retinylidene chromophore. The chromophore is covalently bound within the bundle of transmembrane helices through a protonated Schiff's base linkage to Lys296. The crystal structure of rhodopsin in the dark, inactive state has previously been solved to high resolution. However, no high-resolution structural data are available for metarhodopsin II, the active state of rhodopsin. My thesis work describes how structural constraints obtained by solid-state Nuclear Magnetic Resonance (NMR) spectroscopic measurements of the metarhodopsin II intermediate are combined with restrained molecular dynamics simulations to understand how rhodopsin converts light into a chemical signal.

Retinal isomerization leads to steric strain within the retinal binding site between the retinal β-ionone ring and helix 5 (H5), and between the retinal C19/C20 methyl groups and the second extracellular loop (EL2). These interactions lead to a rearrangement of hydrogen bonding networks involving H5 and EL2 triggering the motion of EL2 away from the retinal, deprotonation of the Schiff base nitrogen and protonation of Glu113. Displacement of EL2 is coupled to the motion of H5 in metarhodopsin II. Motion of the β-ionone ring is coupled to the motion of Trp265 on H6, which triggers a shift of H6 and H7 into active conformations and rearrangement of the hydrogen bonding network centered on the conserved NPxxY motif on H7. Motion of H5, H6 and H7, in turn, is coupled to the rearrangement of electrostatic interactions involving the conserved ERY motif at the cytoplasmic end of H3, exposing the G-protein binding site on the cytoplasmic surface of the protein**.** The location of the retinal and structural reorganization of the protein upon activation provides a blue print for understanding the action of agonists and antagonists in the large family of class A GPCRs.

For my mummy and papa

# Table of Contents

# List of Figures

# List of Tables

# Abbreviations

β2-AR, β2-Adrenergic Receptor

C1-C20, carbon positions 1 through 20 in retinal

cGMP, cyclic guanidine monophosphate

CL1 – CL3, cytoplasmic loops 1 through 3 in rhodopsin

CP, cross polarization

DARR, dipolar assisted rotational resonance

DDM, n-dodecyl β-maltoside

DMEM, Dulbecco's Modified Eagle medium

DOPC, dioleoylphosphotidylcholine

DOPE, dioleoylphosphotidylethanolamine

EL1 – EL3, extracellular loops 1 through 3 in rhodopsin

EPR, electron paramagnetic resonance

FBS, fetal bovine serum

GDP, guanidine diphosphate

GMP, guanidine monophosphate

GPCR, G protein-coupled receptor

GTP, guanidine triphosphate

H1 – H8, helices 1 through 8 in rhodopsin

H-D, Hydrogen-Deuterium

HPLC, high performance liquid chromatography

IR, infrared

LD, linear dichroism

MAS, magic angle spinning

MD, molecular dynamics

meta II (I), metarhodopsin II (I)

NMR, nuclear magnetic resonance

ppm, parts per million

PBS, phosphate-buffered saline

PDE, Phosphodiesterase

PSB, protonated Schiff base

Rho, rhodopsin

ROS, rod outer segment

RT, room temperature

SB, Schiff base

TM, transmembrane

U-$^{13}$C, uniformly $^{13}$C labeled

U-$^{15}$N, uniformly $^{15}$N labeled

UV-Vis, ultraviolet-visible

WT, wild-type

Amino acids in other GPCRs are often reffered in the text based on their Weinstein numbering $^{1}$ as a superscript

# Acknowledgements

Stony Brook, in the last five years has come to be my home away from home. During this time, I have been extremely fortunate to cross paths and share my life with a wonderful set of people, both in the lab and outside of it, all of whom have made my graduate school experience unforgettable and memorable.

First and foremost, I would like to thank Steve, my advisor, for giving me the ideal initiation into the world of scientific research. He placed a lot of faith in me when I had little in myself and constantly encouraged me to push past my limits. I really enjoyed our long scientific discussions, where, he actively sought my critical opinion and ensured that I did not remain a passive participant. His scientific clarity and meticulous attention to detail are the qualities I hope to take with me.

To Martine, who taught me almost everything about NMR I know today. She was my "go-to person" for any and every trouble I encountered down in the NMR lab. More than being a facility manager, she is a wonderful friend. Thank you so much Martine, for all the chrished long talks, awesome cakes and the cooking club sessions.

I had the previlige of learning science with a bunch of amazing, fun-loving and genial group of friends and collegaues. Thank you Evan, Tak, Viktor, Markus, Tony, Darryl, Jay, Jeff, Ian, Miki (Mikster), Mahuiddin and Joe for all the fun times that we shared in the lab and outside. The last four deserve a special mention here - we had some amazing times, be it watching sit-coms like Coupling and Chuck, sharing Ian's awesome mohitos, pizzas and chicken satays, Mahuiddin's stress-busting yoga sessions and of course the frequent hour long odysseys to Hicksville, just for a bite of the heavenly dosas at the House of Dosa. You have made my last two years in this lab unbelievable and I shall never forget those moments. And also, thank you for the SOS running club.

To all my friends – Janaki, Sandeep, Enrique, Bere, Mert, Alin, Dylan, Carlos, Sanjee, Bjorg, Andrew, Daniel, Ryan, Lilla, Joel, Masaki, Stephan and many many more,

who welcomed me with open arms when I was a lone stranger here in Stony Brook. You gave me the social support that helped me stay sane in graduate school. I will never forget the crazy parties, the late night movies and long siedler sessions, hanging out at Kike-bere's place, thanksgiving dinners, Sanjee’s amazing Srilankan food and Janaki’s awesome South-Indian meals.

To Malini, my dance teacher – thank you for opening up the wonderful and colorful world of Indian classical dance (Bharatnatyam) to me. You are a wonderful teacher and a great friend. I used to love and look forward to our classes every week and missed it sorely when the time came for us to part ways. Through you, I have discovered the joy and pleasure of Bharatanatyam, for which I am very grateful. Not to mention the fact that it helped me direct my nervous energy into something useful and wonderful whenever my research became stressful.

To Humeyra, my housemate of four years - you were not just a housemate, but over the years, have become more like a sister. We had lots of great times, shared many laughs, and also had many fights! Now that I look back at my 6 years here, I cannot imagine how life would have been, had you not been randomly assigned to be my roommate?

I would also like to express my sincere gratitude to the late Dr. Bhargava, my teacher during my undergraduate years. Even though my undergraduate institution did not offer any avenues to study biophysics, he constantly encouraged me to not let that act as a hindrance to my interest in the subject and pushed me to explore extra-curricular ways to study the subject. An inspiring teacher, he opened up the wonderful world of Physics to me and was instrumental in shaping my desire to pursue graduate school.

To my parents, and my sister Shilpa. Their constant unconditional love and affection, unflinching support and care has moulded me into who I am today. I could not have done any of this without them.

Last but not the least, I would like to thank my best friend and an amazing husband, Raman. For his unconditional love, support, encouragement and above all infinite pateince. He belived in me even when I did not believe in myself. Thank you.

# Chapter 1

# Introduction

## *1.1 Signal transduction across the cell membrane*

Signal transduction simply refers to a transmission of signals from outside of the cell (extracellular) to the inside (intracellular) across the cell membrane. It enables cells to communicate with their environment. In a multicellular organism communication between different cells is key to proper, well coordinated functioning of various tissues and organ systems. This intercellular communication is mostly carried out by secretion of signaling chemicals by one cell, which are then received by the target cell and translated into a downstream response such as enzymatic activity, gene expression, cell proliferation, cell death and stimulation of locomotion. These signals can take the form of peptides, proteins, hormones, steroids, neurotransmitters and growth factors. The cellular machinery amplifies the signal during a cascade, extracting a large intracellular response from a small extracellular signal.

In a multicellular, complex organism, these signaling cascades are also initiated by environmental, physical stimuli, for example, light hitting the retina in the eye, odorants and bitter and sweet tastes. Malfunction of these intracellular signaling pathways is responsible for a number of diseases such as cancer, asthma, night blindness and parkinson’s disease.

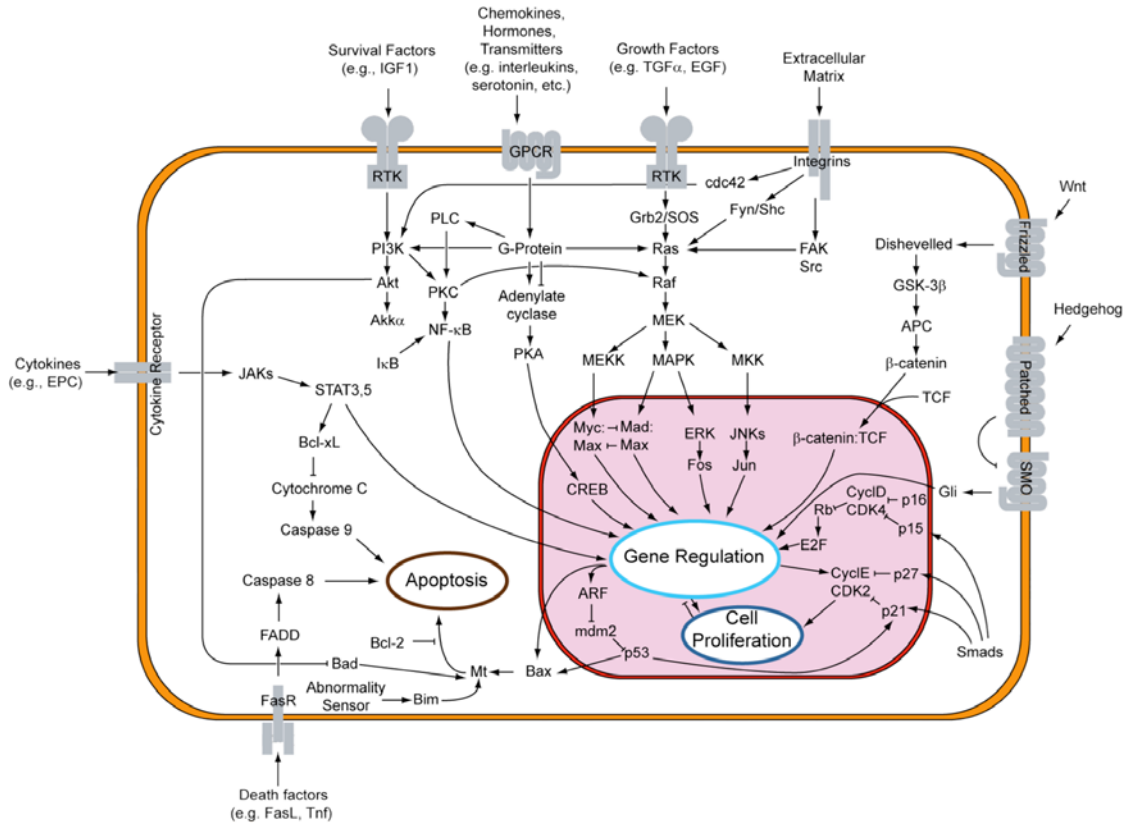


**Figure 1.1: An overview of the signal transduction pathway**.
http://en.wikipedia.org/wiki/Image:Signal_transduction_v1.png

Some of the extracellular chemical signals are small, nonpolar and lipophilic chemical molecules, such as testosterone, estrogen and cortisol that can readily diffuse across the hydrophobic plasma membrane around a cell. Inside the cell, the ligand (hormone) binds to intracellular receptors either in the cytoplasm or the nucleus, initiating a cellular response, such as gene transcription. However, most chemical signals are hydrophilic and too large in size to diffuse across the cell membrane. Membrane-associated receptor proteins (cell-surface receptors) facilitate transmission of these signaling molecules inside the cell. As shown in Fig. 1.1, there are many classes of membrane receptors that respond to the extracellular stimuli. These include G-protein

coupled receptors (GPCRs) (e.g., CCR5, rhodopsin), receptor tyrosine kinases (RTKs), (e.g., EGFR), integrins and Toll-like receptors.

These receptors are integral membrane proteins that bind and respond to a wide variety of signaling ligands. They all have an extracellular domain, a transmembrane (TM) domain and a cytoplasmic domain. Ligand binding on the extracellular side of the receptor induces specific structural rearrangements of the receptor such as dimerization and rigid body motion of TM helices that allow the cytoplasmic part of the receptor to become active inside the cell, initiating the intracellular signaling cascade. We are interested in studying the class activation mechanism of G-protein coupled receptors (GPCRs).

## *1.2 G protein-coupled receptors*

GPCRs represent the largest family of membrane receptors involved in signal transduction of external stimuli and ligands across the cell surface [2,3]. They are responsible for a variety of physiological process such as vision, behavioral regulation, inflammatory response, and controlling various autonomic functions such as heart rate and blood pressure. This impressive broad diversity in GPCR function makes them a very important class of membrane receptors, pharmaceutically. It is estimated that ~30% of the drugs currently available, target GPCRs for diseases such as cancer, allergies, asthma and stroke [4,5]. They share a common architecture consisting of 7 TM α-helices [6-8]. The first step in the activation mechanism of most GPCRs is the binding of a signaling ligand. Ligand binding to the extracellular loops or within the TM helical bundle of these receptors leads to an allosteric conformational change that allows it to bind and activate several heterotrimeric guanylate nucleotide-binding protein, known as G-proteins [9] inside the cell.

Apart from the above, it has been proposed recently that GPCRs upon phosphorylation by G protein-coupled receptor kinases (GRKs) [10] may play an important role in signaling cascades independent of the G-proteins and similar to the ones normally initiated by the growth factor receptors [11,12].

A recent, detailed analysis of the human genome [13,14] has revealed around ~950 genes that code for GPCRs. These include ~460 olfactory receptors [13,15,16]. Based on sequence similarities within the 7 TM hydrophobic domains, mammalian GPCRs have been grouped under six distinct families [7]:

- Class A, Rhodopsin-like
- Class B, Secretin-like
- Class C, Metabotropic glutamate / pheromone
- Class D, Fungal pheromones
- Class E, cAMP receptors
- Frizzled/Smoothened family

An interesting point to note is that even though GPCRs have structural and functional similarities they bind and respond to a wide variety of signaling ligands (agonists, antagonists and inverse agonists), for example, glycoprotein hormones, neurotransmitters, small peptides, chemokines and vitamin A derivatives [17] and possess diverse ligand binding domains. The lengths of N- and C-terminal domains and the extracellular and intracellular loops vary significantly among the various families of GPCRs. Additionally, sequence analysis of GPCRs has revealed that they have widely divergent sequences with no significant homology. However, within a subfamily significant sequence homology is observed [6,8]. In fact, one of the only structural features that is conserved among most members of the large family of 7 TM receptors is the disulfide bond between cysteine residues found on the extracellular end of TM H3 and the second extracellular loop (EL2). However, in spite of these apparent differences, a wealth of biophysical and biochemical data exists that provides evidence for similar conformational changes of the

receptors upon activation [18-24]. My thesis work has concentrated on studying the activation mechanism of rhodopsin, a member of the class A GPCRs. Studying this one receptor provides insights into a mechanism for the entire family of class A GPCRs

Class A GPCRs constitute one of the largest families of GPCRs. Members of this family are further divided into subfamilies based on the similarity of the ligands they bind. Apart from the visual family of receptors, some of the other subfamilies of class A GPCRs include the amine receptors (e.g. adrenergic receptors, histamine receptor and serotonin receptor), bradykinin receptors, olfactory receptors, hormone receptors (e.g. follicle stimulating hormone (FSH) receptor) and peptide receptors (e.g. CCR5 and CXCR1 chemokine receptors). They are characterized by a short N-terminal tail and presence of at least one highly conserved residue (sequence identity > 90%) in each of the 7 TM domains. These conserved residues include the disulfide bond between the EL2 and TM H3, the (D/E)RY motif on the cytoplasmic end of H3, the NPxxY$(x)_{5,6}$F at the cytoplasmic end of TM H7, and conserved prolines in the middle of the H5, H6 and H7 that impart a degree of flexibility to these helices. Additionally, there are several charged residues found on TM helices H1, H2 and H4. These signature residues mediate helix-helix interactions important for locking the receptor in the inactive state [25]. It is believed that activation of class A GPCRs upon ligand binding involves significant rigid body motion of these TM helices through a coupling between the various conserved motifs [26].

## *1.3 Rhodopsin: a class A GPCR*

Rhodopsin is the visual photoreceptor responsible for black and white vision in low light that is found in the rod cells of the human retina. It is a 40 kDa eukaryotic membrane protein, composed of 348 amino acids that belongs to the large, pharmaceutically important family of class A GPCRs [3]. Rhodopsin, in its membrane embedded region has a chromophore, 11-*cis* retinylidene, covalently linked to Lys296 in the TM H7 through a Schiff base that is protonated in the dark [27]. The chromophore is an aldehyde derived

from vitamin A [28]. Upon absorption of a photon of light, the 11-*cis* retinal isomerizes to an all-*trans* conformation inducing significant conformational changes in the surrounding protein. These changes trigger a shift of the protein into an active conformation where it binds and activate the G-protein, transducin [29].

Heinrich Müller, who attributed the reddish purple color of the rod cells to hemoglobin, first discovered rhodopsin in 1851. Later in 1878, Kühne [30] isolated the pigment from the rod outer segments of the frog's retina and studied its regeneration and photolability. He named this pigment "visual purple" (rhodopsin).

Rhodopsin is found in the disk membranes of the rod outer segment (ROS) in the rod photoreceptor cells. Rod cells are highly specialized and differentiated epithelial cells, with outer and inner segments (as shown in Fig. 1.3), Rod cells are capable of detecting a single photon. Mammalian ROS are typically 1μm in length and contain an array of 1000-2000 flattened disk-like vesicular structures about 160 Å thick. Rhodopsin is contained in the membrane of these disks, as shown in Fig. 1.4. Rhodopsin forms > 90% of the protein content of the disk membranes and it occupies about 50% of the surface area of a disk membrane. The rest of the space is occupied by lipids and cholesterol. In the human retina there are 120 million rod cells; a single rod cell on an average contains $10^8$ molecules of rhodopsin. Such a high concentration of rhodopsin helps in efficient detection of photons of light which travels in a straight line and cannot diffuse through the membrane like other soluble ligands to reach the photoreceptor.

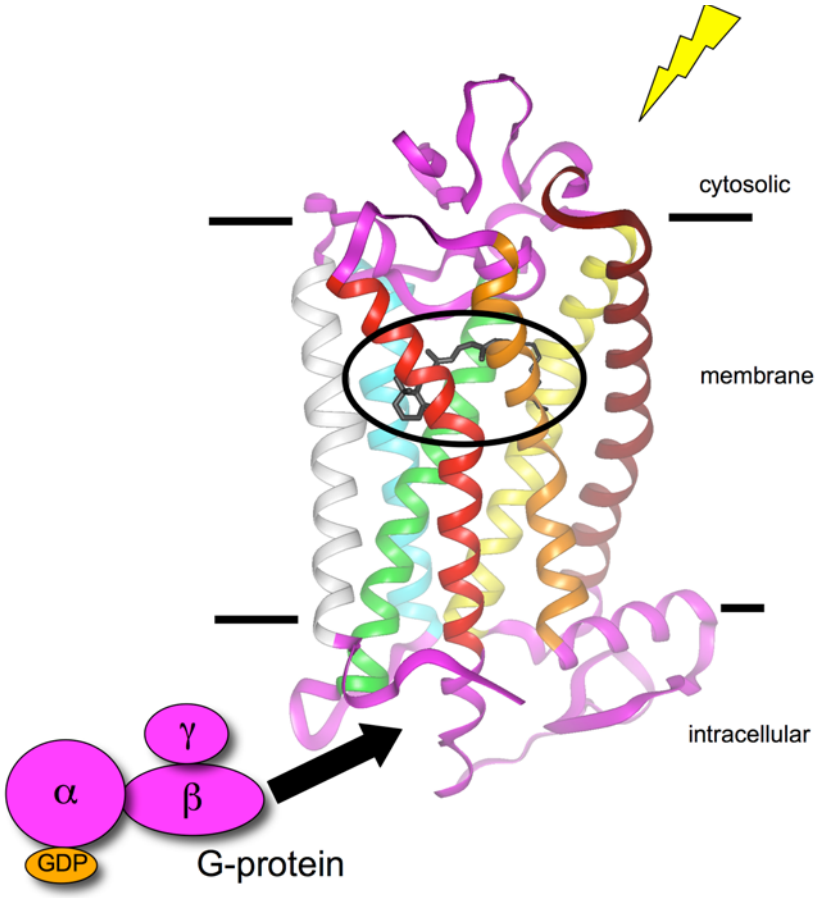


**Figure 1.2: A view of the rhodopsin crystal structure** [31]. It has 7 TM helices and three extracellular and 3 intracellular loops. The black circle highlights retinal covalently linked to H7 in rhodopsin. The G-protein binds to the intracellular loops for activation.

### *1.3.1 Rhodopsin phototransduction cascade*

The phototransduction cascade is a process by which light is converted into a chemical signal by the rod cells in the retina of the eye. The rod cells then pass this chemical signal to the retinal nerve cells, which in turn relay the signal along the visual pathway. Apart from rhodopsin, the other auxiliary proteins (such as transducin and phosphodiesterase) that aid in the efficient conversion of light into a chemical signal are also present in the rod outer segments. Rhodopsin serves as the input stage for this visual cascade. In dark

rhodopsin, the 11-*cis* retinylidene chromophore has an absorption maxima ($\lambda_{max}$) around 500 nm. Hubbard and Kropf [32] demonstrated that the visual phototransduction cascade (reviewed by Menon et al. 2001 [33] and Hubbell *et al*. 2003 [34] and the references cited in them) is initiated by an 11-*cis* to all-*trans* isomerization of the retinal chromophore upon absorption a single photon of light. In fact this is the only light dependent step of the visual cascade. The photoisomerization of the 11-*cis* retinal chromophore occurs within 200 fs of photoactivation. It has been documented as the fastest photochemical process known [35] with a high quantum yield of ~0.67 [36,37], as compared with ~0.2 of the protonated retinylidene Schiff base in organic solvent.

Photoisomerization is followed by thermal relaxation of the receptor through a series of spectrally well characterized photointermediates to form the active state known as metarhodopsin II (meta II) also designated as R* absorbing maximally ($\lambda_{max}$) at 380 nm. The active species, R* binds to the $\alpha$-subunit ($G_{t\alpha}$(GDP)) of the heterotrimeric G-protein, transducin ($G_{t\alpha\beta\gamma}$(GDP)) [29,38]. Formation of the complex between R* and $G_{t\alpha\beta\gamma}$(GDP) induces conformational changes in the $G_{t\alpha\beta\gamma}$(GDP) that catalyzes the exchange of GDP to GTP in the nucleotide binding site on the $G_{t\alpha}$ subunit. GTP binding to $Gt_{\alpha}$ triggers another conformational change that results in the dissociation of the active $Gt_{\alpha}$ ($Gt_{\alpha}$*(GTP)) from $G_{t\alpha\beta\gamma}$. The active $Gt_{\alpha}$*(GTP) subsequently binds to the cyclic guanosine monophosphate (cGMP) phosphodiesterase (PDE) and activates it by dissociating its inhibitory $\gamma$-subunit. The active PDE catalyzes the hydrolysis of cGMP to 5'GMP thereby reducing the cellular concentration of cGMP. Fall in the concentration of cGMP leads to closure of the cGMP-gated-$Na^+$ channels that reside in the plasma membrane surrounding the ROS. In the dark, these channels are kept open by the bound cGMP. Their closure blocks the influx of $Na^+$ ions causing hyperpolarization of the rod plasma membrane (see Fig. 1.3).

Hubbell *et al*. [34] discuss the various stages of signal amplification along the visual transduction pathway that account for the high gain of the rod cell response. First, each

molecule of R* can activate ~500 molecules of the G-protein, tranducin. Second, each activated PDE can hydrolyze ~$10^3$ molecules of cGMP to 5'-GMP. Third, hundreds of $Na^+$ channels respond to the drop in level of the cGMP; in total about $10^6$-$10^7$ $Na^{2+}$ ions are prevented from entering the cell per second causing the hyperpolarization of the rod cell membrane by ~1 mV. An important point to note here is that even though the visual system (including both rod and cone cells) functions over a large ($10^6$-fold) range of light intensity, the rod cells are sensitive enough to detect a single photon of light [39]. One of the reasons for this high sensitivity of rhodopsin is the coupled effect of signal amplification during the visual cascade (as discussed above) and extremely low levels of dark noise [39]. Thermal isomerization of rhodopsin at physiological temperature has been estimated to occur once every ~470 years [40]. The low level of basal activity for rhodopsin is because the presence of 11-*cis* retinal stabilizes the inactive state of rhodopsin as an efficient inverse agonist.

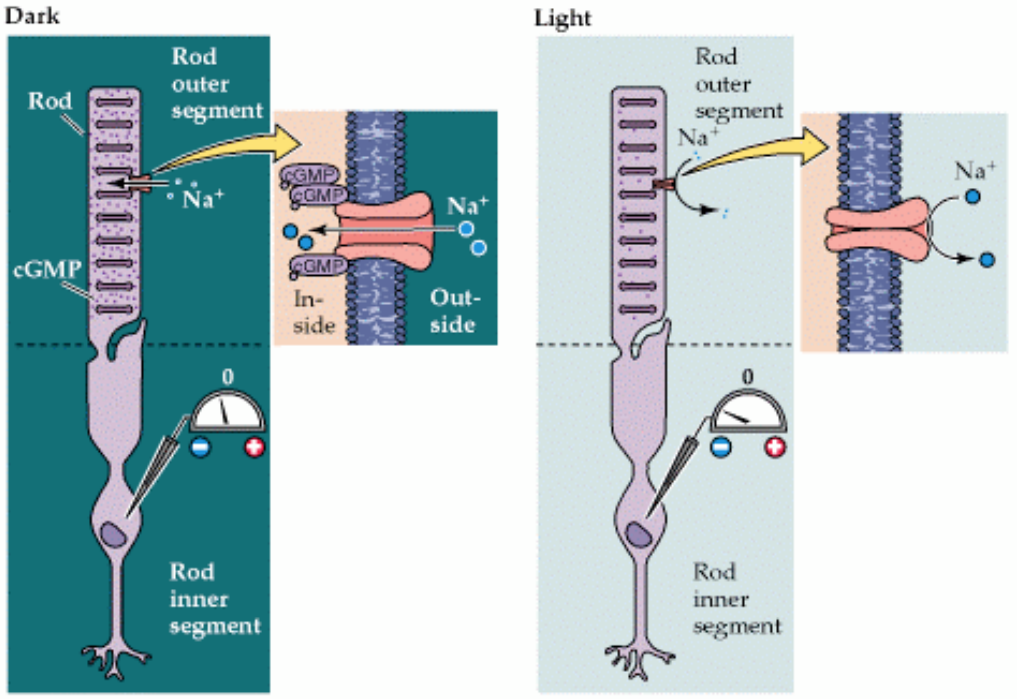


**Figure 1.3: A cartoon representation of cyclic GMP-gated channels in the Rod outer segment.** (Purves *et al.* Neuroscience, McNamara, & Williams, 2nd edition, 2001)

A number of processes work in parallel with the visual cascade to revert the rod cells to the resting dark state even before the activation process reaches peak potential [41]. At the level of rhodopsin, the cascade is shut down through phosphorylation of the C-terminal tail of the receptor, which is rich in serine and threonine residues. A rhodopsin specific kinase (RK; rhodopsin kinase [42,43]) phosphorylates the C-terminal domain of R*, triggering the binding of the inhibitory protein arrestin to the cytoplasmic loop. Arrestin binding uncouples R* from the G-protein, thereby inhibiting its activity [44]. Around the same time a regulator of G-protein signaling (RGS) protein inactivates transducin by hydrolyzing the bound GTP to GDP [45]. This leads to dissociation of transducin from PDE and facilitates its inactivation by allowing the inhibitory γ-subunits to associate with PDEs [46]. The inactive PDE can no longer hydrolyze the cGMP molecules. In addition, the

sodium channels that close in response to the drop in the level of cGMP also control the influx of $Ca^{2+}$. Therefore, the cellular concentration of $Ca^{2+}$ drops, which stimulates the GMP cyclase to replenish the concentration of cGMP to levels before receptor activation. The cGMP then binds to the $Na^{+}$ channels, returning the rod cell to its resting state. The membrane potential returns to its original level within 1-2 s following a brief photoexcitation. These various shutdown processes help in prolonging the lifetime of the rod cells and enable them to adapt to changes in the intensity of the stimulus over a wide range of baseline levels of stimulation and adds to the high sensitivity of rod cells.

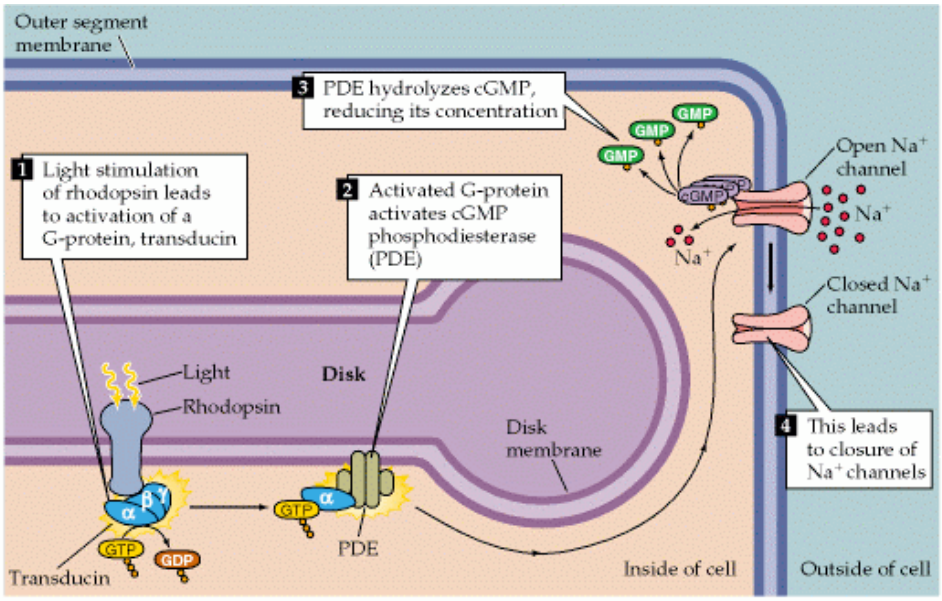


**Figure 1.4: Details of the phototransduction cascade in Rod cells.** (Purves *et al.* Neuroscience, McNamara, & Williams, 2nd edition, 2001)

### *1.3.2 A brief overview of the rhodopsin structure*

Rhodopsin was the first GPCR to be sequenced [47,48] and the first whose inactive state crystal structure was obtained at atomic resolution [31,49,50]. Recently, high-resolution crystal structures have been presented for the β2-adrenergic receptor [51,52] and the invertebrate squid rhodopsin [53]. Rhodopsin is embedded in the disc membrane of the ROS as a 7 TM helical receptor. The N-terminal tail of rhodopsin extends into the intradiscal (extracellular) space whereas the C-terminal tail is present in the cytosol (cytoplasmic side) of the Rod cells. Some of the physical characteristics that have been elucidated by having a high-resolution crystal structure of rhodopsin [14]: height: ~75 Å perpendicular to the membrane; width: ~48 Å; thickness: ~35 Å. The surface area occupied by intracellular and extracellular loops and tails projecting outside the phospholipid bilayer is ~1200 $Å^2$

Rhodopsin is made up of an apoprotein opsin and the chromophore, 11-*cis* retinal. The chromphore is covalently linked to Lys296 on H7 through a SB that is protonated in the dark (Fig. 1.2). The chromophore is what absorbs the photon of light. Glu113 on H3 acts as the counterion for the PSB [54,55]. The salt bridge that exists between the PSB and Glu113 on H3 plays an important role in stabilizing the inactive state structure of rhodopsin [56]. In other GPCRs, such as the dopamine [57], acetylcholine [58] and serotonin [59] receptors, interactions are observed between the ligand and residues on H7 analogous to Lys296 in rhodopsin. Disruption of the salt bridge is essential for the activation of rhodopsin [60].

Rhodopsin folds into 7 TM (H1, 34-64; H2, 71-100; H3, 106-140; H5, 200-230; H6, 241-276; H7, 286-309) [50] α-helices that are irregular and kinked. They tilt at various angles with respect to the membrane normal except the N-terminal segments of H4 and H6 that are oriented roughly parallel to the membrane normal [31,49,50]. The proline residues at positions 53, 170, 171, 215, 267 and 303 cause the kinks in helices H1, H4, H5, H6

and H7, respectively. All the prolines except Pro53 on H1 are among the most highly conserved residues across the family of class A GPCRs. The kinks in the helices allow them to pack more closely and to create a tight binding pocket for the 11-*cis* retinal chromophore [50]. In H2, a kink is observed due to the presence of two consecutive glycine residues at positions 89 and 90. They allow a hydrogen bond to form between the side chain of Thr92 and the main chain carbonyl of Phe88 causing a distortion of the helix. The kink in H3 is observed around the counterion Glu113.

The kinks in the helices also allow formation of extensive 3D interhelical or water mediated hydrogen bonding networks within the TM core of rhodopsin. One such hydrogen bonding network extends from Trp265 in the retinal binding pocket all the way to the intracellular end of the H7 through the highly conserved NPxxY (Asn302, Pro303, Tyr301) motif on H7. Other members of this hydrogen bonding network include Asn55 at the kink in H1, Asp83 on H2, Met257 on H6 and Ser298, Ala299 and Tyr301 on H7 (Fig. 1.5A). Tyr306, of the conserved NPxxY motif couples this hydrogen bonding network to residues on H8 via a packing interaction with Phe313. Interestingly, most of the residues involved in this hydrogen bonding network are conserved either across the family of class A GPCRs (e.g. Trp265, Ser298, Ala299, Tyr301 and Asn302) or in rhodopsin like GPCRs (e.g. Asn55, Asp83 and Met257) [1,50,61]. This hydrogen bonding network is essential from transmitting steric and electrostatic rearrangements from the retinal binding site to the cytoplasmic side of rhodopsin. A number of studies have shown that this hydrogen bonding network rearranges upon rhodopsin activation [50,62-66].

The second hydrogen bonding network extends from the kink in H3 around the counterion Glu113, to the second extracellular loop (EL2) [31,50] (Fig. 1.5B). The kink in H3 is a result of a water mediated hydrogen bond between the side chain carboxyl and the backbone carbonyl of Glu113. The side chain of Glu113 is also hydrogen bonded to the amide group of Cys187 on EL2. Other members of this hydrogen bonding network include Glu181, Gly182, Gln184, Ser186, Gly188, Tyr191 and Tyr192 on EL2 and

Tyr268 on H6. This hydrogen bonding network on one side extends to amino acids on the third extracellular loop (EL3) between H6 and H7 through water molecules and on the other side extends all the way to the extracellular ends of H4 and H5 [31,50]. This well-defined extensive network of interactions help in stabilizing the structure of EL2 above the retinal in the binding pocket. In fact, according to the crystal structure the extracellular loops of rhodopsin have lower thermal-factors than the cytoplasmic loops [31].

Another hydrogen bonding network extends from the second kink in H3 around the β-ionone ring. This triangular network of hydrogen bonds connects the side chain of Trp126 on H3 to the side chain of Glu122 on H3 and the side chain of His211 on H5 (Fig. 1.5C). The side chain of Glu122 is also hydrogen bonded to the backbone carbonyl of His211, which is not involved in the main chain hydrogen bonding due to the presence of a highly conserved Pro215 (H5), responsible for the kink observed in H5. The side chain on His211 forms another hydrogen bond with the hydroxyl group of Tyr206, which in turn is hydrogen bonded to backbone carbonyl of Ala166 on H4 [31,50]. FTIR studies have shown that Glu122 is protonated in rhodopsin and meta II [63]. However, it becomes more weakly hydrogen bonded in meta II [63]. UV-absorption studies have shown that the indole nitrogen of Trp126 becomes more weakly hydrogen bonded in meta II [66]. All the hydrogen bonding networks discussed above play an important role in stabilizing the inactive state structure of rhodopsin and they are modulated upon activation.

In rhodopsin, most of the highly conserved signature residues (with sequence identities > 90%) are located in the TM domains. These residues include, the NPxxY motif at the cytoplasmic end of H7 and the ERY (Glu134, Arg135 and Tyr136) motif on the cytoplasmic end of H6. The Arg135 forms an interhelical salt bridge with Glu134 and is interacts closely with Glu247 on H6. This “ionic lock” is important for stabilizing the cytoplasmic ends of H3 and H6 in an inactive conformation. This interaction is disrupted in meta II [18,67] and opsin [68].

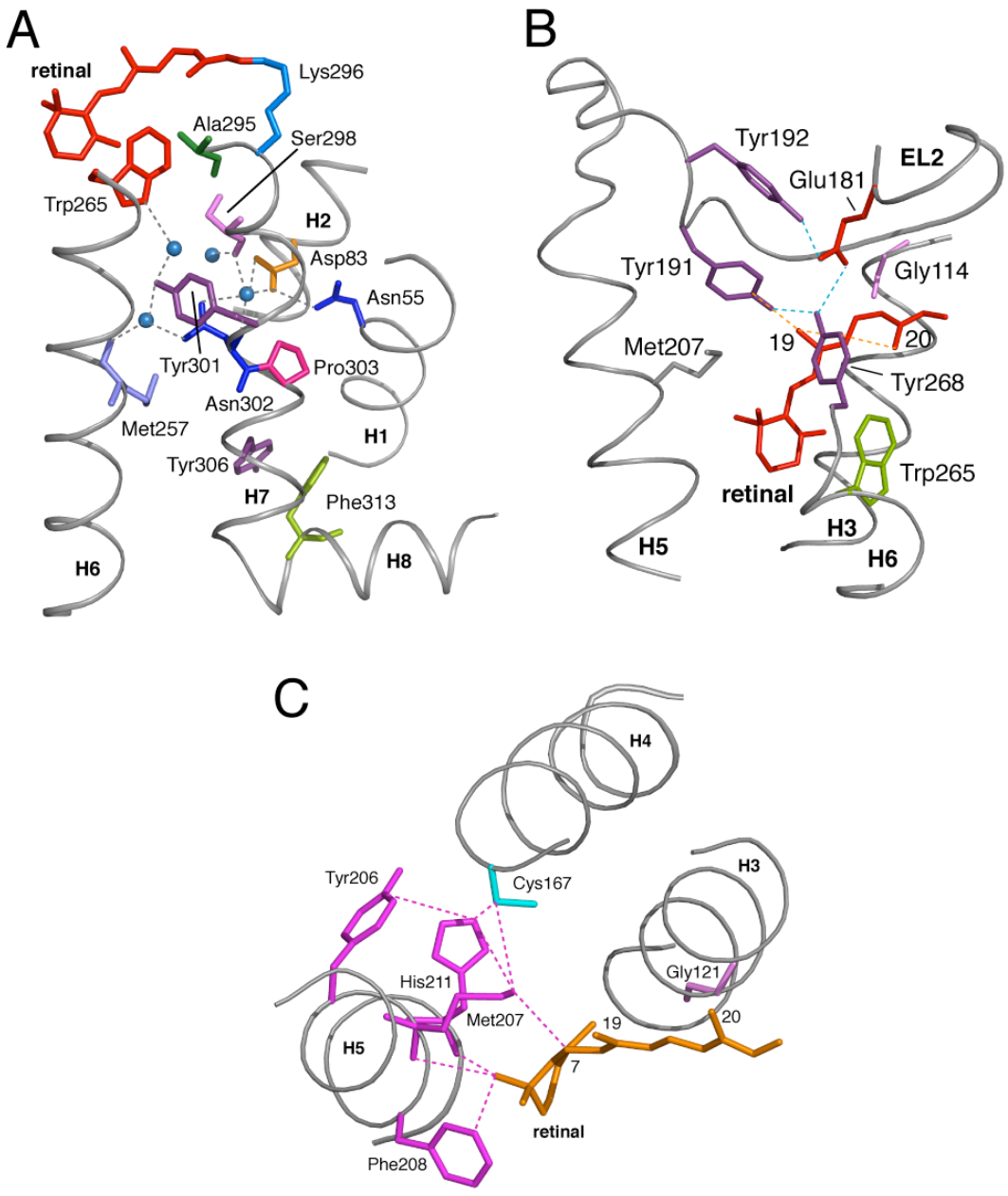


**Figure 1.5: Three hydrogen bonding networks that are important in stabilization of the inactive state of the receptor:** (A) The hydrogen bonding network involving the NPxxY motif on H7. (B) Part of the hydrogen bonding network involving EL2 and the PSB in the retinal binding pocket. (C) Hydrogen bonding network centered around H5.

The extracellular domain of rhodopsin includes the N-terminal tail and three interhelical loops (EL1, EL2 and EL3). The extracellular domains are more structured than the cytoplamic loops as demonstrated by the lower thermal-factors for the intradiscal loops in the crystal structure for the ground state of the receptor [69]. The three extracellular loops (EL1, EL2 and EL3) include 4 short β-strands β1 (4-6), β2 (9-11), β3 (177-180) and β4 (187-190) that fold into two β-hairpins: β1-β2 and β3-β4. The N-terminus is glycosylated at Asn2 and Asn15. The oligosaccharide chains project away from the extracellular loops [31,50]. Mutation of Asn15 effects G-protein activation [70]. The crystal structure of rhodopsin indicates that EL2 extends from Trp175 on H4 to Thr198 on H5. The intriguing aspect about the EL2 sequence is that it folds into a highly ordered and stable structure consisting of the two short β-strands (β3 and β4) that form a lid over the retinal-binding site [31,49,50] (Fig. 1.5). Motion of EL2 is constrained by a conserved disulfide bond between Cys110 at the end of H3 and Cys187 on β4 that is critical for the correct folding of rhodopsin into a fully functional conformation [71,72]. Other than the Cys110-Cys187 disulfide bond, the EL2 sequence is not conserved among the class A GPCRs.

The cytoplasmic domain of rhodopsin consists of the C-terminal tail (310-348) and 3 cytoplasmic loops (CL1, 65-69;CL2, 141-149; CL3, 231-240) [50]. CL2 and CL3 have been shown to be important for G-protein recognition and binding [73-75]. One of the interesting features that came out of the crystal structure for rhodopsin, and is seen only in class A GPCRs, is the fourth cytoplasmic loop, which folds into a putative alpha helix H8, that extends from amino acid Asn310 to Leu321 and lies almost perpendicular to the helices. H8 is amphiphatic in nature and is anchored to the lipid bilayer through palmitoyl groups attached to Cys322 and Cys323 [50]. The residues on H8 have multiple interactions with residues on surrounding helices, especially H7 and H1. Studies have shown that H8 is important for modulating interactions with the G-protein [76]. However, truncation of H8 beyond Asn315 does not affect transducin activation [77]. This suggests that H8 does not havw a primary role in G-protein activation. The C-terminal tail of rhodopsin is rich in

serine and threonine residues. In the activated state, the receptor gets phosphorylated at these amino acids by rhodopsin kinase phosphorylation facilitates binding of an inhibitory protein, arrestin, to switch off the active receptor.

### *1.3.3 Functional microdomains and group conserved residues*

Helix-helix interactions in rhodopsin are mediated by two sets of conserved residues. The first set consists of the highly conserved signature residues that have sequence identities > 90% across the family of class A GPCRs. For example, H5, H6 and H7 have the highly conserved prolines and the NPxxY motif on H7 (as discussed above). These signature residues are important for both function and stability of the receptor. In efforts of implicating these conserved sequences in a global activation mechanism, the concept of functional microdomains has been introduced [26].

Sequence similarities among class A GPCRs have identified a number of motifs corresponding to five proposed microdomains, which appear to be conserved throughout class A GPCRs. They include, a cluster of aromatic amino acids centered on the extracellular side of H6, a conserved ERY or DRY motif at the intracellular end of H3, and an NPxxY sequence on H7 [21,78]. In addition, there exists a number of conserved hydrogen bonding networks, such as the one of which is centered on Asn55 and Asp83 of H1 and H2, another involving His211 on H5. The challenge has been to develop a comprehensive model that explains the function of these conserved regions in the class A GPCRs.

Apart from the signature residues, there exists another family of conserved residues known as the group-conserved residues [79,80]. These include the small and weakly polar amino acids such as glycine, alanine, serine, cysteine and theronine. These residues have low sequence identities (< 40%) when considered individually but are highly conserved as a group, with sequence identity > 95%, across the family of class A GPCRs.

These small and weakly polar amino acids have high propensities for transmembrane helical interfaces and can facilitate tight packing between helices by mediating strong van der Waals interactions between helices. These closely packed helices can in turn facilitate the formation of interhelical hydrogen bonds between strongly polar (asparagine, glutamine, arginine, histidine and lysine) and weakly polar (serine, cysteine and threonine) amino acids [79,80].

Sequence analysis of rhodopsin revealed that most of these group-conserved amino acids were found on helices H1 (Gly51), H2 (Ala80 and Ala82), H3 (Ala124 and Ala132), H4 (Ala164 and Ala168) and H7 (Ala295 and Ala269) and surprisingly none were located on H5 and H6. The distribution of the small and weakly polar group-conserved amino acids has led to the proposal that helices H1-H4 form a tightly packed core stabilized by strong interhelical hydrogen bonding interactions in the inactive state of rhodopsin that do not change significantly upon receptor activation. TM helices H5, H6 and H7 each exhibit multiple interactions with the core that are responsible stabilizing the inactive state of rhodopsin. Retinal isomerization modulates each of these interactions in a concerted fashion leading to activation [79,80]. For example, in the rhodopsin crystal structure [31,50] a hydrogen bonding interaction exist between Asn78 (H2) and Trp161 (H4). Both of these residues are highly conserved across the family of class A GPCRs. This hydrogen bond is mediated by the presence of two group-conserved amino acids located one helix turn from two group-conserved amino acids, Ala82 on H2 and Ala164 on H4. Similarly, group-conserved residues were found to stabilize the H2-H4 core in the β2-AR receptor [81].

### *1.3.4 Rhodopsin, a prototypical GPCR*

Rhodopsin is one of the most well studied GPCRs. Rhodopsin quickly rose to the foreground becoming the prototypical GPCR. Rhodopsin has historical importance due to its role in vision, and is readily isolated in pure functional form from bovine retina

(~0.7 mgs per retina). Several methods have been developed for efficient expression and purification of rhodopsin from ROS and several eukaryotic recombinant expression systems [82-85]. Over the past decade or more, a wealth of biophysical and biochemical data have been collected on rhodopsin that provides useful insights into its structure and function [18,67,86-88]. A number of high-resolution crystal structures have been determined for the inactive state [31,49,50] [4068] and various photointermediates [89,90] of rhodopsin. Recently, a high-resolution crystal structure has been proposed for the ligand free opsin state following the decay of the active state [68]. It shows significant rigid body motion of TM helices that might be representative of the active state of rhodopsin.

However, rhodopsin as a member of the visual family of receptors has unique features that make it different from rest of the GPCRs. First of all, it does not bind a ligand as in other GPCRs for activation. It has a covalently linked chromophore that upon absorption of light behaves like an agonist. Interaction between other GPCRs and their ligand is completely non-covalent in nature [60]. However, it has been shown recently that the covalent link between the retinal and the apoprotein is not necessary for rhodopsin activation [91]. Additionally, it has been shown that adding all-*trans* retinal as a diffusible agonist similar to other GPCRs can activate some mutants of rhodopsin [54,92]. For example, adding all-*trans* retinal to the empty receptor in the dark can activate M257A the mutant of rhodopsin [92]. Therefore, all the reasons stated above show that rhodopsin is a perfect system for understanding and deducing a mechanism for activation of class A GPCRs.

In the following chapters, I use solid state NMR to understand the molecular mechanism of rhodopsin activation. In Chapter 3, I discuss in detail the conformation of the retinal, particularly the retinal β-ionone ring. I compare the $^{13}C$ chemical shifts of the retinal chromophore in rhodopsin and meta II to understand how the geometry and chemical nature of the surrounding protein changes upon activation. In Chapter 4, I discuss the role of the second extracellular loop (EL2) in the stability of the dark state and

the active state. I have obtained a range of distance constraints between amino acids on EL2 and the surrounding helices and between amino acids on the $\beta_4$ strand of EL2 and the retinal chromophore to understand how the interactions between EL2 and the surrounding protein gets modulated upon activation. In the following chapters, I present the structural rearrangements induced in TM helices H5, H6 and H7 and H8 as a result of retinal isomerization, which represent the functional state of the receptor.

# Chapter 2

# Methods and Materials

## *2.1 Expression and purification of $^{13}$C-labeled rhodopsin*

Rhodopsin was expressed in stable tetracycline-inducible HEK293S cells [93] containing the wild-type opsin gene [94]. The cells were grown in Dulbecco's modified Eagle's medium formulation [95] prepared from cell culture-tested components (Sigma, St. Louis, MO). For suspension growth, the medium was supplemented with specific $^{13}$C-labeled amino acids (Cambridge Isotope Laboratories, Andover, MA), Heat inactivated and dialyzed fetal bovine serum (10%), Pluronic F-68 (0.1%), heparin (50 mg/L), penicillin (100 units/mL) and streptomycin (100 μg/mL) [96,97]. The cells were induced with 2.0 mg/L tetracycline on day 5 [93] and harvested on day 7. The HEK293S cell pellets containing opsin were resuspended in 40 mL/L cell culture + protease inhibitors [94] and unlabeled 11-*cis* retinal was added in two steps to a final concentration of 15 μM to regenerate rhodopsin from opsin.

## *2.2 Purification and reconstitution of rhodopsin in n-dodecyl-β-d-maltoside micelles for metarhodopsin II studies*

Rhodopsin was purified from the cell pellets by immunoaffinity chromatography using the rho-1D4 antibody (National Cell Culture Center, Minneapolis, MN) [94].

The cell pellets (40 ml/L of cell culture) were extruded through an 18.5 gauge needle and solubilized in 1.0% n-dodecyl-β-D-maltoside (DDM) detergent in phosphate buffered saline (PBS) at pH 7.0 at room temperature for 4 hours. Following solubilization the lysate was centrifuged at 50,000 g for 30 mins at 4°C. The supernatant was collected separately in an autoclaved bottle.

The supernatant was loaded on a column packed with beads slurry (2.0 ml/mg of rhodopsin: CNBr beads coupled to rho-1D4 antibody; the rho-1D4 antibody recognizes the last 9 amino acids of the C-terminus tail of rhodopsin) at a slow rate of 1.0 ml/min to ensure efficient coupling at room temperature (RT). Subsequently, the column was washed with 50 column volumes (=1.0 ml/mg of rhodopsin) of 0.02% DDM in PBS at pH 7.0 and equilibrated with 10 column volumes of 0.02% DDM in 2 mM sodium phosphate (NaPi) buffer at pH 6.0. During each step small aliquots of the flow through were tested by UV-Vis spectroscopy to ensure that no rhodopsin was coming off the column during any of the steps mentioned above.

Rhodopsin was eluted off the column with equilibration buffer (0.02% DDM in sodium phosphate (NaPi) buffer at pH 6.0) containing a 100μM concentration of a 9 amino acids peptide (9-mer) corresponding to the last 9 amino acids of the rhodopsin C-terminus as the antibody epitope. Rhodopsin was eluted at flow rates of 1.0 ml/min at RT. Elution fractions containing rhodopsin were collected and concentrated using Centricon cones (Amincon, Bedford, MA) with a 10 kDa cutoff to a final volume of ~400 μL.

## *2.3 Purification and reconstitution of rhodopsin in digitonin micelles for metarhodopsin I studies*

As mentioned above, the cell pellets (40 mL/L of cell culture) were extruded through an 18.5 gauge needle and solubilized with 1.0 % DDM in PBS at pH 7.0 at room temperature for 4 hours. Following solubilization the lysate was centrifuged at 50,000 g for 30 mins at 4°C. The supernatant was collected separately in an autoclaved bottle.

The supernatant was loaded on a column packed with beads slurry (2.0 ml/mg of rhodopsin: CNBr beads coupled to rho-1D4 antibody) at a slow rate of 1.0 ml/min to ensure efficient coupling to the column at RT.

Subsequently, the column was washed with 10 column volumes (=1.0 ml/mg of rhodopsin) of 0.02% DDM in PBS at pH 7.0. DDM was exchanged with digitonin detergent on the column by first washing with 30 column volumes of 0.1% digitonin in PBS at pH 7.0 followed by washing with 20 column volumes of digitonin in PBS at pH 7.0. Following that the column was then equilibrated with 10 column volumes of 0.02% digitonin in 2.0 mM NaPi at pH 7.0. During each step small aliquots of the flow-through were tested by UV-Vis spectroscopy to ensure that no rhodopsin was coming off the column during any of the steps mentioned above.

Rhodopsin was eluted off the column with equilibration buffer (0.02% digitonin in sodium phosphate (NaPi) buffer at pH 7.0) containing the 9-mer epitope at a concentration of 100 μM. Elution was done at flow rates of 1ml/min at RT. Elution fractions containing rhodopsin were collected and concentrated using Centricon cones (Amincon, Bedford, MA) with a 10 kDa cutoff to a final volume of ~400 μL. All the buffers and solutions were prepared fresh, just a day before the purification to prevent

precipitation of digitonin in the column that can result in low yields of purified rhodopsin.

The concentrated protein in DDM or digitonin was stored frozen at -80°C until required for NMR data acquisition.

## *2.4 Synthesis of $^{13}$C-labeled retinals and regeneration into rhodopsin*

Synthetic retinals with specific $^{13}$C-labels were produced by standard methods [98] and purified by established protocols [99] to obtain $^{13}$C labeled 11-*cis* retinal.

Our collaborator, Prof. Mordechai Sheves provided specific $^{13}$C labeled all-*trans* retinal in hexane. The all-*trans* retinal was dried to a film under a steady stream of argon. The film was re-dissolved in 0.5 ml of dried acetonitrile and illuminated for 20 min with white light (using a low power fiber optic light source from Dolan-Jenner) on ice. This was done to obtain different isomers of retinal (13-*cis*, 11-*cis*, 9-*cis*, 7-*cis* etc). The isomer mixture in acetonitrile was blown down to a film using argon gas in the dark room. The film was re-dissolved in 3.0 ml of dried hexane and the solution was filtered through a 0.45 μm syringe driven filter units (Millipore, non-sterile, LCR(PTFE) membrane) before being used for purification.

High pressure liquid chromatography (HPLC) was used to purify 11-*cis* retinal from the mixture of isomers using an Econosphere silica 10μ column from Alltech (length 250 mm, ID 10 mm) [96]. The mobile phase contained 96% hexane and 4% ethyl acetate. The flow rate was maintained at 8ml/min throughout the purification. Fig. 2.1 show the HPLC profile for the mixture of retinal isomers under the above-mentioned conditions.

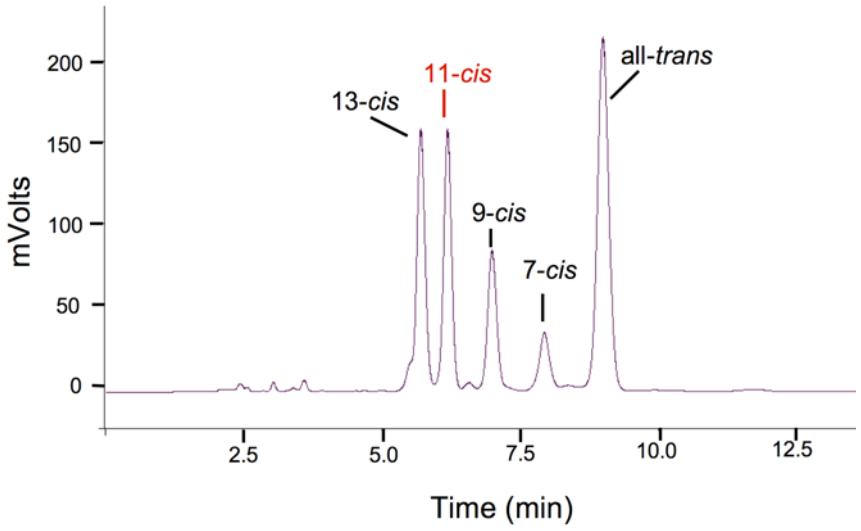


**Figure 2.1: HPLC profile of illuminated all-*trans* retinal.**

11-*cis* retinal was collected separately in a round bottom flask covered with aluminum foil to prevent light from isomerizing it to all-*trans* retinal. The purified fraction in hexane and ethyl acetate was blown down to a film under argon and re-dissolved in smaller, known quantities of dried hexane. The concentration was measured using UV-Vis spectroscopy. The 11-*cis* retinal in hexane was kept at -80°C until required for regenerating rhodopsin.

Rhodopsin pigment in DDM or digitonin micelles was regenerated with a 2:1 molar ratio of $^{13}$C-labeled 11-*cis* retinal to protein [100]. Rhodopsin samples were equilibrated with 11-*cis* retinal (dissolved in a small, known quantity of ethanol) in the dark room before being illuminated with a 400 W lamp with a > 495nm cutoff filter for ~45-60 sec at RT. It is important that the ethanol concentration must not exceed 1.0% of

the total volume in DDM or digitonin as it can affect the efficiency of trapping rhodopsin in the active state.

Following illumination, the sample (rhodopsin + 11-*cis* retinal) was nutated for an hour at RT in the dark room to allow efficient regeneration of rhodopsin with the labeled retinal. Regeneration efficiency was calculated based on the recovery of the 500 nm peak in the UV-Vis spectra. It usually took about 30 min at RT to regenerate ~90-95% of the sample to rhodopsin in DDM micelles and about 24 hours at RT for samples reconstituted in digitonin.

The regenerated samples were blown down by evaporation using a steady stream of argon gas to a volume of about 60 μL or less. Samples were then packed into 4 mm Bruker zirconia NMR rotors fitted with a small Teflon spacer to block the bottom 1/4$^{th}$ of the rotor volume and frozen at –80 °C until NMR data acquisition.

## *2.5 Structure determination of membrane proteins by solid-state nuclear magnetic resonance spectroscopy*

3D structural elucidation of proteins is the key to understanding various biological functions. Questions involving how different proteins interact with one another, how mutations affect protein function, how information is exchanged between cells of a multicellular organism, how cells are organized into different tissues and many other similar questions can be answered more thoroughly if one possesses a deeper understanding of the structure of the proteins involved. This understanding is essential for guiding the efficient development of various therapeutic drugs.

Membrane proteins are involved in a number of cellular and physiological processes such as signaling between cells, transport across cell membranes and energy

transduction processes. About 30% of the human genome codes for membrane proteins and therefore, they are very important drug targets [4]. However, despite the importance of membrane proteins their high-resolution structure determination and functional elucidation has remained an under-explored territory.

In recent years, huge advancements have been made in the 3D structure determination of proteins using X-ray crystallography and solution-state Nuclear Magnetic Resonance (NMR). However, it is often difficult to obtain well-ordered crystals of large hydrophobic membrane proteins needed for high-resolution diffraction data. Solution NMR has increasingly been used for studying structure and dynamics of small detergent-solubilized membrane proteins (≤ 40 kDa) as they can tumble freely at nano-second timescales [101,102]. However, large proteins (> 40 kDa) reconstituted in detergent micelles or phopholipid bilayers (to mimic their native environment), are not amenable to this technique as they have slower tumbling rates and longer rotational correlation times. In recent years, solid-state NMR (ssNMR) has emerged as a powerful tool for the structural elucidation of membrane proteins in their functional native environment. It provides site-specific, atomic level structural constraints on samples in a variety of crystalline or amorphous environments and can be applied to proteins that are greater than 100 kDa in size [103]. In fact there is no upper limit on the size of the protein that can be studied using solid-state NMR. Solid-state NMR can provide detailed information on the topology, dynamics and three-dimensional structure of molecules. In the past decade tremendous progress has been made in this field to obtain structural constraints on proteins, including distance information between pairs of amino acids as well as orientational and torsional constraints that can be translated into molecular structures. Structural information along with other biochemical data (such as mutational analysis and assays to determine protein activity) can then collectively provide a comprehensive understanding of the mechanism by which an individual membrane protein functions.

In my thesis project I have extensively used solid-state NMR for structural studies on the inactive and active state of the G-protein coupled receptor, rhodopsin.

### *2.5.1 A brief review of NMR spectroscopy*

NMR is a powerful technique that employs the use of high static magnetic fields (of the order of Tesla) and alternating (radio frequency; RF) fields to manipulate spin states of magnetically active nuclei, such as $^{1}H$, $^{13}C$, $^{15}N$, $^{31}P$ and $^{17}O$. Isidor Rabi first described NMR on molecular beams in 1938. Edward M. Prucell and Felix Bloch later improved the technique for use on solution and solids in 1946, for which they received the Nobel Prize in 1952. Most of the discussion below will focus on solid-state NMR application to systems of spin 1/2 nuclei such as $^{13}C$ and $^{1}H$.

#### *Nuclear spin interaction hamiltonian*

In a solid sample the molecular motion is restricted. As a result a solid-state NMR spectrum has very low resolution with line widths of the order of 10-100 kHz resulting from anisotropic internal interactions that exist at a molecular level within the sample. In solution NMR most of these interactions are averaged to their isotropic value due to rapid molecular motion or tumbling. The nuclear spin hamiltonian ($\mathcal{H}$) describes all the interactions (external and internal) experienced by the spin that results in an NMR spectrum [104-106]. The Hamiltonian is described below:

$$\mathcal{H} = \mathcal{H}_{Z} + \mathcal{H}_{RF} + \mathcal{H}_{CS} + \mathcal{H}_{D}^{II} + \mathcal{H}_{D}^{IS} + \mathcal{H}_{J} + \mathcal{H}_{Q} \qquad (2.1)$$

$$\mathcal{H} = \mathcal{H}_{ext} + \mathcal{H}_{int} \qquad (2.2)$$

The external spin hamiltonian ($\mathcal{H}_{ext}$) describes the interaction between the nuclear spin and the applied external static ($\mathbf{H_O}$) and oscillating magnetic fields ($\mathbf{H_{RF}} = H_1\cos(\omega t)$).

$$\mathcal{H}_{ext} = \mathcal{H}_Z + \mathcal{H}_{RF} \tag{2.3}$$

Interaction with the external static longitudinal magnetic field ($\mathbf{H_O}$) is known as the nuclear Zeeman hamiltonian ($\mathcal{H}_Z$). It is of the order of 100 MHz and is described by the following equation:

$$\mathcal{H}_Z = -\gamma \mathbf{H}_O \bullet \mathbf{I} \tag{2.4}$$

$-\gamma\mathbf{H_O}$ is defined as the Larmor procession frequency ($\omega$) of spin I with gyromagnetic ratio ($\gamma$). The other term in equation (1.2) is known as the radiofrequency hamiltonian ($\mathcal{H}_{\mathbf{RF}}$). It is of the order of 10-100 kHz and it is described by the following equation:

$$\mathcal{H}_{RF} = -2\gamma H_1(\cos\omega t) I_x \tag{2.5}$$

The rest of the terms in equation (1.1) are derived from internal interactions at the molecular level within the sample. They constitute the internal spin interaction hamiltonian ($H_{int}$). They are described by the following equations:

$$\mathcal{H}_{cs} = -\gamma \mathbf{H}_o \bullet \hat{\sigma}(\Theta) \bullet \mathbf{I}$$
$$\mathcal{H}_D^{II} = \sum_{i \neq j} (\gamma_i \gamma_j \hbar) I_i \bullet \mathcal{D} \bullet I_j$$
$$\mathcal{H}_D^{IS} = \sum_i (\gamma_I \gamma_S \hbar) I_i \bullet \mathcal{D} \bullet \mathbf{S} \qquad (2.6)$$
$$\mathcal{H}_J = \sum_i I_i \bullet \mathcal{J} \bullet I_j$$
$$\mathcal{H}_Q = \frac{(eQ)}{2I(2I-1)\hbar} \mathbf{I} \mathcal{V} \mathbf{I}$$

The chemical shift term ($\mathcal{H}_{CS}$) presents the indirect interaction between the nuclear spin (**I**) and the external magnetic field ($\mathbf{H_o}$) through the electrons surrounding the nucleus. It depends upon the distribution of electrons around the nucleus (under consideration), which in turn depends on the nature of the chemical bond that the nucleus is involved in. The external magnetic field ($\mathbf{H_o}$) induces a polarization in the electron cloud surrounding the nucleus. These circulating electrons in turn generate a magnetic field called the induced magnetic field ($\mathbf{H}_{ind}$) [105]. This induced magnetic field shields the nuclear spin from the external field ($\mathbf{H_o}$) and changes the value of the total magnetic field experienced by the nuclear spin, thus modulating its Larmor frequency (ω). The chemical shift interactions are of the order of 10-30 kHz and depend on the orientation of the molecule ($\Theta$) with respect to the external magnetic field. They are represented by a second rank chemical shift tensor, $\sigma(\Theta)$, represented by a 3x3 matrix. Chemical shift tensor can be placed into its principal axis system (PAS) by diagonalization of the matrix. The eigen values that result from diagonalization are denoted as $\sigma_{11}$, $\sigma_{22}$ and $\sigma_{33}$. They are the three principal values of the chemical shift anisotropy tensor, $\sigma(\Theta)$. The individual $\sigma_{ii}$ depends on the molecular orientation ($\Theta$) but their sum does not. In solution, molecular tumbling averages out this anisotropic component of the chemical shift leaving only the isotropic component. The isotropic component of $\sigma(\Theta)$, $\sigma_{iso}$ is the average of the tensor, which is nothing but 1/3$^{rd}$ the trace of the matrix, as shown below:

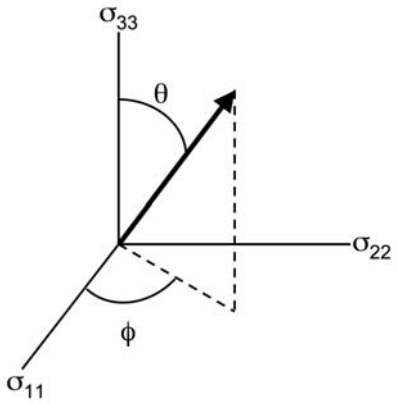


$$\sigma_{iso} = \frac{1}{3}(\sigma_{11} + \sigma_{22} + \sigma_{33})$$
$$\mathcal{H}\text{cs} = \gamma \mathbf{H_o}[1 - (\sigma_{11}\sin^2\Theta\cos^2\phi + \sigma_{22}\sin^2\Theta\sin^2\phi + \sigma_{33}\cos^2\Theta)]Iz \qquad (2.7)$$
$$= \gamma \mathbf{H_o}[1 - (\sigma_{iso} + \Delta\sigma(3\cos^2\Theta - 1) + \eta_{\text{cs}}\sin^2\Theta\cos 2\phi)]Iz$$

By convention, $\sigma_{33} \geq \sigma_{22} \geq \sigma_{11}$.

Therefore, $\Theta$ is the angle between the distribution of electrons around the nucleus and $\mathbf{H_o}$. This is known as chemical shift anisotropy (CSA). As mentioned earlier, $\sigma_{ii}$ depends on the molecular orientation, therefore CSA can be used to obtain information on the orientation of the molecule.

The dipolar interaction term in the Hamiltonian ($\mathcal{H}_{\mathbf{DD}}$) represents the direct interaction between nuclear spins [105]. The field generated by the second nuclear spin (S) modulates the total field experienced by first nuclear spin (I). Dipolar interactions can be intermolecular or intramolecular. The direct dipole-dipole coupling between like and unlike spins is represented by the homonuclear ($\mathcal{H}_{\mathbf{DD}}^{\mathbf{II}}$) and heteronuclear ($\mathcal{H}_{\mathbf{DD}}^{\mathbf{IS}}$) dipolar Hamiltonian terms in equation (1.6). The strength of the dipolar coupling ($\mathcal{D}_{ij}$) depends on the gyromagnetic ratios of the nuclear spins involved ($\gamma_I$, $\gamma_j$), distance separation between the two nuclei ($r_{ij}$) and the angle that the line joining the two nuclei makes with the external magnetic field ($\Theta_{ij}$).

$$Dij = \frac{\mu_0}{4\pi}\frac{\gamma_i\gamma_j}{2r_{ij}^{3}}\hbar(3\cos^2\Theta_{ij} - 1) \qquad (2.8)$$

In solution NMR the fast Brownian motion of the molecules averages the dipolar coupling between nuclear spins to zero. In solid-state NMR dipolar couplings are not averaged out due to restricted motion and therefore contribute 10-100 kHz of broadening to the line widths in the spectrum.

The *J*-coupling Hamiltonian ($\mathcal{H}_J$) in equation (1.6) arises due to the indirect interaction between nuclear spins through the electrons [105]. These interactions are of the order of 100 Hz and are very useful in establishing connectivities between nuclei in solution state NMR. They provide information on the local environment of a molecule. However, they are often ignored in solid-state NMR because they are masked by other stronger and bigger interactions, such as dipole-dipole couplings and CSA.

The last term in the internal spin interaction Hamiltonian is known as the quadrupolar spin Hamiltonian ($\mathcal{H}_Q$). Quadrupolar couplings are observed for nuclei with spin > 1/2, for example, $^2$H and $^{17}$O. Nuclei with spin > 1/2 has electric quadrupole moments apart from magnetic dipole moments. The quadrupolar interaction arises due to the interaction between the electric quadrupolar moment (Q) and the electric field gradient (EFG) "V" created by the charges surrounding the nucleus (see equation (1.6)). It is a 2$^{nd}$ rank symmetrical tensor. Quadrupolar interactions can be huge, of the order of 5 MHz. However, this term is not applicable in case of spin 1/2 nuclei.

*Magic Angle Spinning (MAS) and Heteronuclear Decoupling*

In solids, the presences of orientation dependent interactions such as chemical shift anisotropy (CSA), homonuclear and heteronuclear dipole-dipole couplings greatly contributes to broadening of the resonance lines in the NMR spectrum, leading to loss of resolution.

$$\mathscr{H}\text{cs} = \gamma \mathbf{H_o}[1 - (\sigma_{iso} + \Delta\sigma(3\cos^2\Theta - 1) + \eta_{\text{cs}}\sin^2\Theta\cos 2\phi)]Iz \qquad (2.9)$$

From equation (1.8) and (1.9), we have seen that both CSA and dipole-dipole coupling depend on the factor of ($3\cos^2\Theta$-1) that describes the orientation dependence. In solution, as mentioned above, these interaction are present but are averaged out by the rapid tumbling of the molecules. In solids, these anisotropic contributions can be averaged manually by spinning the sample mechanically about an axis that is tilted at 54.7° with respect to the external static magnetic field ($\mathbf{H_o}$) increasing the resolution for better identification and analysis of the spectrum (see Fig. 2.2). At this angle, the ($3\cos^2\Theta$-1) is equal to zero and therefore the orientation dependent interactions vanishes. This is known as magic angle spinning (MAS) [107-110].

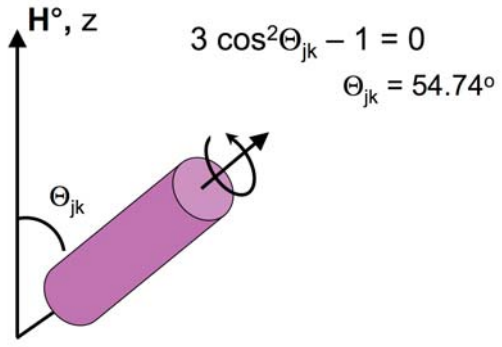


**Figure 2.2: Representation of a rotor spinning at magic angle with respect to the $H_O$**

If the spinning frequency ($\omega_r$) is much greater then the line width of a resonance in the NMR spectrum then it results in a single, narrow peak at the isotropic chemical shift of the nuclei. However, if $\omega_r$ is smaller than the anisotropic contributions to the line width then the resulting spectra exhibits a narrow, most intense peak at the isotropic chemical shift, flanked on either side by spinning side bands spaced at the spinning frequency ($\omega_r$). These spinning side bands are a result of refocusing of the NMR signal every rotor period, generating rotational echoes in the time domain. These rotational echoes, when fourier transformed produce a pattern of spinning side bands in the frequency domain. These spinning side bands carry information on the CSA and dipolar couplings between molecules and in some cases provide information on the mobility of a molecule.

MAS is most effective at averaging out dipolar coupling when $\omega_r$ is greater than the dipolar coupling between the nuclei. The most widely studied nuclei in protein solid-state NMR are $^{13}C$ and $^{15}N$. They are spin 1/2 nuclei and therefore, the quadrupolar coupling term is not present in their interaction Hamiltonians. However, they are dilute spins as compared to $^{1}H$ nuclei (protons), the more abundant spins found in proteins. The homonuclear dipole-dipole couplings between $^{13}C$ or $^{15}N$ are of the order of 2-5 kHz and therefore, can be easily averaged out by MAS. However, heteronuclear dipole-dipole coupling between $^{1}H$- $^{13}C$ and $^{1}H$- $^{15}N$ are larger, of the order of 30 kHz. These interactions lead to considerable broadening to the NMR spectrum and cannot be effectively averaged by MAS as we typically spin at spinning speeds (< 15 KHz) much smaller than the strength of dipolar couplings. However, it is possible to decouple the protons ($^{1}H$) from the observed $^{13}C$ and $^{15}N$ by applying high power radio frequency (RF) magnetic fields at the proton frequency. This is known as heteronuclear decoupling [111,112].

## *Cross Polarization (CP) from the abundant nuclei ($^{1}H$)*

In solid-state NMR, heteronuclei such as $^{13}C$ and $^{15}N$ have very low sensitivity because of long spin lattice relaxation times ($T_1$) also known as longitudinal relaxation times, as compared to solution. As a result, signal averaging can take longer than in liquids. This leads to low signal accumulation and therefore low sensitivity. Additionally, $^{13}C$ and $^{15}N$ have lower gyromagnetic ratios ($\gamma$) as compared to $^{1}H$'s and therefore, the extent of polarization is lower as compared to $^{1}H$. Additionally, they have very low natural abundance ($^{13}C$ ~1.1%) as compared to $^{1}H$ that is naturally 100% magnetically active and it has faster relaxation times. This problem is circumvented by a technique known as cross polarization [113-115]. In order to obtain high-resolution $^{13}C$ or $^{15}N$ NMR spectra, polarization is transferred from the abundant nuclei ($^{1}H$) to the heteronuclei by satisfying the Hartmann-Hahn condition in the rotating frame of reference.

$$\gamma_X H_{1C} = \gamma_H H_{1H}$$
$$\omega_C = \omega_H \qquad (2.9)$$

The rotating frame of reference is a coordinate system that rotates about the external magnetic field ($\mathbf{H_O}$) at the Larmor precession frequency ($\omega$). $H_1$ is the amplitude of the RF field for $^{1}H$ and heteronuclei (X=$^{13}C$ or $^{15}N$). By appropriately choosing the $H_{1,}$ field strengths for $^{1}H$ and X (e.g. $H_{1C} \cong 4H_{1H}$ because $\gamma_H \cong 4\gamma_C$) we can satisfy the Hartmann-Hahn condition and facilitate energy exchange between the X and $^{1}H$ nuclei. One of the advantages of CP from $^{1}H$ is that the experiment can be repeated at a rate determined by the much faster relaxation time of $^{1}H$ instead of that of $^{13}C$.

### *2.5.2 Obtaining structural constraints on rhodopsin using solid-state NMR*

Magic angle spinning, cross polarization (CP) and heteronuclear decoupling are used routinely in solid-state NMR to enhance the resolution of 1D and 2D $^{13}C$ or $^{15}N$ NMR spectra. The chemical shifts obtained from 1D $^{13}C$ or $^{15}N$ CP experiments provide significant information on the local chemical environment of the nuclei. For example, the

$^{13}C$ chemical shifts for the carbonyl and alpha carbons of an amino acid in a protein are sensitive to its secondary structure ($\alpha$-helical, $\beta$-sheets or random coil). Chemical shifts are also sensitive to the protonation state of the molecule, proximity of polar, charged or aromatic residues and provide information on the strength of the hydrogen bonding interactions with neighboring amino acids.

As mentioned previously, hetero- and homonuclear dipole-dipole interactions depend on the internuclear distance between two spins and therefore can be used for obtaining structural constraints on proteins. However, MAS averages out this important information. In the past 20 years, a slew of methods have been developed to reintroduce dipolar couplings in the MAS experiment [116-120]. A number of 2D recoupling solid-state NMR sequences have been introduced for obtaining long-range distance information by measuring weak dipolar couplings [117,120]. Several problems associated with 2D recoupling methods are: First, inhomogeneous RF field ($H_1$) across the length of the NMR sample can lower sensitivity because of mismatch of the Hartmann-Hahn condition over part of the sample. Second, dipolar truncation [121] makes it difficult to measure a weak dipolar coupling in the presence of a strongly coupled network of spins. To overcome the first problem, as much as possible we restrict our sample in the middle of the 4 mm rotor used for running NMR experiments (explained below). The $H_1$ field is most intense and homogeneous in the center of the rotor at the center of the RF coil in the NMR probes. The bottom $1/4^{th}$ of the rotor contributes negligible signal due to $H_1$ field inhomogenity and is blocked off with an appropriately sized piece of Teflon. In order to overcome the problem of dipolar truncation we selectively isotope ($^{13}C$ and $^{15}N$) label our protein as explained in the section above on expression of selectively $^{13}C$ labeled bovine rhodopsin in HEK293S stable cell lines. Selective labeling of proteins also help in obtaining the resolution required for making precise and accurate measurements on non-crystalline samples with broad lines and large natural abundance signal coming from detergents or lipids used for reconstituting the protein.

We use 2D dipolar assisted rotational resonance (DARR) NMR technique [120] to selectively reintroduce dipole-dipole couplings between pairs of $^{13}C$ spins. This techniques enables us to measure long-range $^{13}C...^{13}C$ correlations between pairs of nuclei that ≤ 6.0 Å apart in space. DARR is a homonuclear recoupling sequence similar to proton driven spin diffusion (PDSD) [120]. Using a series of model compounds and some selectively $^{13}C$ labeled rhodopsin samples we have shown previously that DARR is more efficient that radio frequency driven spin diffusion (RFDR) [118] at measuring long range, through space distance constraints [122]. DARR was shown to be more insensitive to $H_1$ field inhomogeniety as compared to RFDR and has been shown to be more robust against dipolar truncation [120,122].

## *Dipolar Assisted Rotational Resonance Spectroscopy (DARR)*

Fig. 2.3 presents the pictorial representation of the pulse sequence a 2D $^{13}C…^{13}C$ DARR experiment [120]. The DARR pulse sequence has four parts: preparation of magnetization, evolution of spins, mixing period, where spins are allowed to interact with each other and exchange information and finally an acquisition period [105,123,124].

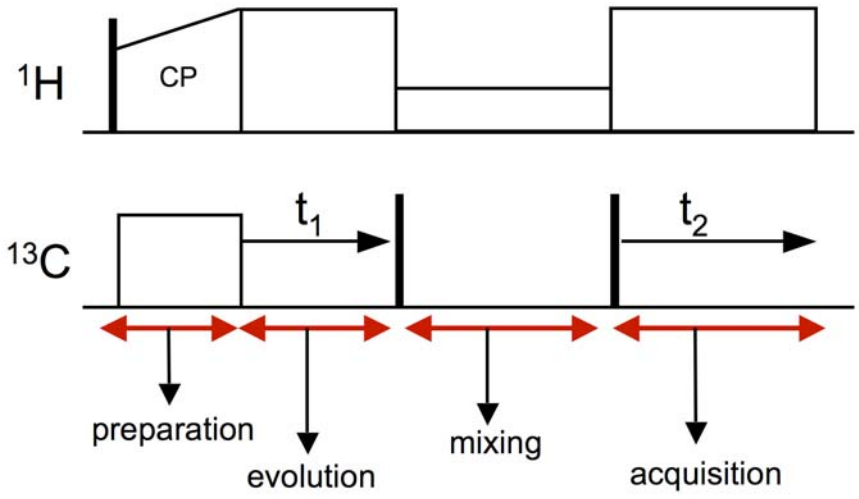


**Figure 2.3: A schematic representation of the DARR pulse sequence.**

During preparation, $^{13}$C magnetization is generated using variable amplitude cross polarization (VACP) [115] from the abundant $^{1}$H nuclei. In the 1D CP experiment the preparation of magnetization is immediately followed by acquisition on the $^{13}$C channel with a high power decoupling on $^{1}$H during acquisition (Fig. 2.3). Application of decoupling helps in increasing the resolution of the final NMR spectrum by averaging the strong heteronuclear dipolar couplings between $^{1}$H and $^{13}$C nuclei. During acquisition, the $^{13}$C spins are allowed to precess in the transverse plane about the static magnetic field. This precession induces an oscillating current in the RF coil in the probe that exponentially decays with a time. This is known as free induction decay (FID). It is detected, amplified and digitized by the spectrometer.

In a 2D DARR experiment, preparation is followed by the evolution period, where the $^{13}$C spins evolve only under their own chemical shift. A high power decoupling is employed during the evolution period on the $^{1}$H channel. This is done to assure that

frequency evolution of $^{13}C$ spins depends on their chemical shifts (i.e. the only prevalent interaction is chemical shift not dipolar couplings) and is not influenced by the strong dipole-dipole interactions between $^{1}H$ and $^{13}C$ nuclei. The length of the evolution time is denoted by "$t_1$" and is of the order of milliseconds.

The evolution time is followed by the mixing period. During which the dipolar coupling between $^{13}C$ nuclei are selectively reintroduced [120]. At the beginning of the mixing period a 90° pulse is applied to the $^{13}C$ channel to restore the $^{13}C$ magnetization back along the z-axis for the rest of the mixing period. There is no irradiation of $^{13}C$ during the mixing time but a low power constant wave (cw) recoupling pulse is applied to the $^{1}H$ channel. The strengths of the recoupling pulse satisfy the rotary resonance condition, $\omega_1=n\omega_r$ (n=1 or 2) [120]. DARR uses a combination of rotor driven and $^{1}H$-driven polarization transfer mechanisms [120]. Therefore, during mixing the $^{13}C$ resonance lines are broadened by recoupling of $^{1}H$ to $^{13}C$ and $^{1}H$ to $^{1}H$. And magnetization is exchanged between the dipolar broadened pattern of one $^{13}C$ spin with the spinning side band of the other $^{13}C$ spin [120] and vise versa. As exchange of magnetization during mixing period is done between $^{13}C$ nuclei along the z-axis, DARR pulse sequence does not suffer from signal decay due to dephasing of $^{13}C$ magnetization in the transverse plane during the mixing period and therefore allow the use of longer mixing times. Mixing time are usually of the order of 10-100 ms. The exact length depends on the extent of spin diffusion desired. Based of a series on studies on model compounds and selectively $^{13}C$ labeled rhodopsin samples, we have previously determined that a mixing time of 600 ms is sufficient for observing weak dipolar couplings between $^{13}C$ nuclei separated by $\leq 6.0$ Å in space [122]. The dipolarly coupled between 13C nuclei close together in space give rise to crosspeaks in the 2D DARR spectrum.

The mixing period is followed by acquisition time "$t_2$". High power decoupling is applied on the $^{1}H$ channel during the entire length of the acquisition time to enhance the resolution of the peaks observed in the NMR spectrum.

To obtain a 2D experiment, a series of 1D experiments (rows) are collected as the length of the evolution time "$t_1$" is sequentially incremented. The signal collected during each acquisition "$t_2$" is being modulated by $\sin(\omega t_1)$, where $\omega$ is the Larmor procession frequency. Fourier transform of the oscillating signal acquired during $t_2$ (acqusition) of each generates the direct dimension of the 2D spectrum. And a second Fourier transform of the rows obtained by incrementing $t_1$ gives the second dimenson of the 2D $^{13}C\ldots^{13}C$ DARR spectrum.

All solid-state NMR experiments described below were performed on 7-10 mgs of $^{13}C$-labeled rhodopsin sample at 14.1 T (600 MHz $^{1}H$ frequency) on a Bruker AVANCE spectrometer using 4 mm magic angle spinning (MAS) probes as previously described [65]. 1D $^{13}C$ NMR spectra were collected at MAS spinning rates between 8 and 12 KHz using ramped amplitude cross polarization [125] with contact times of 2 ms in all experiments.

2D $^{13}C$ DARR NMR measurements [120] were performed with 1024 points in the direct (f2) dimension and 64 points in the indirect (f1) dimension as described previously [65]. A DARR mixing time of 600 ms was used to maximize homonuclear recoupling [122]. The $^{1}H$ radiofrequency field strength during the mixing period was matched to the MAS speed for each sample, satisfying the n=1 matching condition. Two-pulse phase-modulated proton decoupling [111] or SPINAL64 proton decoupling [112] were used during the acquisition and evolution periods. The decoupling field strengths were typically 80-90 kHz. In order to obtain the observed signal-to-noise ratios for each data set discussed below, a 2D spectrum typically required a week of signal averaging, which is approximately equal to 5K scans for each of the 64 rows in the f1 dimension of the 2D spectrum. The carbonyl resonance of powered glycine at 176.02 ppm relative to TMS was used as an external $^{13}C$ reference. All experiments were conducted at -80°C.

In a DARR NMR spectrum, the peaks at the isotropic chemical shifts of all the $^{13}C$ labels in our sample are seen along the diagonal of the 2D plot (see Fig. 2.4). The dipolar couplings between the $^{13}C$ nuclei that are $\leq$ 6 Å apart are seen as off diagonal crosspeaks in the 2D DARR plot (see Fig. 2.4). Based on series on DARR measurements conducted on model compounds we can qualitatively correlate the intensity of the crosspeak to a range of separation between the two $^{13}C$ labels close together in space. A strong crosspeak is typically observed for $^{13}C\ldots{}^{13}C$ distances of 4.5 Å or less, a weak crosspeak is observed for distances between 4.5 and 6.0 Å. Typically, we do not observe crosspeaks for distances greater than 6.0 Å.

In order to get structural information on rhodopsin and meta II we incorporate $^{13}C$ labels in the retinal and the protein. We then obtain distance correlations between these labels in the inactive state and then repeat the measurements on the active intermediate to characterize how these distances change in meta II (Fig. 2.5) by comparing the intensities of the crosspeaks obtained between different $^{13}C$ labels in rhodopsin and meta II.

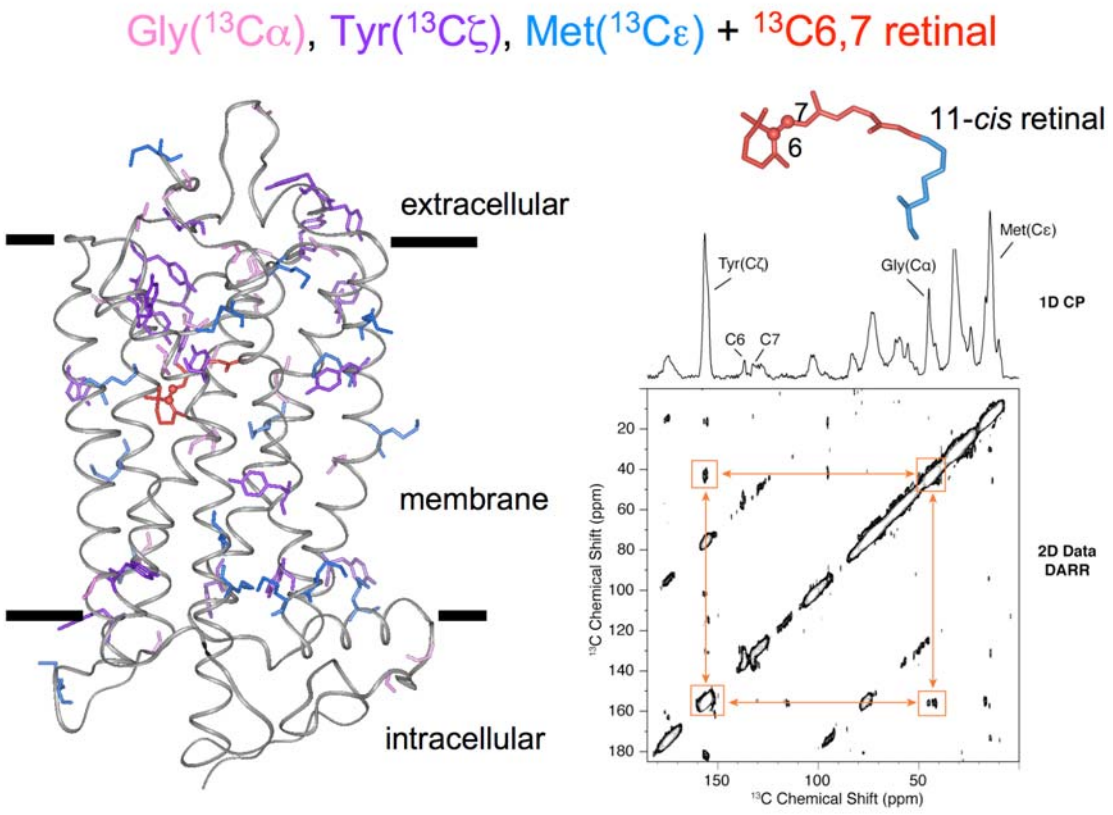


**Figure 2.4: An example of a 2D DARR NMR data on rhodopsin**. Rhodopsin was selectively $^{13}$C labeled at all the Gly(Cα), Tyr(Cζ) and Met(Cε). This sample was regenerated with 11-*cis* retinal, which was chemically synthesized with $^{13}$C labels incorporated at the C6 and C7 carbons on the polyene chain. 1D CP and 2D DARR NMR data were collected on this sample (~10 mgs) on a 600MHz Bruker spectrometer at a sample temperature of 190K. Peaks along the diagonal are at the isotropic chemical shift of all $^{13}$C labels in our sample (as shown in the 1D CP spectra). The off-diagonal crosspeaks (as highlighted in the boxed region; orange) in this example represent the strength of the dipolar coupling between a $^{13}$Cζ-Tyr and a $^{13}$Cα-Gly. On the right is a view of the crystal structure of rhodopsin [31] highlighting the location of all the $^{13}$C labeled amino acids in this sample.

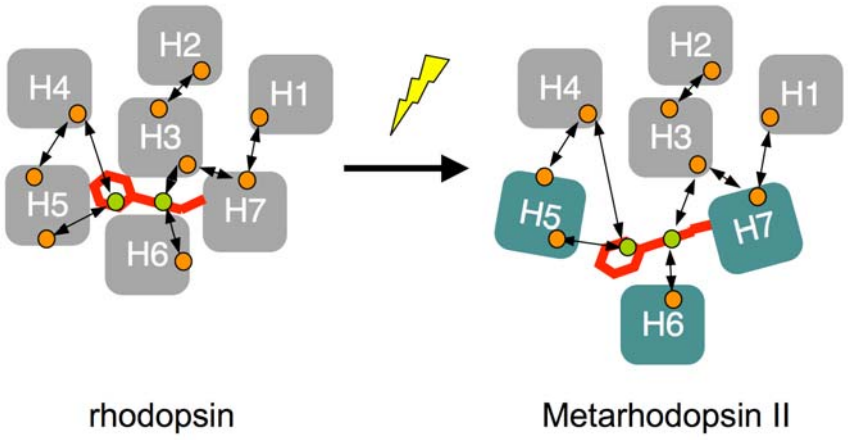


**Figure 2.5: The plan of action.** Orange filled circles represent isotopic ($^{13}C$, $^{15}N$) labels on the protein and green filled circles represent isotopic ($^{13}C$) labels on the retinal.

## *2.6 Trapping of the metarhodopsin II intermediate in n-dodecyl-β-d-maltoside micelles.*

Upon light activation of rhodopsin, the active meta II intermediate is formed within milliseconds in rod outer segment (ROS) membranes and decays with a half-time of ~10 min at pH 6.0 and 20°C [126]. Lowering the temperature to -80°C blocks the decay of the meta II intermediate; this is essential for long periods of data acquisition required for the 2D NMR experiments. However, in ROS or model membranes one typically obtains a mixture of meta I and meta II after photoreaction of the retinal and low temperature trapping. In order to quantitatively (>85%) trap the sample in the meta II intermediate, we solubilized rhodopsin in DDM detergent.

Rhodopsin samples were irradiated for 45 – 60 sec at room temperature in the 4 mm NMR rotor using a 400 W lamp equipped with a > 495 nm high pass filter. Following illumination and immediately put in the NMR probe with the probe stator

warmed to 5°C. Under slow spinning (~2 KHz) the sample was frozen within 3 min of illumination using $N_2$ gas cooled to –80°C [100].

To confirm that we have trapped meta II and completely converted the sample from rhodopsin and meta I, we monitor the chemical shift changes of the $^{13}C$ labels of the retinal that are sensitive to the protonation state of the Schiff base nitrogen and the configuration of the C11=C12 double bond. Meta II is the only intermediate with an all-*trans* retinal and an unprotonated Schiff base. We observe no residual rhodopsin or meta I after illumination, and typically are able to trap > 85% of our original sample in the meta II state based on integration of the retinal $^{13}C$ resonances in rhodopsin and meta II [100] (see Fig. 3.8).

The linewidths of the resolved protein and retinal NMR resonances are generally between 1 and 2 ppm in both rhodopsin and meta II. The absence of line broadening or resonance splitting indicates we have trapped a spectroscopically well-defined meta II state. In particular, MD simulations and $^{2}H$ NMR measurements on rhodopsin have suggested that there are two major conformations of the β-ionone ring, one with a positively twisted C6-C7 single bond and one with a negatively twisted C6-C7 single bond [127,128]. As described below in Chapter 3 and 5, $^{13}C$ chemical shift and DARR NMR measurements suggest only a single conformation exists in rhodopsin and in meta II.

Meta II in DDM has been found to be functionally equivalent to meta II in ROS membranes as it can activate transducin [73,129]. Also, it has been shown that the vibrational frequencies observed in FTIR difference spectrum of meta II minus rhodopsin are identical for rhodopsin in DDM or ROS membranes [63,130]. As a result, the detergent-stabilized meta II structure captures the critically important conformational features of the activated receptor.

The half mean time for proton uptake of meta II in DDM is 25 ms [131]. As mentioned above the time between illumination and freezing of the sample is approximately 3 min. Therefore, we can assume that the proton uptake in our sample is complete and we are observing the form of meta II that activates transducin. Thus, we have trapped a well-defined intermediate between meta I and opsin containing a retinal chromophore whose structure is characteristic of meta II and whose protein vibrations are the same as in meta II trapped in ROS membranes.

## *2.7 Trapping of the metarhodopsin I intermediate in digitonin micelles*

As mentioned above, in ROS or model membranes one typically obtains a mixture of meta I and meta II after photoreaction of the retinal and low temperature trapping. In native ROS membranes, an equilibrium is known to exist between the meta II and the inactive meta I (absorption maximum, $\lambda_{max}$ = 480 nm) intermediate that is characterized by an all-*trans* retinal and protonated SB [132-134]. In DDM micelles, we (as shown by shift in retinal $^{13}C$ NMR resonances upon activation) and others [135] observe a complete conversion of rhodopsin to meta II. The SB deprotonation is complete in DDM micelles. And therefore to quantitatively (> 85%) trap the sample in the inactive meta I intermediate, we solubilized rhodopsin in digitonin micelles at pH 7.0. Studies have shown that digitonin helps stabilize rhodopsin in the inactive meta I intermediate [136].

Digitonin micelles containing rhodopsin were equilibrated at 4° C for an hour before illumination on ice. Samples were irradiated for 45 – 60 sec at room temperature in the 4 mm NMR rotor using a 400 W lamp equipped with a > 495 nm band pass filter. Following illumination the sample was immediately put in the NMR probe with the probe stator warmed to 5°C. Under slow spinning (~2 kHz) the sample was frozen within 5 min of illumination using $N_2$ gas cooled to –80°C. The UV-visible spectra collected on the rhodopsin samples solubilized in digitonin before and after illumination at 4°C shows

a shift in the absorption maxima from 500 nm for rhodopsin to 480 nm for meta I. We did not see any absorption peak at 380 nm (corresponding to meta II) indicating a complete conversion to meta I without any contamination from meta II. In digitonin micelles, meta I is stable for almost an hour at 4°C.

# Chapter 3

## Structure and photoreaction of the retinylidene chromophore

Activation of rhodopsin is initiated by photoisomerization of its 11-*cis* retinal chromophore. The retinal is covalently bound to Lys296 through a protonated Schiff base (PSB) and is tightly packed within the bundle of helices (Figs. 3.1A and B). The retinal binding site is restricted along the axis of the retinal polyene chain by transmembrane helices H5 and H7, and is enclosed on the extracellular side of the dark, inactive state of rhodopsin by the second extracellular (or intradiscal) loop (EL2). The retinal binding site in the inactive state of rhodopsin can accommodate the 7-*cis*, 9-*cis* and 11-*cis* isomers of retinal, but not the longer all-*trans* or 13-*cis* isomers (Fig. 3.2) [137].

According to the crystal structure of rhodopsin [31] there are 35 amino acids within 6 Å of the retinal in its binding pocket (see Fig. 3.1A). The space-filling model in Fig. 3.1B, where spheres represent the van der Waals radii of the retinal and the amino acids surrounding it in its binding site, highlights how tightly the retinal is packed in its binding pocket. Therefore, one can appreciate that within this restricted space, the rapid 11-*cis* to -*trans* isomerization results in a highly strained retinal that induce significant perturbations in the surrounding protein. However, the question of how the absorbed light energy leads to structural changes

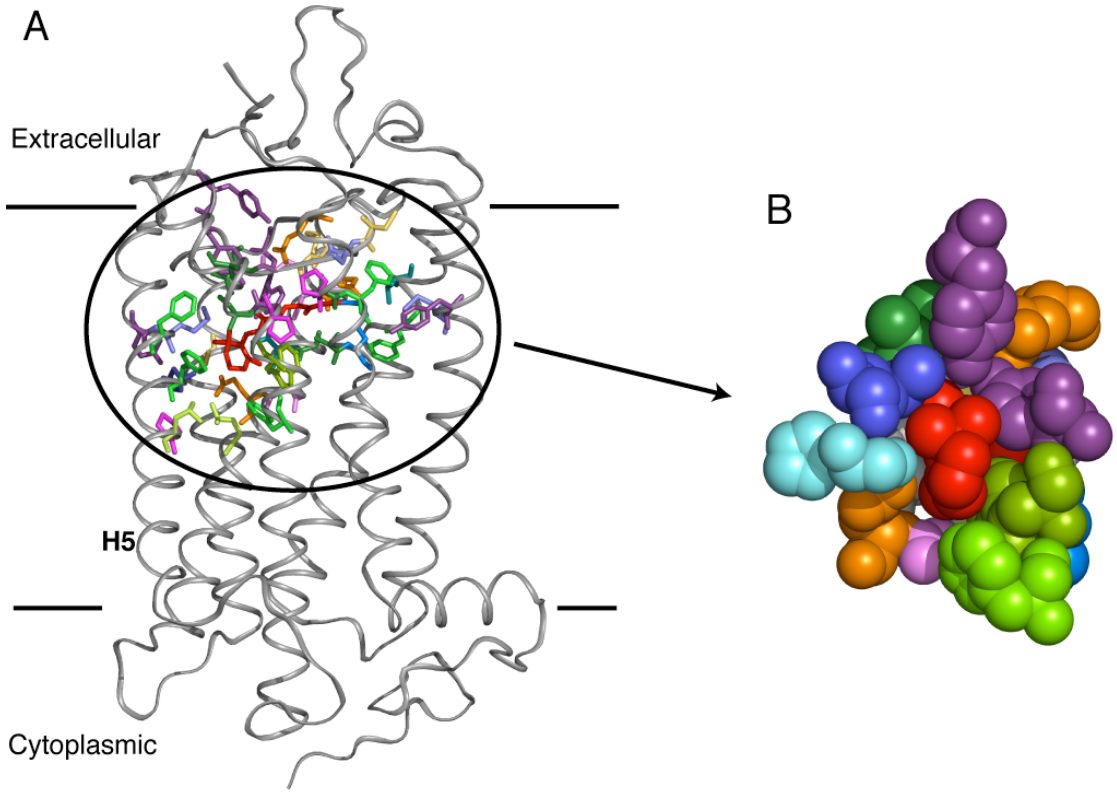


**Figure 3.1:** (A) A view from the rhodopsin crystal structure [31] highlighting most of the amino acids that are within 6 Å of the retinal (red) in its binding pocket. (B) The atoms comprising the amino acids surrounding the retinal are presented as spheres at their van der waals radii in order to appreciate the tight packing of retinal in its binding site.

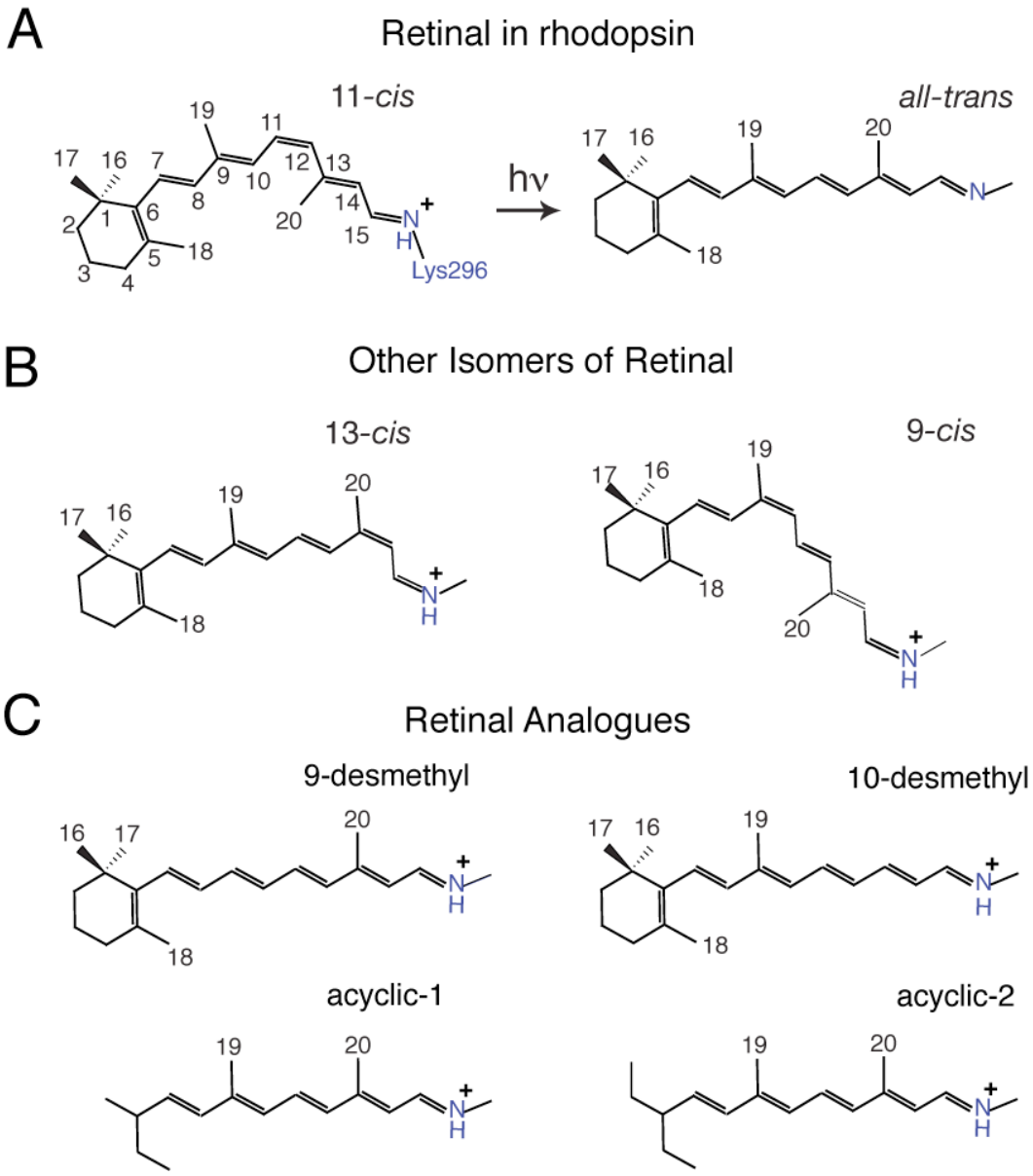


**Figure 3.2: Different isomers and analogues of retinal.** (A) Structures of the 11-*cis* and all-*trans* retinal chromophores in rhodopsin. (B) 13-*cis* and 9-*cis* isomers of retinal. (C) Analogues of retinal used in a number of studies [138,139]. 9-desmethyl and 10-desmethyl retinal shifts the meta I/meta II equilibrium toward meta I and behaves like partial agonists. Acyclic retinal generated by partial deletion of the β-ionone ring leads to reduced formation of meta II with a fast decay rate.

within the rhodopsin protein has not been fully answered since Hubbard and Wald first established that the retinal undergoes a large conformational change upon light absorption [140].

## *3.1 Photoreaction of 11-cis retinal in rhodopsin*

In rhodopsin, the chromophore has an absorption maximum ($\lambda_{max}$) around 500 nm. Upon absorption of a photon of light, the twisted 11-*cis* form of the chromophore in its binding cavity isomerizes to the all-*trans* conformation accompanied by distinct conformational changes in the surrounding receptor. The salt bridge between retinal PSB and Glu113 (H3) side chain is broken upon *metarhodopsin II* formation. Similar interactions have been shown to be important for ligand binding in other class A GPCRs, e.g., for the β2-adrenergic receptor a metal binding site engineered between an Asp residue on H3 and a residue on H7, one helical turn above Lys296 (H7) in rhodopsin, enabled activation by binding of the metal ions $Zn^{2+}$ and $Cu^{2+}$ instead of the catecholamines [141].

The photoisomerisation of retinal occurs within the first 200 femtoseconds upon absorption of a photon of light to form the first photointermediate, *photorhodopsin* at room temperature. It is one of the fastest reactions known [35] with a high quantum yield of ~0.67 [36,37], as compared with ~0.2 of the protonated retinylidene Schiff base in organic solvent. It is predicted that the constrained nature of the 11-*cis* retinal in its binding site and its multiple interactions with the surrounding protein are responsible for its exquisite sensitivity and high quantum yield.

*Photorhodopsin* decays within picoseconds to form *bathorhodopsin* ($\lambda_{max}$ = 550 nm) that stores about 35 kcal/mol of photon energy, as an increase in enthalpy [142], required for formation of subsequent photointermediates (see Fig. 3.3). The X-ray crystallographic data collected on *bathorhodopsin* trapped at cryogenic temperatures revealed a highly distorted all-*trans* retinal [90]. The crystal structure and other biophysical studies such as

ssNMR [143] and resonance Raman spectroscopy [144] demonstrated that the primary distortions were restricted to the chromophore. Resonance Raman spectra of bathorhodopsin exhibit intense hydrogen out-of-plane modes indicating that the retinal is conformationally distorted [145] due to the rapid change in chromophore structure from 11-*cis* to all-*trans* within a tight binding site. The protein environment surrounding the chromophore did not change significantly upon *bathorhodopsin* formation.

*Bathorhodopsin* decays to form the *blue-shifted intermediate (BSI)* with a $\lambda_{max}$ of 543 nm followed by formation of *lumirhodopsin* ($\lambda_{max}$ = 497 nm) and *metarhodopsin I* ($\lambda_{max}$ = 480 nm). A recent 2.8 Å resolution crystal structure determined for *lumirhodopsin* clearly demonstrates the formation of a nearly complete, more relaxed all-*trans* form of retinal with limited structural changes in the protein surrounding the chromophore. The structure shows a rearrangement of the protein in the middle of H3 [89].

No high-resolution crystal structures are available for *metarhodopsin I (meta I)*. However, a 2D electron microscopic study on meta I showed no significant rigid-body motion of helices as compared to the ground state of rhodopsin [146]. *Meta I* exists in a pH and temperature dependent equilibrium with the active intermediate *metarhodopsin II (meta II)* [133]. Meta II is characterized by an all-*trans*-retinal and a deprotonated Schiff which catalyzes guanine nucleotide exchange by the rod cell heterotrimeric G protein, transducin. It was observed that binding of the G-protein, transducin shifts the meta I/meta II equilibrium more towards the active, meta II state [147]. Deprotonation causes the absorption ($\lambda_{max}$) to shift from 480 nm for meta I to 380 nm for meta II. Photoisomerisation to the all-*trans* conformation of the retinal is analogous to agonist binding in other GPCRs.

As shown in Fig. 3.4 [148,149], the photoreaction of rhodopsin is divided into 3 main phases: (1) 11-*cis* to all-*trans*

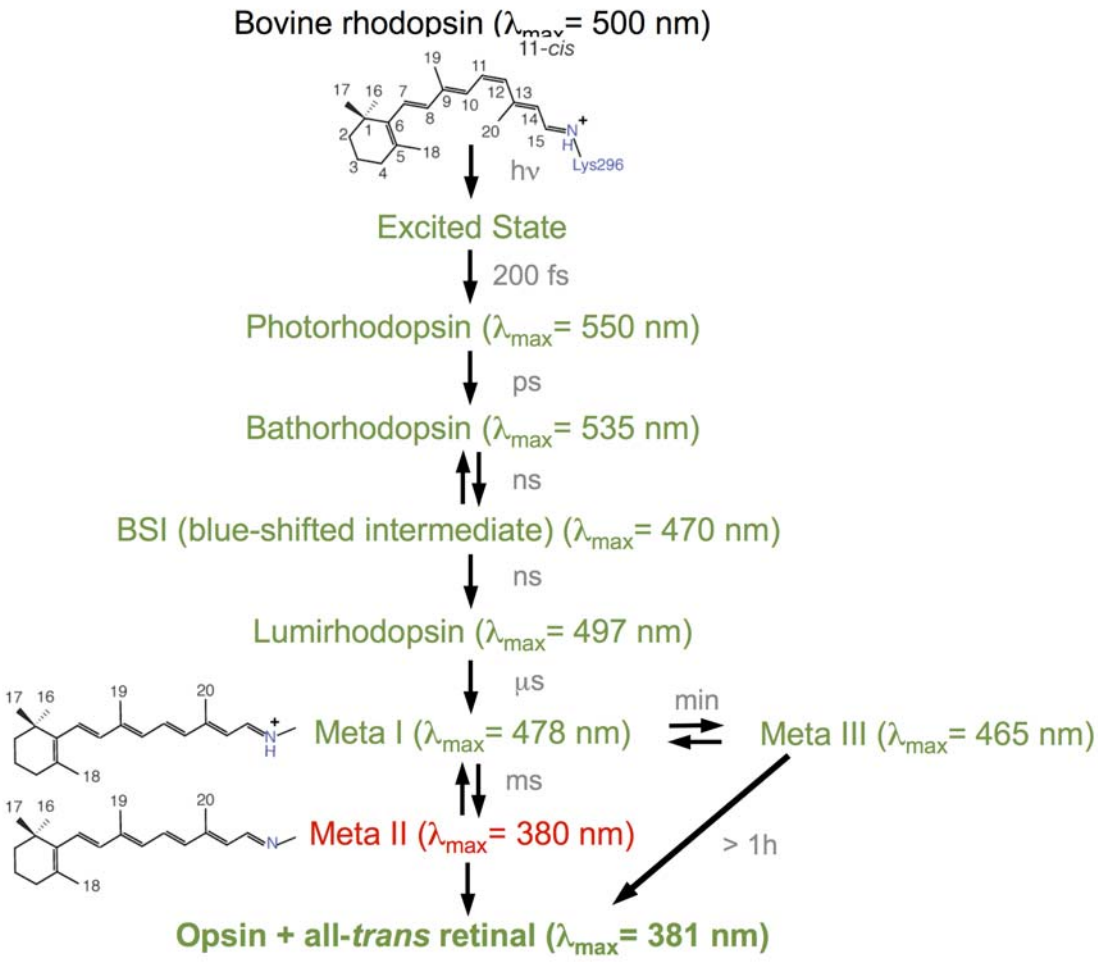


**Figure 3.3: Rhodopsin photoreaction**. Upon absorption of a photon of light the 11-cis retinal chromophore in vertebrate (bovine) rhodopsin (black) isomerizes to an all-trans form within the first 200 fs [150]. Following isomerization, the photoproduct relaxes through a series of spectrally well-characterized photointermediates with defined absorption maxima and life times [151]. Meta II is the active form of rhodopsin that binds and activates the G-protein, transducin.

isomerization of retinal chromophore upon absorption of a photon leading to formation of *bathorhodopsin*; (2) Thermal relaxation of the retinal-protein complex from *bathorhodopsin* to meta I and (3) a G-protein dependent equilibrium between meta I and meta II. Thermodynamic studies [133,152] have shown that following isomerization, the relaxation of *bathorhodopsin* to *lumirhodopsin* and *meta I* occurs with a decrease in enthalpy and entropy. Whereas formation of meta II following meta I, happens with an increase in the enthalpy of the system. Therefore, for the photoreaction to proceed to the active state of the receptor the entropy of the system has to increase. The transition to meta II is accompanied by loss of stabilizing interactions and an increase in flexibility of the receptor that might be responsible for an increase in the entropy of the system.

As mentioned above, *metarhodopsin II* is characterized by deprotonation of the Schiff base linkage between the retinal chromophore and Lys296 on H7 [153]. Glu113 on H3 takes up the proton. Deprotonation of the Schiff base (SB) ruptures the stabilizing salt bridge interaction with Glu113 [54]. Breaking of this salt bridge is considered obligatory for the activation of rhodopsin [154]. Besides proton transfer within the receptor, formation of meta II is also linked to proton uptake by the protein from the aqueous phase [131]. Formation of meta II increases the pH of the aqueous medium indicating that its formation must accompany proton uptake from the milieu. Also, formation of meta II is favored at acidic pH [155].

However, according to Anis and Hoffmann [131], the proton uptake from the aqueous phase happens after the translocation of the internal proton. They were able to kinetically isolate the two isochromic forms of meta II (meta $II_a$ and meta $II_b$), by solubilizing the protein in flexible detergent, DDM. Transfer of a proton from the Schiff base to the counterion (Glu113 on H3) leads to formation of the photoproduct designated as meta $II_a$ ($MII_a$). Its formation can be tracked by the blue shift of the UV/Vis absorption

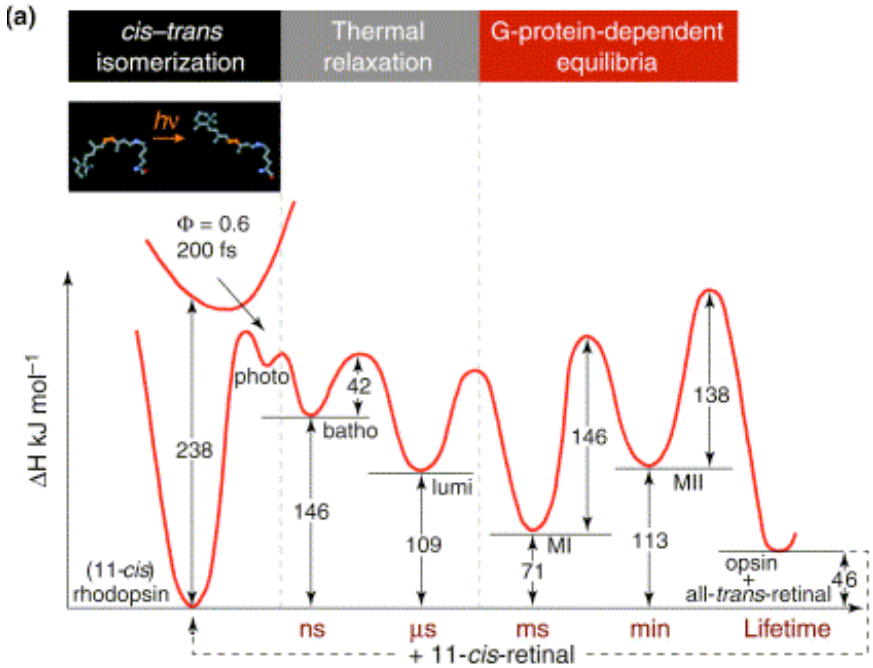


**Figure 3.4: Reaction coordinates of rhodopsin activation suggested by Okada *et al.*** [148]. Following phtotoexcitation retinal in rhodopsin isomerizes to form photorhodopsin that thermally decays within milliseconds to a G-protein dependent equilibrium between meta I and meta II. The figure presents the enthalpies and activation enthalpies of rhodopsin and its photointermediates. Interestingly an increase in enthalpy is observed in meta I to meta II transition.

maxima from 500 nm to 380 nm. It is an endothermic reaction with an activation energy, $E_a$ = 160 KJ/mol and is an entropy driven process [131]. Its formation depends on the hydrophobic nature of the medium surrounding the protein (i.e. membrane or detergent).

Subsequently, the fully active state meta $II_b$ ($MII_b$) state is formed upon proton uptake from the aqueous phase [131]. This is a slightly exothermic reaction with an $E_a$ = 60 kJ/mol [131]. According to a series of FTIR [67,156] and EPR [157] studies on mutants of rhodopsin, the most likely candidate for proton uptake is Glu134 of the highly conserved (E/D)RY motif at the cytoplasmic end of H3. Kinetic studies conducted on rhodopsin solubilized in DDM at pH 7 [131] suggest that formation of the active meta II intermediate from meta I is a two-step process where the proton transfer from the Schiff base and proton uptake by ERY happens as two separate consecutive events where the half-life of $MII_a$ ($\tau(MII_a)$=7 ms) is an order of magnitude faster than proton uptake from the aqueous phase ($\tau(MII_b)$=25 ms) that titrates with a pKa of 6.75.

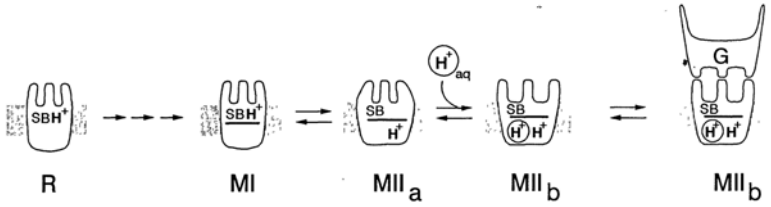


**Figure 3.5: A cartoon representation of the formation of the active state of rhodopsin suggested by Arnis *et al.* [131].** Upon illumination the earlier intermediates give way to meta I, represented by a PSB followed by meta $II_a$ ($MII_a$), represented by a deprotonated SB and a change in the free volume in the hydrophobic core of the protein (depicted as a change in the shape). $MII_a$ leads to the formation of meta $II_b$ ($MII_b$), where a proton is taken up by the protein from the milieu and it undergoes additional conformational rearrangement required for G-protein binding and activation.

This reaction scheme was recently extended by time resolved EPR studies conducted on rhodopsin that was solubilized in detergent, DDM [158]. They proposed that

deprotonation of the Schiff base ($MII_a$) is followed by conformational changes in the protein as seen by the movement of the cytoplasmic end of TM helix H6 ($MII_b$), which in turn is followed by proton uptake from the milieu ($MII_bH^+$). The reaction scheme is represented in the figure below:


**Figure 3.6: Reaction scheme for formation of the active intermediate of rhodopsin as suggested by Hubbell and coworkers [158].**

Kinetic data collected by Hubbell and co-workers [158] showed that at 30°C and neutral pH, deprotonation of the Schiff base (as followed by the rise in absorption at 380 nm) is an order of magnitude faster than movement of TM helix H6 (as seen by changes in EPR spectrum of the nitroxide spin labels incorporated at the cytoplasmic ends of TM helix H5 (Val227) and H6 (Val250)) and has a higher activation energy. However, motion of TM H6 and proton uptake from the solution happens on the same time scale.

However, this does not tell us whether motion of H6 is a cause or consequence of proton uptake from solution. In order to resolve this issue, Hubbell and co-workers [158] collected pH dependent EPR and UV-Vis data. They observed that the extent of deprotonation of the Schiff base and motion of H6 stayed almost independent of the pH change from pH 5.0 to pH 8.0. However, the proton uptake signal titrated with a pKa of 6.5. For example, at pH greater than 7.0, where proton uptake is essentially inhibited, they observed a motion of TM H6. This proves that proton uptake from solution is a consequence of H6 motion. Movement of H6 exposes the charged residues on the cytoplasmic side of rhodopsin that ultimately leads to proton uptake from solution.

Eventually, meta II decays to *opsin* and free all-*trans* retinal. The Schiff base linkage between the retinal chromophore and Lys296 is hydrolysed. Removal of the all-*trans* retinal from the protein is necessary for regeneration with fresh 11-*cis* retinal to form rhodopsin. In the absence of all-*trans* retinal chromophore, *opsin* exhibits very low levels of transducin activity, ~$10^{-6}$ times the activity of meta II [159]. However, FTIR studies have shown that at very low pH *opsin* adopts a conformation very similar to the active meta II state [160].

Recently, Park *et al.* [68] presented a crystal structure of the ligand-free native *opsin* obtained from bovine retinal rod cells at 2.9 Å resolution. The crystal structure for *opsin* shows significant structural changes in the apoprotein as compared to rhodopsin. A rearrangement of interactions is observed involving the conserved ERY sequence at the cytoplasmic end of TM helix H3 and the NPxxY motif of helix H7. Significant movement is also observed of TM helices H5, H6 and H7, particularly the cytoplasmic end of H6 that tilts outwards by 6-7 Å. The authors predict that some of these features are representative of the active state meta II. The *opsin* crystal structure [68] also discloses two openings in the retinal binding pocket that might serve as the entry/exit point for the retinal chromophore.

The decay of meta II to *opsin* also involves a parallel pathway that leads to formation of another intermediate known as *metarhodopsin III*, considered as the retinal storage form of the receptor [126]. It is an inactive intermediate characterized by an intact Schiff base that is protonated and has an absorption maxima at $\lambda_{max}$ = 470 nm. However, the retinal binding site becomes more accessible to hydroxylamine in meta III, leading to hydrolysis of the PSB to form *opsin* and retinal [161]. Formation of meta III is observed under more alkaline conditions in parallel to hydrolysis. For example at pH 8.0, 30% of the decay product is meta III [161]. Meta III can be illuminated to form a species that absorbs at 380 nm and is likely to be identical to meta II [126,162]. In the long term, meta III decays to opsin and free all-*trans* retinal by hydrolysis of the Schiff base.

Recent FTIR studies have provided evidence that meta III might also arise from thermal decay of meta I. During the formation of meta III, the retinal thermally isomerizes about the Schiff base C=N double bond from an 15-*anti* conformation in meta I/meta II to a 15-*syn* geometry in meta III [161,163]. Meta III is known as the retinal storage form because it keeps a fraction of the photoisomerized chromophore away from the regeneration pathway in which the all-*trans* retinal is released from the protein [164]. Thus, retinal remains bound to its original binding site. Interestingly, in isolated membranes, devoid of any other regulatory proteins, meta III remains stable for hours (e.g. $t_{1/2}$=100 mins at pH 7.3 and 30°C [126,164] ). On the other hand, it is formed only transiently *in situ*. It decays within minutes and returns to the normal regeneration pathway [164]. This apparent conflict was solved by a study conducted by Hofmann and co-workers, using a series of fluorescence, UV-Visible and FTIR spectroscopic techniques [164]. They observed that the presence of the G-protein, transducin in the native membranes, triggers the decay of meta III. The interaction between transducin and meta III induces the transition of meta III to meta II facilitating the hydrolysis of the Schiff base linkage. This allows the all-*trans* retinal to be released back into the normal regeneration pathway. Thus, the G-protein plays a significant role in the metabolism of retinal [164].

## *3.2 Physico-chemical properties of the retinal chromophore in rhodopsin*

In rhodopsin, 11-*cis* retinal is tightly packed on the extracellular side of the receptor within the bundle of TM helices, covalently linked to the ε-carbon of Lys296 on H7 through a Schiff base that is protonated in the dark. A glutamate residue (Glu113) located on H3 acts as the counterion for the positively charged Schiff base linkage [54,165].

The absorption maximum ($\lambda_{max}$) of retinal protonated Schiff base (RPSB) in solution (e.g. all-*trans*-N-retinylidene-n-butylamine in $CHCl_3$) is about 460 nm [96,166,167]. In the protein it is red shifted to ~500 nm. This change in the absorption maximum of the retinal upon incorporation in the protein is known as the opsin-shift and is an indication of the effect of the binding cavity of the protein on the retinal conformation. This spectral tuning by opsin is even more pronounced in the three cone pigments responsible for trichromatic vision (color). For example, the $\lambda_{max}$ for the red cone pigment is 557 nm, the green cone pigment is 530 and the blue cone pigment is 425 nm [149].

The absorption maximum ($\lambda_{max}$) of the chromophore is modulated by a number of factors. (1) The protonation state of the retinal Schiff base has a dramatic influence on the $\lambda_{max}$. The retinal Schiff base in rhodopsin has a full positive charge. The conjugated nature of the polyene chain induces a partial delocalization of the positive charge throughout the π-electron system [168]. This induces a bathochromic (red) shift in $\lambda_{max}$. (2) Twists about single (C-C) induces a blue shift whereas twists double bonds (C=C) are also known to induce a red shift in the $\lambda_{max}$ [169-171]. Honig *et al.* demonstrated that changing the C6-C7 single bond torsion angle modulated the $\lambda_{max}$ of the retinal model compounds [168]. (3) Electrostatic interactions between the retinal and any polar or charged residues in the binding cavity [172,173] can induce a shift the $\lambda_{max}$. According to Sekharan *et al.* [174] the biggest contribution to the opsin shift comes from the interaction with the counterion (Glu113 on H3). The positively charged SB forms a salt bridge with Glu113 that modulates the $\lambda_{max}$. However, the presence of other polar or charged residues close to the retinal in the binding site contribute to increasing the charge delocalization along the polyene chain away from the SB. In the rhodopsin crystal structure [31], a charged residue, Glu181 on EL2, is interacting with the C12 carbon on the retinal. (4) Lastly, steric interaction within the protein can lead to distortions in the retinal structure that may effect the charge delocalization along the polyene chain and hence the $\lambda_{max}$ [174]. Therefore, any mechanism that would induce an increased delocalization of the positive charge between

the β-ionone ring and the SB and reduce bond alteration would contribute to the red shift of the absorption maximum ($\lambda_{max}$) [168].

Interestingly, a study conducted by Steinberg *et al* [175] suggested that the pKa of the PRSB in rhodopsin is higher than 16. The high pKa is apparently maintained by the interaction with the counterion, Glu113 on H3. Mutation of Glu113 to neutral glutamine dramatically reduced the pKa of the PSB from > 16 to 6, rendering it prone to deprotonation [54,165].

Upon absorption of a photon of light the retinal isomerizes to an all-*trans* conformation. The photoisomerisation of retinal occurs within the first 200 fs upon absorption of a photon of light to form the first photointermediate, *photorhodopsin* at room temperature. 11-*cis* retinal chromophore acts as an extremely efficient inverse agonist for rhodopsin. It has a very low thermal isomerization rate, once every 470 years at physiological temperatures [176]. Apparently, the low thermal isomerization rate of the retinal is due to the high pKa of the RPSB [177].

In the ground state (inactive) of rhodopsin, the retinal chromophore exists in a highly twisted 11-*cis* conformation. This has been demonstrated by the presence of hydrogen-out-of-plane (HOOP) modes in resonance Raman spectroscopy [172,178-180], FTIR spectroscopy [181] and circular-dichroism [182] studies. This twisted conformation of the 11-*cis* retinal and its multiple interactions with the surrounding protein are believed to be responsible for the efficient isomerization to the all-*trans* form.

Solid-state deuterium NMR spectroscopy of aligned samples of rhodopsin regenerated with deuterated retinal demonstrated a negative pre-twist of the retinal polyene chain about the C11=C12 double bond in rhodopsin [31,183] that relaxed considerably in the meta I intermediate in rhodopsin photoreaction (see section 3.1). Brown and co-workers [183], also observed that the β-ionone ring is twisted about the C6-

C7 single bond in rhodopsin and maintained its twisted conformation in the inactive, meta I intermediate. This was further corroborated by measurements of the carbon-carbon bond lengths and tortional angles in the polyene chain of the retinal chromophore in rhodopsin and meta I by double quantum solid-state NMR spectroscopy [184].

Therefore, the primary role of the protein environment is to stabilize the distorted conformation of the 11-*cis* retinal chromophore needed for the ultra fast transformation to an all-*trans* conformation. In the same way, that the interactions between the protein and the chromophore are important in determining the spectral properties of the retinal, studying the properties of the retinal can help us gain understanding of the binding cavity, where it resides and hence help us understand the changes that the protein undergoes on activation. Therefore, retinal is an important tool for mapping the binding cavity of the protein both in the inactive and active state of the protein.

Much less is known about the conformation of the retinal in the active state of rhodopsin, meta II, than in dark rhodopsin. The structure of a photoactivated intermediate of rhodopsin having an unprotonated Schiff base has been reported [185]. However, the low resolution in both the dark state and the photointermediate makes it difficult to establish how the chromophore or the receptor changes structure upon illumination. In contrast, solid-state NMR is well suited for structural studies that target specific regions of membrane proteins in native membrane environments. High-resolution magic angle spinning (MAS) NMR methods have been used to investigate ligand conformation in ligand-activated GPCRs, such as the histamine [186] and the neurotensin receptors [187], as well as the structure of the retinal-containing membrane proteins. For example, analysis of $^{13}C$ chemical shifts has previously been used to investigate the conformation of the retinal chromophore in bacteriorhodopsin [167,188] and rhodopsin [189-192].

In the sections below, I have explained how solid-state magic angle spinning NMR spectroscopy has been used to obtain the $^{13}C$ chemical shifts of the retinal chromophore and the $^{15}N$ chemical shift of the Schiff base nitrogen in rhodopsin and metarhodopsin II. The $^{13}C$ chemical shifts obtained of the eleven conjugated carbons along the retinal polyene chain (C5 - C15) and the five methyl carbons (C16, C17, C18, C19, C20) are sensitive to the conformation of the retinal and molecular interactions within the protein binding site.

I have also measured the $T_1$ relaxation time of the C18 methyl group on the β-ionone ring of the retinal in rhodopsin and metarhodopsin II using solid-state magic angle spinning (MAS) NMR to determine the conformation of the β-ionone ring of the retinal about C6-C7 single bond.

Comparison of the metarhodopsin II chemical shifts with those of retinal model compounds and the 11-*cis* retinal in rhodopsin suggests that the retinal is in a polar environment in metarhodopsin II with significant protein interactions near the β-ionone ring (C5, C17). Additionally, I show that the unusual chemical shift of the retinal C12 carbon in rhodopsin is due to its interaction with the charged Glu181 residue on EL2. This strong perturbation at C12 of the retinal due to Glu181 disappears in the E181Q mutant of rhodopsin and in metarhodopsin II.

## *3.3 Characterization of meta II trapped at low temperature in DDM detergent*

Meta II is the only intermediate in the rhodopsin photoreaction with an unprotonated Schiff base nitrogen. We first confirmed that the all-*trans* retinal chromophore in meta II trapped in DDM is bound to Lys296 through an unprotonated SB nitrogen, and that only a single intermediate is present in the NMR sample. $^{15}N\varepsilon$-lysine was incorporated into

rhodopsin, and the $^{15}$Nε chemical shifts were obtained of the 11-*cis* retinal PSB in rhodopsin and the all-*trans* unprotonated retinal SB in meta II using solid-state MAS NMR. In Fig. 3.7A, the $^{15}$Nε resonance for the PSB nitrogen in rhodopsin solubilized in DDM is observed at 156.8 ppm, identical to the chemical shift for rhodopsin reconstituted in DOPC [96]. In meta II (Fig. 3.7A), the $^{15}$Nε resonance shifts to 282.2 ppm. The resonances at ~10.0 ppm in rhodopsin and 8.1 ppm in meta II correspond to the other lysines in the protein. The natural abundance $^{15}$N signal from the amide nitrogens is observed as a broad resonance at ~95.0 ppm, and the intense peak at ~50 ppm results from $^{15}$N-labeling of arginine.

The large change in the $^{15}$N chemical shift of the SB in meta II is attributed to the deprotonation of the SB upon activation. In bacteriorhodopsin, two resolved M intermediates are observed with $^{15}$Nε chemical shifts of 288.6 ppm (Mn) and 296.4 ppm (Mo) [193]. In contrast, the all-*trans*-N-retinylidene-n-butylimine SB is observed at 315.3 ppm [194]. The upfield chemical shift of the M states relative to the model compound, as well as the upfield shift of Mn relative to Mo was attributed to stronger basicity/hydrogen bonding in the upfield shifted Schiff base [193]. The upfield shift in meta II relative to these forms suggests that the environment of meta II is more polar than in the M states of bacteriorhodopsin.

In rhodopsin, the $^{13}$Cε-Lys296 is observed at 49.1 ppm and on conversion to meta II shifts downfield to 60.8 ppm and overlaps the region of the $^{13}$Cβ-serine in the protein as seen in the difference spectra between rhodopsin and meta II in Fig. 3.7B. The 11.7 ppm shift in the $^{13}$Cε-Lys296 resonance between rhodopsin and meta II is again primarily due to deprotonation of the SB upon conversion to meta II. Rest of the free lysine residues in rhodopsin and meta II are observed as a broad peak around ~39.6 ppm. The $^{13}$Cε-Lys296 chemical shift is unique because it is the only lysine in the protein that forms a Schiff base with the retinal chromophore. These chemical shifts serve as good markers for the active intermediate of rhodopsin.

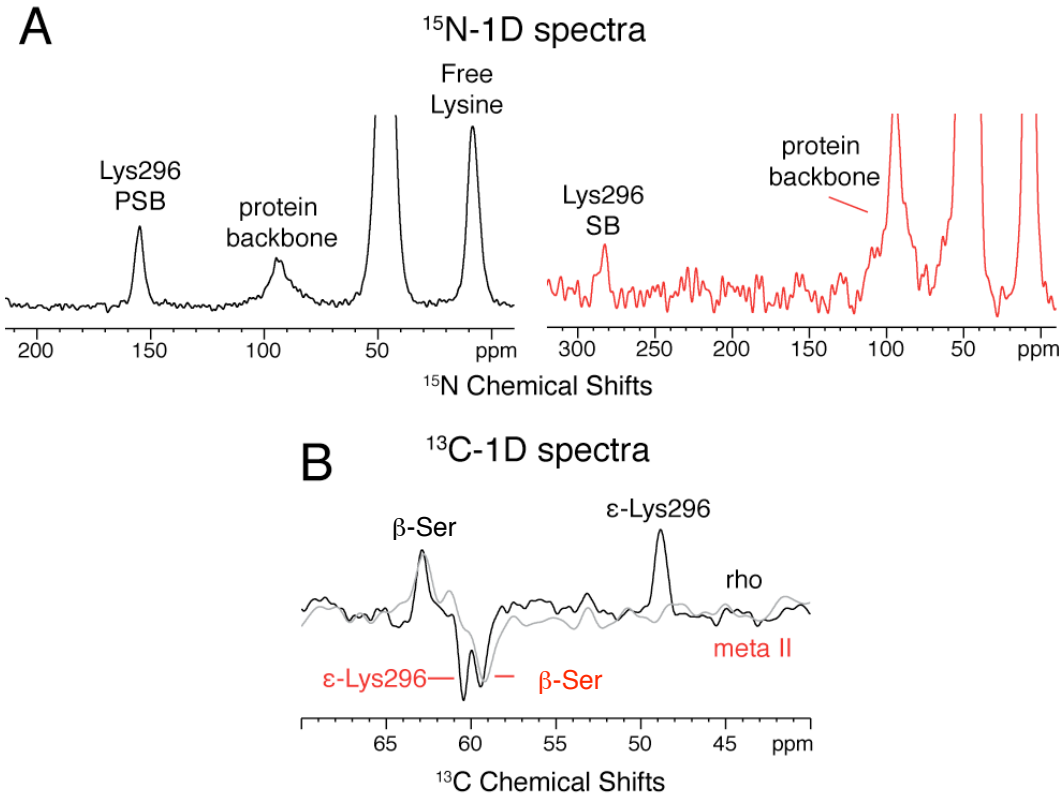


**Figure 3.7: $^{15}$N and $^{13}$C chemical shifts for Lys296 (H7) that is covalently linked to retinal.** (A) 1D $^{15}$N CP spectra of rhodopsin labeled at $^{15}$Nε-lysine. The $^{15}$Nε-Lys296 is observed as a distinct narrow peak at 156.8 ppm in rhodopsin (black) and it shifts ~125 ppm downfield to 282.2 ppm in meta II (red). The $^{15}$Nε resonance for the rest of the free lysines in rhodopsin is observed as a broad peak ~8.0 ppm. (B) 1D $^{13}$C difference spectra between rhodopsin (positive peaks) and meta II (negative peaks) labeled with $^{13}$Cε-lysine and $^{13}$Cβ-cyteine. The $^{13}$Cε-Lys296 is observed as a distinct peak at 49.1 ppm and on conversion to meta II shifts downfield to 60.8 ppm and overlaps the region of the $^{13}$Cβ-serine in the protein. The other negative peak around 59 ppm and the positive peak around 63 ppm belongs to $^{13}$Cβ-serine residue in meta II and rhodopsin respectively.

The $^{13}C$ chemical shifts of the retinal carbons along the polyene chain also provide a way to characterize the ability to trap a homogeneous meta II intermediate at low termperature. In this case, rhodopsin solubilized in DDM was regenerated with 11-*cis* retinal selectively $^{13}C$ labeled within the β-ionone ring and along the conjugated polyene chain. One-dimensional $^{1}H$-$^{13}C$ cross polarization (CP) MAS NMR experiments [65](as explained in the methods section; Chapter 2) were performed to obtain the chemical shifts of the retinal carbons in rhodopsin and meta II. Fig. 3.8 presents regions of the 1D $^{13}C$ MAS spectra for rhodopsin regenerated with retinal $^{13}C$ labeled at the C5, C8, C9 and C13 carbons along the polyene chain. The $^{13}C$ MAS spectra of rhodopsin (black) have been overlaid with the MAS spectra of meta II (red). The quaternary odd numbered carbons (C5, C9 and C13) with attached methyl groups exhibit the largest chemical shift changes of the retinal carbons.

The retinal C5 and C9 resonances are observed in rhodopsin at 131.0 ppm and 148.9 ppm, respectively, and shift to 126.0 and 139.6 ppm in the meta II intermediate. The broad resonance at 127.0 ppm is due to the natural abundance $^{13}C$ signal from the aromatic carbons in the protein. The $^{13}C$ resonance of C13 at 168.5 ppm in rhodopsin overlaps the broad natural abundance $^{13}C$ signal from carbonyls centered at ~175 ppm. A 20 ppm change in the $^{13}C13$ chemical shift to 148.2 ppm is observed in meta II. In contrast, the C8 resonance does not shift significantly between rhodopsin and meta II.

Integration of the $^{13}C$ resonances shows that we convert > 85% of rhodopsin to meta II. The retinal $^{13}C$ resonances are narrow (1.0-1.2 ppm) in both rhodopsin and meta II, exhibiting no signs of splitting or differential broadening. The chemical shifts are reproducible to within 0.3 ppm. For comparison, the histamine ligand bound to the H1 receptor exhibits broad $^{13}C$ resonances (4-8 ppm) suggesting conformational heterogeneity [187].

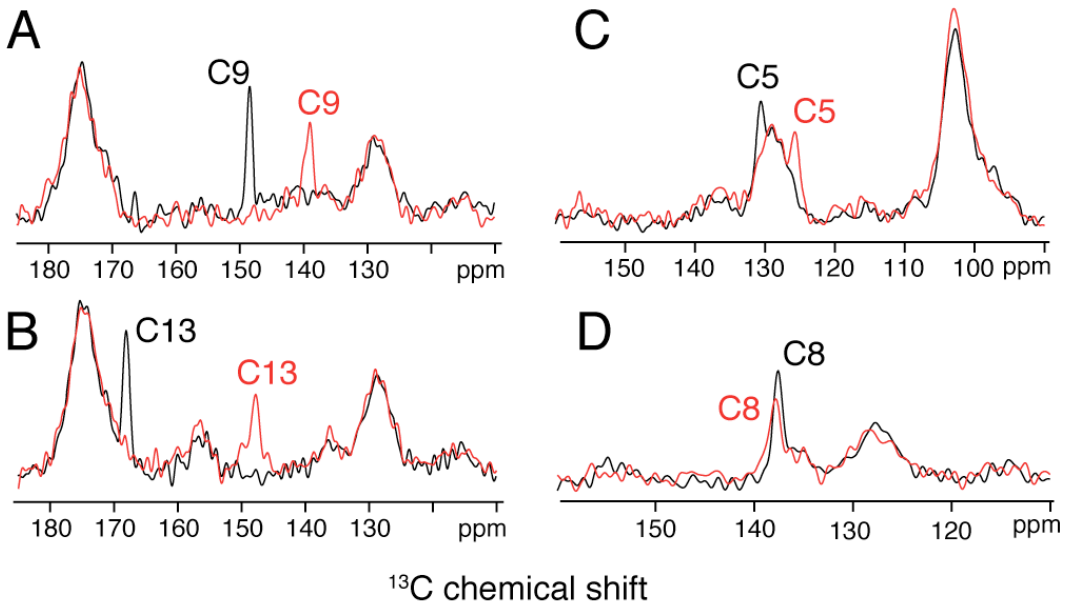


**Figure 3.8: Representative one-dimensional $^{13}$C MAS NMR spectra of the dark state of rhodopsin (black) and the active meta II intermediate (red) containing $^{13}$C-labeled retinal chromophores.** Regions of the $^{13}$C spectra from ~110-180 ppm are shown for rhodopsin and meta II containing retinal $^{13}$C-labeled at the C9 (A), C13 (B), C5 (C) and C8 (D) positions. The C5 resonance overlaps the natural abundance signal from the aromatics in the protein.

After decay of meta II to opsin and free retinal, the $^{13}C$ retinal resonances broaden considerably and are not observed. The origin of the broadening most likely results from heterogeneous interactions of the retinal with the protein and detergent after hydrolysis of the Schiff base linkage. Together these observations indicate that the conformational heterogeneity of the retinal in rhodopsin and meta II is similar and limited. Recently, A $^{13}C$ NMR study [187] conducted on another class A GPCR, $H_1$ receptor (Histamine receptor) bound to its Histamine ligand, showed that the binding cavity of the receptor was able to accommodate both charged (dicationic) and an uncharged (monocationic) form of the ligand. This is analogus to the equllibrium between the charged (PSB) meta I and the uncharged (SB) meta II form of the retinal in rhodopsin. They also observed very broad $^{13}C$, $^{15}N$ resonances for the ligand, both in 1D and 2D data sets suggesting conformational heterogeneity for the ligand in its bound state to the receptor as compared to the narrow signals (~1.0-1.2 ppm) observed for the retinal (inverse agonist) in rhodopsin.

Table 3.1 lists the chemical shifts for C5-C20 of the retinal in rhodopsin obtained from our current studies using rhodopsin solubilized in DDM detergent. We [100] and others [135] have found that DDM facilitates the conversion of rhodopsin to meta II. In a comprehensive comparison of spin labeled rhodopsin, Hubbell and coworkers [135] found that the same outward tilt of H6 in meta II trapped in both DDM and lipids. The most notable difference between the two environments is that the receptor conformations have increased flexibility in detergent. The $^{13}C$ chemical shifts reported in Table 3.1 are in agreement within experimental error (0.3-0.4 ppm) with those reported earlier by Degroot and co-workers [192] for rhodopsin reconstituted in lipids. The similar chemical shifts (and absorption spectra) indicate that the conformation of the retinal in the binding cavity in rhodopsin solubilized in DDM is the same as for rhodopsin reconstituted into a lipid environment.

| Position | Rhodopsin (ppm) | PSB (ppm) | ΔRho (ppm) |
|---|---|---|---|
| 5 | 131.0 | 132.1 | -1.1 |
| 6 | 137.1 | 137.2 | -0.1 |
| 7 | 132.8 | 132.3 | 0.5 |
| 8 | 139.3 | 137.2 | 2.1 |
| 9 | 148.9 | 147.8 | 1.1 |
| 10 | 128.0 | 126.4 | 1.6 |
| 11 | 141.6 | 138.7 | 2.9 |
| 12 | 132.2 | 128.7 | 3.5 |
| 13 | 168.5 | 165.8 | 2.7 |
| 14 | 122.1 | 120.5 | 1.6 |
| 15 | 165.7 | 163.3 | 2.4 |
| 16 | 30.6 | 28.9 | 1.7 |
| 17 | 26.1 | 28.9 | -2.8 |
| 18 | 21.6 | 22.1 | -0.5 |
| 19 | 14.7 | 12.6 | 2.1 |
| 20 | 16.4 | 18.8 | -2.4 |

**Table 3.1:** Assignment of the $^{13}C$ chemical shifts of the retinal in WT rhodopsin and comparison with the PSB of the model compound, N-(11-cis-retinylidene)-n-propyliminium trifluroacetate in solution [195] to obtain Δ(Rho).

## *3.4 Charge delocalization along the retinal polyene chain in rhodopsin*

Table 3.1 compares the $^{13}C$ chemical shifts of rhodopsin with those of the 11-*cis* retinal PSB model compound in $CDCl_3$ having a trifluoroacetate counterion (N-(11-*cis*-retinylidene)propyliminium trifluroacetate) [195]. The differences in chemical shifts (ΔRho) listed in Table 3.1 are shown as a histogram in Fig. 3.9A. ΔRho represents the effect of the protein on the conformation and environment of the retinal PSB. The unusual features of the histogram, as noted previously [189], are the positive ΔRho values observed for the C8-C15 carbons along the retinal polyene chain. Since partial charges on the retinal carbons typically alternate between partial negative on the even number carbons and partial positive on the odd numbered carbons, the most unusual chemical shift in Fig. 3.9A is consequently that observed for C12. We previously attributed the large downfield chemical shift at C12 to a specific interaction with a negative charge in the retinal binding site [196]. This observation was confirmed by the crystal structure of rhodopsin [49], which revealed that Glu181 on EL2 is oriented toward the retinal with the side chain carboxyl group ~4 Å from C12.

In order to test whether the unusual chemical shift at C12 is due to a charged Glu181 carboxyl group, we obtained NMR spectra of the E181Q rhodopsin mutant regenerated with 11-*cis* retinal $^{13}C$-labeled at C12. The E181Q mutation results in a reduction of the anomalous ΔRho shift from +3.5 ppm to +1.1 ppm (Table 3.2). The reduction in ΔRho confirms that Glu181 is responsible for unusual shift at C12, which implies that Glu181 is also responsible for the accumulation of excess positive charge along the polyene chain and suggests that Glu181 is charged in rhodopsin. The large change in the C12 chemical shift is consistent with FTIR data that Glu181 is

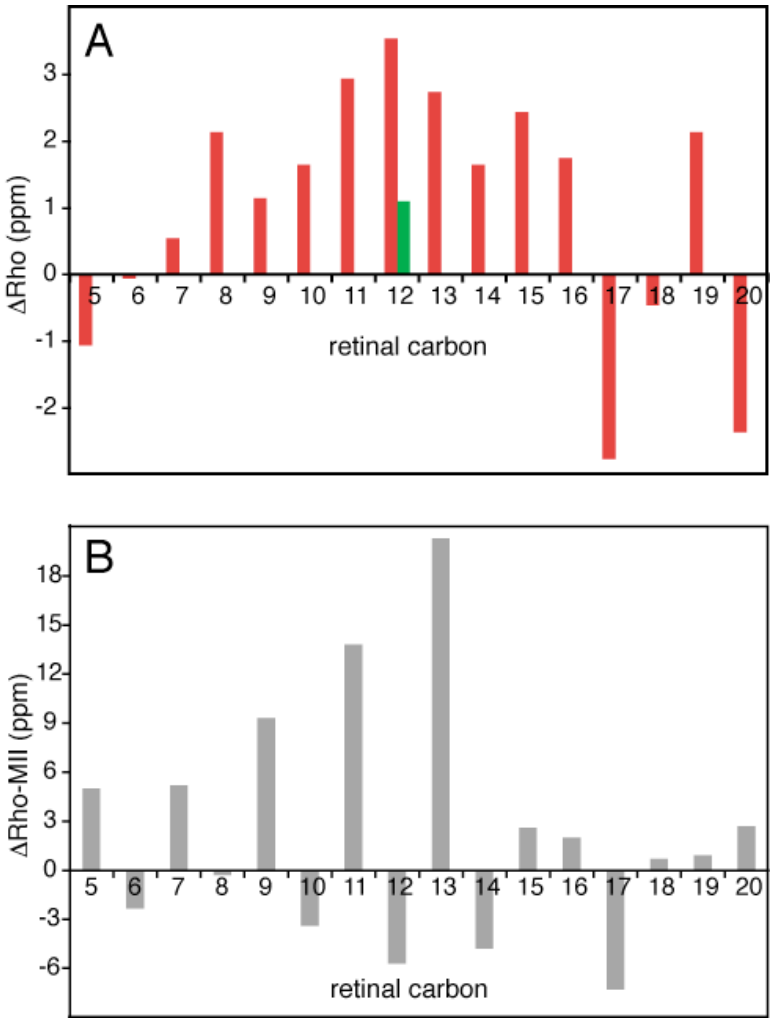


**Figure 3.9: Comparison of retinal $^{13}C$ chemical shifts in rhodopsin with an 11-*cis* retinal PSB model compound and with meta II.** (A) Differences Δ(Rho) between the retinal chemical shifts for C5-C20 in rhodopsin and in the N-(11-cis-retinylidene)-n-propyliminium trifluroacetate model compound in solution [195]. (B) Differences Δ(Rho-MII) between the retinal chemical shifts for C5-C20 in rhodopsin and meta II. All chemical shifts are externally referenced to TMS.

deprotonated in meta II, but is in contrast to the lack of a change in the absorption spectra between wild-type rhodopsin and the E181Q mutant.

In meta II spectra of the E181Q mutant, the C12 chemical shift did not display any significant variation from its chemical shift in wild-type meta II (Table 3.2). While the influence of protein charges on retinal chemical shifts should be much weaker for the unprotonated retinal Schiff base compared to the PSB, the absence of an influence on the C12 chemical shift would be consistent with C12 not interacting with Glu181 in meta II because Glu181 moves away from the retinal upon activation or that Glu181 is protonated in meta II. FTIR studies concluded that the conformation is less constrained in the E181Q mutant of meta I compared with wild-type meta I and that mutation of Glu181 can lower the high pKa of the retinal PSB chromophore characteristic of rhodopsin [197].

| Compound | Wild Type (ppm) | E181Q Mutant (ppm) |
|---|---|---|
| Rhodopsin | 132.2 | 129.8 |
| Meta II | 137.9 | 137.4 |

**Table 3.2**: $^{13}C$ chemical shifts in rhodopsin and meta II for retinal C12 carbon on the polyene chain of the retinal for WT and E181Q mutant.

| Position | Meta II (ppm) | $M_{NP}$ in $CDCl_3$ (ppm) | $M_P$ in $CD_3OH$ (ppm) | $\Delta MII_{NP}$ (ppm) | $\Delta MII_P$ (ppm) |
|---|---|---|---|---|---|
| 5 | 126.0 | 130.4 | 129.3 | -4.3 | -3.3 |
| 6 | 139.5 | 138.5 | 138.2 | 1.0 | 1.3 |
| 7 | 127.6 | 128.5 | 128.2 | -0.8 | -0.6 |
| 8 | 139.6 | 138.2 | 138.2 | 1.5 | 1.4 |
| 9 | 139.6 | 138.6 | 138.2 | 1.0 | 1.4 |
| 10 | 131.4 | 130.7 | 130.5 | 0.8 | 1.0 |
| 11 | 127.8 | 128.5 | 128.2 | -0.6 | -0.4 |
| 12 | 137.9 | 136.8 | 136.0 | 1.2 | 1.9 |
| 13 | 148.2 | 144.6 | 146.8 | 3.7 | 1.4 |
| 14 | 126.9 | 130.2 | 129.3 | -3.2 | -2.3 |
| 15 | 163.1 | 160.0 | 161.4 | 3.2 | 1.7 |
| 16 | 28.6 | 29.7 | 28.6 | -1.0 | 0.0 |
| 17 | 33.4 | 29.7 | 28.6 | 3.8 | 4.8 |
| 18 | 20.9 | 22.4 | 21.1 | -1.4 | -0.2 |
| 19 | 13.8 | 13.5 | 11.9 | 0.4 | 1.9 |
| 20 | 13.7 | 13.7 | 12.2 | 0.1 | 1.5 |

**Table 3.3: Assignment of the $^{13}C$ chemical shifts of retinal in the active intermediate metarhodopsin II and comparison with the model compound,** (NP) N-all-*trans*-retinylidene-*tert*-butylamine in a non polar solvent, $CDCl_3$ to obtain Δ(MII) and (P) all-*trans*-retinylidene-*tert*-butylamine model compound in a polar solvent ($CD_3OD$).

## *3.5 Metarhodopsin II chemical shifts suggest a polar retinal binding site*

On conversion to the active meta II intermediate, the 11-*cis* retinal adopts a an all-*trans* conformation and the Schiff base deprotonates. Table 3.3 lists the $^{13}C$ chemical shifts of the C5-C20 carbons of the all-*trans* retinal in meta II. The plot of the chemical shift differences in Fig. 3.9B between rhodopsin and meta II shows a strong alternation of chemical shift from C5 to C15, due to a difference in electron delocalization along the polyene chain [196]. The odd numbered carbon resonances are shifted downfield and the even numbered carbon resonances are shifted upfield, with the most pronounced downfield shifts being associated with the odd numbered carbons. This pattern reflects the dominant influence that the protonation state of the Schiff base has on electron delocalization. The retinal C16-C20 carbons do not exhibit significant shifts, indicating that they are not affected by charge delocalization along the retinal polyene chain.

The isotropic $^{13}C$ chemical shifts of the retinal chromophore are sensitive to their environment and have been used in the past to map the polarity of the retinal binding site in rhodopsin [189,192]. Table 3.3 and Fig. 3.10 (orange) present the chemical shift differences ($\Delta MII_{NP}$) between meta II and the all-*trans*-N-retinylidene-n-butylimine model compound in a nonpolar solvent ($CDCl_3$). Since the retinal SB is unprotonated in both meta II and the all-*trans* retinal propylimine model compound, one would expect smaller differences than for $\Delta$Rho. However, significant differences are seen at retinal carbons C5, C13, C14, C15 and C17. In order to account for the affect of the choice of solvent on the model compound spectra, we compared the chemical shifts of meta II with an all-*trans*-N-retinylidene-n-butylimine model compound in a polar solvent ($CD_3OD$) (Fig. 3.10, blue).

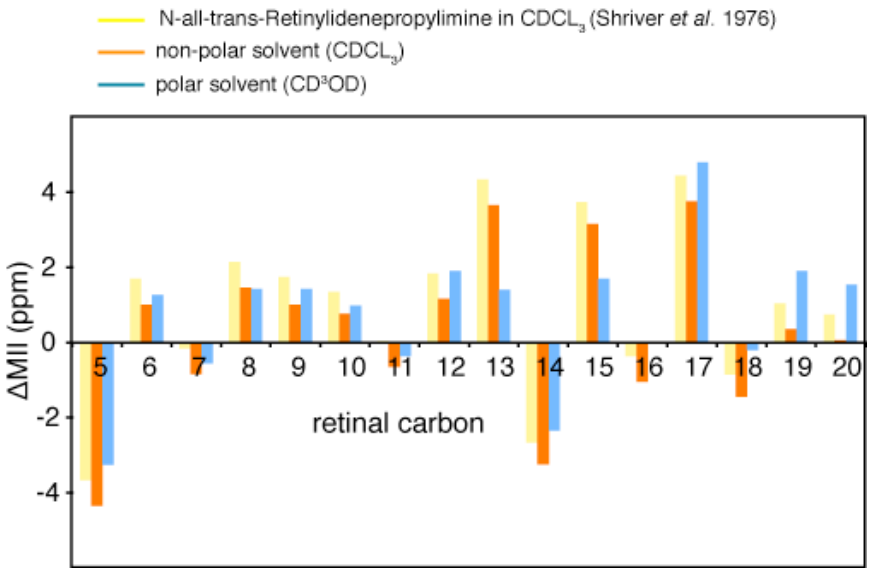


**Figure 3.10: A histogram representing the comparison of retinal $^{13}C$ chemical shifts between meta II and all-*trans* retinal model compounds.**; Differences are shown between meta II and the N-all-*trans*-retinylidenepropylimine in $CDCL_3$ by shriver *et al.* [198] in yellow, N-all-*trans*-retinylidene-*tert*-butylamine model compound in a non-polar solvent ($CDCl_3$) ($\Delta MII_{NP}$; orange) and the N-all-*trans*-retinylidene-*tert*-butylamine model compound in a polar solvent ($\Delta MII_P$; $CD_3OD$) (blue). The smaller differences between retinal carbons (13, 14 and 15) in meta II and the butylamine model in a polar solvent compound suggests that the binding cavity is more polar near the SB end of the retinal in meta II. All chemical shifts are externally referenced to neat TMS at 0 ppm.

The downfield shifts for the retinal resonances along the polyene chain (C13, C14 and C15) are reduced, suggesting that the binding cavity near the SB end of the retinal is more polar in meta II. This observation is consistent with experiments showing that the retinal binding cavity becomes more accessible to water and hydroxylamine in meta II [199,200] and is also consistent with the upfield shift of the $^{15}N\varepsilon$ resonance of the unprotonated SB nitrogen in meta II (mentioned above).

The accessibility to water and hydroxylamine is consistent with motion of EL2 away from the retinal SB in meta II (explained in more detail in Section 4.3). Weaker interactions between the retinal and EL2 in meta II are consistent with several of the chemical shift changes of the retinal carbons. First, the lack of chemical shift changes at the C12 position in meta II as observed for the E181Q mutation are consistent with the loss of a strong E181 interaction with the retinal chain. Second, the chemical shifts of the C19 and C20 methyl groups in rhodopsin, are unique (Table 3.1, Fig. 3.9) due to the conformation and environment of the protein within a tight retinal-binding cavity. However, in meta II they are roughly the same as in all-*trans* SB model compounds in solution suggesting a reduced interaction with the protein upon isomerization.

The retinal $^{13}C14$ chemical shift is sensitive to isomerization about the C=N bond of the SB [201]. In rhodopsin, the PSB linkage between the retinal and Lys296 on H7 is characterized by a 15-*anti* C=N geometry [49,180,202,203]. When the C=N is in a *syn* conformation, the steric interaction between the proton attached to C14 and the protons on the ε-carbon of Lys296 leads to an upfield shift of the isotropic resonances at both positions, referred to as a γ-effect [201,204]. In our case, the ~3.0 ppm upfield shift of the C14 is not associated with a corresponding upfield shift in the Lys296 Cε resonance, which is observed at 60.9 ppm in meta II (mentioned above), in agreement with FTIR studies that the geometry of the C=N double bond remains 15-*anti* [161]. The assignment of

the C=N bond as 15-*anti* suggests that the C14 upfield shift is due to a specific protein interaction

## *3.6 6-s-cis conformation of the β-ionone ring*

The β-ionone ring of the 11-*cis* or all-*trans* retinal model compounds are known to assume either a 6-s-*cis* or a 6-s-*trans* conformation about the C6-C7 single bond due to steric constraints within the compound [205]. The energy difference between the two conformers (6-s-*cis* or a 6-s-*trans*) is very small and depends on the extent of π-electron delocalization along the conjugated polyene chain of the retinal. This π-electron delocalization extends all the way into the β-ionone ring in the 6-s-*trans* isomer and is broken in the 6-s-cis retinal [205]. In rhodopsin due to the multiple interactions between the retinal and the protein, the β-ionone ring has a defined conformation about the C6-C7 single bond in rho and meta II. The high-resolution crystal structure of rhodopsin [31] and experimental solid-state $^{13}C$ [206] and $^{2}H$ [128] NMR measurements carried out on rhodopsin in ROS membranes regenerated with selectively $^{13}C$ and $^{2}H$ labeled 11-*cis* retinal respectively, have demonstrated that the β-ionone ring has a twisted 6-s-*cis* conformation about the C6-C7 single bond in rhodopsin and is largely retained in the meta I state. However, no conclusive data is available for the conformation of the ring in the active state, meta II.

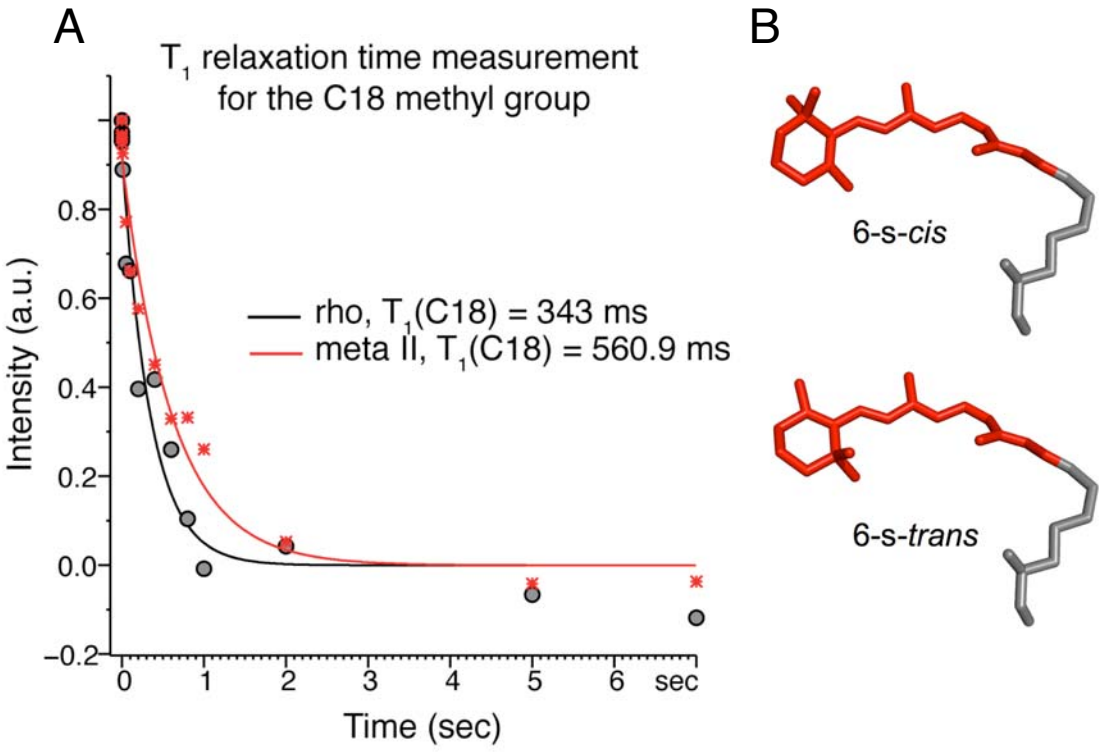


**Figure 3.11:** (A) $T_1$ relaxation curves for the C18 methyl of the β-ionone ring in wild-type rhodopsin (black) and meta II (red) at 190K and 600MHz $^1$H field. (B) Molecular structure of 11-cis retinal in a 6-s-*cis* or 6-s-*trans* conformation of the β-ionone ring about the C6-C7 single bond.

| Compound | Temperature (K) | $^{13}$C5 (ppm) | $^{13}$C8 (ppm) | $^{13}$C-18 ($T_1$) (sec) |
|---|---|---|---|---|
| 6-s-*trans** | 296 | 134.6-144.8 | 131.6-133.4 | 25.6-31.7 |
| 6-s-*cis** | 296 | 126.7-129.4 | 138.2-140.6 | 0.41-3.69 |
| 6-s-*trans* retinoic acid (monoclinic) | 190 | 136.5 | 131.3 | 12.3 |
| 6-s-*cis* retinoic acid (triclinic) | 190 | 129.6 | 139.7 | 0.14 |
| Rhodopsin | 190 | 131.0 | 139.3 | 0.34 |
| Meta II | 190 | 126.0 | 139.6 | 0.56 |

**Table 3.4:** Comparison of the $^{13}$C chemical shifts of retinal C5 and C8 along with the $T_1$ relaxation measurement for the C18 methyl group in wild-type rhodopsin in the inactive and the active states, with a variety of model compounds. *Chemical Shifts are taken from Harbison *et al.* [188].

We measured the $T_1$ relaxation times for the $^{13}$C18 methyl group on the β-ionone ring to assess the conformation of the ring about the C6-C7 single bond of retinoic acid crystals in organic solvents (monoclinic and triclinic forms) and the retinal chromophore in the inactive and active form rhodopsin, solubilized in detergent, DDM, at 190K, using a standard solid-state NMR cross-polarization inversion-recovery sequence [188] (as explained in the methods and material chapter). A similar study was conducted by Harbison *et al.* [188] on bacteriorhodopsin and retinal model compounds where they measured very long $T_1$ relaxation times of the order of seconds for the 6-s-*trans* conformation of the β-ionone ring and very small $T_1$ relaxation times of the order of milliseconds for the 6-s-*cis* conformation. The large disparity in the $T_1$ relaxation times for the retinal $^{13}$C18 methyl group between the two conformers is primarily due to the steric interaction between the proton on C7 and the C18 methyl group in the 6-s-*trans* conformation. In the 6-s-*cis* conformation, the retinal C18 methyl group is out of the plane of the conjugated polyene system and therefore does not experience the same steric hindrance.

Table 3.4 summarizes the $T_1$ relaxation times for the $^{13}$C18 methyl group of the retinal chromophore in rhodopsin, metarhodopsin II and a variety of retinal model compounds (with 6-s-*cis* or 6-s-*trans* ring conformations). Fig. 3.11 presents the $T_1$ relaxation time measurements of the C18 methyl group in rhodopsin (black) and meta II (red) at 190K. In rhodopsin, the $T_1$ relaxation time is 343 ms is within the range of 6-s-*cis* model compounds and well outside the range of 6-s-*trans* model compounds. In meta II, the $T_1$ relaxation time is 560.9 ms, again within the range of 6-*cis* model compounds.

The $^{13}$C chemical shifts of the C5 and C8 retinal carbons are also sensitive to the 6-s-*cis* or 6-s-*trans* conformations of the β-ionone ring. Analysis of the $^{13}$C chemical shift tensors of retinal model compounds has shown that the C5 resonance is very sensitive to charge delocalization along the polyene chain [188]. In the twisted 6-s-*cis* conformation,

the C5=C6 double bond, that is part of the β-ionone ring, is not very efficiently conjugated with the rest of the retinal polyene chain and as a result the π-electron delocalization does not extend all the way to the C5 carbon in the ring [205]. Comparison of the chemical shifts of the crystalline retinal derivatives, show that the $^{13}$C5 chemical shift for 6-s-*cis* model compounds is ~7-9 ppm upfield from the 6-s-*trans* model compounds (Table 3.4). In contrast, the $^{13}$C8 chemical shift appears to be predominantly influenced by steric interactions. In the 6-s-*trans* conformer, the C8 proton is located between the C16 and C17 methyl groups on the β-ionone ring. This steric interaction causes a ~5-8 ppm upfield shift of the $^{13}$C8 resonance as compared to the 6-s-*cis* model compounds. In dark rhodopsin, we observe the $^{13}$C5 resonance at 131.0 ppm and the $^{13}$C8 resonance at 139.3 ppm indicating a 6-s-*cis* conformation of the β-ionone ring [188,189].

In meta II, the $^{13}$C5 and $^{13}$C8 chemical shifts are observed at 126.1 ppm and 139.6 ppm, respectively, in agreement with a 6-s-*cis* conformation of the ring. The $^{13}$C5 isotropic resonance is shifted significantly upfield in both rhodopsin and meta II (see Fig. 3.9A and 3.10). Since, the $^{13}$C5 chemical shift depends strongly upon the orientation of the β-ionone ring, one explanation for the observed $^{13}$C5 chemical shift in meta II is that the ring is significantly more non-planar (with respect to the retinal polyene chain) than in the retinal model compounds. It is known that the C6-C7 conformation influences the absorption maxima ($\lambda_{max}$) of the pigment; in a planar conformation, the C5=C6 double bond is fully conjugated with the π-electron system between C5 and C15. The planar 6-s-*trans* retinal chromophore in the M intermediate of bacteriorhodopsin absorbs at 412 nm. The $\lambda_{max}$ of meta II at 380 nm is the same as that of 6-s-*cis* unprotonated SB model compounds, suggesting that the C6-C7 conformation is not dramatically more non-planar.

A second possible explanation for the upfield $^{13}$C5 chemical shift in meta II is the protein environment. In the crystal structure of dark rhodopsin, the ionone ring is in contact with Trp265 and Phe261 on H6, Gly121 and Glu122 on H3 and Phe208, His 211 and Phe212 on H5. In meta II, we observed that the β-ionone ring moves towards H5

and this motion leads to a rearrangement of packing interactions with residues on helices H5 and H6 (explained in Chapter 5). Consequently, one possibility for the upfield shift of $^{13}$C5 resonance could be the shielding by ring current from the surrounding aromatic residues (Phe208, His211 and Phe212 on H5; Trp265 on H6) [207,208].

The 6-s-*cis* conformation defines how the β-ionone ring is packed within the tight confines of the retinal binding site. Retinal analogs in which the ionone ring is replaced with two ethyl groups are not able to fully activate rhodopsin [139]. In membranes, rhodopsin activity is reduced to approximately 20% of wild type as assayed by GTPγS binding to transducin. However, no GTPγS binding is detected for rhodopsin regenerated with this retinal analog, solubilized in DDM. Fourier transform infrared spectroscopy confirmed that the meta II intermediate was not formed [139]. Therefore, steric interactions between the retinal and H5 are absent in retinal analogs lacking the β-ionone ring. Without these interactions, changes in the structure or position of H5 (explained in Chapter 5), which may be necessary for rhodopsin activation, do not occur.

## *3.7 β-ionone ring inversion and assignment of $^{13}$C16-$^{13}$C17 chemical shifts*

According to IUPAC nomenclature, the C1-C16 bond is oriented into the page in Fig. 3.2, while the C1-C17 bond is oriented out of the plane of the page. In solution, the $^{13}$C16 and $^{13}$C17 resonate at the same chemical shift of 28.9 ppm for both 11-*cis* and all-*trans* retinal model compounds [192]. In rhodopsin, the C16 and C17 methyl group resonances are observed at 30.6 ppm and 26.1 ppm (Table 3.1). The difference in chemical shift is attributed to the tight binding site of the retinal and the inability of the different ring conformations to rapidly interconvert. Ring inversion can change the position of the methyl groups from an axial orientation to an equatorial orientation. In an axial orientation, the protons of the methyl group are in steric contact with the proton of the C3

carbon of the retinal β-ionone ring. This interaction produces an upfield chemical shift (referred to as a γ effect) of the methyl group. The resonance at 26.1 ppm is assigned to the methyl group in the axial orientation [192]. An open question has been whether the 26.1 ppm resonance corresponds to the C16 or the C17 methyl group.

In Chapter 5, I discuss in detail, an extensive $^{13}C$ NMR study that defines the position of the β-ionone ring in rhodopsin and in meta II on the basis of distance measurements between $^{13}C$ groups on the retinal and amino acids lining the retinal binding site. For example, 2D DARR NMR spectra have been obtained using rhodopsin containing $^{13}C$-labels at the carbonyl carbons of Met207 and the carbonyl carbon of His211 on H5, and regenerated with retinal $^{13}C$-labeled at both the C16 and C17 methyl groups. In the $^{13}C$ DARR NMR spectra, the strongest crosspeaks between the carbonyl and methyl group resonances, corresponding to the shortest internuclear distances, are observed to the methyl group resonating at 30.6 ppm. Now, according to the rhodopsin crystal structure (pdb code: 1U19), the C16 methyl group is closer to the carbonyl of Met207 (4.9 Å) and carbonyl of His211 (4.9 Å) on H5 than the C17 methyl group that is 7.0 Å away from Met207 and 7.2 Å away from His211 [31]. Therefore, we can assign the resonance 30.6 ppm to C16 methyl group and the resonance at 26.1 ppm to the C17 methyl group. Additionally, based on the argument mentioned in the previous paragraph we can definitively say that in rhodopsin the C17 methyl group in an axial orientation and the C16 methyl group in an equatorial orientation on the β-ionone ring.

On conversion to meta II, the retinal moves toward H5 and is positioned between Met207/His211 and Phe208/Phe212. The C16 and C17 methyl group resonances are observed at 28.6 ppm and 33.4 ppm, respectively. These assignments are based on the following observations. First, a relatively strong DARR crosspeak is observed between the methyl resonance at 28.6 ppm and both the carbonyl carbons of Met207 and His211 (data presented in Section 5.2.1). Second, 2D DARR NMR data show that the side chain of Met207 in meta II is positioned between the β-ionone ring and Cys167 on H4. Third,

a relatively stronger crosspeak is observed between a $^{13}C$ methyl resonance at the ring carbons of Phe208/Phe212 at 33.4 ppm in meta II (data presented in Section 5.2.1) shows that these constraints are only consistent with an assignment of the resonance at 28.6 ppm to the C16 methyl group.

The upfield shift in the resonance is attributed to an axial orientation of the retinal C16 methyl group and the γ-effect produced by interaction with the protons attached to C3 on the β-ionone ring. As a consequence, in the rhodopsin to meta II transition the C16 methyl resonance changes from 30.6 ppm to 28.6 ppm, and the C17 methyl resonance changes from 26.1 ppm to 33.4 ppm. These assignments, in turn, indicate that there is an inversion in the ring conformation upon activation. Buss and coworkers [209,210] have calculated that there is substantial energy barrier for ring inversion, between 5-6 kcal/mol. Moreover, these results show that in both rhodopsin and meta II, the $^{13}C16$ and $^{13}C17$ chemical shifts are unique and that averaging does not occur in the retinal binding site of the protein.

## *3.8 Conclusion*

The observation that the retinal C18 methyl group has a short $T_1$ relaxation time in both the dark-state of rhodopsin and the meta II intermediate demonstrates that the β-ionone ring of the retinal chromophore has a 6-s-*cis* conformation about the C6-C7 single bond in rhodopsin and it does not change upon activation. The 6-s-*cis* conformation is in contrast with the 6-s-*trans* conformation observed for the retinal chromophore in bacteriorhodopsin [188]. Further, comparison of the metarhodopsin II chemical shifts with those of retinal model compounds and the 11-*cis* retinal in rhodopsin suggests that the retinal near the SB end is in a polar environment in metarhodopsin II with significant protein interactions near the β-ionone ring (C5, C17) and the Schiff base (C14). And with the help of E181Q mutant of rhodopsin we have shown that a strong perturbation at C12 of the retinal in rhodopsin is due to Glu181 on EL2. And this perturbation is not seen

in metarhodopsin II, consistent with a movement of EL2 loop away from the retinal binding site upon activation.

# Chapter 4

# Displacement of the Second Extracellular Loop (EL2) Upon Rhodopsin Activation

## *4.1 Introduction*

GPCRs comprise a simple architectural core of seven transmembrane (TM) helices (H1 to H7) connected often by short extracellular and cytoplasmic loops. Sequence variability within the TM helices and extracellular loops allow them to respond to diverse stimuli including light and a wide variety of ligands. Small molecule ligands can bind within the helical core of the receptor, whereas larger peptide and protein ligands bind at the extracellular loops. The second extracellular loop (EL2) in particular has been the target of a number of functional studies indicating that it plays an integral role in activation of GPCRs that bind either small molecules or large peptide ligands [211-214].

The extracellular domains of rhodopsin are more structured than the cytoplasmic loops as demonstrated by the lower B-factors for the intradiscal loops in the crystal structure [69]. The three extracellular loops (EL1, EL2 and EL3) include 4 short β-strands β1 (4-6), β2 (9-11), β3 (177-180) and β4 (187-190) that fold into two β-hairpins: β1-β2 and β3-β4 (see Fig. 4.1A). The crystal structure of rhodopsin indicates that EL2 extends from Trp175 on H4 to Thr198 on H5.

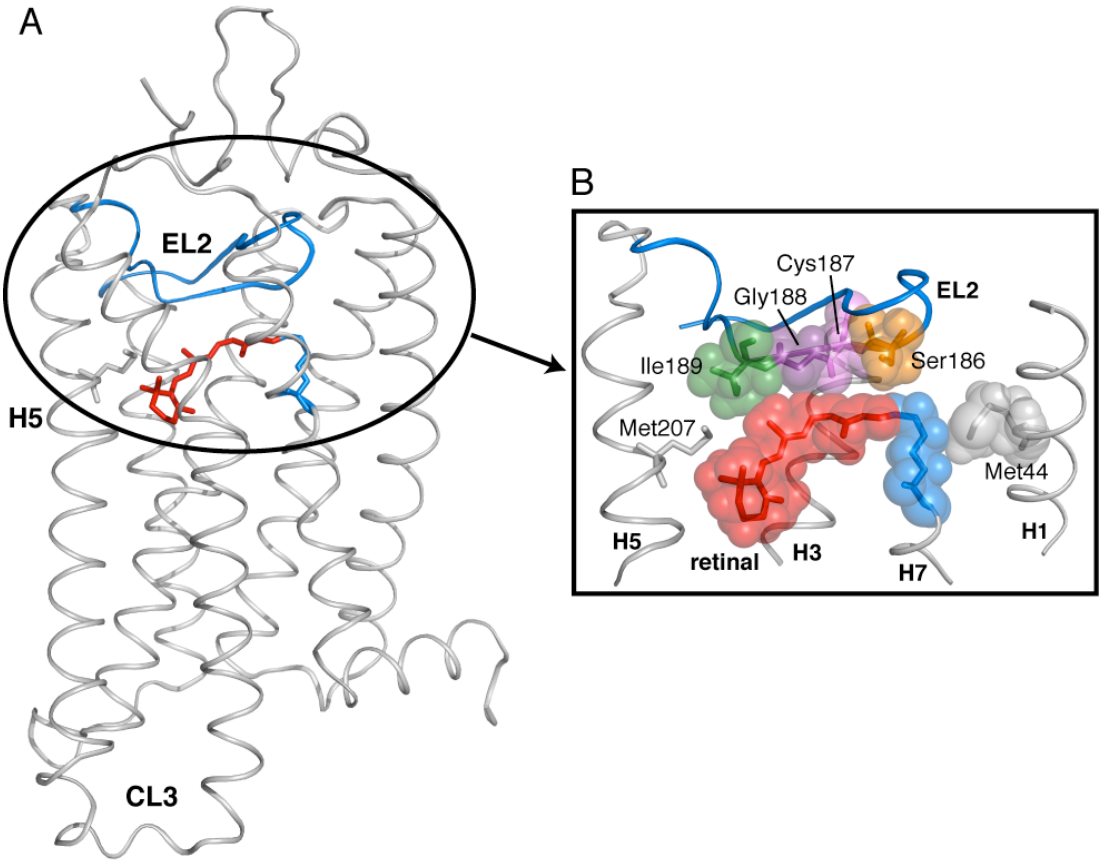


**Figure 4.1: Location of extracellular loop 2 (EL2) in rhodopsin**. (a) A view of the rhodopsin crystal structure [50] highlighting the location of EL2 (blue). It folds into two β-sheets (β3 and β4) that form a lid over the retinal binding pocket. (b) View of the β4 strand of EL2 from the rhodopsin crystal structure [50] highlighting the tight packing of Ile189, Gly188, Cys187 and Ser186 with the polyene chain of the retinal.

The intriguing aspect about the EL2 sequence is that it folds into a highly ordered and stable structure consisting of the two short β-strands (β3 and β4) that form a lid over the retinal-binding site [31,49] (Fig. 4.1). Motion of EL2 is constrained by a conserved disulfide bond between Cys110 at the end of H3 and Cys187 on β4 that is critical for the correct folding of rhodopsin into a fully functional conformation [71,72]. Other than the Cys110-Cys187 disulfide bond, the EL2 sequence is not conserved among the class A GPCRs. However, nine residues from Pro170 near the kink on H4 to Asp190 at the end of the β4 strand are highly conserved among the visual pigments for example, Pro170, Pro171, Gly174, Trp175, Arg177 and Asp190.

The structure of EL2 in rhodopsin is stabilized by a number of polar residues that form a well-defined hydrogen bonded network (Fig. 4.2). At the center of this network is Glu181 on the β3 strand. Glu181 is highly conserved in vertebrate opsins and cone pigments [215]. In squid rhodopsin the residue corresponding to Glu181 serves as the counterion for the retinal protonated Schiff base in the inactive state. All across the visual pigment family, either a glutamic or aspartic residue is found at the position corresponding to Glu181 in rhodopsin except in the red and green cone pigments that have a histidine residue in the corresponding location [216]. The side chain of Glu181 is situated very close to the C11=C12 double bond of the retinal. It is only 4.7 Å from C12 on the polyene chain [49]. Our $^{13}C$ NMR data have shown an anomalous chemical shift for C12 in the dark state of rhodopsin as compared to retinal model compounds [196,217]. Upon mutation of Glu181 to Gln, we observed a marked reduction in this anomalous chemical shift for C12 (explained in detail in Chapter 4). Sakmar and co-workers have shown that Glu181 is charged in the dark and have suggested that Glu181 in conjunction with Glu113 on H3 serves as a complex counterion for the retinal PSB in the dark. However, in meta I, Glu181 serves as the primary component of the complex counterion to the PSB. This counterion switch model was based on a series of UV-Vis, resonance Raman and FTIR studies conducted on mutants of Glu181 [197].

Glu181 is hydrogen bonded to Tyr192 (β4) and Tyr268 (H6), and is connected through water-mediated hydrogen bonds to Ser186 (EL2) and to Glu113 (H3), which serves as the counterion to the retinal PSB [31]. Glu113 is hydrogen bonded to the backbone carbonyl of Cys187 (EL2) through a water molecule and is within hydrogen bonding distance to the hydroxyl group of Thr94 (H2) [31]. The involvement of Glu113 in this stable hydrogen bonded network is thought to be important in significantly raising the pKa of the Schiff base (above 16) [175] and ensuring that it remains protonated in the dark state of rhodopsin [218,219].

Besides the conserved disulfide bond and the hydrogen bonding network involving Glu181, there are a striking number of hydrogen bonding interactions between the β-strands and the ends of the TM helices. The ends of the β-hairpins that connect β3 to H4 and β4 to H5 are stabilized by a number of hydrogen bonds (e.g. Trp175-Ser202, Ser176-Thr198, Arg177-Asp190, Tyr178-Ala168) (see Appendix A.2). Computational studies identified this region as part of a stable folding core of rhodopsin [220], suggesting that EL2 is important for maintaining a stable, inactive receptor conformation. This was further supported by a mutational study conducted by Janz and coworkers on Arg177 on β3 and Asp190 on β4. These amino acids form a salt bridge holding the β-hairpin together. They demonstrated that disruption of this salt bridge rendered the Schiff base very prone to hydrolysis in the dark leading to formation of a thermally unstable mutant of rhodopsin [221]. Also, mutation of Tyr191 and Tyr192 to leucines has been shown to decrease the stability of the binding pocket leading to faster meta II decay rates [222].

A series of studies based on FTIR and time resolved Raman spectroscopy on different intermediates in the rhodopsin photoreaction have demonstrated a rearrangement of these hydrogen bonding interactions upon illumination. A dramatic weakening of the Schiff base hydrogen bonding was observed in bathorhodopsin to lumirhodopsin transition whereas full recovery of the Schiff base hydrogen bonding was observed in the meta I intermediate, immediately before meta II formation [179].

In contrast to the role of EL2 as a stable cap on the extracellular side of GPCRs, several studies have suggested that EL2 is dynamic and mediates both receptor activity and ligand binding. Baranski and colleagues proposed that in the C5a receptor, EL2 serves as a negative regulator [213] where the loop inserts between the TM helices to block receptor activity, and then is released upon ligand binding. Holst and Schwartz suggested that a short EL2 in the melanocortin receptor, which is unable to insert into the helical TM core, leads to a high level of constitutive receptor activation [223]. In the recent crystal structure of the β2-adrenergic receptor (β2-AR) with a bound partial inverse agonist [52], EL2 is not closely associated with the ligand-binding site. The β2-AR structure, along with the observation that short loops may be correlated with constitutively active GPCRs, raises the question of whether the role of EL2 as a stable cap is unique to rhodopsin due to the crucial requirement that visual pigments must have very low basal activity in the dark.

Here, I use $^{13}C$ magic angle spinning (MAS) NMR spectroscopy to determine the position of EL2 in dark rhodopsin and in the active meta II intermediate. Chemical shift measurements of the conserved Cys110-Cys187 disulfide bond and distance measurements between the retinal chromophore and amino acids on the β4 strand of EL2 are consistent with motion of EL2 away from the agonist all-*trans* retinal Schiff base upon receptor activation. Mutational studies on Glu181 (EL2) and Met288 (H7) show that the hydrogen bonding network on EL2 is coupled to the hydrogen bonding network centered on H5 involving His211, thus explaining how EL2 motion may be transmitted through H5 to the conserved Glu-Arg-Tyr sequence on the intracellular side of the receptor.

## *4.2 Chemical shift changes in Ser186 and Cys187 suggest structural changes in the EL2*

The Cys110-Cys187 disulfide bond is the only conserved feature in EL2 and the only disulphide bond in rhodopsin. Fig. 4.2B presents $^{13}$C DARR NMR spectra of rhodopsin (black) and meta II (red) labeled with $^{13}$Cβ-cysteine. The β-carbon resonances in disulfide bonds occur in a unique chemical shift window (34-50 ppm) and are sensitive to the secondary structure with a range of 34 to 43 ppm for α helices and 36 to 50 ppm for β sheets [224]. In Fig. 4.2B, we observe strong crosspeaks between the Cys110-Cys187 β-carbon resonances at 36.4 ppm and 46.8 ppm, respectively. The 46.8 ppm chemical shift of Cys187 is consistent with its location in the β4 strand of EL2. Upon conversion to meta II, the Cys187 resonance shifts to 50.1 ppm due to a change in the conformation of EL2 or a change in the environment around Cys187. The chemical shift of Cys110 does not change significantly (-0.2 ppm), indicating that the secondary structure of H3 near Cys110 does not change in meta II. In agreement with our data, Nakamichi et al observed a change in the electron density around the S-S disulphide bond between Cys187 and Cys110 in bathorhodopsin. They observed a dislocation of the disulphide bond upon illumination [90]. The eight reduced cysteines in rhodopsin are observed as a broad resonance around 25 ppm (not shown).

In addition to the chemical shift changes observed in Cys187, we also observe a ~1.6 ppm change in the chemical shift of the $^{13}$Cβ carbon of Ser186. The $^{13}$Cβ-Ser186 chemical shift was assigned on the basis of the 2D DARR NMR crosspeak observed between the $^{13}$Cβ-Ser186 and the $^{13}$C1(carbonyl)-Cys185 resonances in rhodopsin (black) and meta II (red), as presented in Fig. 4.3B. In rhodopsin the crosspeak is observed at 63.3 ppm for $^{13}$Cβ-Ser186 and 169.7 ppm for $^{13}$C1-Cys185. On conversion to meta II, the crosspeak shifts to 61.7 ppm for $^{13}$Cβ-Ser186 and 170.4 ppm for $^{13}$C1-Cys185. The shift of ~1.6 ppm in the resonance of $^{13}$Cβ-Ser186 between rhodopsin and meta II can be

attributed to a change in the hydrogen bonding interaction of Ser186 with surrounding residues on EL2 and transmembrane helix H3.

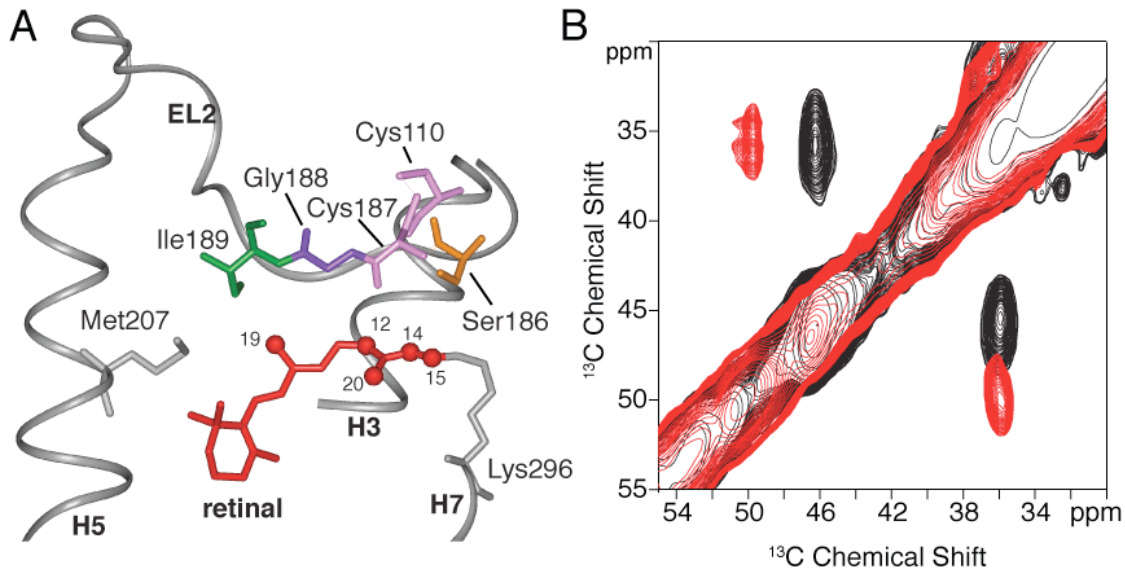


**Figure 4.2: Structural changes involving the conserved Cys110 - Cys187 disulfide link on activation of rhodopsin.** (a) View of the β4 strand of EL2 from the rhodopsin crystal structure[31] highlighting the interactions of Ile189, Gly188, Cys187 and Ser186 with the polyene chain of the retinal. Cys110 on the extracellular end of H3 forms a conserved disulfide link with Cys187 in β4. (b) A region from the 2D DARR NMR spectrum of rhodopsin selectively labeled with $^{13}$Cβ-cysteine. The figure highlights the crosspeak between Cys187 (46.8 ppm) and Cys110 (36.4 ppm) in rhodopsin (black). On conversion to meta II (red) there is a distinct shift in the crosspeak to 50.1 ppm for Cys187. The $^{13}$Cβ chemical shift of Cys110 at ~36 ppm does not change significantly between rhodopsin and meta II.

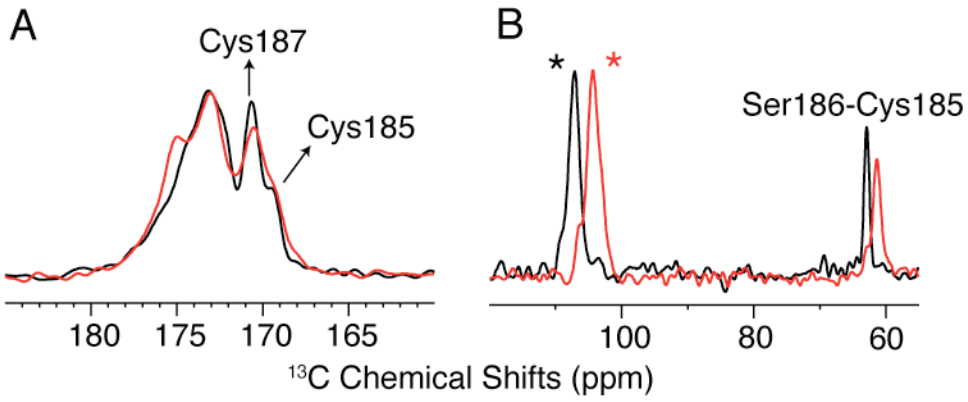


**Figure 4.3: 1D and 2D $^{13}$C NMR spectra of rhodopsin and meta II labeled with $^{13}$C1-cysteine and $^{13}$Cβ-serine.** (a) Overlap of 1D $^{13}$C NMR spectra for $^{13}$C1-cysteine residues in rhodopsin (black) and meta II (red). The backbone carbonyl of Cys187 on EL2 is observed as a sharp resonance at 170.8 ppm in rhodopsin. The assignment is based on the crosspeaks observed between $^{13}$C1-Cys187 and $^{13}$C12, $^{13}$C20 retinal in rhodopsin, as shown in Fig. 4.4B. In meta II, the resonance for $^{13}$C1-Cys187 has been tentatively assigned to the resonance at 170.9 ppm. The backbone carbonyl of Cys187 is hydrogen bonded to Glu113 in rhodopsin[50] and the lack of significant changes in the chemical shift for Cys187 in meta II suggest that its hydrogen bonding interactions remain intact upon activation. The shoulder at 169.8 ppm has been assigned to the backbone carbonyl of Cys185 on EL2 in rhodopsin (black); the assignment is based on the crosspeak observed between $^{13}$Cβ-Ser186 and $^{13}$C1-Cys185 in rhodopsin and meta II as explained below. The broad resonance observed at ~174.0 ppm represents the backbone carbonyls of the rest of the cysteines in rhodopsin and meta II. (b) Rows through the $^{13}$C1-Cys185 diagonal resonance of the 2D DARR NMR spectra of rhodopsin (black) and meta II (red) highlighting the crosspeak with $^{13}$Cβ-Ser186 on EL2. A strong crosspeak is observed between $^{13}$C1-Cys185 (169.8 ppm) and $^{13}$Cβ-Ser186 (63.3 ppm) in rhodopsin consistent with a separation of 3.5 Å. On conversion to meta II (red), the crosspeak shifts to 170.5 ppm for $^{13}$C1-Cys185 and 61.7 ppm for $^{13}$Cβ-Ser186. The 1.6 ppm change in the $^{13}$Cβ-OH chemical shift of Ser186 between rhodopsin and meta II is significant and may correspond to a weakening in the hydrogen bonding interaction of Ser186 upon activation. The asterisks indicate spinning side bands.

## *4.3 EL2 is displaced away from the retinal binding site upon activation.*

The β4 strand of EL2 lies directly on top of the retinal polyene chain in the binding cavity. It is aligned almost parallel to the retinal in the binding site with Cys185 close to the PSB end of the retinal and with Ile189 close to the retinal β-ionone ring (Fig. 4.1). We observe contacts between the retinal $^{13}$C14 and $^{13}$C15 carbons and $^{13}$Cβ-Ser186 (Fig. 4.4A), between the retinal $^{13}$C12 and $^{13}$C20 carbons and $^{13}$C1-Cys187 (Fig. 4.4B), and between the retinal $^{13}$C12 and $^{13}$C20 carbons and $^{13}$Cα-Gly188 in rhodopsin (Fig. 4.4C). These contacts are lost in meta II. Moreover, we were not able to observe contacts in rhodopsin or meta II between the retinal $^{13}$C9 and $^{13}$C12 carbons and U-$^{13}C_6$-Ile189 (Fig. 4.4D).

On the basis of measurements in model compounds and in the dark state of rhodopsin, we typically observe strong crosspeaks for $^{13}$C…$^{13}$C distances of ~4.0 Å or less, moderate crosspeaks for distances of up to 5.0 Å and weak crosspeaks for distances up to 6.0 Å. Consequently, the lack of crosspeaks in the DARR spectrum of meta II indicate that retinal – EL2 distances are on the order of 6.0 Å or more. In rhodopsin, we observed strong contacts between the carbonyl of Cys187 on EL2 and the C12 and C20 carbons on the retinal polyene chain (Fig. 4.4B). In the rhodopsin crystal structure [31], Cys187 is 4.21 Å and 6.22 Å from the retinal C12 and C20 carbons, respectively. On conversion to meta II, both retinal contacts with Cys187 are lost, consistent with an increase in separation between EL2 and the retinal.

Further support for the increase in distance between retinal and EL2 in meta II comes from assignment of a crosspeak at 46.5 ppm between the $^{13}$C20 methyl carbon on the retinal and a $^{13}$Cα-glycine residue. There are only two glycines in the binding cavity close to the C20 methyl group, i.e. Gly114 on H3 and Gly188 on EL2 (Fig. 4.5). In meta II, we assign the C20-Gly crosspeak to Gly114 (H3) based on the presence of this

resonance in the 2D DARR spectrum of the G188A mutant of meta II (see Appendix A.3 and Section 5.4.2).

The model in Fig. 4.4 shows the crystal structure of rhodopsin containing the 11-*cis* (red) retinal PSB tightly packed against EL2. The distances between the C20 methyl group and the $^{13}$C-labeled positions on Gly114, Cys187 and Gly188 are shown as dotted lines. Crosspeaks between the retinal C20 methyl group and each of these amino acids are observed in the dark. We superimpose the position of the all-*trans* retinal SB (orange) in meta II predicted using restrained MD simulations (see Appendix A.1). In order to satisfy distance constraints derived from our NMR measurements, in the MD simulations the retinal chromophore shifts slightly toward the cytoplasmic side of the retinal binding site and EL2 moves toward the extracellular surface.

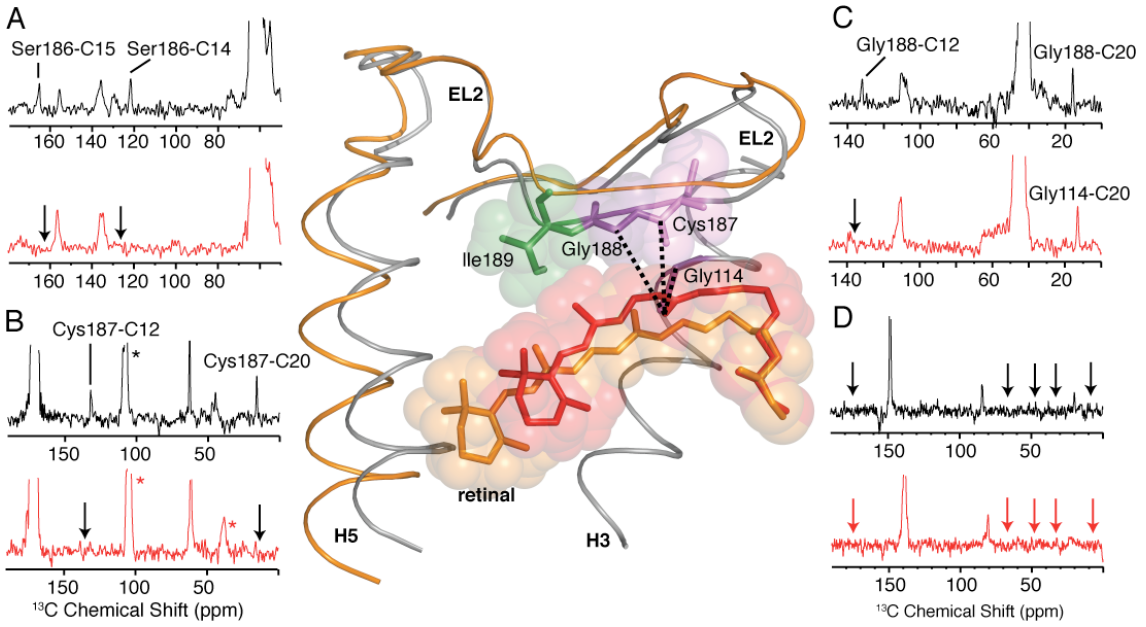


**Figure 4.4: 2D $^{13}$C DARR NMR spectra of retinal – EL2 interactions. Rows are shown from the 2D $^{13}$C DARR NMR spectra of rhodopsin (black) and meta II (red).** (a) Rhodopsin labeled with $^{13}$Cβ-serine and $^{13}$C14,15 retinal. Crosspeaks are observed between Ser186 (63.3 ppm) and the $^{13}$C14 and $^{13}$C15 resonances in dark rhodopsin, and are lost (arrows) in meta II. (b) Rhodopsin labeled with $^{13}$C1-cysteine and $^{13}$C12,20 retinal. Crosspeaks are observed between Cys187 (170.8 ppm) and the $^{13}$C12 and $^{13}$C20 resonances in dark rhodopsin, and are lost (arrows) in meta II. (c) Rhodopsin labeled with $^{13}$Cα-glycine and $^{13}$C12,20 retinal. Crosspeaks are observed between Gly188 (42.0 ppm) and the $^{13}$C12 and $^{13}$C20 resonances in dark rhodopsin, and are lost (arrows) in meta II. However, a new Gly-C20 contact is observed, which is assigned to Gly114 (see text). (d) Rhodopsin labeled with U-$^{13}C_6$- isoleucine and $^{13}$C9 retinal. No contacts were observed between Ile189 and C9 on the polyene chain of the retinal in either rhodopsin (black arrows) or meta II (red arrows). The structure of EL2 in rhodopsin is shown (center) indicating the contacts observed between the C20 methyl group and Cys187,Gly188 and Gly114 in rhodopsin. The Cys187 and Gly188 contacts with the retinal are lost in meta II despite the rotation of the C20 methyl group toward Gly114. In order to illustrate the displacement of EL2 needed to satisfy the NMR constraints, we have superimposed the rhodopsin crystal structure with the meta II model (orange) obtained from MD simulations guided by our experimentally determined retinal-protein contacts. * corresponds to the spinning side bands.

## *4.4 Rearrangement of the hydrogen bonding networks involving EL2 and H5 upon rhodopsin activation.*

The changes observed in the chemical shifts for the Cys110-Cys187 disulfide bond (Fig. 4.2B) and the loss of EL2-retinal contacts in meta II (Fig. 4.4) indicate that EL2 changes position upon receptor activation. The next question is whether the hydrogen bonding network involving EL2 remains intact or is it disrupted in meta II? Tyrosines are an integral part of the EL2 hydrogen bonding network [31]. Fig. 4.5 presents a view of the extracellular end of rhodopsin showing the positions of six key tyrosines: Tyr10, Tyr178, Tyr191, Tyr192, Tyr206 and Tyr268. Tyr191 (EL2), Tyr192 (EL2) and Tyr268 (H6) are involved in the hydrogen bonding network with Glu181 on EL2. Tyr206 on H5 is involved in a second hydrogen bonding network with His211 (H5), Glu122 (H3), Trp126 (H3) and Ala166 (H4).

The $^{13}C$ chemical shift for the ζ-carbon of tyrosine is sensitive to its chemical environment and hydrogen bonding strengths [225]. The $^{13}C\zeta$ resonances of the 18 tyrosines in rhodopsin are not resolved (see Fig. 4.6A, black). However, the difference spectrum between rhodopsin and meta II highlights the $^{13}C\zeta$-tyrosine resonances that change upon rhodopsin activation (Fig. 4.6B). There are two well-resolved shoulders in the meta II portion of the difference spectrum (Fig. 4.6B). The downfield resonance at 159.3 ppm is reflective of a more strongly hydrogen bonded tyrosine, while the 153.6 ppm resonance is characteristic of a more weakly hydrogen bonded tyrosine [225]. These two tyrosines must be coupled to the hydrogen bonding network involving Glu181 on EL2 since both the 159.3 and 153.6 ppm resonances are lost in the tyrosine difference spectrum of the E181Q mutant (Fig. 4.6C). There is no evidence for a tyrosinate anion [226], which would have a chemical shift closer to 165 ppm [225]. In order to assign these tyrosines, difference spectra were collected for a series of rhodopsin mutants (Y268F, Y192F, Y191F, Y178F and Y206F), where different tyrosines in the retinal binding cavity were mutated one at a time to phenylalanine (Fig. 4.6D-H).

### *4.4.1 Tyr206 becomes more weakly hydrogen bonded in meta II*

In the $^{13}$Cζ-tyrosine (rhodopsin minus meta II) difference spectrum (Fig. 4.6B), we observe a distinct meta II resonance at 153.6 ppm. We have assigned this upfield peak to Tyr206 on H5 on the basis of the loss of a Cζ-Tyr resonance at 153.6 ppm in the meta II component of the Y206F difference spectrum (Fig. 4.6H). The upfield shift of $^{13}$Cζ-Tyr206 resonance is consistent with a weaker Cζ-OH hydrogen bond in meta II.

In rhodopsin, the Tyr206 (Cζ-OH) is hydrogen bonded to the side chain of His211 on H5 and the backbone carbonyl of Ala166 on H4. Tyr206 is part of a hydrogen bonding network that changes upon meta II formation. We have previously shown that the backbone carbonyl of His211 (H5) is hydrogen bonded to the side chain of Glu122 in rhodopsin and that this hydrogen bond is disrupted in meta II [227]. The $^{13}$Cζ-Tyr206 resonance in rhodopsin is assigned at 154.8 ppm on the basis of a loss of intensity at this position in the rhodopsin half of the Y206F difference spectrum (Fig. 4.6H) and on contacts with His211 on H5 in rhodopsin and meta II (see Appendix A.4). We propose that the weaker Tyr206 hydrogen bond in meta II is caused by rotation of H5 and the loss of the Tyr206 interaction with the backbone carbonyl of Ala166 on H4.

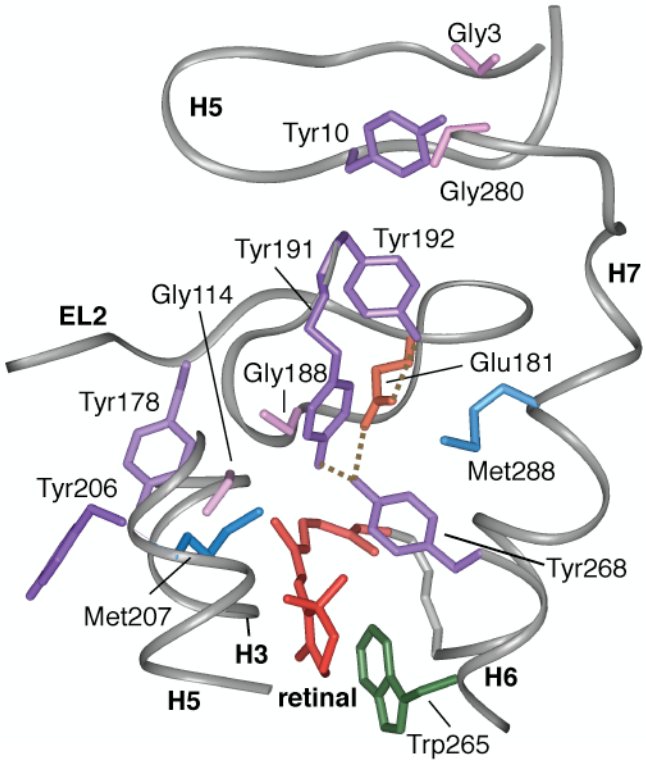


**Figure 4.5: A view of the extracellular side of the rhodopsin from the crystal structure [31].** The figure highlights the relative position of six tyrosines: Tyr10, Tyr178, Tyr191, Tyr192, Tyr206 and Tyr268. Of these tyrosines, Tyr191, Tyr192 and Tyr268 are involved in the hydrogen-bonding network with Glu181. Tyr268 and Tyr191 are also in close contact with Met288 on H7. Tyr206 on H5 is involved in a second H-bonding network with His211 (H5), Glu122 (H3), Trp126 (H3) and Ala166 (H4) (not shown). Additionally, the figure shows Tyr-Gly interactions on the extracellular side of rhodopsin between Gly188-Tyr268, Gly3-Tyr10-Gly280 and Gly114-Tyr178.

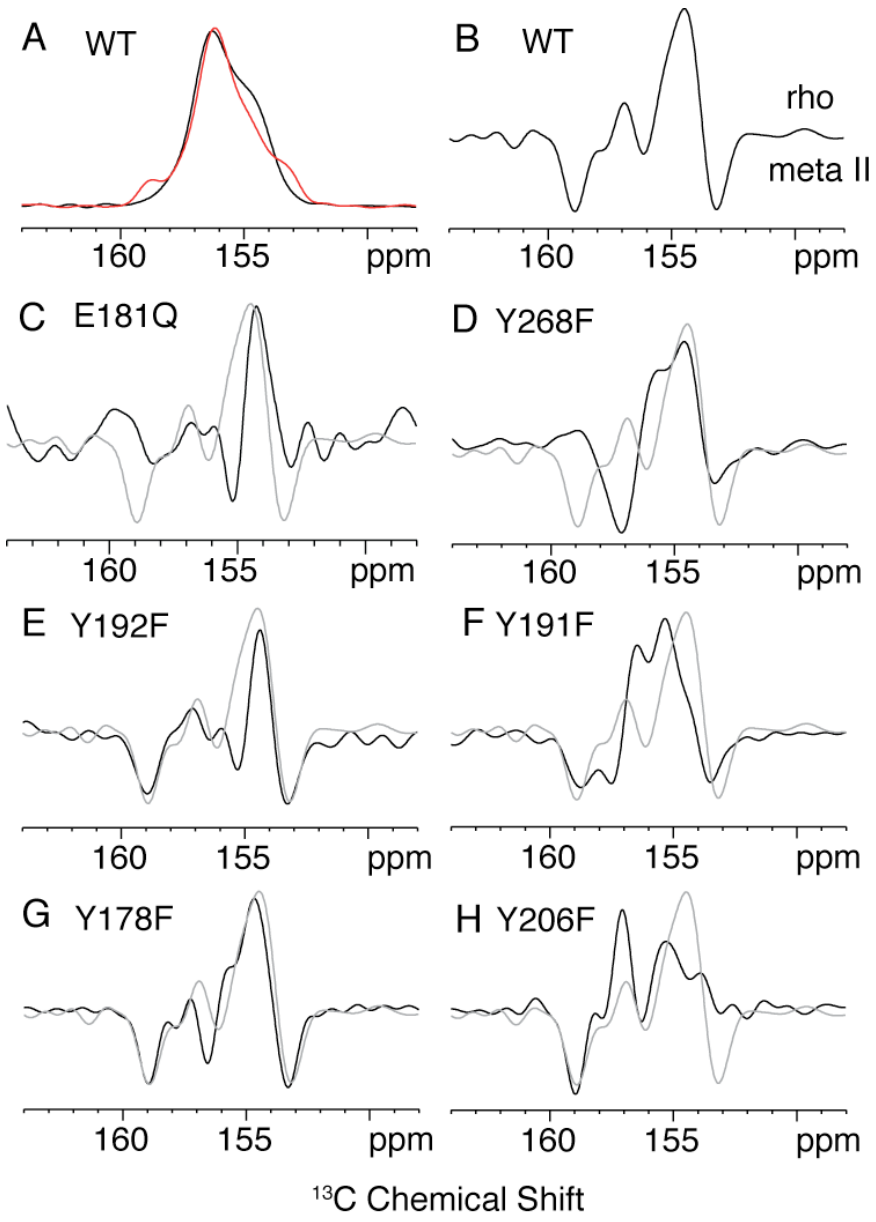


**Figure 4.6: One dimensional (1D) $^{13}$C CP-MAS spectra of rhodopsin and meta II labeled with $^{13}$Cζ-tyrosine.** (a) Overlap of the $^{13}$C 1D CP-MAS spectra of the $^{13}$Cζ-tyrosine resonance in rhodopsin (black) and meta II (red). Difference spectra for wild-type rhodopsin (b) and several rhodopsin mutants, E181Q (c), Y192F (d), Y178F (e), Y206F (f), Y191F (g), Y268F (h). The difference spectrum in gray corresponds to the wild-type protein.

### *4.4.2 Tyr191 becomes more strongly hydrogen bonded in meta II*

None of the $^{13}$Cζ-tyrosine difference spectra (Fig. 4.6C-H) exhibit a complete loss of the negative peak at 159.3 ppm, except the Y268F mutant where the negative peak at 159.3 ppm appears to shift to 157.5 ppm. Unfortunately, we were not able to assign conclusively the 159.3 ppm resonance to Tyr268 because of the appearance of a positive peak at 159.3 ppm in the dark spectrum of the Y268F mutant. The appearance of the 159.3 ppm resonance in rhodopsin suggests that the mutation of Tyr268 is causing another tyrosine in the vicinity to become more strongly hydrogen bonded. Additionally, in the difference spectrum of the Y191F mutant, the negative peak at ~159 ppm is split into two components as compared to the wild-type difference spectrum.

Nevertheless, the loss of the 159.3 ppm resonance in the E181Q mutant and its sensitivity to mutation of Tyr268 and Tyr191 strongly suggest an assignment to one of the tyrosines (Tyr191 and Tyr268) associated with EL2. This assignment is supported by 2D DARR data obtained on rhodopsin labeled with $^{13}$Cζ-tyrosine and $^{13}$Cε-methionine. In the rhodopsin crystal structure (1U19), there are 5 Met($^{13}$Cε) - Tyr($^{13}$Cζ) pairs (Met288-Tyr268, 3.9 Å; Met207-Tyr191, 4.8 Å; Met288-Tyr191, 5.2 Å; Met253-Tyr206, 5.5 Å; Met288-Tyr192, 5.7 Å). In Fig. 4.7A, we observe two crosspeaks between tyrosine and methionine that we assign to the closest Met-Tyr pairs (i.e. Met288-Tyr268 and Met207-Tyr191). Conversion to meta II generates a crosspeak between the tyrosine resonance at 159.4 ppm and a methionine resonance at 12.8 ppm. We can assign this methionine to Met288 on H7 based on the loss of this crosspeak in the M288L mutant (orange, Fig. 4.7B).

The M288L data along with the tyrosine difference spectra above indicate that the 159.3 ppm resonance belongs to either Tyr191 or Tyr268 in meta II. We assume that the strong hydrogen bonding interaction for a tyrosine at 159.3 ppm is due to its interaction with Glu181 and that the appearance of a resonance at 159.3 ppm in the Y268F rhodopsin

spectrum and in the Y191F meta II spectrum is because these mutations lead to the rearrangement of the EL2 hydrogen bonding network. We tentatively assign the 159.3 ppm resonance in meta II to Tyr191 since we observe a crosspeak at 156.5 ppm between a tyrosine and the retinal C20 methyl group [100] that was assigned to Tyr268. The C20 methyl group is closer to Tyr268 (4.2 Å) than to Tyr191 (8.0 Å) in rhodopsin, and we expect that motion of EL2 away from the retinal would only increase the $^{13}$C20-Tyr191($^{13}$Cζ) distance. Together these data argue that Tyr191 becomes more strongly hydrogen bonded in meta II and and that the hydrogen bonding network involving the tyrosines and Glu181 on EL2 remains intact.

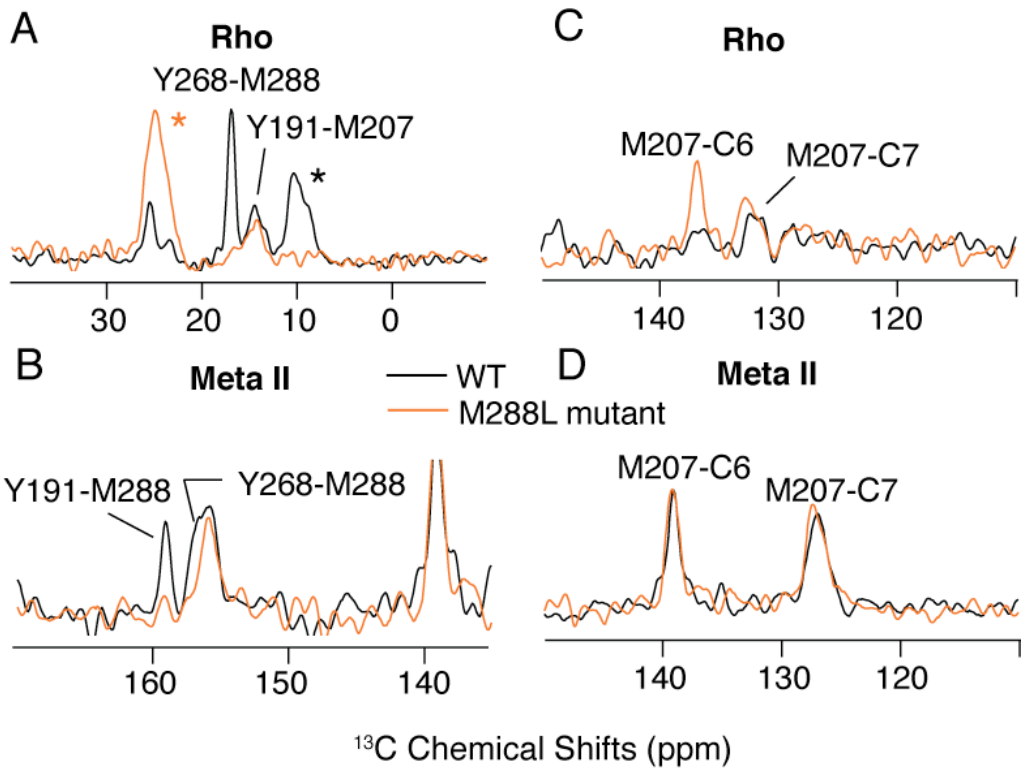


**Figure 4.7: 2D DARR NMR of Tyr(Cζ) - Met(Cε) contacts in rhodopsin and the M288L rhodopsin mutant**. (a) Rows through the $^{13}$Cζ-Tyr diagonal resonance from 2D DARR NMR spectra of rhodopsin (black) and the M288L rhodopsin mutant (orange) labeled with $^{3}$Cζ-tyrosine and $^{13}$Cε-methionine. (b) Following conversion to meta II, the figure presents an overlap of rows through the $^{13}$Cε-Met diagonal resonance from 2D DARR NMR spectra of WT meta II (black) and the M288L mutant meta II (orange) labeled with $^{3}$Cζ-tyrosine and $^{13}$Cε-methionine. (c) Rows through the $^{13}$Cε-methionine diagonal resonance of rhodopsin (black) and the M288L rhodopsin mutant (orange) showing the crosspeaks to the retinal $^{13}$C6 and $^{13}$C7 resonances. (d) Same as in (c) following conversion to meta II. In the M288L mutant of rhodopsin, we observe a contact between Met207 and C6 that is not present in wild type rhodopsin. This change in the Met207-retinal contact in the M288L mutant of rhodopsin can be interpreted as either a change in the position of the retinal or in the position of Met207 on H5 upon mutation of Met288 (H7) to a leucine. Upon activation, the Met207 – retinal interactions in the M288L mutant are identical to those in wild-type meta II. * corresponds to the spinning side bands.

## *4.5 Tyrosine – Glycine changes in meta II*

Motion of EL2 also explains the loss of tyrosine-glycine contacts in meta II. In the rhodopsin crystal structure (1U19), there are six Tyr(Cζ)-Gly(Cα) contacts all located in the extracellular region of rhodopsin involving: Tyr10-Gly3, 3.9 Å; Tyr10-Gly280, 4.4 Å; Tyr29-Gly101, 4.0 Å; Tyr178-Gly114, 4.5 Å; Tyr191-Gly188, 5.2 Å; Tyr268-Gly188, 5.3 Å. Fig. 4.8 presents rows through the $^{13}$Cζ-tyrosine diagonal resonance from 2D DARR spectra in the region of Tyr-Gly crosspeaks for wild-type rhodopsin, and for the Y178F and Y206F rhodopsin mutants. In wild-type rhodopsin, we observe at least four (of five possible) crosspeaks: three well defined peaks and a shoulder at ~40.0 ppm (Fig. 4.8A).

The $^{13}$Cα-Gly resonance at 42.0 ppm has previously been assigned to Gly188 [100] based on a crosspeak observed between retinal C19 methyl group and Gly188 in rhodopsin. In Fig. 4.8A, the Tyr-Gly crosspeak at 42.0 ppm is tentatively assigned to a contact between Tyr268 (H6) and Gly188 (EL2) in rhodopsin, although there may be other contributions to this resonance as the Tyr268-Gly188 distance of 5.3 Å is greater than that of the other four Tyr-Gly pairs. Importantly, this EL2-H6 contact is lost in meta II.

The crosspeak at 45.5 ppm (Fig. 4.8A) is assigned to a contact between Tyr178 and Gly114 based on the loss of this crosspeak in the corresponding dark spectrum of the Y178F mutant (Fig. 4.8B). In the meta II spectrum of the Y178F mutant, we lose a resonance at 44.9 ppm (Fig. 4.8B). There are only two glycines within 10 Å of Tyr178 in rhodopsin, Gly114 (H3) and Gly188 (EL2) [31]. In wild-type meta II, we have assigned the 46.5 ppm resonance to Gly114 (explained in Section 5.4.2). As a result, the crosspeak between Tyr178 and glycine at 44.9 ppm in meta II cannot be assigned to Gly114, and we tentatively assign it to Gly188 on EL2. These assignments imply that an EL2-H3 contact (Tyr178-Gly114) is lost in meta II and an EL2-EL2 contact (Tyr178-Gly188) is gained.

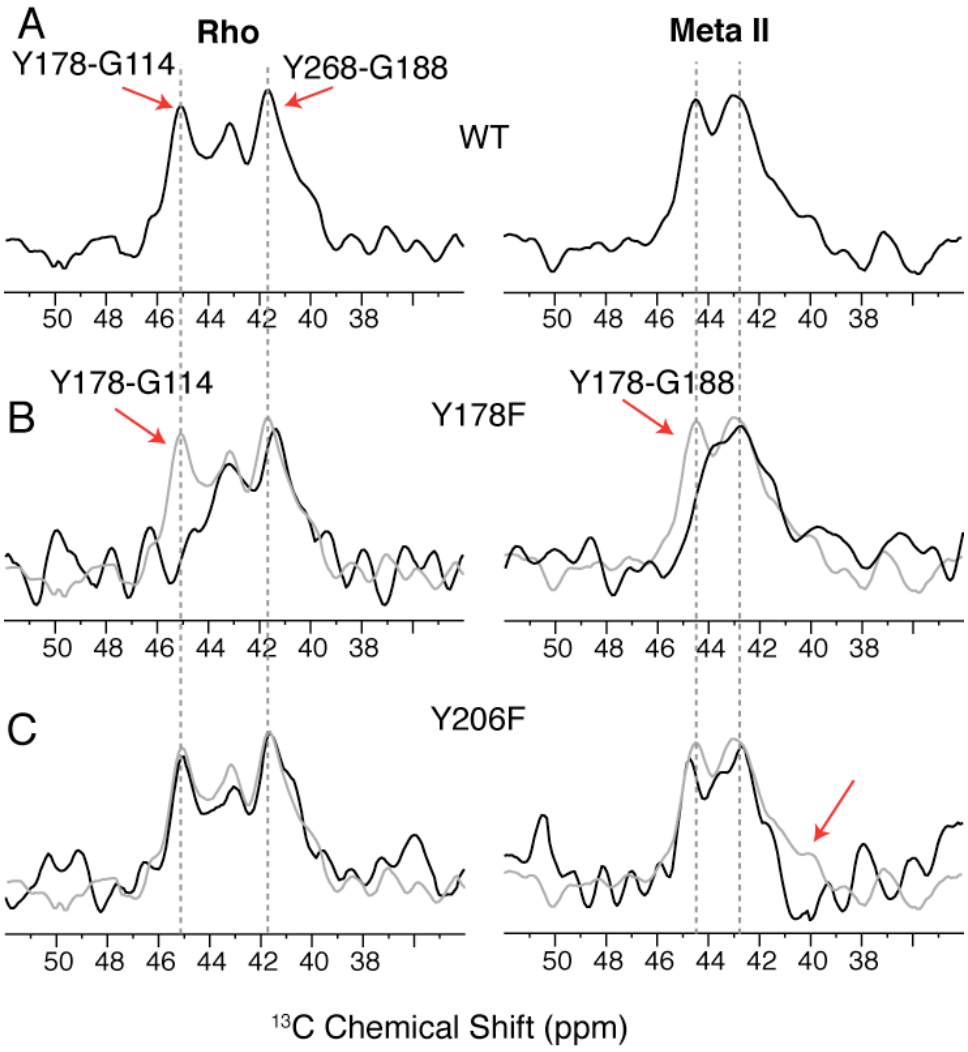


**Figure 4.8: 2D DARR NMR of Tyr($^{13}$Cζ)-Gly($^{13}$Cα) contacts in rhodopsin and meta II.** (a) Row through the $^{13}$Cζ-tyrosine diagonal resonance from 2D DARR NMR spectra of rhodopsin (left) and meta II (right). (b) Same as (a) for the Y178F rhodopsin mutant. The loss of the resonance at 45.5 ppm in the mutant enables us to assign the crosspeak to a contact between Tyr178 and Gly114 at 45.5 ppm in rhodopsin. In meta II, the resonance at 44.9 ppm that is lost in the Y178F mutant is tentatively assigned to the Y178-G188 contact. (c) Same as (a) for the Y206F rhodopsin mutant. The Tyr-Gly crosspeaks appear identical to those in (a) except that the broad shoulder observed at ~40.0 ppm in wild-type meta II is lost in the meta II spectrum of the Y206F mutant.

There are no changes in the tyrosine-glycine crosspeaks in the dark spectrum of the Y206F mutant (Fig. 4.8C). However, in the meta II spectrum for the Y206F mutant the low frequency shoulder at ~40.0 ppm seems to disappear. This shoulder cannot correspond to a contact between Tyr206 and a glycine, as there are no glycines within 12.6 Å of Tyr206 [31]. Consequently, the shoulder must correspond to contacts involving Tyr10 or Tyr29 on the extracellular loops of rhodopsin (Fig. 4.5). Tyr206 is not close to either of these tyrosines, but rather is part of a hydrogen bonding network involving residues on H5 (His211) and H3 (Glu122 and Trp126). Our data suggests that disruption of this hydrogen bonding network in the Y206F mutant is coupled to the changes in the extracellular loops.

The data presented above on the E181Q, M288L (in section 4.4.2) and Y206F (in section 4.5) mutants suggest that light-induced structural changes in EL2 are strongly coupled to the hydrogen bonding network centered on H5 involving residues such as His211 (H5), Glu122 (H3) and Trp126 (H3). First, in the E181Q (EL2) mutant (Fig. 4.6C) the resonance at 153.6 ppm assigned to Tyr206 (H5) and the resonance at 159.3 ppm assigned to Tyr191 are lost. Second, in the M288L mutant (H7) we observed something really interesting, a contact is gained between the ε-$CH_3$ group of Met207 (H5) and the retinal C6 carbon (Fig. 4.7C), which is not detected in wild-type rhodopsin. The Met207-retinal contacts in meta II are the same for the M288L mutant and the WT

## *4.6 Conclusion*

### *4.6.1 EL2 controls access to the retinal binding site.*

The major conclusion from our studies is that EL2 changes position upon activation and that this change is coupled to motion of H5, H6 and H7. In the following chapter 5, I

define the location of the retinal chromophore in meta II and our current measurements between the β4 strand and the retinal indicate that there is an increase in separation between the retinal and EL2 upon activation. The hydrogen bonding network involving Glu181 remains intact but rearranges in meta II, and consequently the displacement of EL2 does not appear to be large.

Our observations can be compared with the crystal structures of opsin [68] and a 'photoactivated' (deprotonated) intermediate of rhodopsin [185]. In both of these structures, EL2 has not moved to any significant extent. Also, in contrast to the structural changes observed here, in the opsin structure Tyr178 is within 4 Å of Gly114 and remains hydrogen bonded to the backbone carbonyl of Ala168. Glu181 does not hydrogen bond to any of the tyrosines on EL2 or H6 (i.e. Tyr178, Tyr191, Tyr192 or Tyr268). Rather Glu181 directly interacts with Ser186 and Gly188. Met288 is within 5.0 Å of Tyr191, but is ~8.3 Å from Tyr268. These differences between meta II and opsin suggest that the all-*trans* retinal Schiff base is holding EL2 in an active conformation in meta II. Release of retinal to form opsin allows the binding site residues to rearrange and EL2 to shift back to roughly its position in rhodopsin.

Displacement of EL2 away from the retinal is consistent with studies showing that the retinal binding site becomes more accessible to water and hydroxylamine in meta II [54,165]. Mutation of many of the residues in the hydrogen bonding network involving EL2, such as Glu181 [228] and Tyr192 [229], results in increased accessibility of the retinal PSB to hydroxylamine in the dark. In agreement with these mutational studies, Furutani *et al.* [230] observed the appearance of an N-D amide A vibration at 2366 $cm^{-1}$ in meta II that they attributed to access of the EL2 β-hairpin to hydrogen-deuterium (H-D) exchange in the meta I-to-meta II transition. Interestingly, neither disruption of the Cys110-Cys187 disulfide bond by mutation to alanine nor disruption of the salt bridge between Arg177 and Asp190 on EL2 increases hydroxylamine accessibility [221,231] suggesting that the hydrogen bonding network involving Glu181 is alone sufficient to keep EL2 tightly

capped over the retinal binding site. Displacement of EL2 is also consistent with studies where a significant increase in transducin activation was observed for rhodopsin, in the dark, regenerated with 11-*cis* retinal analogues with a longer R group (ethyl or propyl) attached to the retinal C9 carbon. The methyl group attached to the retinal C9 carbon is packed between Tyr268 (H6) and Tyr191 and Ile189 on EL2 in rhodopsin. Therefore, increase in bulk volume around the retinal C9 carbon may lead to a displacement of EL2 and hence activation of the receptor. This provides further evidence for the displacement of EL2 as an important trigger for rhodopsin activation.

In a parallel fashion, EL2 may serve to control the access of small molecule ligands to interior binding sites within the ligand-activated GPCRs. For example, alanine scanning mutagenesis of the M1 muscarinic acetylcholine receptor revealed that the access of ligands to the binding site was increased by mutation of EL2 residues [232]. Furthermore, substituted cysteine accessibility studies of the dopamine D2 receptor showed that the extracellular part of H5 is accessible to hydrophilic reagents [233]. Finally, the recent crystal structure of the β2AR with a bound partial inverse agonist [52] shows that EL2 does not cap the amine-binding site, as in rhodopsin. Taken together, the studies on GPCRs activated by small molecule ligands suggest that there is a dynamic role of EL2 in allowing water and ligands to enter the interior binding sites.

### *4.6.2 EL2 functions as a negative regulator in GPCR activation*

Several studies have suggested that EL2 serves a role as a negative regulator in the class A GPCRs. The simple idea is that EL2 has multiple interactions with the extracellular ends of the TM helices in the inactive state and that displacement of EL2 upon ligand binding allows TM helices H5, H6 and H7 to adopt active conformations. For example, Baranski and colleagues [213] showed that a high degree of constitutive activity is associated with the mutation of residues in EL2 of the C5a receptor. They proposed that mutation of EL2 increases the flexibility of the loop and releases inhibitory constraints.

The high degree of basal activity in the melanocortin receptor, which has a short EL2 and lacks the conserved disulfide bond, was explained by a related mechanism [223]. Finally, crosslinking in the putative ligand binding site [24,87] and metal binding sites [23] in the vicinity of EL2 modulate receptor activity. These modifications were designed to mimic the movement of the TM helices, and for this to occur, EL2 was envisioned to change conformation or position consistent with a role as a negative regulator.

In rhodopsin, EL2 has also been implicated as a negative regulator of receptor activity. It is known that mutation of Tyr191 and Tyr192 to leucine decreases the stability of the binding pocket leading to faster meta II decay rates [222], and that mutation of Ser186 (EL2) to alanine and Glu181 (EL2) to phenylalanine strongly perturbs the kinetics of rhodopsin activation [234]. However, none of the EL2 mutants tested in rhodopsin have been shown to display constitutive activity. This may be due to the presence of additional regulatory elements, such as the interaction between the retinal PSB and its Glu113 counterion and the tight packing between the 11-*cis* retinal and conserved Trp265 on H6, which all contribute to low dark noise in rhodopsin.

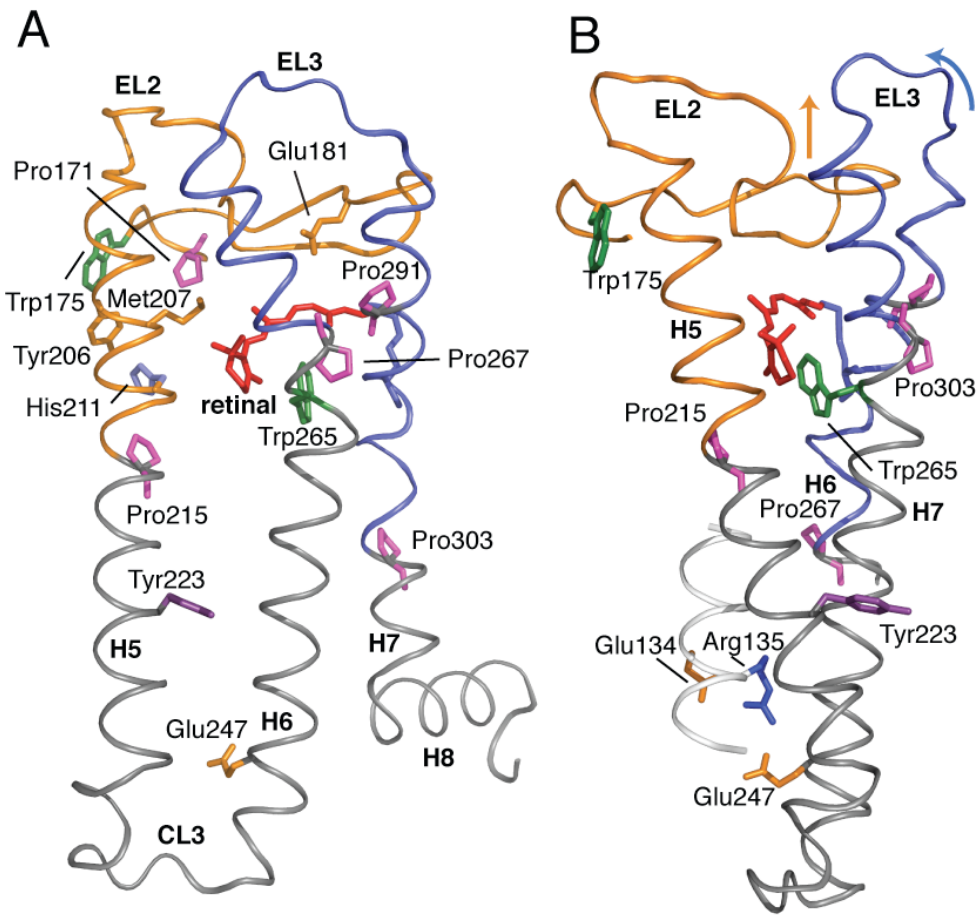


**Figure 4.9: Crystal structure of rhodopsin [50] highlighting the two helix-loop-helix (HLH) segments proposed to interact upon rhodopsin activation.** The H4 (Pro171)-EL2-H5(Pro215) segment is shown in orange and the H6(Pro267)-EL3-H7(Pro291) segment is shown in blue. (a) Retinal isomerization within the tightly packed binding site results in steric contacts between the β-ionone ring and H5, and between the retinal C19 and C20 methyl groups and EL2. These interactions trigger the simultaneous displacement of EL2 and H5. Motion of the β-ionone ring is also coupled to the motion of Trp265. Trp265 is packed against the β-ionone ring and C20 of the retinal, as well as Gly121 on H3 and Ala295 on H7. Movement of the Trp265 sidechain away from these critical contacts triggers the shift of helices H6 and H7 into active conformations. The coupled motions of helices H5-H7, in turn, are coupled to the rearrangement of electrostatic interactions involving the conserved ERY sequence at the cytoplasmic end of H3, exposing the G protein binding site on the cytoplasmic surface of the protein. (b) View of the rhodopsin crystal structure highlighting the interaction between EL2 and EL3 on the extracellular side of the receptor, and the positions of Tyr223 and the conserved Glu135-Arg135-Tyr136 sequence on the intracellular side of the receptor. Motion of EL2 away from the retinal binding site may allow the H6-EL3-H7 segment to pivot in toward the center of the protein.

### *4.6.3 EL2-H5 forms a structural unit in GPCRs*

One of the challenges in understanding the mechanism of GPCR activation is to establish how retinal isomerization [18,86] or ligand binding [22,23] produces rigid body motion of the TM helices. The influence of the E181Q and M288L mutations on retinal-H5 interactions suggests that structural changes in EL2 are coupled to the motion of H5. We propose that the functional unit is in fact the EL2-H5 sequence. In this regard, it is interesting to note the structural changes involving H5 in the recent crystal structure of opsin [68]. On the extracellular side of H5, the hydrogen bonding interaction between the Glu122 side chain and the His211 backbone carbonyl is broken upon activation and a new interaction is observed directly between side chains in meta II. These changes are observed in NMR measurements on meta II [227]. On the cytoplasmic side of H5, Tyr223, a residue that is highly conserved across the GPCR family, has rotated around to interact with Arg135 and stabilize the "ionic lock" in what may be the active conformation.

The crystal structure of rhodopsin shows that the β-strands in EL2 are extensively knit together by hydrogen bonding interactions and that the hydrogen bonding network centered on Glu181 extends to the Tyr268 on H6 and Glu113 on H3 [50]. If the motion of EL2 is coupled to motion of H5, then the Pro170-Pro171 sequence at the H4-β3 boundary may serve as a flexible hinge leading to observable changes in the hydrogen bonding interactions linking β3-to-H4 and H4-to-H5. We observe that many of the hydrogen bonding contacts involving the extracellular end of H4 change in meta II (see Appendix A.2).

Tight coupling between EL2 and H5 is supported in studies on ligand-activated GPCRs [235-238]. Wurch *et al.* [236] addressed the coupling of EL2 and H5 by replacing the EL2-H5 sequence from the $5HT_{1D}$ serotonin receptor with the corresponding sequence from the $5HT_{1B}$ serotonin receptor. They found that it was necessary to replace the entire

EL2-H5 sequence in order to recover antagonist binding; replacing either the EL2 or H5 sequence alone significantly decreased binding. Also, the idea that EL2 is a structured unit is reflected in GnRH receptor studies where Pfeger *et al.* [238] showed that exchange of the entire EL2 from another species had less effect on ligand binding affinity than point mutations of EL2 within a species.

The EL2-H5 sequence advocates that helix-loop-helix (HLH) segments stretching from a proline in one helix to a proline in an adjacent helix may form structural units. Fig. 4.9 highlights the HLH segments involving EL2 and EL3, and suggests how motion of EL2 away from the retinal binding site may allow the extracellular end of the H6-EL3-H7 segment to pivot in toward the center of the protein and conversely allow the intracellular end of H6 to rotate outward as shown by spin labeling studies [18,88]. Oprian and coworkers have previously shown that rhodopsin containing an engineered disulfide bond between V204$^{5.39}$C (H5) and F276$^{6.59}$C (H6) retains the ability to activate transducin [87], indicating that the extracellular end of H6 does not move outward upon activation. The inward motions of the extracellular ends of H6 and H7 are captured in the global toggle switch model proposed by Schwartz and coworkers [23].

Additionally, Fig. 4.9 shows the positions of two key tryptophan residues in rhodopsin, Trp265 (H6) and Trp175 (H4). Trp265 (H6) is conserved throughout the class A GPCRs and its motion toward the extracellular surface is an important element of the activation mechanism of rhodopsin [65]. Trp175 (H4) is at the junction of EL2 with H4. In rhodopsin, the W175F mutation is one of the only mutations in the H4-EL2-H5 segment that leads to constitutive activity [239]. The interesting aspect of this mutant is that it displays a UV-Vis spectrum and light induced G-protein activation similar to WT rhodopsin. The fact that this tryptophan is highly conserved in the visual receptors, but not in other class A GPCRs, suggests that the entire H4-EL2-H5 sequence is specific to different subfamilies of class A GPCRs.

In conclusion, the structural constraints described above provide insights into how EL2 and its extensive hydrogen bonding interactions play a role in coupling retinal isomerization to the activation of rhodopsin. The subfamily specific H4-EL2-H5 unit in rhodopsin holds H5 and the extracellular ends of H6 and H7 in inactive conformations. We propose that the displacement of EL2 away from the retinal binding site is coupled to motion of H5 and to the inward motion of the H6-EL3-H7 unit upon activation. Similar motions are likely to occur in other GPCRs [23,240] suggesting that EL2 may act as a plug or cork that must be released or rearranged for receptor activation.

# Chapter 5

# Location of the retinal in metarhodopsin II: implications for the motion of H5

## *5.1 Introduction*

H5 plays a crucial role in the activation mechanism for rhodopsin and other class A GPCRs. H5 extends from amino acid 200 – 230 [50]. On the extracellular side, H5 is connected to the extracellular loop 2 (EL2), which has been shown to play an important role in ligand binding and receptor activation for not only rhodopsin but also other class A GPCRs [211-214]. The intracellular end of H5 is connected to H6 via the third cytoplasmic loop (CL3) (Fig. 5.1A). As explained in the next chapter, H6 undergoes a significant conformational change upon retinal isomerisation that is important for transducin binding to the activated receptor [18]

One of the highly conserved residues on H5 in class A GPCRs is a proline residue, Pro215$^{5.50}$. It is found in the middle of the transmembrane domain, with a sequence identity of 91% [7]. The backbone hydrogen bonding network in H5 is interrupted due to the presence of this proline, which causes the helix to develop a kink making it more flexible. However, the kink in H5 is not too pronounced in either rhodopsin [31] or the recent β2-AR crystal structure [52]

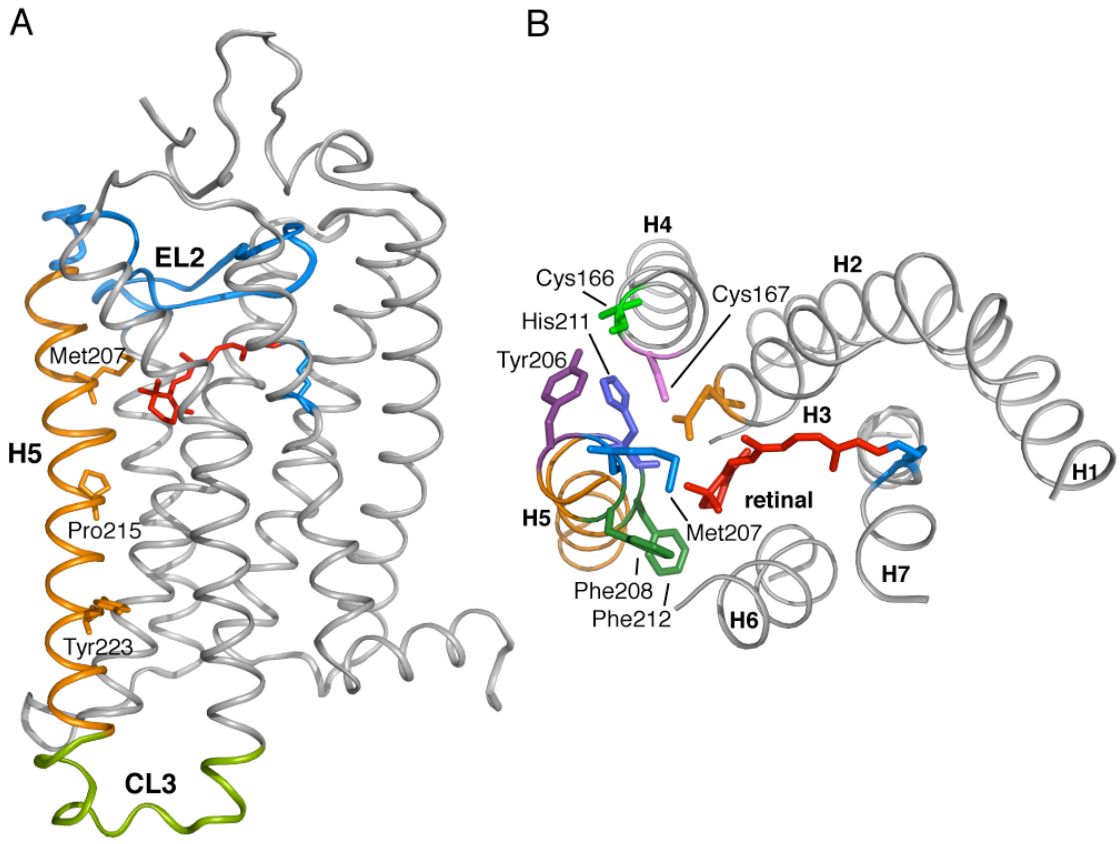


**Figure 5.1: View of the rhodopsin crystal structure highlighting H5.** (A) A front view of the rhodopsin crystal structure (pdb: 1GZM) [50] highlighting the position of H5 (orange). H5 extends from amino acids 200-230. H5 is important as it connected EL2 (blue) on the extracellular side and CL3 (green) on the intracellular side. (B) A view of the retinal binding pocket from the rhodopsin crystal structure from the extracellular side. The figure highlights the positions of residues on H5 (e.g. Met207, His211, Phe208, Phe212 and Tyr206) and their interaction with residues on the surrounding helices (H3 and H4) and retinal (red).

The presence of this proline disrupts the canonical α-helical hydrogen bonding interaction with a histidine residue at the i-4 position, His211on H5. This allows the backbone carbonyl of His211 to hydrogen bond to another residue in the protein. In the rhodopsin crystal structure [31] the His211 carbonyl forms an interhelical hydrogen bond with the side chain of Glu122 on H3. One of the advantages of this conserved proline is that it makes the helix more flexible and allows it to undergo conformational changes upon activation. The formation of a non-helical bulge due to the presence of the conserved proline can facilitate a see-saw movement of the helix where the two sides of H5 (extracellular and intracellular) about the proline can move independent of one another in opposite directions [23]. Mutation of Pro215 to leucine is responsible for autosomal dominant retinitis pigmentosa in patients [241]. Apart from above, there is no biophysical data available for any mutant of Pro215.

The other highly conserved residue on H5 is Tyr223$^{5.58}$ on the intracellular end of the receptor. It has sequence identity of 83% across the family of class A GPCRs. According to the rhodopsin crystal structure [50], the side chain of Tyr223 is facing the lipids and is not interacting with any other residue in the protein. Additionally, there is no mutational data available for this residue in the literature. The recent crystal structure of opsin [68], the unliganded state of rhodopsin following meta II decay, might shed some light on the role of Tyr223 in the activation mechanism of rhodopsin. In opsin, Tyr223 has rotated around to face the interior of the receptor and is involved in a hydrogen bonding interaction with the side chain of Arg135 of the conserved ERY sequence on the cytoplasmic end of H3. This interaction between Tyr223 and Arg135 might be important for stabilizing the conformation of the cytoplasmic end of H5, H6 and CL3 necessary for interaction with transducin. Similarly, in the recent, 2.4 Å crystal structure of the human β2-AR receptor-T4 lysozyme fusion protein bound to a partial inverse agonist, carazolol [52], the side chain of the residue equivalent to the conserved Tyr223 in rhodopsin is pointed in the general direction of the conserved DRY sequence on the cytoplasmic end of the H3.

Phe212 on H5 is 81% conserved in rhodopsin like GPCRs as a tyrosine or a phenylalanine [16]. It is located in the interface between H5 and H6. According to Holst *et al.*[242], the very high constitutive activity of the Ghrelin receptor is abolished by mutation of the residue analogous to Phe212 in rhodopsin. It plays an important role in ligand free activation of rhodopsin like GPCRs. It has been suggested [242] that this conserved phenylalanine on H5 might be important for locking the side chain of the highly conserved Tryptophan on H6 ($Trp265^{6.48}$ in rhodopsin) in a stable active conformation following the rotamer switch [243].

In this chapter, I will discuss the conformational changes that H5 undergoes as a result of retinal isomerisation and translation and its implications on the activation mechanism of rhodopsin and other class A GPCRs.

## *5.2 Location of the retinal in metarhodopsin II*

Analysis of helix-helix packing in rhodopsin shows that the H5-H6 interface is the most loosely packed in rhodopsin [79] and may provide a low energy path for the retinal to enter/exit the retinal binding site. In fact, a recent crystal structure of opsin lacking the retinal chromophore reveals an opening in the H5-H6 interface [68]. These studies are consistent with models where the retinal moves toward and contacts H6, placing the β-ionone ring in the H5-H6 interface.

However, in contrast to the idea that the retinal moves toward H6 following isomerization, studies using retinal analogs that can crosslink to the protein in the dark or following photoreaction place the ionone ring in the H4-H5 interface in meta II. Specifically, Nakanishi and colleagues found a crosslink between the β-ionone ring of retinal and Ala169 on helix H4 after illumination [244]. Bourne and co-workers noted that in the rhodopsin crystal structure a straight line drawn between Lys296 (H7) and Ala169

(H4) passes through helix H3 and suggested that this helix must consequently move upon activation [245]. Additionally, comparison of the recent 2.6 Å crystal structure of lumirhodopsin with the structure of rhodopsin reveals differences in the middle of H3 [89].

Recently, both nuclear magnetic resonance (NMR) and X-ray crystallography have suggested that the β-ionone ring does not change position upon isomerization of the retinal and formation of meta II. Watts and co-workers [246] argued that the β-ionone ring anchors the retinal in position and that retinal isomerization leads to motion of H6 by inducing changes in the dihedral angles of Tyr268 and Ala269 and that formation of the active meta II intermediate is largely dependent on the protonation of Glu134 in the ERY sequence in rhodopsin. Also, in a low-resolution crystal structure of a rhodopsin photointermediate having an unprotonated Schiff base [185], only minimal structural changes were observed relative to rhodopsin on the extracellular side of the receptor (see Fig. 5.9B). Both models suggest that the energy stored in bathorhodopsin is largely dissipated by structural changes in helix H6 and the cytoplasmic loops..

We have previously presented solid-state NMR measurements of rhodopsin showing that there is movement of the retinal toward H5 in meta II [100]. In this study [100], the retinal was labeled with $^{13}C$ at the C19 and C20 methyl groups, and at the C14 and C15 carbons of the polyene chain close to the retinal PSB linkage with Lys296. These measurements reported only on the position of the retinal methyl groups and the region of the retinal near the Schiff base, and consequently provided only weak constraints on the final position of the β-ionone ring relative to helix H5. As a result, it was not possible to distinguish between different models that had previously been proposed for the location of the retinal in meta II. Here, we extend our solid-state NMR studies on rhodopsin and meta II using retinals isotopically labeled on the retinal chain (C7, C12, C19, C20) and the β-ionone ring (C5, C6, C16, C17 and C18). These retinals are incorporated into rhodopsin containing $^{13}C$ labels on different amino acids (methionine, histidine, glycine, cysteine, lysine, tyrosine, tryptophan, threonine and phenylalanine) to define the location

of the retinal in the activated meta II intermediate. High-resolution structural constraints on rhodopsin and meta II were established using the two-dimensional (2D) dipolar-assisted rotational resonance (DARR) NMR experiment.

### *5.2.1 Location of the β-ionone ring relative to H5 in metarhodopsin II*

In this study we have used additional $^{13}$C DARR NMR measurements on rhodopsin to establish whether the β-ionone ring increases its contact with H5 upon activation. We targeted the terminal ε-methyl group of Met207, which is on the face of H5 oriented toward the β-ionone ring of the retinal. For these experiments, rhodopsin containing $^{13}$Cε-labeled methionine was regenerated with 11-*cis* retinal $^{13}$C-labeled at the C6 and C7 carbons (Fig. 5.1B).

Fig. 5.2A presents the 2D DARR NMR spectra of rhodopsin showing only the region containing crosspeaks between the $^{13}$C6, $^{13}$C7 retinal resonances and the $^{13}$Cε resonance of methionine. The rhodopsin spectrum (black) exhibits a weak crosspeak between the $^{13}$C7 resonance of the retinal chromophore and Met207 (14.7 ppm). The weak intensity of the Met207-C7 crosspeak (Fig. 5.2A) is consistent with the separation of 4.9 Å observed in the rhodopsin crystal structure [31]. No crosspeaks are observed between the $^{13}$Cε resonance of Met207 and the $^{13}$C6 resonance of the retinal; the 5.4 Å distance between these $^{13}$C labels is near the upper limit of the distance range of the DARR experiment [122]. Upon conversion to meta II (red), both the $^{13}$C6 and $^{13}$C7 resonances exhibit strong crosspeaks with the $^{13}$Cε-Met207 resonance at 13.8 ppm. The intensity of the meta II crosspeaks indicates that the C6 and C7 carbons are in van der Waals contact with Met207.

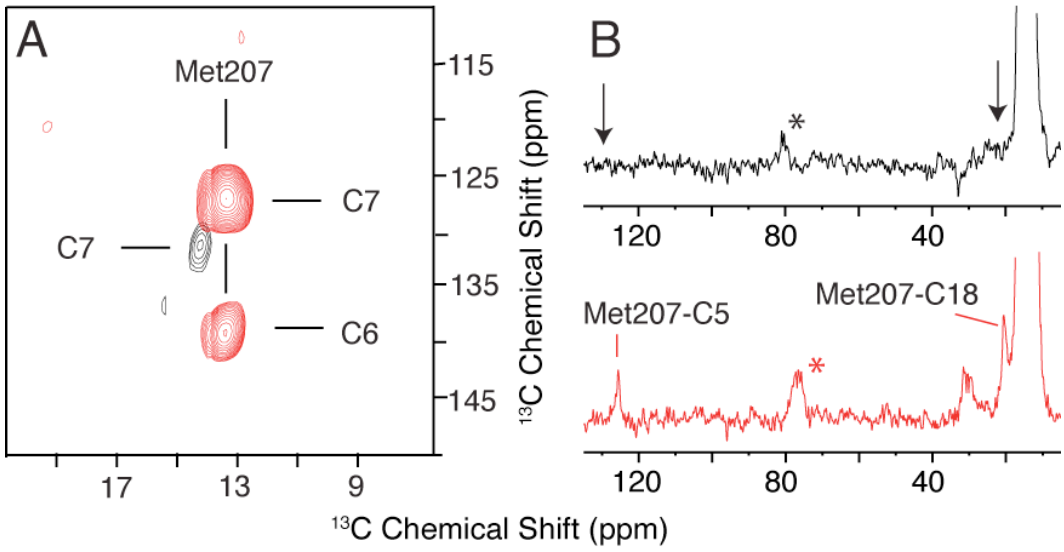


**Figure 5.2: 2D DARR NMR of rhodopsin and meta II labeled with $^{13}$Cε-methionine and regenerated with $^{13}$C6, $^{13}$C7-retinal or with $^{13}$C5, $^{13}$C18-retinal.** (A) Regions of the 2D DARR NMR spectra are shown for rhodopsin (black) and meta II (red) labeled with $^{13}$Cε-Met and regenerated with $^{13}$C6, $^{13}$C7-labeled retinal. A weak crosspeak is observed between the $^{13}$C7 resonance of the retinal (132.8 ppm) and the $^{13}$Cε resonance of Met207 (14.6 ppm) on H5 in rhodopsin. In meta II, the crosspeak between the $^{13}$C7 (127.6 ppm) retinal resonance and Met207 (13.8 ppm) gains intensity, and a new crosspeak is observed between the $^{13}$C6 (139.5 ppm) retinal resonance and Met207. (B) Rows through the $^{13}$Cε-Met diagonal resonance from the 2D DARR NMR spectra of rhodopsin (black) and meta II (red) labeled with $^{13}$Cε-Met and regenerated with 11-*cis* retinal labeled at $^{13}$C5 and $^{13}$C18 on the β-ionone ring. In rhodopsin, there were no crosspeaks observed between Met207 (14.7 ppm) and the $^{13}$C5 (131.0 ppm) or $^{13}$C18 (21.6 ppm) resonances of the retinal. On conversion to meta II, strong contacts are observed between the $^{13}$Cε methyl resonance of Met207 (13.8 ppm) and both the $^{13}$C5 (126.0 ppm) and $^{13}$C18 (20.9 ppm) resonances of the retinal.

NMR measurements were also made on rhodopsin containing $^{13}$Cε methionine and regenerated with $^{13}$C5, $^{13}$C18-labeled retinal. In the DARR NMR spectra for rhodopsin, crosspeaks were not observed between Met207 and either the $^{13}$C5 or $^{13}$C18 resonances of the retinal β-ionone ring. In the rhodopsin crystal structure [31], the Met207(Cε) – retinal C5 (6.7 Å) and the Met207(Cε) – retinal C18 (7.7 Å) distances are outside the range of the DARR NMR experiment. However, upon conversion to meta II, we observed strong crosspeaks between Met207 and both the $^{13}$C5 and $^{13}$C18 resonances on the β-ionone ring (Fig. 5.2B).

The Met207-C5/C6/C7/C18 contacts are consistent with our previous observation of movement of the retinal toward H5 [100]. However, the data do not tightly constrain the location of the ionone ring relative to H5 due to the flexibility of the long methionine side chain. In order to better establish the position of the ionone ring relative to H5 in meta II, additional $^{13}$C-$^{13}$C recoupling experiments involving the retinal and several amino acids in the H4-H5 and H5-H6 interfaces were undertaken.

To address the trajectory of the retinal suggested by retinal crosslinking to Ala169 on helix H4 [244], we obtained 2D DARR NMR spectra of rhodopsin $^{13}$C labeled at the Cβ carbon of Cys167 and at the C5, C6 and C7 carbons of retinal. On the basis of molecular modeling of the retinal binding site, Cys167 should be in close proximity to one of these carbons if the retinal adopts the position in the H4-H5 interface suggested by crosslinking to Ala169. In rhodopsin, the β-carbon of Cys167 and the C5-C7 carbons are separated by >7.8 Å. In the 2D DARR NMR spectrum of rhodopsin, no cysteine-retinal crosspeaks were observed (data not shown). Similarly, in the 2D DARR NMR spectrum of meta II we were unable to detect cysteine-retinal crosspeaks, arguing that the retinal C5-C7 carbons are more than 6 Å from the β carbon of Cys167 (Data not shown).

To observe contacts between the retinal chromophore and phenylalanine in the H5-H6 interface, we $^{13}$C-labeled the C16 and C17 methyl groups on the retinal β-ionone ring, as well as the ring carbons of phenylalanine. The $^{13}$C resonances of the aromatic ring of phenylalanine at 120-145 ppm are well resolved from the $^{13}$C resonances of the C16 and C17 retinal methyl groups between 25 and 33 ppm. Fig. 5.3A presents the one-dimensional MAS difference spectrum between rhodopsin (positive) and meta II (negative) in the region of the retinal methyl resonances. The positive peaks at 30.6 and 26.1 ppm have previously been assigned to the $^{13}$C16 and $^{13}$C17 resonances in rhodopsin [192]. On the basis of IUPAC nomenclature, the C1-C16 bond is oriented into the page in Fig. 3.2, while the C1-C17 bond is oriented out of the plane of the page. The difference in the $^{13}$C chemical shifts (4.5 ppm) of the C16, C17 resonances is attributed to one methyl group being in an equatorial orientation and the other methyl group being in an axial orientation with respect to the β-ionone ring. A steric contact between the methyl group in the axial orientation and the proton on C3 of the β-ionone ring results in an upfield chemical shift [192,206]. The negative peaks at 28.6 and 33.4 ppm correspond to the chemical shifts of the C16 and C17 methyl groups in meta II. The difference in chemical shift (4.8 ppm) of the $^{13}$C16- and $^{13}$C17-labeled methyl groups is again consistent with a difference in the relative orientation of the methyl groups. However, the shift of C16 from 30.6 to 28.6 ppm and C17 from 26.1 to 33.4 ppm indicates that C16 has now moved to the axial position in meta II.

Figs. 5.3B and C present rows extracted from the 2D DARR NMR spectra of rhodopsin containing $^{13}$C-ring-labeled phenylalanine and regenerated with 11-*cis* retinal $^{13}$C-labeled at the C16 and C17 positions. The rows are taken through the $^{13}$C resonance of the aromatic phenylalanine ring on the diagonal of the 2D spectrum. Vertical lines drawn from the MAS difference spectrum indicate the positions of the retinal-phenylalanine crosspeaks. There are 31 phenylalanines in rhodopsin. In the rhodopsin crystal structure, the closest ring carbons of Phe208 are 4.2 Å from C17 and 4.7 Å from

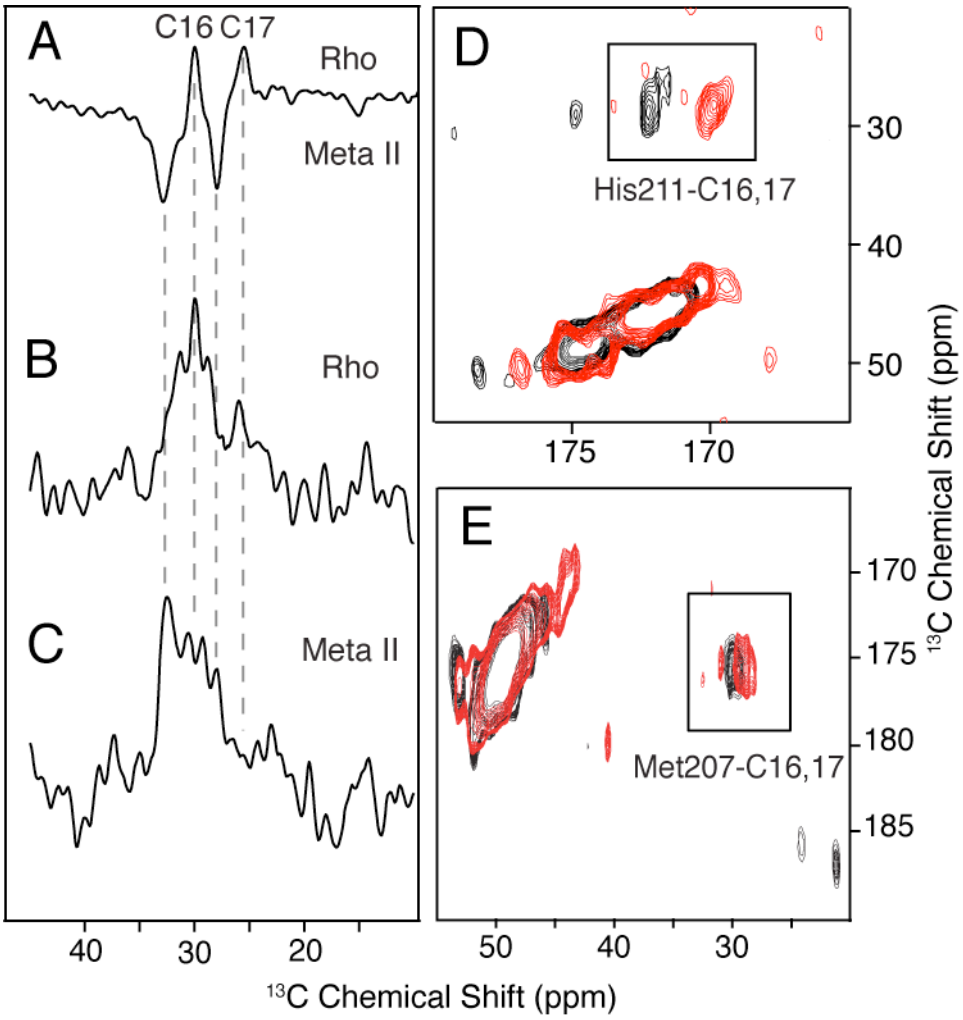


**Figure 5.3: Retinal $^{13}$C16 and $^{13}$C17 contacts with phenylalanine, histidine and methionine.** (A) NMR difference spectrum of rhodopsin (positive) minus meta II (negative) showing only the region of the $^{13}$C16 and $^{13}$C17 resonances of the retinal. (B) Row taken from the 2D DARR NMR spectrum of rhodopsin containing $^{13}$C-ring-labeled phenylalanine. The row passes through the diagonal $^{13}$C-ring resonances of phenylalanine, although only the region of the crosspeaks to the retinal $^{13}$C16 and $^{13}$C17 resonances is shown. (C) Row taken from the 2D DARR NMR spectrum of meta II of the same sample as in (B). Vertical lines are drawn to indicate the positions of Phe-retinal crosspeaks. (D) 2D DARR NMR spectra of rhodopsin (black) and meta II (red) using rhodopsin labeled at $^{13}$C1-histidine and regenerated with $^{13}$C16, $^{13}$C17 11-*cis* retinal. *E,* 2D DARR NMR spectra of rhodopsin (black) and meta II (red) using rhodopsin labeled at $^{13}$C1-methionine and regenerated with $^{13}$C16, $^{13}$C17 11-*cis* retinal. Boxes outline the regions of interest.

C16. Phe212 is the only other phenylalanine within 7 Å of the C16 and C17 methyl groups. Therefore, the contacts detected between phenylalanine and the $^{13}$C16 and $^{13}$C17 resonances at 30.4 and 26.1 ppm, respectively, in Fig. 5.3B are assigned to Phe208 and/or Phe212. While the 4.2 Å and 4.7 Å distances are within the range of the DARR experiment, the low signal intensity (compared to an isolated pair of $^{13}$C spins separated by the same distance) is due to dipolar truncation [121,247-249], which makes it difficult to measure a weak dipolar coupling in the presence of a strongly coupled network of spins.

Upon conversion to meta II, the crosspeaks assigned to retinal-phenylalanine contacts in rhodopsin disappear. New crosspeaks of similar intensity appear at the chemical shifts assigned to the $^{13}$C16 and $^{13}$C17 resonances in meta II (Fig. 5.3C). These contacts are also assigned to Phe208 and/or Phe212 based on the proximity of the retinal to Met207 discussed above. The similar intensities of the C16, C17-phenylalanine crosspeaks in the inactive and active states are consistent with the β-ionone ring maintaining an approximate distance of 4-5 Å from Phe208 and/or Phe212 in meta II.

To further characterize the interaction of retinal with H5, DARR NMR measurements were made between the retinal $^{13}$C16, $^{13}$C17 methyl groups and the backbone carbonyls of Met207 ($^{13}$C1) and His211 ($^{13}$C1). Fig. 5.3D presents the 2D DARR NMR spectra of rhodopsin (black) and meta II (red) containing $^{13}$C1-histidine and $^{13}$C16, $^{13}$C17-labeled retinal. His211 is the only histidine within 15 Å of the C16 and C17 methyl groups in rhodopsin. The $^{13}$C1-histidine chemical shifts for His211 in rhodopsin (136.9 ppm) and meta II (137.5 ppm) agree with those previously assigned to His211 [227]. Fig. 5.3E presents the 2D DARR NMR spectra of rhodopsin (black) and meta II (red) containing methionine $^{13}$C labeled at the carbonyl position and regenerated with $^{13}$C16, $^{13}$C17-labeled retinal. The Met-retinal crosspeaks in these spectra are assigned to Met207 based on the close proximity of these groups in rhodopsin. While His211($^{13}$C1)-retinal and Met207($^{13}$C1)-retinal crosspeaks are observed in both rhodopsin and meta II, an

increase of intensity upon conversion to meta II is consistent with tighter packing of the β-ionone ring of retinal with the backbone of H5.

### *5.2.2 Location of the polyene chain in metarhodopsin II*

In our earlier work [100], we had concluded that the retinal translates about 4-5 Å towards H5. This conclusion that the retinal moves toward H5 was based largely on the loss of crosspeaks between the retinal C19 methyl group and the Cζ carbons of Tyr191 (EL2) and Tyr268 (H6), as well as on the gain of a tyrosine contact with the retinal C20 methyl group that we had tentatively assigned to Tyr178 (EL2). To conclusively assign the C20-Tyr contact in meta II, we have obtained DARR NMR spectra of the Y178F rhodopsin mutant labeled with $^{13}$Cζ-tyrosine and regenerated with $^{13}$C12, $^{13}$C20-retinal.

Fig. 5.4 presents the DARR NMR spectra of the wild-type rhodopsin (left) and the Y178F mutant of rhodopsin (right). The figure presents rows through the diagonal resonance of tyrosine at ~156 ppm in both the dark-state of rhodopsin (black) and in the meta II intermediate (red). The upper panels (A and C) show the region containing retinal C12-tyrosine crosspeaks, while the lower panels (B and D) show the region containing the C20-Tyr crosspeaks. In rhodopsin (black spectra), we observe crosspeaks between Tyr268 and both the C12 and C20 resonances. The $^{13}$Cζ- carbon of Tyr268 is close to both C12 (4.9 Å) and C20 (4.2 Å) in the inactive state of rhodopsin [31].

In Figs. 5.4B and D, we observe a single retinal – tyrosine crosspeak in both wild-type meta II and the Y178F mutant of meta II (red spectra). The observation of a retinal-tyrosine crosspeak in the Y178F mutant rules out Tyr178 as the tyrosine having a direct contact with the C20 methyl group in meta II. According to the crystal structure, there

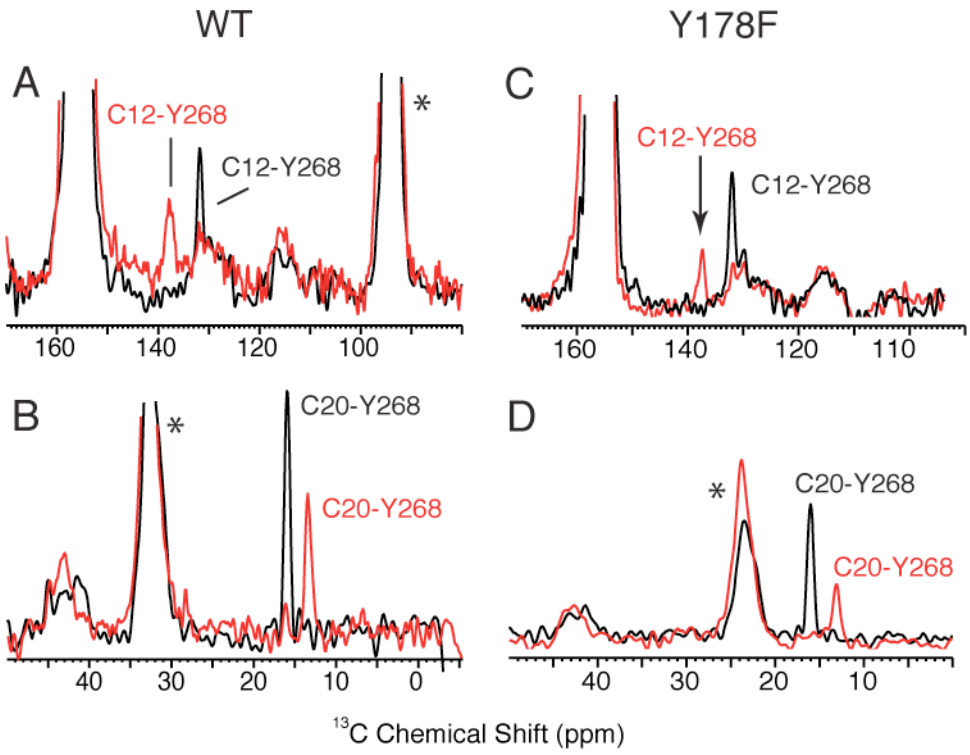


**Figure 5.4**: **2D DARR NMR of wild-type rhodopsin and the Y178F rhodopsin mutant labeled with $^{13}$Cζ-tyrosine and regenerated with $^{13}$C12, $^{13}$C20-retinal.** (A, B) Rows are shown taken through the $^{13}$Cζ-Tyr diagonal from the DARR NMR spectra of wild-type rhodopsin (black) and meta II (red). The region containing crosspeaks to the retinal C12 carbon is shown in *A* and to the retinal C20 carbon in B. (C, D) The same regions of the DARR NMR spectra of the Y178F mutant of rhodopsin (black) and meta II (red) are taken through the $^{13}$Cζ-Tyr diagonal. Asterisks indicate MAS sidebands.

are two other tyrosines in relatively close proximity to the C20 methyl group, Tyr268 on H6 and Tyr191 on EL2. We assign the C20-tyrosine crosspeak in meta II to Tyr268 on H6 (see below).

To assign the C20-tyrosine crosspeak to either Tyr191 (EL2) or Tyr268 (H6), DARR NMR measurements were made on rhodopsin and the Y178F mutant of rhodopsin $^{13}$C-labeled at $^{13}$Cα-glycine and regenerated with $^{13}$C12, $^{13}$C20-retinal. In the crystal structure of rhodopsin, the two closest glycines to the C20 methyl group are Gly188 on EL2 (6.2 Å) and Gly114 on H3 (7.2 Å) (Fig. 5.5A). We use the assignment of a single C20-glycine contact in meta II to either Gly188 or Gly114 to aid with the C20-tyrosine assignment. Fig. 5.5B presents rows through the C20 diagonal resonance showing contacts with glycines at 42.0 ppm and 45.4 ppm, which are assigned to Gly188 and Gly114, respectively (Fig. 5.5B, top). The chemical shift of 45.4 ppm resonance is consistent with the location of Gly114 in α-helical secondary structure. In meta II, both C20-glycine contacts are lost and a single new contact is observed at 46.4 ppm (Fig. 5.5B, bottom) in both the Y178F mutant and wild-type rhodopsin. We can assign the new 46.4 ppm resonance to Gly114 (H3) rather than Gly188 (EL2) since the same crosspeak is observed in the G188A mutant of rhodopsin (see Appendix, A.3).

The assignment of the C20-glycine contact to Gly114 in meta II has several implications. First, the additional distance constraints described above on Gly114 and in Section 6.2 on Thr118 agree with our previous conclusion [100] that the C20 methyl group undergoes a large rotation (>90°) upon *cis-trans* isomerization of the retinal, whereas the C19 methyl group remains roughly in the same position. Moreover, we find that in rhodopsin the C12 carbon exhibits crosspeaks to both Gly114 and Gly188, consistent with the crystal structure of rhodopsin [31]. However, these crosspeaks are lost in meta II indicating that the C12-C13-C20 plane is oriented such that the C20 methyl group is closer to Gly114 on the extracellular side of the binding site and C12 is pointing away from Gly114 (H3) toward the cytoplasmic side of the binding site.

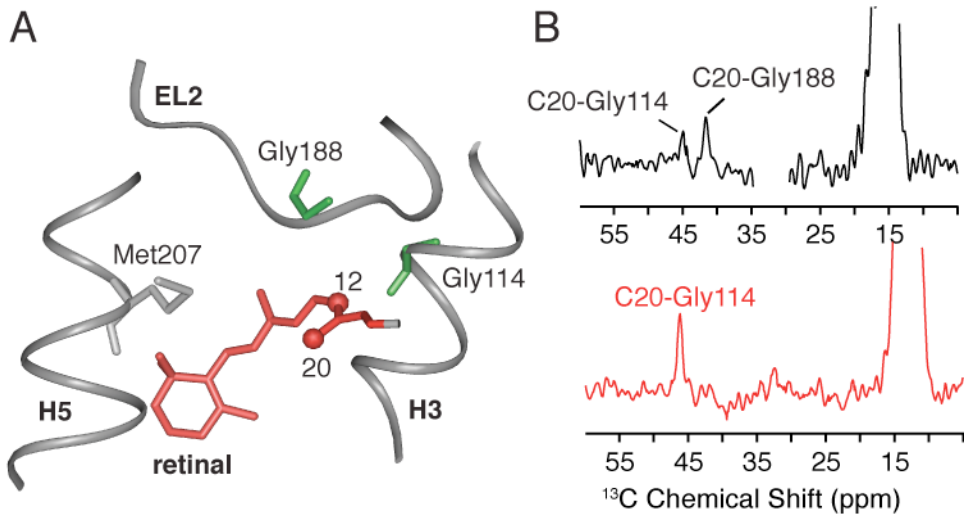


**Figure 5.5**: **2D DARR NMR of rhodopsin and meta II labeled with $^{13}$Cα-glycine and regenerated with $^{13}$C12, $^{13}$C20 retinal.** (A) View of the retinal-binding pocket highlighting the interaction of retinal with Gly188 on EL2 and Gly114 on H3. (B) Rows through the $^{13}$Cα-glycine diagonal of rhodopsin (black) and meta II (red). The crosspeaks between C20 and Gly188 on EL2 observed at 42.0 ppm and Gly114 on H3 at 45.4 ppm in rhodopsin are lost and a new crosspeak is observed between C20 and Gly114 on H3 at 46.4 ppm in meta II. (The rhodopsin spectrum in *B* is of the Y178F mutant obtained with a high signal-to-noise ratio; in wild-type rhodopsin we observe a single crosspeak at 42.0 ppm, which we assign to the closer C20-Gly188 contact.)

MD simulations (see Appendix A.1) using the C20-Gly114 assignment produce a model of the all-*trans* retinal in meta II with the C13-C20 bond oriented toward H3 at an angle of ~60° to the membrane normal. Independently, site-directed deuterium NMR studies on meta I by Brown and coworkers [183] have shown that the C13-C20 bond is oriented at an angle of 59±3°. Although the deuterium NMR studies are on meta I, they support the assignment of the C20-Gly114 contact in meta II.

Second, the assignment suggests that EL2 moves away from the retinal chromophore upon activation. The large rotation of the C20 methyl group agrees with the crystal structure of bathorhodopsin [90,250] that reveals a clockwise rotation of the C20 methyl group (viewed from the Schiff base end of the retinal) and a number of computational [31,251] and biophysical [183] studies. Such a rotation would place the C20 methyl group close to Gly188 on EL2 in the absence of EL2 motion. We had previously assumed that the position of EL2 did not change in the formation of meta II [100] because of the network of hydrogen bonding interactions involving EL2 and the extracellular ends of the transmembrane helices. This new data challenges this assumption. Moreover, recent DARR NMR distance measurements (explained in detail in Section 4.3) show that contacts between the retinal chromophore and the β4 strand of EL2 are lost in meta II.

Third, the assignment of the C20-Gly contact to Gly114 in meta II suggests that the C20-tyrosine contact is with Tyr268 rather than with Tyr191. In rhodopsin, the C20 methyl group has contacts with Tyr268 and Trp265, while the C19 methyl group has contacts with Tyr191 and Tyr268 [100]. In meta II, there are no tyrosine crosspeaks associated with C19, and, as noted, we observe only a single tyrosine crosspeak to C20. We had previously argued for a 4-5 Å translation of the retinal toward H5 in order to move the C19 methyl group away from Tyr191 and Tyr268. The distance constraints presented here and in the previous Chapter 4 on the motion of EL2, indicate that the translation of the retinal is more modest (~2 Å) and that EL2 moves away from the retinal

upon activation. Motion of EL2 away from the retinal chromophore would increase both the C19-Tyr191 distance and the C20-Tyr191 distance, leaving only Tyr268 in relatively close proximity to the C20 methyl group. We have not been able to confirm this assignment by mutational studies since mutation of Tyr268 to phenylalanine appears to alter its interactions with EL2 .

### *5.2.3 Location of the retinal Schiff base in metarhodopsin II*

The DARR NMR measurements described above between the β-ionone ring and amino acids on H5, and the C18 methyl group and Gly121, argue for a small (~2 Å) shift of the retinal toward H5. To obtain further support for motion of the retinal toward H5, we also measured the distance between the ε-carbon of Lys296 on H7 and the ε-$CH_3$ carbon of Met44 on H1 (Fig. 5.6B). The $^{13}$Cε-Met44 -to-$^{13}$Cε-Lys296 distance in rhodopsin is 4.7 Å. Fig. 5.6A presents rows through the $^{13}$Cε- diagonal resonance of methionine in the DARR NMR spectrum of rhodopsin (black) and meta II (red). The Met44-Lys296 crosspeak intensity decreases in the conversion to meta II consistent with an increase in the internuclear distance.

## *5.3 Rearrangement of H3-H4-H5 contacts in metarhodopsin II*

In this section, we describe additional solid-state NMR measurements to address the impact of retinal movement on the position of helix H5. Solvent accessibility studies [252] and recent DEER EPR measurements [88] have shown that the cytoplasmic end of H5 does not undergo large, rigid body motion as observed for H6. However, we have recently shown that an interhelical hydrogen bond between His211 on H5 and Glu122 on H3 is broken in meta II [227] suggesting a change in helix-helix packing and H5 motion. Below, we take advantage of

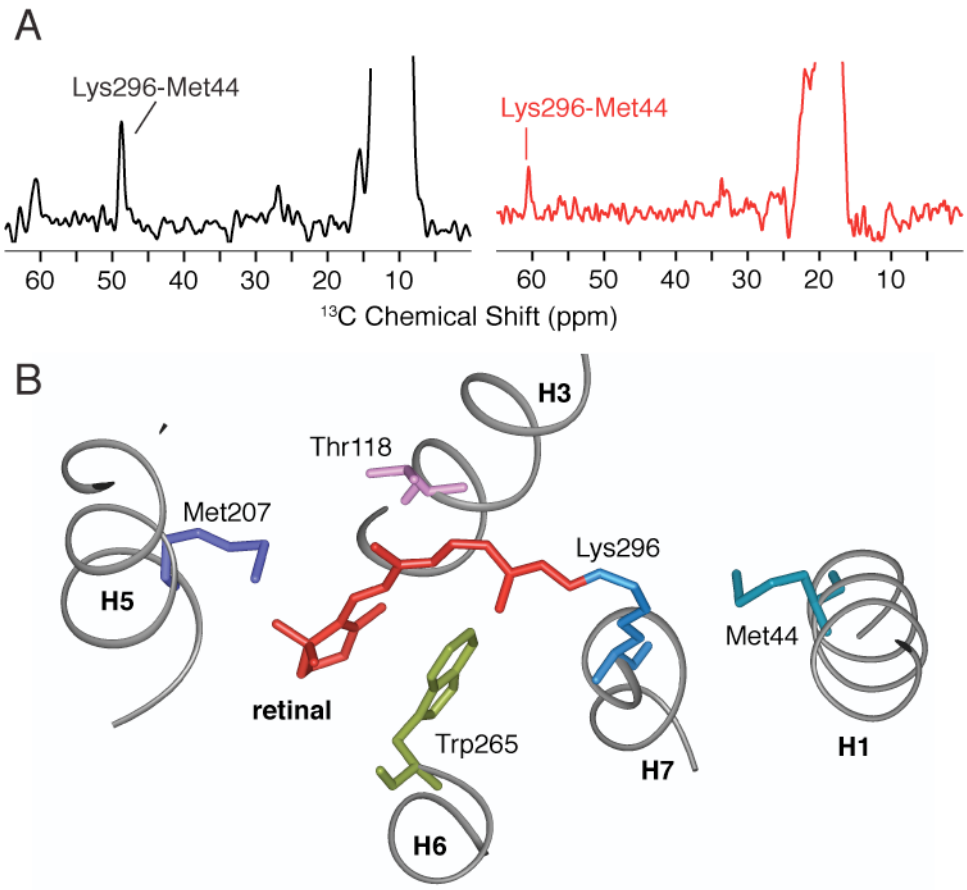


**Figure 5.6: 2D DARR NMR of rhodopsin and meta II labeled with $^{13}$Cε-methionine and $^{13}$Cε-lysine. (**A) Rows through the 2D DARR NMR spectra of rhodopsin (black) and meta II (red) taken through the Met44 (H1) diagonal resonance at 10.5 ppm showing the crosspeak with $^{13}$Cε-Lys296 (H7) at 49.1 ppm. On conversion to meta II (red) the crosspeak becomes weaker consistent with an increase in separation between Met44 (19.4 ppm) and Lys296 (60.8 ppm). (B) A view of the retinal binding site in rhodopsin (pdb code: 1U19) from the extracellular side of the protein highlighting the orientation of the retinal with respect to specific residues on H1 (Met44), H3 (Thr118), H5 (Met207), H6 (Trp265) and H7 (Lys296).

the known chemical shifts of His211, Met207 and Tyr206 to probe how the H4-H5 interface changes in meta II.

Fig. 5.7 shows the 2D DARR NMR spectra of rhodopsin (black) and of meta II (red) labeled with $^{13}$Cβ-cysteine, $^{13}$Cε-methionine, and $^{13}$Cε1-histidine in the region of the Met-Cys, His-Cys and His-Met crosspeaks. There are 10 cysteines, 16 methionines, and 6 histidines in rhodopsin. Fig. 5.7A shows the Cys-Met region of the full 2D NMR spectrum. In rhodopsin, there are no Cys-Met contacts observed since the closest Cys-Met pair is separated by more than 7.6 Å. In meta II, we observe a contact between Cys167 at 25.3 ppm and Met207 at 13.8 ppm, indicating that they are in close proximity (< 5.0 Å). The Met207 chemical shift in meta II is identical to that defined by the methionine-retinal ($^{13}$C6, $^{13}$C7) crosspeaks (Fig. 5.2A), while the Cys167 chemical shift is identical to that defined by the His211-Cys167 crosspeak (Fig. 5.7B).

A mutation of His211 to alanine allows us to unambiguously assign the resonance at 136.9 ppm in rhodopsin to His211 [227]. The $^{13}C\varepsilon_1$ resonances of the other 5 histidines in rhodopsin are observed as a broad line between 130 and 140 ppm. Above the 2D spectrum in Fig. 5.7B, we show rows taken through the diagonal of His211 in rhodopsin (black) and meta II (red). There is only one cysteine within 17 Å of His211, i.e. Cys167 at a distance of 3.9 Å. The His211-Cys167 crosspeak is observed at 23.7 ppm in rhodopsin. Similarly, the only methionine in close proximity to His211 is Met163 at a distance of 4.1 Å in rhodopsin. The next closest methionine in rhodopsin is Met207, which is 9.7 Å away. The broad His211-Met crosspeak at 13.1 ppm is consequently assigned to Met163.

In meta II (Fig. 5.7B, red), the His211-Cys167 crosspeak loses intensity and shifts to 25.3 ppm. The assignment to Cys167 can be made because it is the only cysteine within 17 Å of His211. The decrease in intensity of the histidine-cysteine crosspeak indicates that there is an increase in the His211-Cys167 distance.

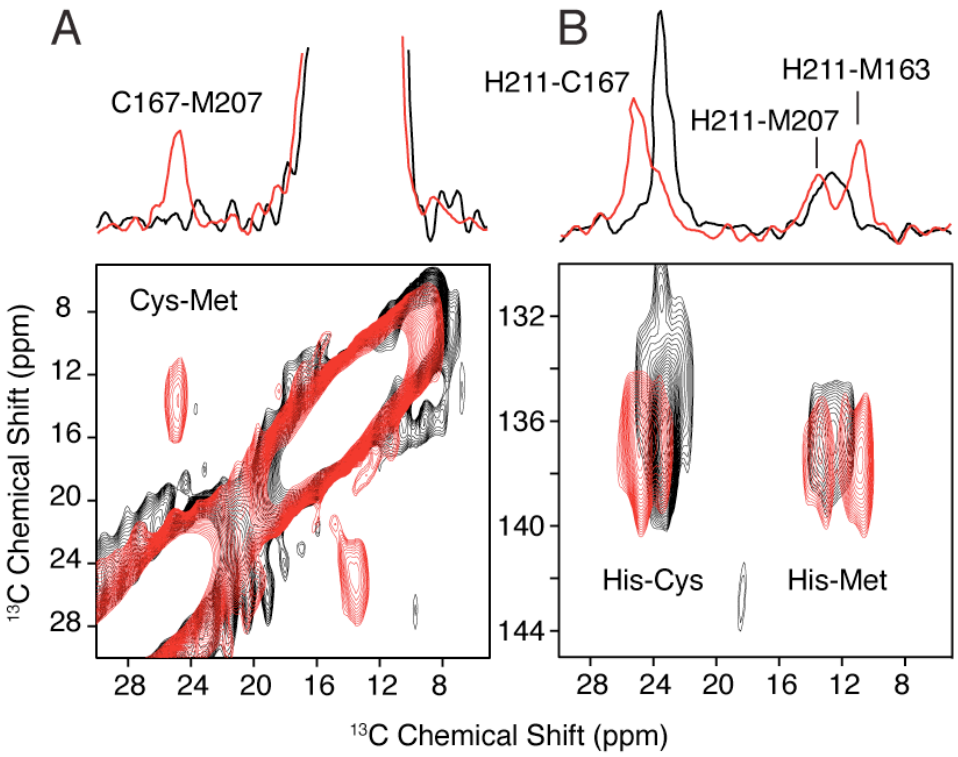


**Figure 5.7: 2D DARR NMR spectra of rhodopsin and meta II labeled with $^{13}$Cβ-cysteine, $^{13}$Cε-methionine and $^{13}$Cε1-histidine.** (A) Cys-Met contacts in rhodopsin (black) and meta II (red). Above the 2D spectrum are rows taken through the Met207 diagonal. A crosspeak with Cys167 at 25.3 ppm appears in meta II. (B) His-Cys and His-Met contacts in rhodopsin and meta II. Above the 2D spectrum are rows taken through the His211 diagonal in rhodopsin (136.9 ppm) and meta II (137.5 ppm). In rhodopsin, crosspeaks are observed with Cys167 at 23.7 ppm and Met163 at 13.1 ppm. In meta II, crosspeaks are observed with Cys167 at 25.3 ppm, Met207 at 13.8 ppm and Met163 at 11.2 ppm.

The His-Met region of the 2D DARR NMR spectrum in Fig. 5.7B also places constraints on the position of H5 in meta II. Two crosspeaks (red) are observed between His211 and methionine in meta II. There are only two methionines within 16 Å of His211 in rhodopsin. The crosspeak at 13.8 ppm is assigned to Met207 based on the chemical shift of the crosspeak observed between Met207 and the retinal $^{13}$C6, $^{13}$C7 carbons (Fig. 5.2A). The crosspeak at 11.2 ppm is assigned to Met163. These data indicate that the terminal methyl groups of both Met163 and Met207 are within 6.0 Å of His211.

The multiple contacts observed for Met207 in meta II provide strong constraints on its location. The Met207 side chain must be positioned between Cys167 and the retinal since we do not observe a retinal-Cys167 crosspeak in meta II. The chemical shift of Met207 undergoes a small (0.9 ppm) shift in frequency upon conversion from rho to meta II. The unique shift and narrow linewidth indicate that the Met207 side chain is not disordered. The decrease in intensity of the His211-Cys167 crosspeak and the appearance of a new Met207-Cys167 contact in meta II are consistent with motion of the extracellular end of the H5 helix and/or rearrangement of the side chains in the H4-H5 interface.

In rhodopsin, Tyr206 on H5 is also part of the hydrogen bonding network centered on H5. Tyr206 (Cζ-OH) is H-bonded to the side chain of His211 on H5 and the backbone carbonyl of Ala166 on H4. We have previously shown that the backbone carbonyl of His211 (H5) is H-bonded to the side chain of Glu122 in rhodopsin and that this hydrogen bond is disrupted in meta II [227]. The $^{13}$Cζ-Tyr206 resonance in rhodopsin is assigned at 154.8 ppm on the basis of a loss of intensity at this position in the rhodopsin half of the Y206F difference spectrum between rhodopsin and meta II (see Fig. 4.6, in Chapter 4) and on contacts with His211 on H5 in rhodopsin and meta II (explained below). In meta II we observe a distinct resonance at 153.6 ppm. We have assigned this upfield peak to Tyr206 on H5 on the basis of the loss of a Cζ-Tyr resonance at 153.6 ppm in the meta II component of the Y206F difference spectrum (see Fig. 4.6, in Chapter 4).

This upfield shift of $^{13}$Cζ-Tyr206 resonance is consistent with a weaker Cζ-OH hydrogen bond in meta II. We propose that the weaker Tyr206 hydrogen bond in meta II is caused, at least in part, by the loss of the Cζ-Tyr206 interaction with the Nε2-His211.

In the crystal structure of rhodopsin [31], Tyr206(Cζ) is the only tyrosine within 5.5 Å of His211(Cε1); the next closest tyrosine is 12.1 Å away. In rhodopsin, we observe a strong crosspeak between $^{13}$Cε1-His211 at 136.9 ppm and $^{13}$Cζ-Tyr206 on H5 at 154.8 ppm (see Appendix A.4). Upon conversion to meta II, the crosspeak shifts to 137.3 ppm for $^{13}$Cε1-His211 and 153.7 ppm for $^{13}$Cζ-Tyr206 (see Appendix A.4). The intensity of the crosspeak does not change significantly between rhodopsin and meta II indicating that the distance between the Cζ-Tyr206 and Cε1-His211 does not change appreciably upon activation.

Recently, Watts and co-workers have argued that the position of the β-ionone ring does not change upon the formation of meta II on the basis of an analysis of the $^{13}$C chemical shifts of the C16 and C17 methyl groups [246]. This conclusion is essentially correct relative to the large translation proposed by Nakanishi and co-workers [244]. However, the small, but significant, changes we observe, which are in disagreement with the detailed model proposed on the basis of an immobile ionone ring [246], are critical for rearrangement of Trp265 on H6, as discussed in Chapter 6. Changes in the chemical shifts observed due to sample illumination in the previous study [246] (~0.7 ppm for C17) are smaller than those observed here (2-3 ppm for both C16 and C17). The differences can arise from incomplete trapping of meta II or differences in the meta II intermediate trapped in lipid and detergent environments. We [253,254] and others [63,135] find that illumination of rhodopsin in DDM detergent results in nearly quantitative conversion (> 85%) to meta II, while illumination of rhodopsin in unsaturated lipids and ROS membranes results in a mixture of intermediates containing both protonated and unprotonated retinal Schiff bases at pH 7.0 [255].

## *5.4 Conclusions*

### *5.4.1 Rearrangement of the H3-H4-H5 interface*

The crosspeaks observed between the $^{13}C$ labels on the retinal and histidine, phenylalanine and methionine on H5 tightly constrain the position of the β-ionone ring between Met207 and Phe208 in meta II. Moreover, the observation of a new Met207-Cys167 contact and the lack of a contact between the retinal and Cys167 in meta II rules out the possibility that the β-ionone ring is located in the H4-H5 interface. These data argue that the position of the retinal derivative used in the crosslinking studies of Nakanishi and co-workers [244] is different than in wild-type meta II.

A structural model resulting from MD simulations guided by our NMR data (see Appendix A.1.) suggests an explanation for the role of the β-ionone ring in the formation and stability of meta II (Fig. 5.8). The crystal structure of rhodopsin shows a hydrogen bonding contact between the side chain of Glu122 on H3 and the backbone carbonyl of His211 on H5. The His211 carbonyl does not participate in main chain hydrogen bonding due to the highly conserved Pro215 at the i+4 position. In the meta II model derived from guided MD simulations, the β-ionone ring contacts the side chain of Glu122 on H3 as well as the backbone of H5 near His211. Retinal movement disrupts the hydrogen bond between the main chain carbonyl of His211 and the side chain of Glu122 as observed previously by solid state NMR [227]. The position of H5 now allows the formation of a new hydrogen bond between Glu122 and the His211 δ-nitrogen, which stabilize the meta II structure. Weakening of the hydrogen bond between His211 and Glu122 in meta II is further supported by FTIR studies conducted on WT rhodopsin and

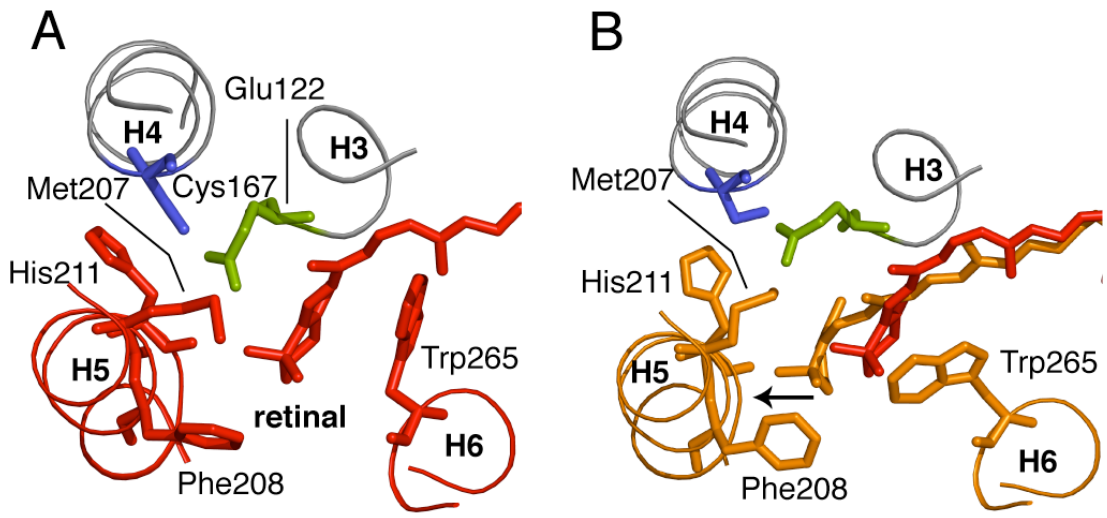


**Figure 5.8: Influence of retinal motion on H3-H5 interactions.** (A) A view of the rhodopsin crystal structure (pdb code: 1U19) from the extracellular surface showing the 11-*cis* retinal and key amino acids on H3, H4 and H5. (B) Structure of meta II obtained from a restrained molecular dynamics simulation (see supplemental data) showing the relative positions of all-*trans* retinal (orange) and helices H3-H5 after retinal isomerization. The position of the 11-*cis* retinal chromophore in rhodopsin is shown in red. The β-ionone ring of retinal contacts the side chain of Glu122 on H3 as the retinal moves forward upon formation of meta II. This motion of the retinal disrupts the hydrogen bonding interaction between the backbone carbonyl of His211 (H5) and the side chain of Glu122 (H3) and leads to a rearrangement of other bonding and non-bonding interactions between pairs of residues (such as Cys167-Met207, Trp126-Glu122, and His211-Tyr206) in the H3-H4-H5 interface. This rearrangement is essential for H5 to adopt an active conformation. Displacement of the β-ionone ring of the retinal allows the side chain of Trp265 and/or the backbone of H6 to move toward the extracellular side of the receptor triggering a shift in the positions of helices H6 and H7. The black arrow indicates the motion of retinal and the orange arrow indicates the direction of rotation and/or motion of H5 in meta II.

E122Q mutant [63] in DDM where an upshift of the carbonyl stretching vibration for Glu122 suggesting a weakening of its hydrogen bonding interaction was observed in rhodopsin to meta II transition.

The role of Glu122 and His211 in stabilizing the meta II state is supported by comparative studies between rhodopsin and the cone pigments, which lack these residues. Shichida and coworkers [256] found that substitution of Glu122 in rhodopsin with the corresponding amino acid in the green- or red-sensitive cone pigments converts the rate of retinal regeneration and meta II decay into those characteristic of the respective cone pigments. In contrast, when glutamate is substituted into the green-sensitive cone pigment, the rates of retinal regeneration and meta II decay are similar to those of rhodopsin.

The recent crystal structure of opsin [68], which is formed following the release of all-*trans* retinal in meta II, shows that the position of the helix H5 backbone is the same as in rhodopsin, although some of the side chain interactions predicted for meta II are retained (see Fig. 5.9). For example, the backbone carbonyl of His211 (H5) is no longer hydrogen bonded to the Glu122 (H3) side chain. Instead a new interaction is observed directly between Glu122 (H3) and His211 (H5) side chains consistent with our meta II data. Also, Trp126 (H3) has lost its hydrogen bonding interaction with Glu122 (H3) in opsin and appears to be hydrogen bonded only to His211 on H5. A weakening of the hydrogen bonding interaction for Trp126 was observed in meta II by NMR [65] and UV-visible absorption spectroscopy [66]. However, the hydrogen bonding interactions for Tyr206 in opsin are not consistent with recent NMR results showing that Tyr206 undergoes a significant weakening of hydrogen bonding in meta II. Also, the distance constraints obtained from our NMR experiments for pairs of amino acids in the H3-H4-H5 interface in meta II, such as His211(H5)-Cys167(H4), His211(H5)-Met163(H4), His211(H5)-Met207(H5) and Met207(H5)-Cys167(H4), are not consistent with the arrangement of residues in the

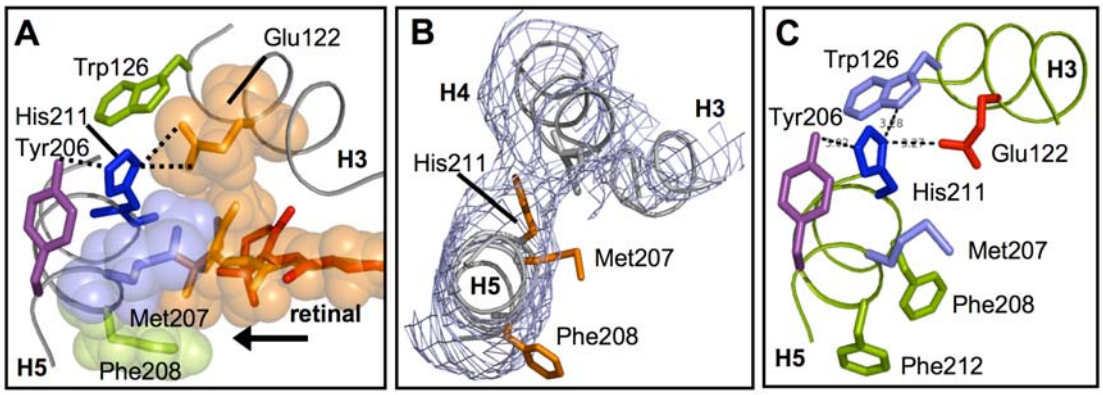


**Figure 5.9: Comparing the H3-H4-H5 interface from our simulation model for meta II (A) with the low resolution crystal structure for the photoactivated intermediate of rhodopsin [185] (B) and the opsin crystal structure [68] (C) influence of retinal motion on H3-H5 interactions.** (A) Upon conversion to meta II, the retinal moves toward H5 and packs between Met207 and Phe208. Retinal translation leads to a rearrangement of bonding and non-bonding interactions between residues in the H3-H4-H5 interface. This rearrangement is essential for H5 to adopt an active conformation. (B) The side chains of amino acids in the H3-H4-H5 interface of the low resolution crystal structure for the "photoactivated" state of rhodopsin are not resolved. (C) The crystal structure of opsin shows that the position of the extracellular end of helix H5 is the same as in rhodopsin, although some of the side chain interactions predicted for meta II are retained. It appears that the all-*trans* retinal chromophore holds helix H5 in an active conformation, and that loss of the retinal allows the receptor to shift (at least partially) back to an inactive conformation.

opsin crystal structure. As a result, it appears that mutiple interactions with the all-*trans* retinal chromophore holds helix H5 in an active conformation, and that loss of the retinal allows the receptor to shift (at least partially) back to an inactive conformation. These changes are in agreement with retinal analog studies where replacement of the β-ionone ring by two ethyl groups inhibited formation of meta II due to the lack of interactions with the protein (particularly H5) that are necessary for stabilizing the active state [139,257]. Ernst and coworkers [258] showed that regeneration of rhodopsin with acyclic analogues of retinal with the C17 and C18 methyl groups preserved formed low amounts of meta II with WT kinetics. However, they observed a fast decay of its activity suggesting that the β-ionone ring is important for stabilizing the active conformation of rhodopsin.

### *5.4.2 Motion of H5 upon retinal isomerization*

As mentioned above, on the extracellular side of H5, the hydrogen-bonding interaction between the Glu122 side chain and the His211 backbone carbonyl has been broken and a new interaction is observed directly between their side chains. This observation suggests that H5 must undergo a rotation/and or motion upon formation of meta II. Additionally observation of strong contacts between the side chain of Met207 (H5) and C6, C7, Cys167 (H4) and His211 (H5) are consistent with a movement of H5, as the data alone cannot be explained by a rearrangement of the Met207 side chain. Further support for the motion of H5 comes from the observation of a weakening of the contact between His211 (H5) and Cys167 (H4) in meta II.

Our observation regarding motion of H5 is not consistent with site directed spin labeling (SDSL), EPR studies conducted by Hubbell and co-workers [88,154], where they did not observe a significant motion of the intracellular end of H5. They observed a single nitroxide label (R1) introduced at site 227 in rhodopsin become more immobile upon meta II formation. The gain in tertiary contacts at 227R1 in meta II has been explained as a restriction of the side chain mobility due to a movement of the cytoplasmic end of H6

towards H5 in meta II as seen by a simultaneous increase in the mobility of an additional spin label at site 250, on the cytoplamic side of H6.

However, they did observe an increase in the mobility of a spin label introduced at site 140 on the cytoplasmic end of H3 in the H3-H5 interface. This observation is consistent with a motion of the cytoplasmic end of H5 away from the H3-H5 interface. Furthermore, the cytoplasmic end of H5 in the recent opsin crystal structure [68] appears to adopt the 'active' conformation of the receptor. The cytoplasmic end of H5 has moved inward and rotated to place conserved Tyr223, i.e. 4 residues below V227 on H5, in contact with Arg135, breaking the ionic lock. The NMR results showing a movement of H5 due to steric interactions with the ionone ring and coupling with EL2 (explained in more detail in Chapter 4 and 6) are consistent with the key role of H5 motion in activation. In light of the above-mentioned observations, the increase in the immobility observed for the spin label at site 227 on H5 in the EPR data [88,154] can be due to the motion of the cytoplasmic ends of H5 and H6 towards each other upon meta II formation.

Nevertheless, further studies defining the position of H5 will be important since this helix connects EL2 and CL3, and recent DEER EPR measurements [88] and crosslinking studies by Oprian and co-workers [87], using engineered disulfide bonds in the H3-H5 (Cys140-225) and the H5-H6 interfaces (Cys204-276) suggest that the motion of H5 is limited.

On the extracellular side, H5 is connected to EL2, which has been shown to be important for ligand binding and activation [211-214]. In the chapter 4, I have explained how our data suggests that the extracellular end of H5-EL2 behave as one structural unit with the extracelular end of H4, which undergoes distinct conformational change upon receptor activation. This is in agreement with the global toggle switch mechanism for GPCR activation introduced by Schwartz and co-workers [242]. The subfamily specific H4-EL2-H5 unit in rhodopsin is designed to hold H5 and the extracellular ends of H6 and H7

in inactive conformations. We propose that the displacement of EL2 away from the retinal binding site, upon retinal isomerisation, is coupled to motion of the H5 and to the inward motion of the H6-EL3-H7 unit (explained in Section 4.6.3). Similar motions are likely to occur in other GPCRs [23,240] suggesting that EL2 may act as a plug or cork that must be displaced for receptor activation.

## *5.5 H5 in other class A GPCRs*

H5 in many other class A GPCRs has been shown to interact with receptor-specific ligands. For instance, in the amine receptors (such as the β2-adrenergic receptors), the amino acids corresponding to Met207, Phe208 and His211 in rhodopsin are conserved as serines (Ser203 (5.42), Ser204 (5.43) and Ser207 (5.46)). These serines, hydrogen bond to the hydroxyl groups on the catechol ring of the amine agonist to stabilize an active receptor conformation [259-261]. These interactions have shown to be critical for agonist binding and stabalization of the active receptor structure. Mutation of these residues to alanines greatly affected the binding efficiency of the receptor to these catecholamine agonists. However, these mutations did not affect the binding affinities to the antagonists. These serines are conserved for all the GPCR subfamilies that bind to agonists with catecholamine ligand such as $\alpha_1$-, $\alpha_{2A}$-, $\alpha_{2B}$, $\beta_1$-, $\beta_2$-adrenergic and $D_2$-dopamine receptors. In the dopamine [233] and serotonin [262] receptors, the amino acids at the positions equivalent to His211 and Phe212 have been shown to interact with their receptor-specific ligands.

These findings have been validated by a high resolution, 2.4 Å crystal structure that was recently obtained for a modified form of the human $\beta_2$-adrenergic receptor [52]. T4-Lysozyme was engineered in place of the third cytoplasmic loop (CL3) to reduce structural heterogeneity and to assist in crystallization. It provides some useful insights into the structure of the amine receptor and its interaction with a diffusible partial agonist, carazolol.

Further support for the involvement of residues on H5 in the activation mechanism of other class A GPCRs comes from metal binding studies conducted on the κ-opioid and NK1 tachykinin receptor, where introduction of a metal binding site at the extracellular end of H5 blocked ligand binding and receptor activation [263,264]. On the contrary, binding of Zn(II) at the natural metal binding site on the extracellular end of H5 in the NK3 tachykinin receptor enhanced agonist binding [265]. Therefore, the exact nature of the role of the extracellular end of H5 maybe sub-family specific but is important in the activation mechanism.

According, to the rhodopsin crystal structure [31] the conserved proline, Pro215 creates an unusual helix bulge on the kinked H5 that allows different parts of the helix above and below the proline to assume different rotational orientation of the side chains. It allows certain amino acids on H5 to orient their side chains toward the retinal binding site. Molecular dynamics simulations have shown the presence of a similar unusual bulge in the pro-kinked H5 of the dopamine receptor [266].

As mentioned previously, Pro215 is highly conserved among the class A GPCRs. However, there are two families of receptor that do not have a conserved proline on H5: glycoprotein harmone receptors, such as TSH, LH and FSH receptors and the melanocortin receptor (MC) family, which includes the cannabinoid and sphingolipid receptors. These families are extremely prone to agonist binding and are easy to activate. In the melanocortin receptor family the extracellular end of H5 is kept close to H4 by a very short EL2 that provides an open ligand binding site and allows movement of the extracellular ends of H6 and H7 inwards towards their active conformations [242]. Therefore, one of the main roles of the extracellular end of H5 in receptor activation could be to hold the receptor in an inactive conformation by preventing the extracellular ends of H6 and H7 from moving inwards [242].

# Chapter 6

# Motion of the β-ionone ring: trigger for motion of H6

## *6.1 Introduction*

A wealth of biophysical data has been collected over the last decade that suggests a movement of the cytoplasmic end of the TM H6 of rhodopsin upon activation. Cysteine crosslinks established between the cytoplasmic ends of H3 and H6, which prevented their relative motion, rendered the receptor inactive and suggested H6 motion is important for activation [18]. A recent EPR study conducted on selectively introduced nitroxide spin labels at the cytoplasmic end of TM helices in rhodopsin is consistent with a 5.0 Å outward movement of the cytoplasmic end of H6 away from H3 [88]. Substituted cysteine accessibility studies on rhodopsin [267] and $\beta_2$-AR [78] are consistent with this model. Similar studies as mentioned above have been conducted on other GPCRs that suggest a movement of H6 upon activation [268,269].

A recent crystal structure proposed for the native opsin, a ligand free state following meta II decay, shows a clear outward movement of the cytoplasmic end of H6 by 6-7 Å [68]. However, SDSL studies performed on mutants of rhodopsin where the salt bridge between Glu113 (H3; counterion) and Lys296 (H7)

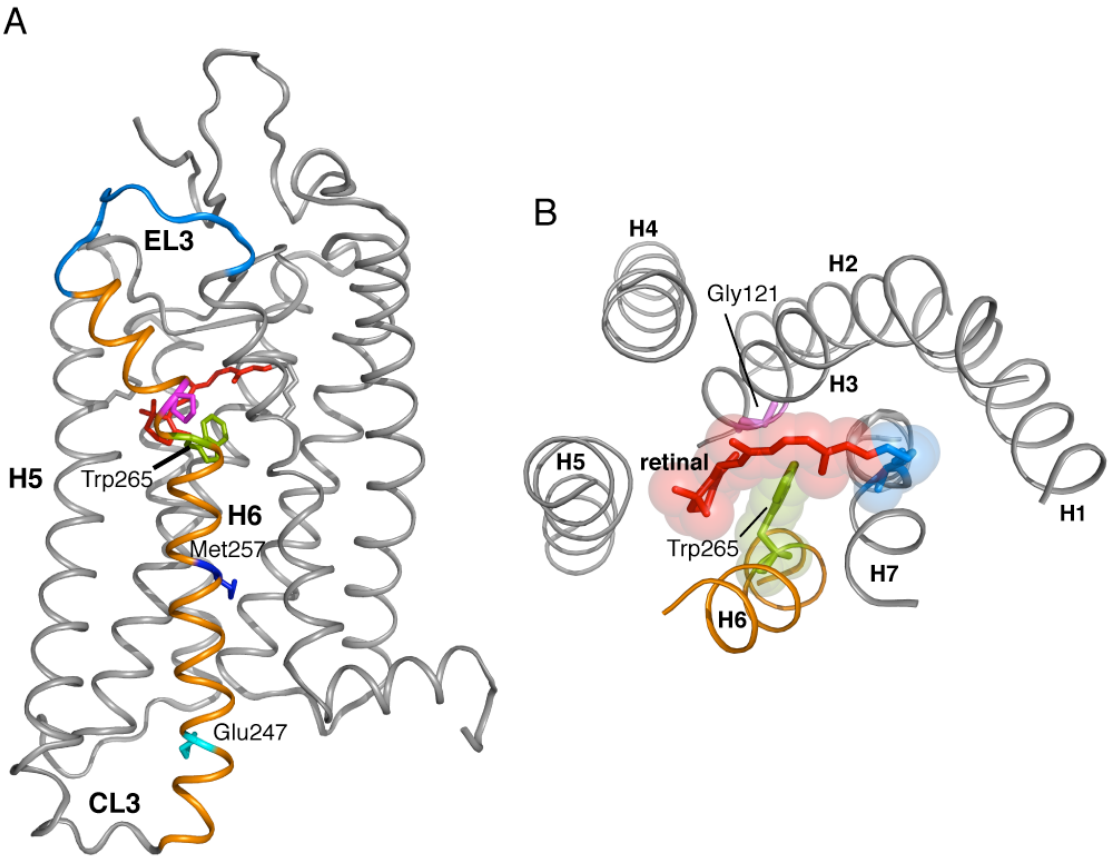


**Figure 6.1: View of the rhodopsin crystal structure highlighting H6.** (A) A front view of the rhodopsin crystal structure (pdb: 1GZM) [50] highlighting the position of H6 (orange). H6 extends from amino acids 241-276. H6 is connected to EL3 (blue) on the extracellular side and CL3 (grey) on the intracellular side. Studies have shown that the cytoplasmic part of H6 undergoes a large motion upon activation. Important residues and their location highlighted on H6 are, Pro267 (magneta), Tyr265 (green), Met257 (dark blue) and Glu247 (cyan) (B) A view of the retinal binding pocket from the rhodopsin crystal structure from the extracellular side. The figure highlights the tight packing between the side chain of Trp265 on H6 and the retinal chromophore (red).

is broken, such as E113Q, A292E and G90D, caused changes in the nitroxide spin labels on the cytoplasmic side of H5 and H6 that indicated a movement of H6 even when the mutant receptor was locked off in the inactive state in the presence of 11-*cis* retinal [154]. All the data presented above suggest that movement of H6 is essential for activation but must be accompanied by additional changes significant for the functional state of the receptor.

H6 extends from amino acid 241-276 [50]. The extracellular side of H6 has a conserved (F/Y/W)XXX(W/Y)XPY motif rich in aromatic residues and a proline (Fig. 6.1). Pro267 is one of the most conserved residues in class A GPCRs, with sequence identity of 99%. In the rhodopsin crystal structure, a strong kink (30°) is observed in H6 around this proline [31]. Computational and experimental studies suggest that Pro267 serves as a hinge to facilitate H6 motion [19,270-272]. The water accessibility studies in the dopamine receptor [273] have shown a kink in TM H6 similar to rhodopsin. Mutagenesis studies on the $\beta_2$-AR receptor have shown that straightening of the kink in H6 drives movement of H6 [272]. Other members of this motif include Phe261 (85%), Trp265 (85%) and Tyr268 (70%). This functional microdomain lines the retinal binding site and has been implicated in ligand binding and activation in rhodopsin and other GPCRs [59,273-277].

Phe261 is highly conserved across the family of class A GPCRs. It plays an important role in spectral tuning of the red and green cone pigments [278]. Mutation of Phe261 to smaller amino acids, such as threonine and alanine produced rhodopsin pigments that exhibited lower light-dependent activation of transducin in detergents and membranes. This effect was rescued by simultaneous mutation of a Gly121 on H3 to larger amino acids (e.g. leucine) [279]. Thus, interactions between H3 and H6 have important implications in transmitting significant conformational changes to the cytoplamic side of the protein upon isomerization of the 11-*cis* retinal.

Another important member of the conserved aromatic motif on the extracellular side of H6 is Trp265. It is highly conserved (91%) in the visual pigments. The side chain of Trp265 lies in an arc created by 11-*cis* retinal and the side chain of Lys296, in the chromophore binding cavity. The indole ring of Trp265 is tightly packed against the β-ionone ring of the 11-*cis* retinal, Gly121 on H3 and Ala295 on H7 in rhodopsin [31]. As a result of this tight packing interaction, Trp265 has one of the lowest thermal B-factors in the rhodopsin crystal structure. The indole side chain of Trp265 is interacting with Asn302, which is part of the highly conserved NPxxY motif on H7, through water-mediated hydrogen bonds. This tight packing and multiple interactions of Trp265 with residues on H7 are thought to be responsible for locking the receptor off in the dark and for the extremely low level of basal activity of the apoprotein.

Crosslinking studies by Borhan *et al.* have shown that strong interactions between the β-ionone ring and the indole side chain of Trp265 are responsible for the inverse agonist behavior of 11-*cis* retinal. Upon isomerisation of the retinal, the ionone ring moves away from Trp265 [244]. Additionally, Javitch and coworkers have proposed the "rotamer toggle switch" mechanism of activation for ligand activated GPCRs, where ligand binding to the aromatic residues on H6 may induce a change in the side chain conformation of a Phe261$^{6.52}$, Trp265$^{6.48}$ and Cys264$^{6.47}$ which may lead to receptor activation by modulating the conformation of H6 about the kink introduced by the highly conserved, Pro267$^{6.50}$ [272]. Apart from the above-mentioned models, mutational studies on Trp265 have demonstrated that mutants of Trp265 significantly reduce the light dependent activation of transducin and hinder the regeneration of rhodopsin by 11-*cis* retinal [280].

Tyr268 is also part of the conserved aromatic motif on the extracellular side of H6. The aromatic ring of Tyr268 is interacting closely with the C11=C12 double bond in the retinal polyene chain [50] and is involved in hydrogen bonding interactions with Tyr191 and Glu181 on EL2 [50]. NMR data presented in Section 4.4 (Fig. 4.6) for the Y268F

mutant suggest that hydrogen bonding network rearranges in meta II with Tyr268 becoming more strongly hydrogen bonded (discussed in Chapter 4). Additionally, it also known that mutation of Tyr268 to phenylalanine reduces the light dependent transducin activation of rhodopsin [280]. This suggests that the aromatic residues lining the binding cavity are not only important for ligand binding but are also essential for maintaining the hydrogen bonding interactions that stabilize the inactive and active state structure of the receptor.

Glu247, present on the cytoplasmic side of H6, is highly conserved among various rhodopsin like GPCRs such as opsin, neurotransmitters and glycoprotein hormone receptors. In rhodopsin [50], it forms an ionic lock with Arg135 (H3), part of the highly conserved ERY sequence on the cytoplasmic side of H3. Mutation of the amino acid corresponding to Glu247 in a number of GPCRs, such as the $\beta_2$-AR [78], the muscarinic acetylcholine receptor [281] and the gonadotropin-releasing hormone receptor [282], has shown an increase in basal activity and agonist dependent activation.

These studies raise the question as to how retinal isomerization on the extracellular side of H6 is coupled to the outward rotation of the cytoplasmic end of H6. In the next section, $^{13}$C DARR NMR measurements are described on rhodopsin $^{13}$C-labeled at Thr118 (H3), Gly121 (H3) and Trp265 (H6) and regenerated with 11-*cis* retinal $^{13}$C-labeled at the C18 and C19 methyl groups to further address how isomerization of the retinal acts as a trigger for the motion of H6.

## *6.2 Location of Trp265 in metarhodopsin II*

We have used solid-state MAS NMR spectroscopy to obtain structural constraints on the position of the side chain of Trp265 and its interaction with other residues on the surrounding helices and retinal carbons in rhodopsin and meta II [65]. The side chain of Trp265 is packed between Gly121 on H3 and Ala295 on H7 [31]. Gly121 on H3 is highly

conserved among all visual pigments. Mutagenesis data [283] mentioned above have shown that mutation of Gly121 to bigger residues leads to formation of thermally unstable pigment that is highly susceptible to hydroxylamine in the dark. The mutants show a high degree of dark activity. We studied changes in $^{13}C\ldots^{13}C$ 2D DARR NMR [65,122] contacts between the uniformly $^{13}C$-labeled indole side chain of Trp265 on H6 and $^{13}C\alpha$-Gly121 on H3. We observed a crosspeak between Trp265 (Cζ3, Cε3 and Cη2) and Gly121 (Cα) in dark rhodopsin consistent with a separation of < 6.0 Å according to the crystal structure [31]. On conversion to meta II, the contact was lost indicating that Trp265 and Gly121 have moved apart (> 6.0 Å) from one another [65]. This observation is consistent with a movement of H6 away from H3 upon activation at the position of Trp265.

The presence of Trp265 close to the highly conserved kink in H6 due Pro267 has led us to suggest that the large indole side chain of Trp265 act as lever for the outward motion of H6 observed upon activation. To further constrain the location of the Trp265 side chain we uniformly $^{13}C$ labeled tyrptophans in rhodopsin and regenerated the sample with retinal $^{13}C$ labeled at the retinal $^{13}C19$ and $^{13}C20$ methyl groups [65]. In rhodopsin, we observed $^{13}C\ldots^{13}C$ DARR NMR contacts between the indole ring of Trp265 and the $^{13}C20$ methyl group on the polyene chain. These contacts were lost upon meta II formation indicating that Trp265 and the C20 methyl groups are greater than 6.0 Å away from one another. However, we observed strong contacts between the $^{13}C19$ methyl group and most of the carbons on the side chain of Trp265 in meta II.

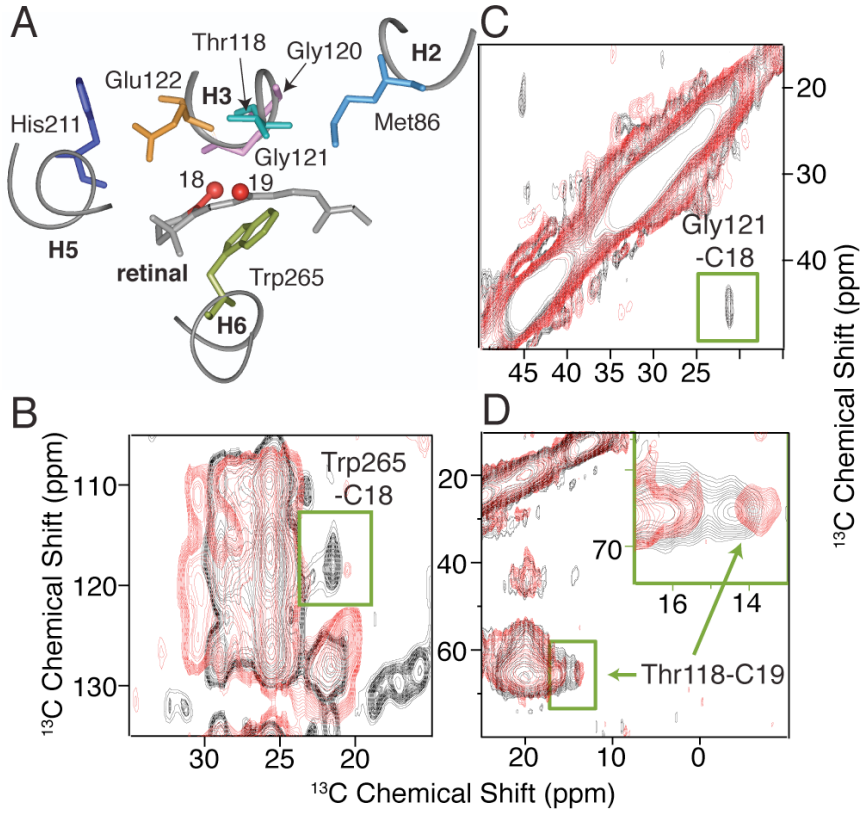


**Figure 6.2: Location of Trp265 in the retinal binding pocket.** (A), View of the retinal-binding pocket highlighting the interaction of the C18 methyl group on the β-ionone ring of the retinal with Gly121 (H3) and Trp265 (H6), and the interaction of the C19 methyl group on the retinal polyene chain with Thr118 (H3). Panels (B), (C) and (D) present 2D DARR NMR spectra of rhodopsin (black) and meta II (red). (B) Region of Gly121-retinal C18 contacts. In rhodopsin, a crosspeak (highlighted by a green box) is observed between the $^{13}C\alpha$ resonance of Gly121 on H3 and the retinal $^{13}C18$ methyl group, consistent with a separation of 3.7 Å (pdb: 1U19). This contact is lost upon conversion to meta II. (C) Region of Trp265-retinal C18 contacts. In rhodopsin, a weak contact is observed between the ring carbons of U-$^{13}C$-Trp265 and the retinal $^{13}C18$ methyl group. This contact is lost in meta II. (D) Region of Thr118-retinal C19 contacts. In rhodopsin, a crosspeak between U-$^{13}C$-Thr118 on H3 and the retinal $^{13}C19$ methyl group overlaps with the intense intra-residue crosspeaks of U-$^{13}C$-Thr118. The crosspeak is more clearly resolved in meta II (red) where the $^{13}C19$ resonance has shifted to a lower frequency. The observation in meta II of a retinal C19-Thr118 crosspeak of roughly the same intensity as in rhodopsin indicates that the retinal-Thr118 distance does not change considerably upon activation.

These contacts were not observed in rhodopsin as the C19 methyl group is about 6.1 Å away from the Trp265 side chain. This suggests that the Trp265 side chain is packed against the C19 methyl group in meta II.

In the rhodopsin crystal structure [31], the side chain of the highly conserved Trp265 (H6) is tightly packed against the β-ionone ring of the retinal (Fig. 6.1B). The retinal C18 methyl group is at 3.7 Å from the nearest indole ring carbon. To test whether the retinal C18 methyl group remains in contact with Trp265 after conversion to meta II, we obtained 2D DARR NMR spectra of rhodopsin and meta II containing U-$^{13}$C-tryptophan, $^{13}$Cα-glycine and $^{13}$C5, $^{13}$C18-retinal. We observe a weak crosspeak between the aromatic ring carbons of Trp265 and the C18 methyl group in rhodopsin (Fig. 6.2B). The crosspeak is not observed in meta II consistent with an increase in the distance between the β-ionone ring and Trp265. We attribute the weak intensity of the C18-Trp265 crosspeak in rhodopsin to dipolar truncation [121,247-249], a problem encountered in the measurement of long internuclear distances (i.e. weak dipolar couplings) using uniformly $^{13}$C labeled amino acids (i.e. in the presence of strongly $^{13}$C coupled networks).

To assess the contribution of dipolar truncation to the observed intensities in rhodopsin containing U-$^{13}$C-tryptophan, $^{13}$Cα-glycine and $^{13}$C5, $^{13}$C18-retinal, DARR NMR experiments were run on a parallel rhodopsin sample containing only $^{13}$Cα-glycine and $^{13}$C5, $^{13}$C18-retinal. Figs. 6.3A and 6.3B correspond to rows through the retinal C5 diagonal at 131.0 ppm of these two rhodopsin samples. The crosspeak at 21.6 ppm arising from the directly bonded C5-C18 carbons increases in intensity when Trp265 is not $^{13}$C-labeled, consistent with dipolar truncation being the cause of the intensity loss in

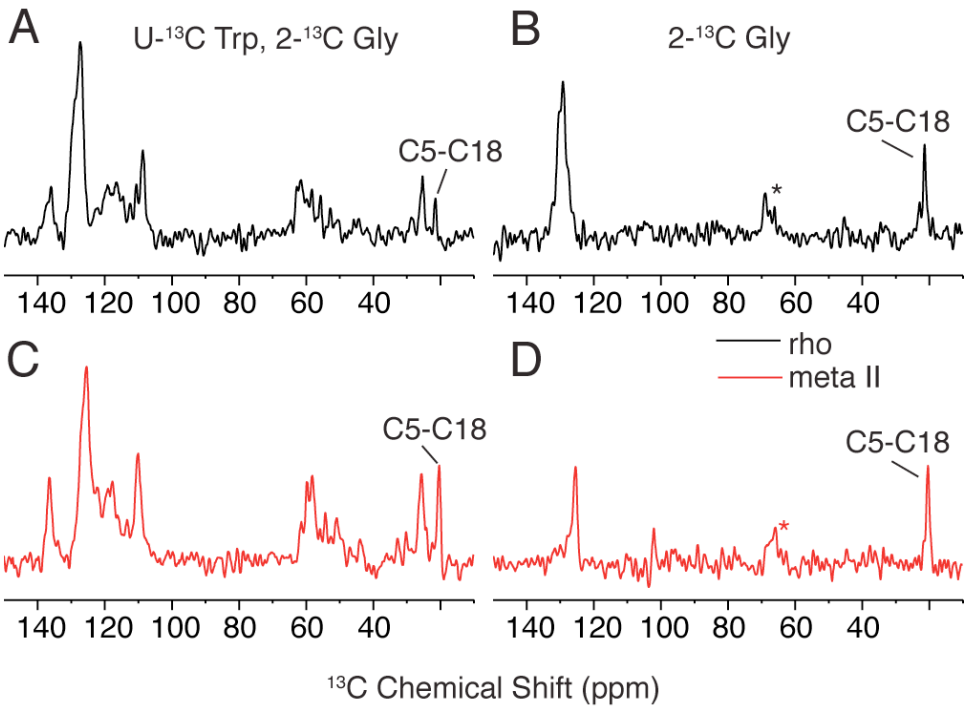


**Figure 6.3: Effect of dipolar truncation on the intensity of DARR crosspeaks.** Rows are shown through the $^{13}$C5 diagonal from the 2D DARR NMR spectra of wild-type rhodopsin (black) and meta II (red) regenerated with $^{13}$C5, $^{13}$C18-labeled retinal and containing either U-$^{13}$C-Trp and $^{13}$Cα-Gly (A & C) or containing only $^{13}$Cα-Gly (B & D). In all four spectra the region containing the crosspeak between the directly bonded $^{13}$C5 and $^{13}$C18 carbons of the retinal is highlighted. In (A) a relatively weak crosspeak is observed between the $^{13}$C5 (131.0 ppm) and $^{13}$C18 (21.6 ppm) resonances as compared to (B). The loss of intensity in the $^{13}$C5-$^{13}$C18 crosspeak between (A) and (B) has been attributed to dipolar truncation due to the presence of U-$^{13}$C-Trp265 in the vicinity of the directly bonded $^{13}$C5-$^{13}$C18 pair in (A) On conversion to meta II, the crosspeak observed in (C) between the $^{13}$C5 (126.0 ppm) and $^{13}$C18 (20.9 ppm) resonances is almost the same in intensity as the one observed in (D) This observation suggests that the presence of U-$^{13}$C-Trp265 is no longer modulating the intensity of the crosspeak between directly bonded $^{13}$C5 and $^{13}$C18 carbons and provides indirect evidence for the increase in separation between the conserved Trp265 (H6) and the β-ionone ring of the retinal in meta II. Asterisks indicate MAS sidebands.

our measurement of the retinal C18–Trp265 contact. In contrast, on conversion to meta II the intensity of the $^{13}$C5-$^{13}$C18 crosspeak (measured through the C5 diagonal at 126.0 ppm) in the sample labeled with U-$^{13}$C-tryptophan (Fig. 6.3C) is comparable to the intensity of the $^{13}$C5-$^{13}$C18 crosspeak in the sample containing unlabeled tryptophan (Fig. 6.3D) suggesting that Trp265 (H6) and C5-C18 have moved away (> 6 Å) from each other in meta II. As a result, the difference in intensity of the $^{13}$C5-$^{13}$C18 crosspeak in Figs. 6.3A and C provides a very interesting piece of indirect evidence consistent with an increase in separation between the retinal C18 methyl group and Trp265 in meta II.

Fig. 6.2A shows the positions of Gly121, Trp265 and the C18 methyl group on the retinal β-ionone ring. In the rhodopsin crystal structure [31], the retinal C18 methyl group is at 3.7 Å from the Cα carbon of Gly121. In the 2D DARR NMR spectrum, we observe a strong crosspeak between these groups (Fig. 6.2C, black). Upon conversion to meta II, the Gly121 – retinal C18 contact is lost (Fig. 6.2C, red) consistent with an increase in their separation. In Section 3.6, I have shown that on the basis of the $T_1$ relaxation measurements of the retinal C18 methyl group that the retinal C6-C7 single bond is in the s-*cis* conformation in both rhodopsin and meta II indicating that the change in distance is not due to a change in the conformation of the β-ionone ring from s-*cis* to s-*trans*. Furthermore, on the basis of an NMR contact between Met86 on H2 and Gly120 on H3, which does not change upon formation of meta II, we have concluded that the position of Gly121, the adjacent residue on H3, does not change upon activation (at least relative to H2) [65]. As a result, we attribute the increase in the Gly121 – retinal C18 distance to motion of the retinal β-ionone ring toward H5 by at least 1.5 Å. Finally, on the basis of the C18-Gly121 contact in rhodopsin, we conclude that the 6-s-*cis* conformation in rhodopsin has a negative twist (i.e. the C18 methyl group is oriented toward H3). In MD simulations on rhodopsin, Lau *et al.* [128] observed two distinct conformations, one conformation with a negative twist about the C6-C7 single bond placing the C18 methyl group near Gly121 (as observed) and one with a positive twist placing the C18 methyl group near Tyr268. DARR NMR experiments on $^{13}$Cζ-tyrosine-

labeled rhodopsin containing $^{13}$C18-labeled retinal failed to exhibit a C18-Tyr crosspeak (data not shown) indicating that if present the positively twisted conformer is only a minor component.

The retinal C18-Trp265 and retinal C18-Gly121 distance constraints described above complement previous Gly121-Trp265 and retinal C19-Trp265 distance measurements in which we observed the loss of a Gly121-Trp265 contact and the gain of a retinal C19-Trp265 contact in meta II [65]. These earlier results were interpreted in terms of rotation or translation of the Trp265 side chain toward the extracellular side of the retinal binding site upon formation of meta II.

The crosspeak between the retinal C19 methyl group and Trp265 provides a point of contact between the retinal chromophore and H6 in meta II. To obtain a corresponding point of contact with H3, we undertook DARR NMR measurements of rhodopsin containing $^{13}$C19-labeled retinal and U-$^{13}$C-threonine (Fig. 6.2D). In the rhodopsin crystal structure [31], the retinal is packed against Ala117, Thr118 and Glu122 on H3. Thr118 is adjacent to the middle of the retinal polyene chain and is the only amino acid among these three that can be selectively $^{13}$C-labeled in our HEK293S expression system. The retinal C19 methyl group is one of the closest points of contact with H3 and is within 5 Å of Thr118. The next closest threonine is over 10 Å away. In meta II, the crosspeak between the $^{13}$C19 methyl group and the unresolved $^{13}C\alpha$ and $^{13}C\beta$ carbons of Thr118 does not change appreciably in intensity indicating that the retinal C19 methyl group maintains contact with H3 at this position (Fig. 6.2D)

As mentioned earlier, the indole nitrogen of Trp265 is involved in a water-mediated hydrogen bonding interaction with Asn302 on H7, which is part of a highly conserved NPxxY motif across the family of class A GPCRs. This interhelical hydrogen bonding interaction is supposed to be important for stabilizing the inactive state structure [284-286]. We obtained $^{15}$N NMR chemical shifts for the indole and amide nitrogen for

Trp265 in rhodopsin and meta II. According to Herzfeld and coworkers [287], the chemical shifts for the indole nitrogen are sensitive to the strength of the hydrogen bonding interaction. They correlated an upfield shift of the $^{15}N$ indole resonance with decreased hydrogen bonding strength based on tryptophan model compounds and bacteriorhodopsin. We have previously observed an upfield shift in the $^{15}N$ indole resonance for Trp265 from 126.5 ppm in rhodopsin to 123 ppm in meta II [65]. The assignment was based on loss of these peaks in the $^{15}N$ spectra for U-$^{15}N$-tryptophan in the W265F mutant. This implies that the Trp265 indole nitrogen is becoming more weakly hydrogen bonded in meta II. These data are consistent with a movement of the aromatic side chain of Trp265 toward EL2 in meta II.

## *6.3 Motion of H6 upon rhodopsin activation*

An aromatic cluster of amino acids at the extracellular (or intradiscal) end of H6 represents a functional microdomain that is key to receptor activation in the class A GPCRs. In rhodopsin, Phe261, Trp265 and Tyr268 on H6 form this cluster. The aromatic side chain of Trp265 lies in the arc created by the 11-*cis* retinal and the side chain of Lys296. We have previously proposed that preventing motion of Trp265 locks the receptor off by inhibiting the motion of H6 [65]. Motion of the β-ionone ring toward H5 in the rhodopsin-to-meta II transition allows motion of the Trp265 side chain or the H6 backbone toward EL2. Previously, we observed that Trp265 comes in close contact with the retinal C19 methyl group in meta II [65] and loses its contact with Gly121 on H3. Moreover, the increase in internuclear distance between the retinal C18 methyl group and both Trp265 and Gly121 supports a model involving coupled motion of the β-ionone ring and Trp265 in meta II.

In our model of meta II generated from guided MD simulations, in order to satisfy the NMR constraints (see Appendix A.1; Table A.1), the Trp265 side chain undergoes significant motion toward EL2 while remaining in van der Waals contact with the C19

methyl group on the retinal polyene chain (see Fig, 6.4B). In the recent opsin crystal structure [68], the indole side chain of Trp265 has moved away from Gly121 and Ala295 consistent with the NMR data, but has not undergone a change in rotameric state or shifted toward EL2 to any significant extent (Fig. 6.5D). This difference with our results can be largely attributed to the lack of all-*trans* retinal in the binding cavity. The location of Trp265 in opsin is consistent with linear dichroism studies where rotation of a tryptophan in the meta I to meta II transition was found to be reversed upon decay of meta II [288].

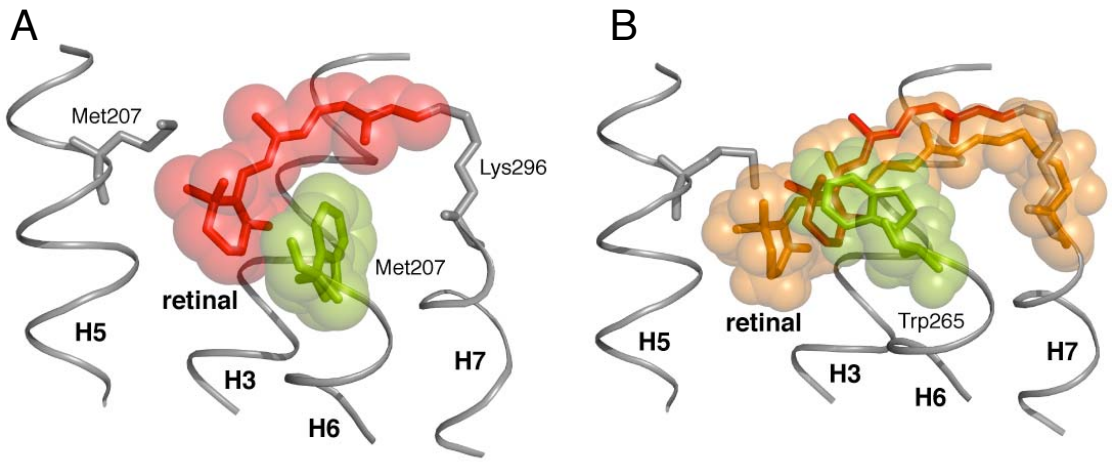


**Figure 6.4: A Model generated by MD simulations for motion of Trp265 or the H6 backbone in meta II.** (A) A view from the rhodopsin crystal structure [31] (pdb:1U19) highlighting the location of the side chain of Trp265 (H6; green), tightly packed against the retinal β-ionone ring (red). (B) Meta II model generated from MD simulations show a movement of retinal (orange) towards H5 that breaks the locking interaction with the side chain of Trp265 (H6) allowing it to move upwards towards EL2 in meta II.

Our conclusions regarding retinal-H6 interactions are in agreement with a wide range of previous studies on both rhodopsin and other GPCRs. For instance, UV absorbance studies on rhodopsin show that Trp265 moves into a more hydrophilic environment and that the plane of the indole side chain of Trp265 changes from an orientation parallel to the bilayer normal to an orientation roughly perpendicular to the bilayer normal [66,288]. Javitch and co-workers [272] proposed the "rotamer toggle switch" for receptor activation based on studies on the $\beta_2$-AR, in the subclass of biogenic amine receptors. In these receptors, ligand binding is thought to induce a change in the side chain conformation of a conserved phenylalanine, which is coupled to changes in the side chain conformations of conserved Cys, Trp and Pro residues on H6. The low-resolution (5.5 Å) crystal structure of metarhodopsin I (meta I) [146] reveals a shift in the electron density close to the bend in H6. This shift has been interpreted as movement of Trp265 in meta I.

Our model is consistent with Borhan *et al.* [244], where the β-ionone ring of the retinal moves away from Trp265 in meta II. However, it is at odds with the model proposed by Spooner et al. [246] where the β-ionone ring is locked in its position by steric constraints and does not move upon isomerisation. According to this model, the cytoplamic end of H6 rotates away from H3 in meta II, by straightening of the helix about the kink produced by Pro267 (H6). It predicts a change in the backbone torsion angles for Trp265 and Ala295 accompanied by disruption of the hydrogen bonding interactions of Tyr268, which is part of the conserved aromatic motif on the extracellular side of H6, upon deprotonation of the Schiff base [246].

We have proposed that preventing motion of Trp265 locks the receptor off by inhibiting the motion of H6, while motion of the β-ionone ring toward H5 in the rhodopsin-to-meta II transition allows motion of the Trp265 side chain or simply of the H6 backbone toward EL2. A counterclockwise rotation of H6 is necessary for satisfying

the NMR contacts observed between Trp265 and retinal (C19) in meta II. This is consistent with studies conducted by Dunham and Farrens [289] where they proposed a counterclockwise rotation of H6 away from H3 when viewed from the extracellular side of the receptor. However, the low-resolution crystal structure presented for the photoactivated intermediate of rhodopsin with a deprotonated Schiff base [185] does not show any significant motion of either Trp265 or H6 (Fig. 6.5C).

The coupled motion of Trp265/H6 and the ionone ring may also influence the position of H7. Trp265 is packed against Ala295 and is hydrogen bonded through a network of water molecules with Asn302, the first residue of the conserved NPxxY sequence on H7. A change in the position of the Trp265 side chain would allow H7 to repack and/or allow the structural water molecules surrounding Asn302 to change their hydrogen bonding pattern. In this regard, we have previously shown that hydrogen bonding of the indole nitrogen of Trp265 is weaker in meta II [65] and that mutation of Met257, on the cytoplasmic side of H6, alters packing of the H6-H7 interface to allow activation of rhodopsin by the addition of all-*trans* retinal as a diffusible ligand [92].

The results mentioned in this chapter are consistent with our helix-loop-helix (HLH) model proposed in chapter 4, which suggests how retinal isomerization and motion towards H5 and motion of EL2 away from the retinal binding site may allow the extracellular end of the H6-EL3-H7 segment to pivot in toward the center of the protein and conversely allow the intracellular end of H6 to rotate outward as shown by spin labeling studies [18,88]. The inward motions of the extracellular ends of H6 and H7 are captured in the global toggle switch model proposed by Schwartz and coworkers [23]. Also, the recent crystal structure of opsin [68] shows that the cytoplasmic side of H6 is tilted outward by 6-7 Å (Fig. 6.5A).

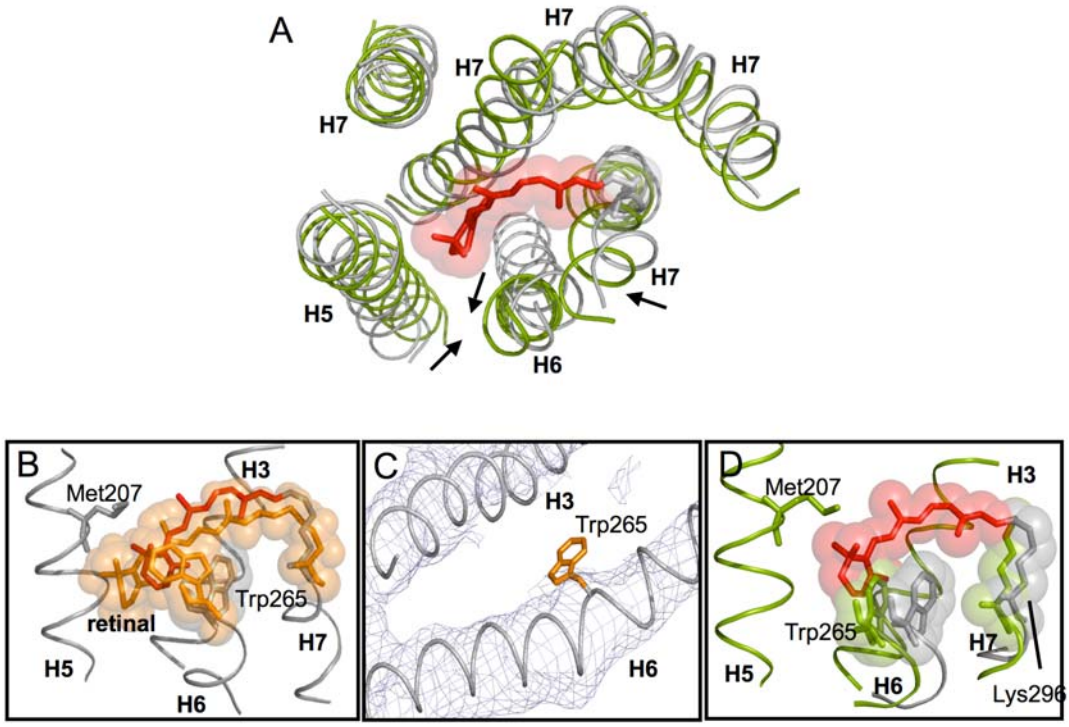


**Figure 6.5: Comparing the motion of Trp265 and H6 backbone from our simulation model for meta II with the low resolution crystal structure for the photoactivated intermediate of rhodopsin [185] and the opsin crystal structure [68] influence of retinal motion on H3-H5 interactions.** (A) presents an overlap of the rhodopsin crystal structure with the opsin crystal structure highlighting, the motion on H5 towards H6, outwards motion of the cytoplasmic part of H6 and a motion of H7 towards H6 in opsin. (B) Motion of the β-ionone ring toward H5 in the rhodopsin-to-meta II transition allows motion of the Trp265 side chain or the H6 backbone toward the extracellular loop 2 (EL2) in our model for meta II. (C) The low resolution crystal structure for the photoactivated state of rhodopsin does not show any significant movement of H6. (D) In the opsin crystal structure, the indole side chain of Trp265 has not undergone a change in rotameric state or shifted toward EL2 to any significant extent.

Studies on other class A GPCRs have shown that motion of H6 is important for their activation. For example, the melanocortin receptors display high levels of constitutive activity. It is thought that the reason is the presence of a short EL2, which is unable to insert into the helical TM core, and is therefore unable to hold the extracellular end of H6 away from H3. As a result, H6 moves inwards, adopting a more active conformation [223]. In the C5a receptor, disruption of the interaction between H3 and H6 by mutation of hydrophobic residues that line the interface caused constitutive activity [268].

## *6.4 Disruption of the "Ionic Lock" between H3 and H6 upon activation*

Movement of TM helix H6 is one of the key elements in the activation of rhodopsin. The general model that has emerged following the pioneering EPR measurements of Hubbell and co-workers [18] is that the relative motion of helices H3 and H6 couple retinal isomerization to the disruption of the "ionic lock" involving the conserved ERY sequence and Glu247 at the cytoplasmic ends of H3 and H6, respectively.

On the basis of our data mentioned above and in the previous chapters we propose that retinal isomerization leads to steric strain within the retinal binding site between the retinal β-ionone ring and helix 5 (H5), and between the retinal C19/C20 methyl groups and the second extracellular loop (EL2). These interactions lead to a rearrangement of hydrogen bonding networks involving EL2 triggering the motion of the EL2 loop away from the retinal, deprotonation of the Schiff base nitrogen and protonation of Glu113. Displacement of EL2 is coupled to the motion of H5 in meta II. Packing of the β-ionone ring against H5 leads to a rearrangement of its hydrogen bonding networks facilitating the rotation of the cytoplasmic end of H5 towards H6. The rotation of H5 places the side

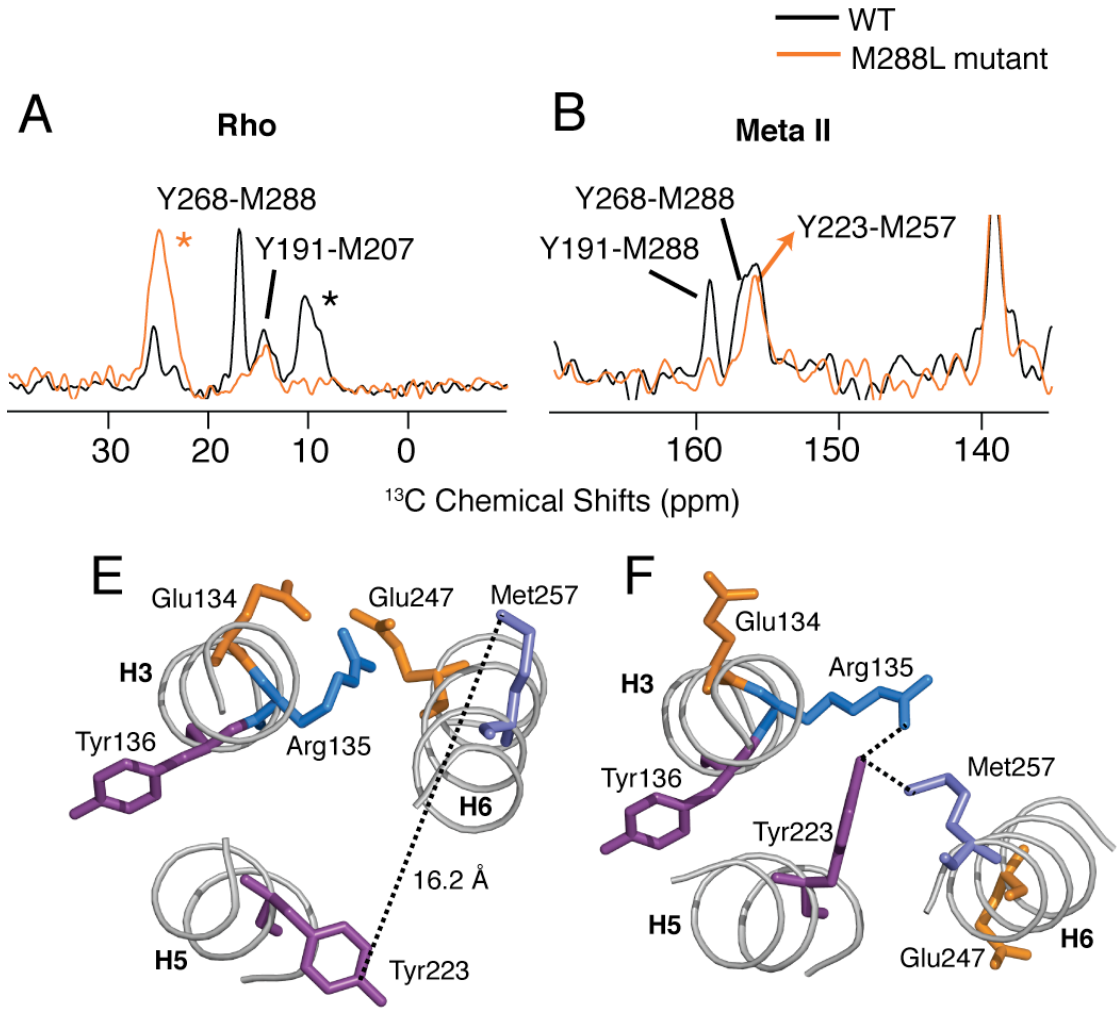


**Figure 6.6: Disruption of the ionic lock between H3 and H6 in meta II and opsin.** (A) data is explained in Section 4.4.2 where we assign some of the Tyr(Cζ) - Met(Cε) crosspeaks observed in rhodopsin and meta II by comparison with M288L mutant data. However, in meta II we a crosspreak in meta II (B) that is very much present in the mutant M288L (orange) spectrum and therefore cannot be assigned to a contact with Met288 (H7). We have tentatively assigned this crosspeaks at ~156 ppm in WT meta II to a contact between Tyr223 (H5) and Met257 (H6). This suggests a rearrangement of the interaction near the ionic lock on H3 in meta II similar to what is seen in the opsin crystal structure as highlighted in (F). (E) and (F) present views of the ionic lock between (ERY) on H3 and Glu247 (H6) in rhodopsin and opsin, respectively. In the dark the distance between Cζ-Tyr223 and the Cε-Met257 is ~16 Å. In opsin, the combined motion of H5 and H6 reduces this separation to < 5 Å.

the side chain of Tyr223 in the vicinity of the ionic lock on the cytoplasmic side of H3 and H6. Motion of the β-ionone ring is coupled to the motion of Trp265 on H6, which allows the outward motion of the intracellular end of H6 disrupting the ionic lock between Glu247 (H6) and Arg135 (H5). The motion of H6 facilitates the formation of a new hydrogen bonding contact between Tyr223 on H5 and Arg135 on H6, effectively breaking the Arg135-Glu247 ionic lock (see Fig. 6.6E and F). The new position of H6 places the side chain of the Met257 (H6) in a direct contact with Arg135 (H3) and Tyr223 (H5) (Fig. 6.6F). In meta II, we observe a contact between a Tyr(Cζ) and a Met(Cε) (Fig. 6.6B) that we have tentatively assigned to Tyr223 on H5 and Met257 on H6. These results indicate that there are two critical H3-H5 interactions that hold helix H5 in an active geometry: Glu122-His211 [227,256] and Arg135-Tyr223 [68,290]. The model of activation that emerges from these studies is one where steric contacts between the retinal β-ionone ring with H5 and the retinal C19 methyl group with EL2 shift the EL2-H5 sequence into an active geometry stabilized by H3-H5 contacts; retinals lacking either the ring [257] or the C19 methyl group fail to activate rhodopsin [291].

Our model is consistent with the opsin crystal structure with [290] and without [68] that shows that the ionic lock is broken. Arg135 is no longer interacting with Glu247 on the intracellular end of H6, instead it is involved in a hydrogen bonding interaction with Tyr223 on H5 and Tyr306 on H7 stabilizing the ionic lock in what appears to be the active conformation (Fig. 6.6E and F).

# Chapter 7

# Coupling retinal isomerization to motion of H7

## *7.1 Introduction*

The cytoplasmic and extracellular ends of H7 are both important in the activation mechanism of rhodopsin [100]. The cytoplasmic end contains the highly conserved NPxxY (Ans302, Pro303, Val304, Ile305 and Tyr306) sequence (Fig. 7.1A). The extracellular end of H7 contains residues that are specific to the subfamily of class A GPCRs [100,239]. For example, in rhodopsin the retinal is attached to Lys296 (H7) as a positively charged protonated Schiff base (PSB) that forms a salt bridge with the negatively charged side chain of Glu113 (H3) (Fig. 7.1A). The salt bridge is essential for stabilizing the ground state of rhodopsin and is broken upon activation [56].

The H7 sequence corresponds to residues 286-309 and contains two prolines, Pro291 and Pro303 [50]. Pro303 is one of the highly conserved signature residues across the family of class A GPCRs, with sequence identity of greater than 80%. The presence of these prolines causes severe kinks in H7. On the extracellular side of Pro303, H7 folds into a $3_{10}$ helix as opposed to a normal $3.6_{13}$ helix (Fig. 7.1). This distortion from the canonical helix ($3.6_{13}$ helix) enables some residues, such as Ala292, Ala295 and Ser298, to face the retinal binding site and allows them to be part of a hydrogen bonding network involving residues on H1, H2, H6 and H7 that contributes to

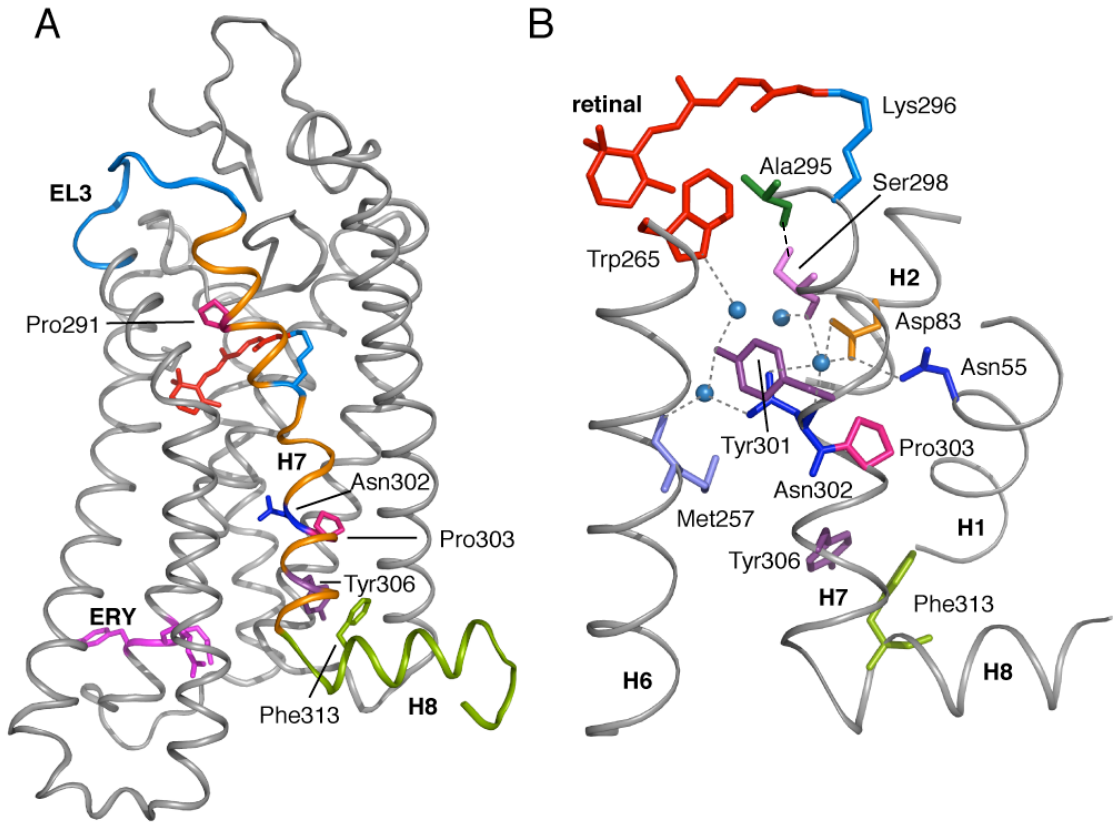


**Figure 7.1: View from the rhodopsin crystal structure [50] highlighting H7.** (A) A front view of the rhodopsin crystal structure (pdb: 1GZM) [50] highlighting the position of H7 (orange). H7 extends from amino acids 286-309. H7 is connected to EL3 (blue) on the extracellular side and H8 (green) on the intracellular side. Important residues and their location highlighted on H7 are, Pro291 and Pro303 (magneta), Asn302 (dark blue), Tyr306 (purple) and Phe313 (green). The ERY sequence is highlighted in magenta on the cytoplasmic side of H3. (B) A view of the water-mediated hydrogen bonding network involving H7. It extends from Trp265 (red; on H6) that lines the retinal binding cavity all the way to Phe313 (green; on H8) through the NPxxY (Asn302 (dark blue) … Tyr306 (purple)) on H7. Other residues involved in this hydrogen bonding network are: Ala295 (H7; green), Ser298 (pink; H7), Tyr301 (purple; H7), Met257 (light blue; H6), Asp83 (orange; H2) and Asn55 (dark blue; H1). Note that the ring of Tyr306 on H7 is packed against the ring of Phe313 on H8.

the stabilization of the inactive state of the receptor [31,50]. Ala295 and Ala299 are two group-conserved residues present on H7. A distorted $3_{10}$ helix is also observed in other GPCRs, where it is thought to be responsible for positioning residues important for ligand binding toward the interior of the protein [266].

According to the rhodopsin crystal structure [50], Ala295 is packed against the side chain of the highly conserved aromatic residue on H6, Trp265 (Fig. 7.1B), which forms a water-mediated hydrogen bond with Asn302 on H7. The backbone carbonyl of Ala299 (H7) is not involved in main chain hydrogen bonding due to the presence of the highly conserved proline (Pro303) at the i+4 position in the middle of H7. Therefore, the backbone carbonyl of Ala299 is free to hydrogen bond to other nearby residues. According to the crystal structure, Ala299 is part of a hydrogen bonding network centered at H7. Members of this hydrogen bonding network include Ala295, Ser298, Ala299, Tyr301 and Asn302 on H7; Met257 on H6; Asn55 on H1, Asp83 on H2 and Gly120 on H3. Tyr306 couples this hydrogen bonding network to residues on H8 via a packing interaction with Phe313 (Fig. 7.1B). Interestingly, most of the residues involved in this hydrogen bonding network are conserved either across the family of class A GPCRs (e.g. Trp265, Ser298, Ala299, Tyr301 and Asn302) or in rhodopsin like GPCRs (e.g. Asn55, Asp83 and Met257) [1,50,61].

The side chain of Tyr306 (H7) is packed against the aromatic ring of Phe313 on H8 [50]. Studies have shown that this hydrophobic interaction is important for stabilization of the helix-turn-helix fold of the NPxxY$(x)_{5,6}$F region in rhodopsin [292]. Thus, the hydrogen bonding network involving H7 couples residues that form the retinal binding site all the way down to H8 through the NPxxY motif (Fig. 7.1B).

The fourth cytoplasmic loop of rhodopsin is connected to the intracellular end of H7 and folds into a putative α-helix designated as H8. H8 is an amphipathic helix oriented perpendicular to seven transmembrane helices (Fig. 7.1). It extends from amino

acid Asn310 to Leu321 and is anchored to the lipid bilayer through palmitoyl groups attached to Cys322 and Cys323 [50]. H8 is known to be important for modulating interactions with the G-protein [76]. Mutation of three amino acids (Asn-Lys-Gln) on the N-terminus of H8 leads to a marked decrease in transducin activation [76].

In the sections below I present 2D DARR NMR data on the position of H7 in meta II and its interaction with the residues on neighboring helices H1, H2 and H6. Following the data section, I discuss the role of the extracellular and intracellular ends of H7 in coupling retinal isomerization to structural changes in H8 and the conserved ERY sequence on the cytoplasmic side of H3.

## *7.2 Interactions involving H7 using solid-state NMR*

We have seen previously how retinal, upon isomerization moves toward H5 and packs between Met207 and Phe208 (explained in detail in Chapter 5). To obtain further support for motion of the retinal toward H5, we measured the distance between the ε-carbon of Lys296 on H7 and the ε-$CH_3$ carbon of Met44 on H1 (explained in Chapter 5, Fig. 5.6). The $^{13}$Cε-Met44 -to-$^{13}$Cε-Lys296 distance in rhodopsin is 4.7 Å [31]. Fig. 5.6A presents rows through the $^{13}$Cε-diagonal resonance of methionine in the DARR NMR spectrum of rhodopsin (black) and meta II (red). The Met44-Lys296 crosspeak intensity decreases in meta II consistent with an increase in the internuclear distance. This suggests that the motion of retinal towards H5 is pulling the side chain of Lys296 on H7 away from H1. This advocates a rearrangement of the extracellular end of H7 in meta II.

As discussed in Chapter 6, the intracellular end of H6 undergoes a significant outward motion and the extracellular end moves inward towards the core of the protein upon activation. We wanted to study if the movement of H6 is coupled to the motion of H7. 2D DARR NMR measurements were used to establish the relative position of Cys264 (H6), Ser298 (H7) and Tyr301 (H7) upon rhodopsin activation. Tyr301 is part of

the hydrogen bonding network that extends from Trp265 down to NPxxY on H7 mediated by water molecules. Ser298 (H7) is highly conserved as a serine or asparagine in rhodopsin-like GPCRs [61]. The side chain hydroxyl (OH) group forms a hydrogen bond with the backbone carbonyl of Ala295 (H7) (Fig.7.1B) to compensate for the elongation of the helix pitch at the start of the $3_{10}$ helix [50].

We observe a crosspeak between $^{13}$Cβ-Cys264 at 25.8 ppm and $^{13}$Cζ-Tyr301 at 156.2 ppm in rhodopsin (see Fig. 7.2A). The intensity of the crosspeak is consistent with the 4.81 Å separation in the rhodopsin crystal structure [31]. Upon conversion to meta II, the crosspeak between $^{13}$Cβ-Cys264 (26.2 ppm) and $^{13}$Cζ-Tyr301 (157.1 ppm) persists and decreases only marginally in intensity, suggesting that the distance between Cys264 on H6 and Tyr301 on H7 remains almost the same in meta II (Fig. 7.2A).

The ζ-carbon of Tyr301 is 4.89 Å away from the β-carbon of Ser298 (H7) [31]. We observe a relatively weak crosspeak between the two in rhodopsin, consistent with the crystal structure. However, on conversion to meta II, a strong crosspeak between$^{13}$Cβ-Ser298 (60.0 ppm) and $^{13}$Cζ-Tyr301 (157.0 ppm) representative of a close interaction between these two side chains is observed (data shown in Fig. 7.2B). The data presented above suggest that the interface between H6 and H7 near the retinal binding site is maintained in meta II and that the portion of H7 on the extracellular side of the kink produced by Pro303 follows the motion of the extracellular end of H6 upon meta II formation.

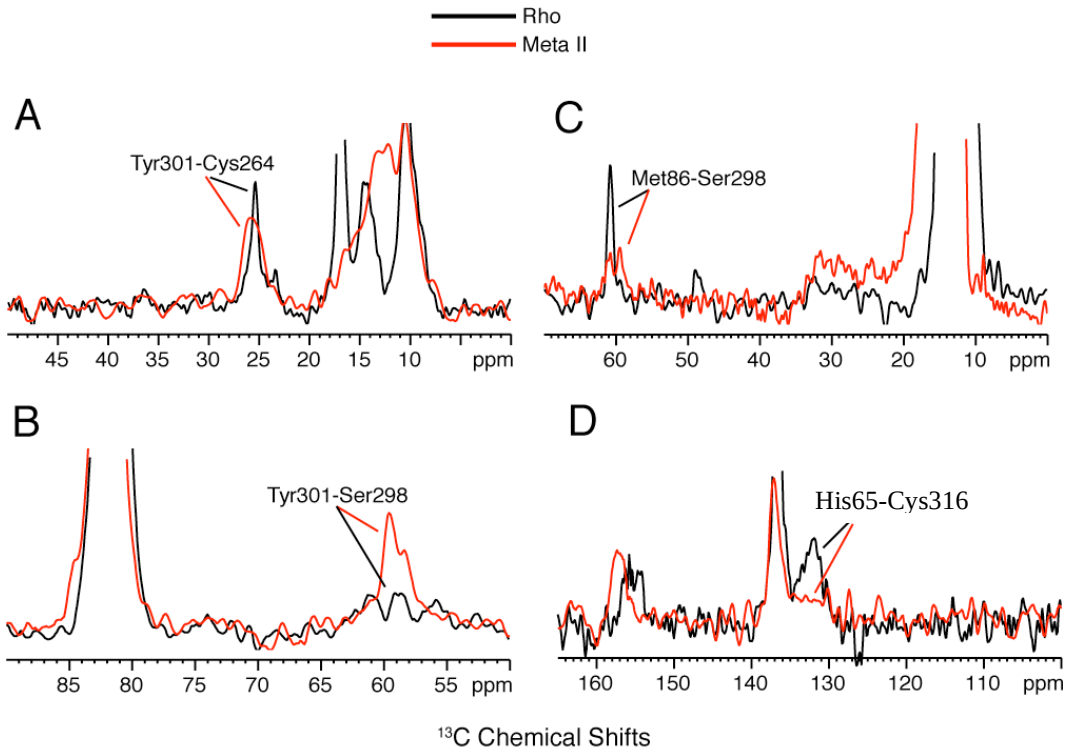


**Figure 7.2: Overlap of 1D rows from 2D NMR data on interactions involving amino acids on H7 in rhodopsin (black) and meta II (red).** (A) A 2D DARR NMR contact was observed between Tyr301 and Cys264 in rhodopsin (black) and meta II (red). Based on the intensity of the crosspeak highlighted the separation between the two amino acids increases only marginally on activation. (B) A weak DARR crosspeak is observed between Tyr301 and Ser298 on H7 in rhodopsin. The crosspeaks becomes a lot stronger in meta II consistent with a decrease in separation between Tyr301 and Ser298 in meta II. (C) A strong crosspeak is observed between Ser298 on H7 and Met86 on H2 in rhodopsin and the crosspeaks becomes a lot weaker is meta II indicating that the two amino acids have moved away from one another upon activation. (D) A weak crosspeak is observed between His65 on H1 and Cys316 on H8 in rhodopsin. The crosspeak is almost non-existent in meta II suggesting a movement of H8 away from H1 in meta II.

To obtain further support for motion of the extracellular end of H7, we studied the interaction between the Cβ-Ser298 on H7 and Cε-Met86 on H2. We observed a strong crosspeak between $^{13}$Cβ-Ser298 (61.2 ppm) and $^{13}$Cε-Met86 (13.3 ppm) consistent with a 4.81 Å separation in rhodopsin [31] (Fig. 7.2C). In meta II, a very weak crosspeak between $^{13}$Cβ-Ser298 and $^{13}$Cε-Met86 was observed consistent with an increase in separation between these two $^{13}$C labels (Fig. 7.2C). Previously, we have obtained a contact between $^{13}$Cε-Met86 and $^{13}$Cα-Gly121 (H3) in rhodopsin that did not change upon conversion to meta II, indicating that the separation between the two residues remains the same in rhodopsin and meta II consistent with TM H1-H4 being a tightly packed core that does not change significantly upon activation [65,79]. This observation suggests that the increase in separation between Cβ-Ser298 and Cε-Met86 is primarily due to the movement of the side chain of Ser298 / H7 away from Met86 /H2, consistent with our hypothesis that H7 follows H6 movement upon activation.

Additionally, we observed a broad crosspeak between $^{13}$C$\varepsilon_1$-His65 (132.3 ppm) on H1 and $^{13}$Cβ-Cys316 (22.8 ppm) on H8 in rhodopsin. This contact was lost in meta II (Fig. 7.2D) consistent with an increase in separation between H8 and H1. This in turn is in agreement with recent EPR studies using double spin labels where an increase in distance was observed between Cys316 on H8 and residues 60-75 connecting the cytoplasmic ends of H1 and H2 [293].

## *7.3 Role of the Lys296 (H7) - Glu113 (H3) salt bridge in the activation of rhodopsin*

Lys296 is present near the break in the helix at the beginning of the stretched $3_{10}$ helical portion of H7. As mentioned above, it is covalently linked to the retinal through a PSB in the dark and forms a salt bridge with the Glu113 counterion on H3 (Fig. 7.3). This

interaction is important for stabilizing the receptor in the inactive state and is broken upon receptor activation [56]. In other GPCRs, such as the dopamine [57], acetylcholine [58] and serotonin [59] receptors, interactions are observed between the ligand and residues on H7, analogous to Lys296 in rhodopsin.

Varying degrees of constitutive activity of opsin were observed for different mutants of Lys296 (H7) [219,294]. For example, the constitutive activity of the K296G mutant was found to be identical to WT meta II. However, regeneration of this mutant with 11-*cis* retinal propylamine (SB) restored the inactive state stability [56]. Upon illumination it displayed 30-40% of wild type transducin activity. These studies are consistent with the idea that the covalent bond between the retinal and the protein might not be essential for activation but is important for efficient activation of rhodopsin. Robinson *et al.* [56] also found that van der Waals interactions with the side chain of the residue at 296 position on H7 plays an important role in stabilizing the inactive state of the receptor. For example, mutation of Lys296 to smaller residues such as glycine favored the formation of meta II suggesting that the steric interactions of Lys296 are lost in meta II. In contrast, mutation of Lys296 to amino acids with longer side chains favored the inactive state of the receptor [294].

Similarly, charge-neutralizing mutations of Glu113, the other member of the salt bridge on H3 produced constitutive activation of opsin. For example, E113Q displays ~25% of the activity of WT meta II [54,219]. Addition of 11-*cis* retinal to the E113Q mutant locks the receptor off in dark, while illumination leads to full transducin activity [54,56]. These studies suggest that the electrostatic interaction between the positively charged retinal PSB with the negatively charged Glu113 counterion is important for stabilizing the inactive state of

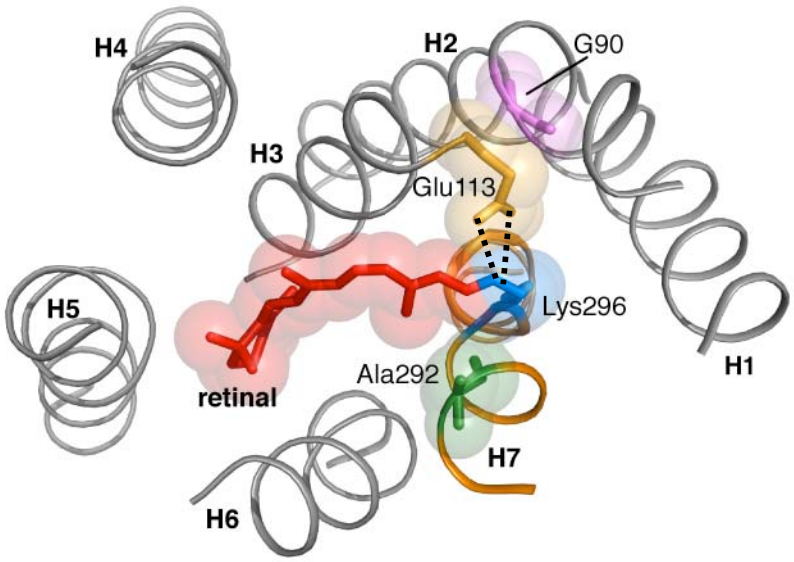


**Figure 7.3: A view of the retinal binding site from the extracellular side of rhodopsin [50] highlighting the Shiff base between Lys296 on H7 and Glu113 on H3**. The figure also presents the location of two additional amino acids (Gly90 on H2 and Ala292 on H7) interacting closely with the Schiff base. Mutation of any of the four amino acids disrupts the salt bridge between Lys296 and Glu113. Mutants such as G90D and Ala292E cause the genetically inherited disease known as congenital stationary night blindness [295,296].

the receptor. Oprian and coworkers have estimated that the salt bridge contributes 2-3 kcal/mol to the inactive state stability [294].

The idea that the Glu113-PSB salt bridge may prevent H7 motion in wild-type opsin [54] does not appear to be confirmed in the opsin crystal structure [68]. In the opsin structure, only very weak electron density was observed for the side chain of Lys296 suggesting that it is not locked into a stabilizing salt bridge with Glu113. Nevertheless, movement of the retinal toward H5 affects the interaction between the retinal PSB and its Glu113 counterion [297].

Studies have isolated four mutations in rhodopsin that break the salt bridge between Lys296 and Glu113 and are responsible for genetically inherited diseases such as retinitis pigmentosa (RP) and congenital stationary night blindness. These include K296E and K296M [60,298] on H7 responsible for retinitis pigmentosa and G90D and A292E on H2 and H7, respectively, responsible for congenital stationary night blindness [295,296]. All of these mutants caused constitutive activation of opsin. However, in the presence of 11-*cis* retinal they behaved similar to wild-type rhodopsin (Fig. 7.3).

The E113Q mutant and other mutations influencing the Glu113-PSB interaction (G90D and A292E) shed light on the structural changes involved in the conversion of meta I to meta $II_a$. Meta $II_a$ results from deprotonation of the SB, [131]) and is the first of the meta II substates. The E113Q mutant regenerated with all-*trans* retinal is able to activate transducin (~47% of light activity) [54]. Sakmar *et al.* [54] concluded that the E113Q mutant made the binding site more flexible allowing it to bind all-*trans* retinal. They [54] estimated the $pK_a$ of the Schiff base in the E113Q mutant to be ~6 as compared to ~16 [175] for the wild-type receptor. Therefore, at neutral pH, the E113Q mutant contains predominantly an unprotonated retinal Schiff base [54]. The lower $pK_a$ would be consistent with access of water to the retinal binding site, which in turn would be consistent with

our model of the displacement of EL2 upon retinal isomerization (as hypothesized in Section 4.4).

In contrast, regeneration of the E113Q, G90D and A292E mutants of rhodopsin with 11-*cis* retinal results in almost no detectable activity [54]. In Chapter 6, we argued that addition of 11-*cis* retinal locks Trp265 in place and prevents the full motion of H6. However, the binding of 11-cis retinal may also stabilize the inactive state by restoring packing interactions with EL2 and H7. However, EPR data [154] acquired on spin labels incorporated on the cytoplasmic side of H5, H6 and H7/H8 of E113Q, G90D and Ala292E show movement of H6 in the dark. This observation suggests that full activity requires not only deprotonation of the retinal, but also isomerization to the all-*trans* geometry.

Interestingly, the double mutants E113Q/M257Y, E113Q/M257N, G90D/M257Y produce strong dark activity in the presence of 11-*cis* retinal [92,154]. Han et al. [92] had previously found that mutation of Met257 alters packing of the H6-H7 interface to allow activation of rhodopsin by the addition of all-*trans* retinal as a diffusible ligand. According to the rhodopsin crystal structure [50], Met257 in conjunction with Leu76 (H2), Leu79 (H2), Leu128 (H3), Leu131 (H3) and Met253 (H6) forms a hydrophobic barrier that seals the hydrogen bonding network involving Trp265 (H6), Asp83 (H2) and the NPxxY motif on H7 from the cytoplasmic side of the receptor. Met257 is at the boundary between the hydrogen bonding network and the hydrophobic barrier and is involved in important steric interactions with Asn302 of the NPxxY motif and therefore prevents helix motion unless triggered by retinal isomerization [50]. Therefore, it is possible that mutation of Met257 can disrupt this packing interaction with H7 facilitating its motion towards an active conformation. This is in fact consistent with the opsin crystal structure [68] where outward rotation of H6 places Met257 in a new position, where it is packed between Arg135 (of the ERY motif on H3), Tyr223 (H5) and Tyr 306 (H7), disrupting the packing interaction with Asn302.

These observations emphasize the fact that full activation of rhodopsin requires modulation of multiple structural elements that stabilize the inactive state of the receptor [154]. This hypothesis is further strengthened by a series of biophysical and biochemical studies [67,131,158,219] that show that apart from disruption of the salt bridge, rhodopsin activation requires deprotonation of the SB (meta $II_a$) and a net uptake of proton from the milieu (meta $II_bH^+$) (explained in Section 3.1).

On the basis of mutational data and FTIR spectroscopy, the most widely accepted candidate for proton uptake from the solvent is Glu134 on the cytoplasmic side of H3 [156,157,299-301]. Glu134 is a member of the highly conserved (D/E)RY sequence on H3 (see Fig. 7.1A and Fig.6.6). It forms an ionic lock with Arg135 on H3 and Glu247 on H6 (Fig. 7.1A & 7.5B). The ionic lock is responsible for stabilizing the cytoplasmic part of rhodopsin [67] as well as other GPCRs [78] in an inactive conformation. Light activation of rhodopsin requires the disruption of this ionic lock. Mutation of Glu134 to uncharged residues leads to constitutive activation of rhodopsin without the ligand and hyperactivity upon illumination or addition of all-*trans* retinal [156,157]. In the presence of 11-*cis* retinal, the mutant displays very modest activation of transducin [156,157]. Other mutations that potentially disrupt the ionic lock between H3 and H6, such as E247A and E251A, also display modest activity in the dark (in the presence of 11-*cis* retinal) and enhanced transducin activity upon illumination [302]. However, more exaggerated activity was observed in the dark for double mutants (as compared to single mutants: E134Q and E247A) such as E134Q/E247A and E134Q/T251A [302].

Hubbell and coworkers [157] presented EPR data on spin labels incorporated at the cytoplasmic side of H3 (C140), H5 (C227), H6 (C250) and H8 (C316) of the E134Q and R135Q mutants in the dark and upon illumination. The data demonstrate a movement of H3 and H8 in the dark, representative of the active state of WT rhodopsin. However,

structural changes observed for H5 and H6 in dark and light resembled closely the changes observed for WT protein.

These observations suggest that disruption of the ionic interaction between Glu134 (H3), Arg135 (H3) and Glu247 (H6) by mutation is not sufficient for H5 and H6 to adopt active conformations. Additional structural rearrangements are required for the full active conformation of H6, such as release of Trp265 (H6) from its tight interaction with the β-ionone ring upon isomerization of the retinal. All of the above-mentioned observations emphasize the fact that there is more than one trigger required to shift the receptor from the inactive to the active state.

## *7.4 Role of the NPxxY motif and H8 in activation of rhodopsin*

Sequence alignment has shown that the NPxxY$(x)_{5,6}$F (Asn302, Pro303, Val304, I305, Ty306 … Phe313) motif on the cytoplasmic end of H7 is highly conserved across the family of class A GPCRs. Mutation of residues in this motif effect transducin activation to varying degrees. For example, the N302A mutation reduces the light induced activation of transducin by 50% [292]. On the other hand, the P303A mutation leads to hyperactivity, increasing transducin activation by ~40%, possibly due to straightening of the $3_{10}$ helix [292]. Mutation of Tyr306 to alanine completely abolishes transducin activation [292].

The side chain of Tyr306 is packed against the aromatic ring of Phe313 and is hydrogen bonded to Asn73 on the cytoplasmic end of H2 (Fig. 7.1B & 7.5A). Ernst and coworkers have shown that the hydrophobic interaction between Tyr306 and Phe313 is significant for maintaining the helix-turn-helix fold of the NPxxY$(x)_{5,6}$F motif on H7 [292]. The Y306A and F313A mutants display very low levels of transducin activation, although they enhance meta II formation.

Cysteine crosslinks introduced between F306C and F313C prevented formation of meta II, but allowed meta II formation in the reduced state [292]. This suggests that rotation of H7 and/or H8 must occur upon rhodopsin activation. In addition to these results, Fritze *et al.* [292] observed increased meta II formation in the Y306A and F313A mutants in the presence of 9-desmethyl retinal (9-dm retinal) or acyclic analogues of retinal (ac-retinal). Normally, 9-dm favors meta I [138] consistent with the idea that the 9-dm group is needed for moving EL2 and H5, while the acyclic derivative results in fast (and reduced) meta II decay [139,258] consistent with the idea that the β-ionone ring is required to hold H5 in an active conformation. Introduction of an additional mutation, E134Q, further enhanced meta II formation in the Y306A mutant pigment regenerated with 9-dm retinal, but did not improve G-protein activation.

These observations make sense in light of a model where interactions between structural elements on the extracellular side of the receptor are coupled to structural motifs on the cytoplasmic side of the receptor. A key hydrogen bonding network mediated by water molecules extends from Trp265 to the highly conserved NPxxY motif on the cytoplasmic end of H7 (Fig. 7.1B).

According to our model of rhodopsin activation, retinal isomerization and motion towards H5 breaks the tight packing between the β-ionone ring of the retinal and the side chain of Trp265. Loss of this stabilizing interaction allows the side chain or the backbone of the extracellular side of H6 to move towards EL2 (as explained in Chapter 6). This movement of Trp265 would potentially disrupt its water-mediated hydrogen bonds with residues on H7 (Ser298, Ala299, Tyr301, Asn302) and Met257 on H6. This is consistent with the NMR [65] (discussed in Chapter 6) and UV-absorption [66] changes that show a weakening of the indole hydrogen bond of Trp265 in meta II.

The motion of the retinal and the extracellular end of H6 is coupled to the motion of EL2 and H5, which in turn leads to deprotonation of the retinal SB. The disruption of

the salt bridge between Lys296 (H7) and Glu113 (H3) would induce a shift in the extracellular end of H7 upwards towards EL2. Our NMR data (discussed above) are consistent with a coupled motion of the extracellular segments of H6 and H7 toward EL2. Therefore, we propose that the change in the position of the retinal leads to concerted motion of the extracellular ends of both H6 and H7; H6 cannot move without rearrangement of H7 and vice versa, in agreement with a global toggle switch mechanism proposed by Schwartz and coworkers for GPCR activation [23].

Movement of H7 towards the core of the protein has shown to be important for the activation of a number of other GPCRs. For example, a metal binding site introduced between the extracellular end of H3 and H7 in the $\beta_2$-AR receptor [141] and the melanocortin receptor [223] promotes activation in the presence of zinc. The bound metal is thought to pull the extracellular ends of H6 and H7 in towards the core of the protein. Similarly, in the C5a peptide receptor, mutation of residues in the putative H3-H7 interface to longer side chain amino acids prevented activation. Therefore, it was proposed that the bound ligand in these receptors pulls the extracellular end of H7 in towards the core of the protein, in the same fashion as retinal pulls the extracellular end of H7 upon isomerization and motion towards H5. In the inactive state of rhodopsin, EL2 folds between the extracellular ends of H6, H7 and H3 preventing their (H6 and H7) motion towards a more active conformation and thus stabilizing the inactive state of the receptor.

The interruption of the hydrogen bonding interactions involving Trp265 would lead to a further rearrangement of the hydrogen bonding network involving Asn302, Asp83 and Asn55. Our hypothesis is that Asn302 rotates toward H2 and is more strongly hydrogen bonded to Asp83 in meta II. This is in accord with FTIR studies on the D83N mutant [63,64], which revealed that Asp83 becomes more strongly hydrogen bonded upon meta II formation.

Studies on other GPCRs, for example thyrotropin-releasing hormone receptor, show complete loss of trandsucin activity upon mutation of Asn55, Asp83 or Asn302 [303]. Interestingly, no loss of activity was observed when Asn302 and Asp83 were interchanged in other receptors [284-286]. These observations suggest that the water-mediated hydrogen bonds between Asn302, Asp83 and Asn55 are responsible for stabilizing both the inactive and active state of the receptor [50].

The combined effect of the motion of the extracellular end of H7 and rotation of Asn302 toward Asn55 (H1) and Asp83 (H2) in meta II would help straighten the extracellular end of H7 that forms a distorted $3_{10}$ helix in rhodopsin. This is consistent with the P303A mutation in rhodopsin that leads to hyperactivity [292].

Rearrangement of the hydrogen bonding network involving H7 and structural changes around Asn302 (H7) would lead to a reorganization of interaction between residues on the cytoplasmic end of H7 and H8 required for the active conformation of the receptor. This rearrangement of H7 is consistent with SDSL studies where small movements of H7 and H8 are observed in conjunction with a large (~5 Å) movement of H6 upon meta II formation [88].

Further support for the rearrangement of H7/H8 comes from mutational studies mentioned above where, disruption of the packing interaction between Tyr306 on H7 and Phe313 on H8 by mutation of either residue enhanced meta II formation. However, as mentioned above both the mutants display very low levels of transducin activation [292]. These studies suggest that either Tyr306 and Phe313 are involved in interaction with the G-protein and/or they control a structural rearrangement of H7/H8 required for activation.

Similar observations have been reported for tyrosine (7.53) of the NPxxY motif in the serotonin 5HT2C receptor [304]. Mutation of Tyr7.53 to a number of amino acids produced three separate constitutive active phenotypes: moderate, high and locked on

constitutive activity. Computational analysis [304] of the serotonin receptor sequence showed that Tyr7.53 is interacting with an aromatic residue at position 7.60 on H8 analogues to Phe313 (H8) in rhodopsin. ). Additionally, we observed a loss of a 2D DARR NMR contact between $^{13}C\varepsilon_1$-His65 (H1) and $^{13}C\beta$-Cys316 (H8) in meta II indicating a movement of H8 away from the cytoplasmic end of H1 (see Fig. 7.2D).

Our NMR data on the Y306F mutant suggest that Tyr306 becomes more strongly hydrogen bonded in meta II (Fig. 7.4 and Appendix A.6). As mentioned before, the 1D $^{13}C\zeta$-Tyr difference spectra (rhodopsin minus meta II) are very sensitive to the strength of the hydrogen bond to the hydroxyl group of a tyrosine [225]. The difference spectrum between rhodopsin and meta II highlights the $^{13}C\zeta$-tyrosine resonances that change upon rhodopsin activation (see Section 4.4, Fig. 4.6B). The 1D $^{13}C\zeta$-tyrosine difference spectrum (between rhodopsin and meta II) for the Y306F mutant looked quite similar to the 1D $^{13}C\zeta$-Tyr difference spectrum for the WT receptor (see Fig. 7.4B) indicating that the hydrogen bonding strength for Tyr306 does not change appreciably between rhodopsin and meta II. However, when we overlapped the difference spectra between mutant rhodopsin and WT rhodopsin with difference spectra between mutant meta II and WT meta II (see Appendix A.6) we observed that the Tyr306 resonance shifts by ~1.6 ppm downfield in rhodopsin to meta II conversion consistent with it becoming more strongly hydrogen bonded in meta II. On the other hand, a similar analysis on Y301F mutant revealed that Tyr301 resonance does not shift considerably between rhodopsin and meta II suggesting that it does not undergo any significant change in its hydrogen bonding interactions. The 1D $^{13}C\zeta$-Tyr difference spectrum for Y301F mutant looked similar to the WT difference spectrum (Fig. 7.4A

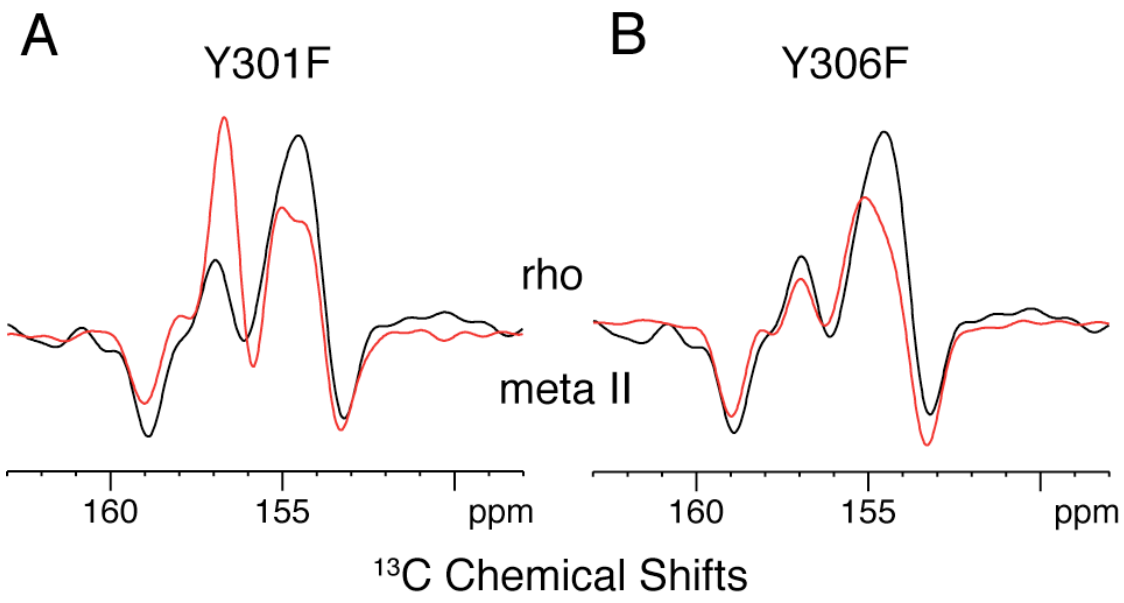


**Figure 7.4: One dimensional (1D) $^{13}$C CP-MAS difference spectra of rhodopsin and meta II labeled with $^{13}$Cζ-tyrosine.** Overlap of the difference spectra for wild-type rhodopsin (black) and rhodopsin mutants (red), Y301F (A), Y306F (B).

The NMR data are consistent with SDSL studies on H8 demonstrating an increase in distance by 2-4 Å between Asn310 and Cys316 upon meta II formation [293,305]. Sakmar and coworkers [306] have proposed that the amphipathic nature of H8 allows it to act as a conformational switch that can adopt different secondary structures depending on its physical environment. Using fluorescence and circular dichroism (CD) they have shown that the structural properties of H8 depends on composition of lipids in the membrane and that it changes conformation from a structured α-helix in rhodopsin to a more unstructured loop like conformation in meta II. However, the opsin crystal structure [68,290] does not show a considerable movement of H8.

Fahmy and coworkers [62] have used fluorescence and IR cross-correlation spectroscopy to correlate changes observed in the emission from the fluorescein label, covalently attached to Cys316 on H8, with changes observed in the FTIR absorption bands upon activation. They found that changes in the conformation of H8, deduced from changes in the emission from the fluorescein label on Cys316, were highly correlated with the changes in the hydrogen bonding strength of Asp83 (H2), which is part of the hydrogen bonding network involving H7. No correlations were observed with changes in the FTIR bands associated with Glu122. Additionally, they [62] were able to assign an FTIR band in meta II at 1643 $cm^{-1}$ to a partial loss in the α-helical secondary structure of H8 upon activation. A similar change in the secondary structure was observed for the synthetic peptide derived from the H8 of the cannabinoid receptor, where a loss of α-helical structure was observed upon G-protein binding [307,308].

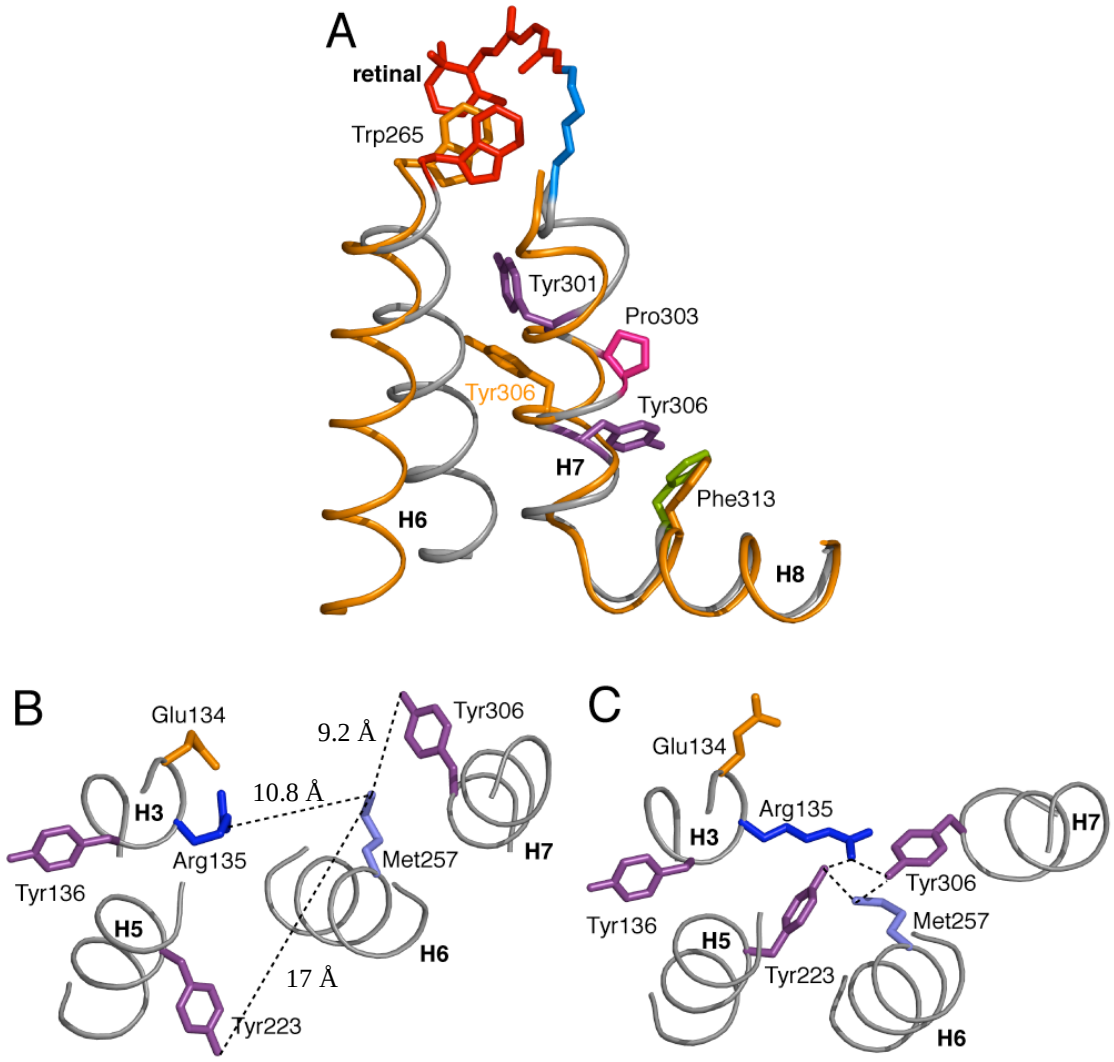


**Figure 7.5: A comparison of the rhodopsin [50] and opsin [68] crystal structures, highlighting the changes in H7**. (A) An overlap of the rhodopsin (grey) and opsin (orange) structures shows a large movement of the side chain of Tyr306 on H7 from its (purple) position in rhodopsin near Phe313 to its new position facing H6 in opsin (orange). The figure also emphasizes the outward motion of the intracellular part of H6 in opsin and the fact that H8/Phe313 do not move significantly from their positions in rhodopsin. Additionally, Trp265 does not show any rotamer change in opsin as compared to rhodopsin. (B) and (C) presents the interaction of amino acids around the ERY motif on H3 in rhodopsin and opsin respectively.

The above mentioned studies are consistent with a model that suggests that the hydrogen bonding network involving Asp83 couples the retinal binding site to the cytoplasmic end of H7 and H8 through the conserved NPxxY motif on H7. This hydrogen bonding network is essential for transmitting steric and electrostatic rearrangements from the retinal binding site to the cytoplasmic side of rhodopsin.

Our proposed model for the conformational changes in H7 and H8 is consistent with the recent the recent crystal structures of opsin where Tyr306 is re-oriented toward Arg135 of the ionic lock [68,290], which is stabilized in an open conformation by elements from H5 (Tyr223), H6 (Met257), and H7 (Tyr306). Together, these observations indicate that retinal isomerization (or ligand-binding in the ligand-activated GPCRs) results in structural changes involving the extracellular end of H7 that allow the cytoplasmic end to adopt an active conformation (see Fig. 7.5). However, in contrast to our model the opsin crystal structure [68,290] does not show any appreciable change in the conformation of Phe313 or H8 (see Fig. 7.5).

How does retinal isomerization and Schiff base deprotonation lead to motion of H7? There are two possibilities. The first possibility is that a change in the position of the retinal directly effects the position of H7 through its covalent linkage to Lys296. We previously proposed a “push-pull” mechanism for activation involving a push on H5 by the ionone ring and a pull on H7 via the covalently attached retinal [100]. As mentioned above, the distance constraints presented here and in Chapter 4 on the motion of EL2 indicate that translation of the retinal toward H5 is more modest (~2 Å) and that EL2 moves away from the retinal binding site upon activation. The reduced motion of retinal toward H5 described above would suggest a more modest role for the direct covalent bond between the retinal and H7. In fact, Oprian and co-workers have shown that a covalent bond between retinal and Lys296 is not required for activation [91].

The second possibility and a more likely possibility for how retinal isomerization and Schiff base deprotonation lead to a change in the position of the extracellular end of H7 is that the H7 helix responds to changes in other structural elements in the protein. The closest elements that change position in meta II are EL2 and H6. The extracellular end of H7 between Met288 and Ala292 packs against EL2 and will likely shift due to displacement of EL2 as a result of changes in both steric and electrostatic interactions. H6 packs against H7 along its entire length, and mutations along the H6-H7 interface modulate activity. For example, Oprian and coworkers showed that mutants of Lys296 result in constitutive activity [219] and that the magnitude of the activity is inversely correlated with residue size [294]. They concluded that the electrostatic Lys296-Glu113 interaction along with a steric contact involving the Lys296 side chain both contribute to preventing receptor activation, presumably by preventing motion of H7. A similar loss of steric interactions between Trp265 and Ala295 (adjacent to Lys296) occurs in the activation of the wild-type receptor. Specifically, as described above, motion of the retinal allows for the rotation of Trp265 away from Ala295 on H7, which in turn may facilitate a shift of H7 into an active orientation.

# Chapter 8

# Conclusion

## *8.1 Model for the photoactivation of rhodopsin*

Rhodopsin is the visual photoreceptor responsible for black and white vision in low light that is found in the rod cells of the human retina. It is a 40 kDa eukaryotic membrane protein that belongs to the large, pharmaceutically important family of G protein-coupled receptors (GPCRs). These receptors have a common architecture consisting of seven transmembrane (TM) helices. Activation of rhodopsin by light is initiated by isomerization of its photoreactive 11-*cis* retinylidene chromophore. The chromophore is covalently bound within the bundle of transmembrane helices through a protonated Schiff base linkage to Lys296. The crystal structure of rhodopsin in the dark, inactive state has previously been solved to high resolution [31,49,50]. However, no high-resolution structural data are available for metarhodopsin II, the active state of rhodopsin.

The work presented in this thesis describes how structural constraints obtained by solid-state Nuclear Magnetic Resonance (NMR) spectroscopic measurements of the metarhodopsin II intermediate are combined with restrained molecular dynamics simulations (see Appendix, A.1) to understand the pathway for light activation of rhodopsin. Since the time scale for the formation of the metarhodopsin II intermediate (> 1 ms) is beyond that readily accessible by molecular dynamics, we use NMR distance restraints from $^{13}C$ dipolar recoupling measurements to guide the simulations. The

simulations yield a working model for how retinal isomerization and thermal relaxation are coupled to receptor activation.

We used $T_1$ (spin-lattice / longitudinal) relaxation time measurements to establish the conformation of the β-ionone ring of the retinal in rhodopsin and meta II. The observation that the retinal C18 methyl group has a short $T_1$ relaxation time in both the dark-state of rhodopsin and the meta II intermediate demonstrates that the β-ionone ring of the retinal chromophore has a 6-s-*cis* conformation about the C6-C7 single bond in rhodopsin and it does not change upon activation. The 6-s-*cis* conformation is in contrast with the 6-s-*trans* conformation observed for the retinal chromophore in bacteriorhodopsin [188]. Furthermore, comparison of the $^{13}C$ chemical shifts for the retinal in meta II with those of retinal model compounds and the 11-*cis* retinal in rhodopsin suggests that the retinal is in a polar environment in meta II with significant protein interactions near the β-ionone ring (C5, C17) and the Schiff base (C14).

Fig. 8.1 presents snapshots from around the retinal binding site to highlight the structural rearrangements observed from our solid-state NMR data upon rhodopsin activation. The model of the activation mechanism of rhodopsin based on our NMR measurements both complements and contrasts with the models of activation proposed on the basis of crystal structures of rhodopsin [49,50] and its photointermediates [68,89,90,185,309]. The emerging picture is that there does not appear to be a single trigger or switch that changes upon receptor activation, but rather changes occur throughout the protein as a result of retinal motion. In contrast, Palczewski and co-workers [185] proposed that GPCR activation might only involve a simple relaxation of a more rigid inactive receptor structure. The structural changes they observed in the crystal structure of a rhodopsin photointermediate

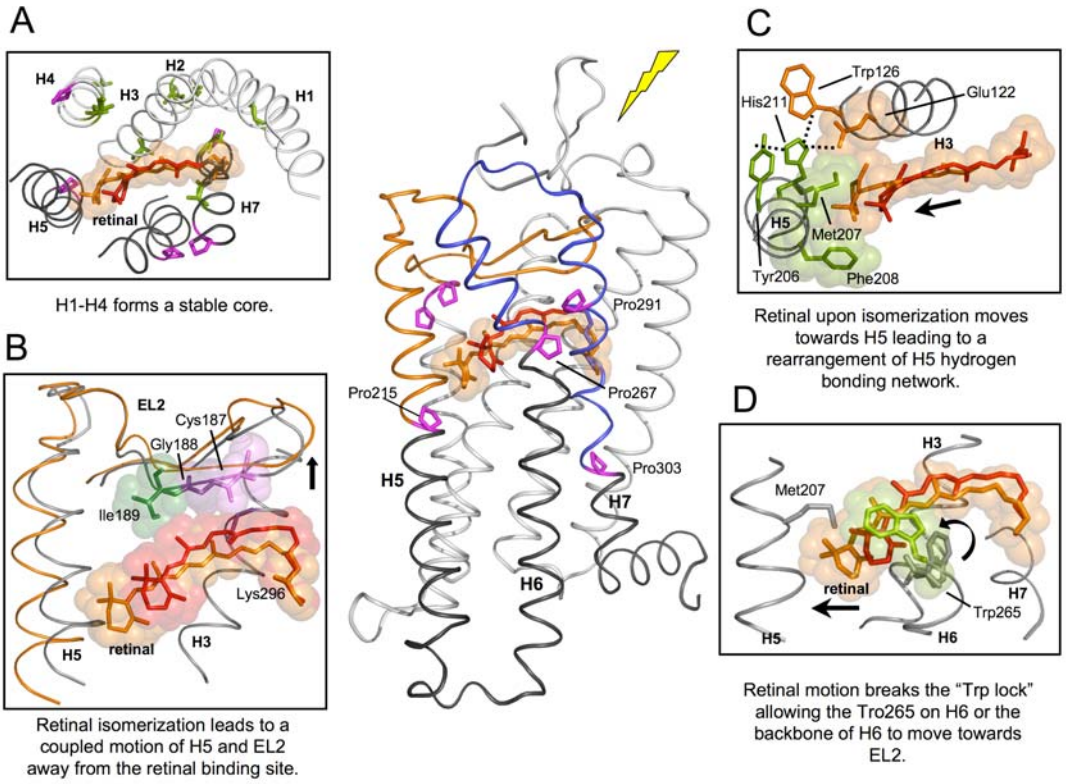


**Figure 8.1: Meta II model generated from restrained molecular dynamic simulations using solid-state NMR data.** The central figure presents a view of the rhodopsin crystal structure [50] highlighting the two helix-loop-helix (HLH) segments proposed to interact upon rhodopsin activation. The H4 (Pro171)-EL2-H5(Pro215) segment is shown in orange and the H6(Pro267)-EL3-H7(Pro291) segment is shown in blue. Retinal isomerization within the tightly packed binding site results in steric contacts between the β-ionone ring and H5, and between the retinal C19 and C20 methyl groups and EL2. These interactions trigger the simultaneous displacement of EL2 and H5. Motion of the β-ionone ring is also coupled to the motion of Trp265. Trp265 is packed against the β-ionone ring and C20 of the retinal, as well as Gly121 on H3 and Ala295 on H7. Movement of the Trp265 sidechain away from these critical contacts triggers the shift of helices H6 and H7 into active conformations. The coupled motions of helices H5-H7, in turn, are coupled to the rearrangement of electrostatic interactions involving the conserved ERY sequence at the cytoplasmic end of H3, exposing the G protein binding site on the cytoplasmic surface of the protein. In (A) the group conserved residues on H1-H4 are represented in green color and the conserved prolines on H4, H5, H6 and H7 are presented in magenta.

with an unprotonated Schiff base are largely limited to the loops on the cytoplasmic surface of the protein [185]. In their study, the retinal chromophore could not be resolved in either the rhodopsin structure or the photoactivated intermediate, with the exception of electron density attributed to the β-ionone ring in one of three photoactivated monomers in the crystallographic unit cell.

More recently, the crystal structure of opsin [68] has revealed several elements that are believe to be associated with the active state. These include outward motion (~6-7 Å) of the cytoplasmic side of H6, a 2-4 Å motion of the cytoplasmic end of H5 towards the intracellular end of H6 and breaking of the Arg135-Glu247 ionic lock. Since opsin exhibits only low basal activity (comparable to many ligand-activated GPCRs) [159], the essential elements required for activation must be missing in the opsin structure.

Based on our data mentioned above and in the previous studies presented on the H1-H4 core [79], it was observed that helices H1-H4 form a tightly packed core stabilized by strong van der Waals interactions between helices mediated by the group-conserved residues (e.g. Ala, Gly, Val, Ser and Thr) and by a series of interhelical hydrogen bonds. This stable core of H1-H4 does not change significantly upon activation. Interestingly, most of the group-conserved residues are found on TM H1-H4 and hardly any on H5, H6 and H7 (details in Chapter 1). However, highly conserved prolines (> 90% sequence identity) are found on helices H5 (Pro215), H6 (Pro267) and H7 (Pro303) providing them a degree of flexibility to undergo conformational changes. This led us to propose that in the inactive state of rhodopsin, helices H1-H4 form a stable core that does not change significantly upon activation and H5, H6 and H7 have multiple interactions with this core that are modulated in a concerted fashion upon activation. Similar group-conserved residues were found to stabilize helices H2-H4 in the β2-AR [81].

The second extracellular loop (EL2) of the rhodopsin forms a cap over the binding site of the photoreactive 11-*cis* retinylidene chromophore. A critical question has been whether EL2 forms a reversible gate that opens upon activation or acts as a rigid barrier. Upon absorption of a photon of light retinal isomerizes from a constrained 11-*cis* to an all-*trans* conformation. Retinal isomerization leads to steric strain within the retinal binding site between the retinal β-ionone ring and helix 5 (H5), and between the retinal C19/C20 methyl groups and the second extracellular loop (EL2). These interactions lead to a rearrangement of hydrogen bonding networks connecting EL2 with the extracellular ends of transmembrane helices H4, H5 and H6, triggering its motion away from the retinal (see Fig.8.1B), deprotonation of the Schiff base nitrogen and protonation of Glu113. This disrupts the salt bridge between H3 and H7 important for stabilizing the inactive state of the receptor.

The retinal C19 methyl acts as a "steric trigger" that is tightly packed between Tyr268 (H6), Tyr191 and Ile189 on EL2 in rhodopsin. The interactions between the retinal C19 methyl group and the surrounding protein drive the formation of meta II. This in turn is consistent with mutational studies on Tyr268. The Y268F mutant displays a marked decrease in transducin activation due to lack of the steric interaction required for efficient coupling of retinal isomerization to formation of meta II. Additionally, rhodopsin regenerated with analogues of retinal lacking the C19 methyl group (9-desmethyl retinal) shifts the equilibrium between meta I and meta II towards meta I, inhibiting transducin activation [129,138]

NMR measurements further reveal that structural changes in EL2 are tightly coupled to changes in the hydrogen bonding networks within the protein core. Displacement of EL2 is coupled to the motion of H5 in metarhodopsin II. The subfamily specific H4-EL2-H5 unit in rhodopsin is designed to hold H5 and the extracellular ends of H6 and H7 in inactive conformations. We propose that the displacement of EL2 away from the retinal binding site, upon retinal isomerization, is coupled to motion of H5 and

to the inward motion of the H6-EL3-H7 unit (explained in chapter 5) involving the extracellular parts of H6 and H7. This is in agreement with the global toggle switch mechanism for GPCR activation introduced by Schwartz and co-workers [242]. Similar motions are likely to occur in other GPCRs [23,240] suggesting that EL2 may act as a plug or cork that must be displaced for receptor activation.

Packing of the β-ionone ring against H5 leads to a rearrangement of its hydrogen bonding networks involving Tyr206 and His211 on H5, Ala166 on H4 and Glu122 and Trp126 on H3. On the extracellular side of H5, the hydrogen bond that exist between the side chain of Glu122 (H3) and the backbone carbonyl of His211 in rhodopsin, is disrupted in meta II and a new interaction is observed directly between their side chains. This observation suggests that H5 must undergo a rotation/and or motion upon formation of meta II. Furthermore, observation of strong contacts between the side chain of Met207 (H5) and retinal C6 and C7, Cys167 (H4) and His211 (H5) (data presented in Chapter 5) are consistent with a movement of H5, as the data alone cannot be explained by a rearrangement of the Met207 (H5) side chain. Further support for the motion of H5 comes from the observation of a weakening of the contact between His211 (H5) and Cys167 (H4) in meta II (data presented in Chapter 5 and Appendix A.4). This rearrangement of the extracellular end of H5 in turn facilitates the rotation of the cytoplasmic end of H5 towards H6. The rotation of H5 places the side chain of Tyr223 in the vicinity of the ionic lock between Arg135, Glu134 and Glu247 on the cytoplasmic side of H3 and H6, respectively (see Fig. 8.2B).

Motion of the retinal β-ionone ring towards H5 is coupled to the motion of Trp265 on H6, disrupting the tight packing interaction between the retinal β-ionone ring and Trp265. Movement of Trp265 breaks the water mediated hydrogen bonding interaction between Trp265 and residues (Ser298, Ala299, Tyr301, Asn302) on H7, Met257 on H6, Asp83 on H2 and Asn55 on H1 (Details in Chapter 7). Removal of the "Trp-Lock" allows the outward motion of the intracellular end of H6 disrupting the ionic

lock between Glu247 (H6) and Arg135 (H5). The motion of H6 facilitates the formation of a new hydrogen bonding contact between Tyr223 on H5 and Arg135 on H6, effectively breaking the Arg135-Glu247 ionic lock and exposing the G-protein binding site on the cytoplasmic surface of the protein. The outward motion of H6 breaks the hydrogen bonding interaction between Met257 (H6) and the NPxxY motif on H7. The new position of H6 places the side chain of Met257 in direct contact with Arg135 (H3) and Tyr223 on H5 (see Fig. 8.2C).

The interruption of the hydrogen bonding interaction involving Trp265 would lead to a further rearrangement of the hydrogen bonding network involving Asn302, Asp83 and Asn55. Our hypothesis is that Asn302 rotates toward H2 and is more strongly hydrogen bonded to Asp83 in meta II (Fig. 8.2C). This is in accord with FTIR studies on the D83N mutant [63,64], which revealed that Asp83 becomes more strongly hydrogen bonded upon meta II formation. The combined effect of the motion of the extracellular end of H7 and rotation of Asn302 toward Asn55 (H1) and Asp83 (H2) in meta II would help straighten the extracellular end of H7 that forms a distorted $3_{10}$ helix in rhodopsin. This is consistent with the P303A mutation in rhodopsin that leads to hyperactivity [292].

Therefore, rearrangement of the hydrogen bonding network involving H7 and structural changes around Asn302 (H7) would lead to reorganization of interactions between residues on the cytoplasmic end of H7 and H8 required for the active conformation of the receptor. This rearrangement of H7 is consistent with our NMR data on Y301F and Y306F mutants (discussed in Chapter 7) and SDSL studies where small movements of H7 and H8 are observed in conjunction with a large (~5 Å) movement of H6 upon meta II formation [88].

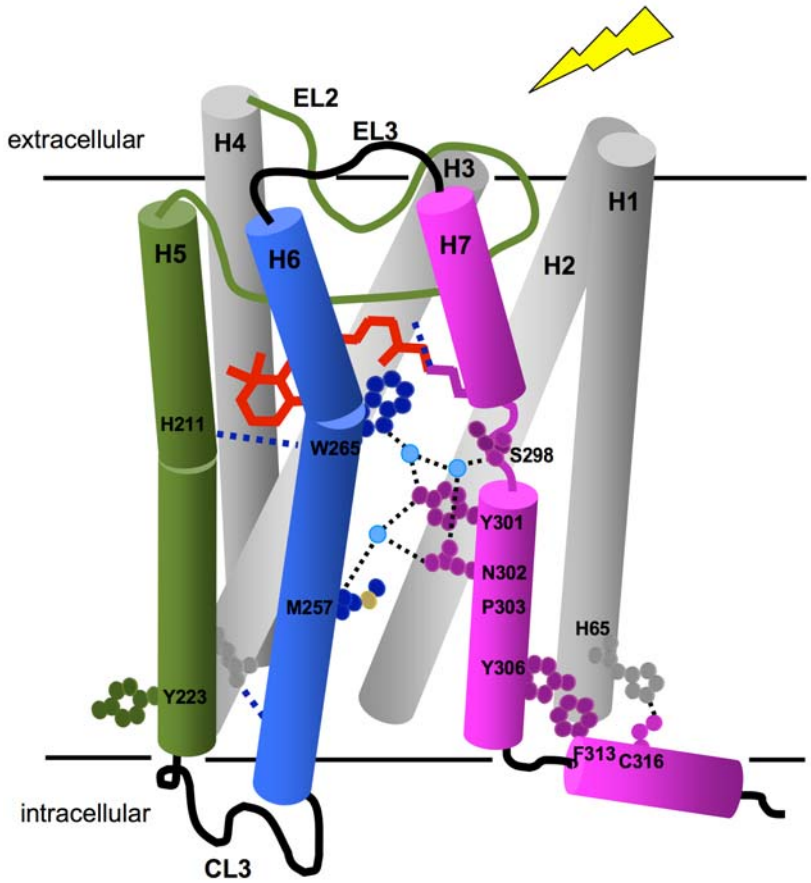


**Rhodopsin**

**Figure 8.2A:** A cartoon representation of changes in rhodopsin upon retinal isomerization and SB deprotonation. H1-H4 core is presented in grey. TM H5 (green), H6 (blue), H7 (magenta) are shown. EL2 is colored green. The salt bridge is shown as a dotted blue line between H3 and retinal. Three hydrogen bonding network stabilizing the inactive state are presented. First, involving H5 is represented as a dotted blue line connecting H5 and H3. Second, involving H7 is shown by a series of water-mediated hydrogen bonds (black) between H7 and H6. Third, the ionic lock between H6 and H3, shown as a dotted blue line. Packing interactions are shown between (1) Phe313 (H8) and Tyr306 (H7); (2) His65 and Cys316 and (3) Trp265 and retinal.

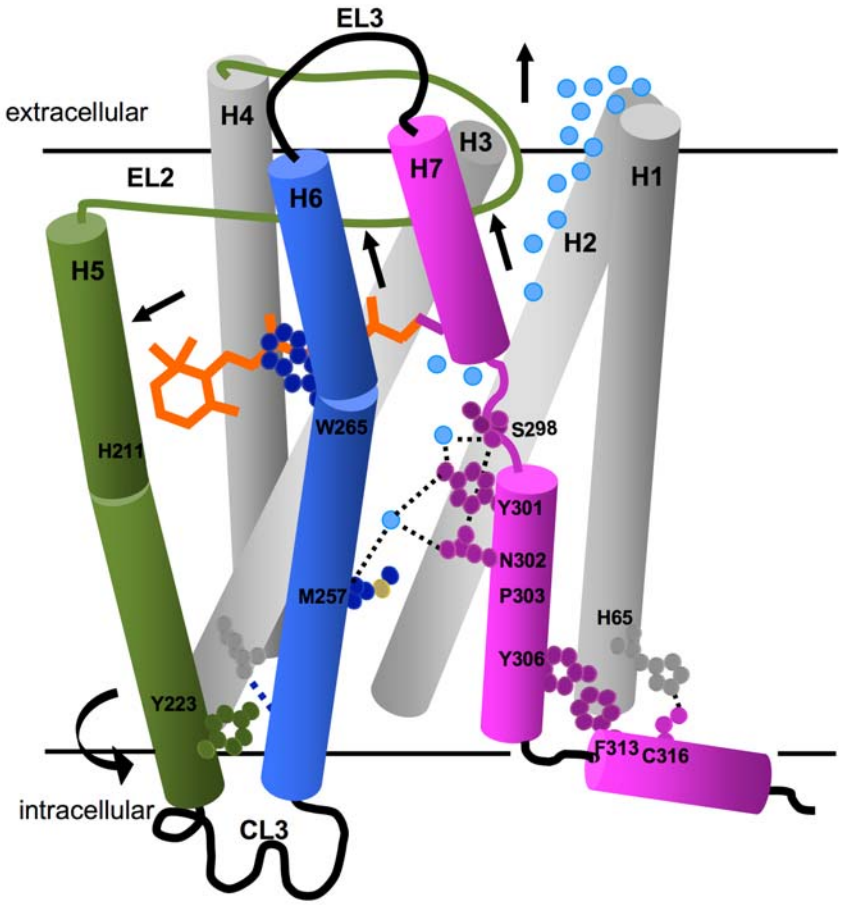


**Meta $II_a$**

**Figure 8.2B:** A cartoon representation of changes in rhodopsin upon retinal isomerization and SB deprotonation: H1-H4 core remains stable. Retinal isomerizes to an all-*trans* conformation (orange) causing a coupled motion of EL2 and H5 (green). EL2 is displaced away from the retinal binding site. Hydrogen bond between His211 carbonyl and Glu122 side chain is disrupted in meta IIa. H5 moves outwards and rotates towards H6 at the cytoplasmic side. This places the side chain of Tyr223 in the vicinity of the ionic lock between H3 and H6. Retinal isomerization breaks the "Trp-lock" and allows the side chain and the extracellular end of H6 to move upwards towards EL2. Retinal motion toward H5 pulls the extracellular end of H7 up and in towards the core of the protein. Movement of EL2 makes the retinal binding site more accessible to water that leads to disruption of disruption of the salt bridge between Lys297 on H7 and H3.

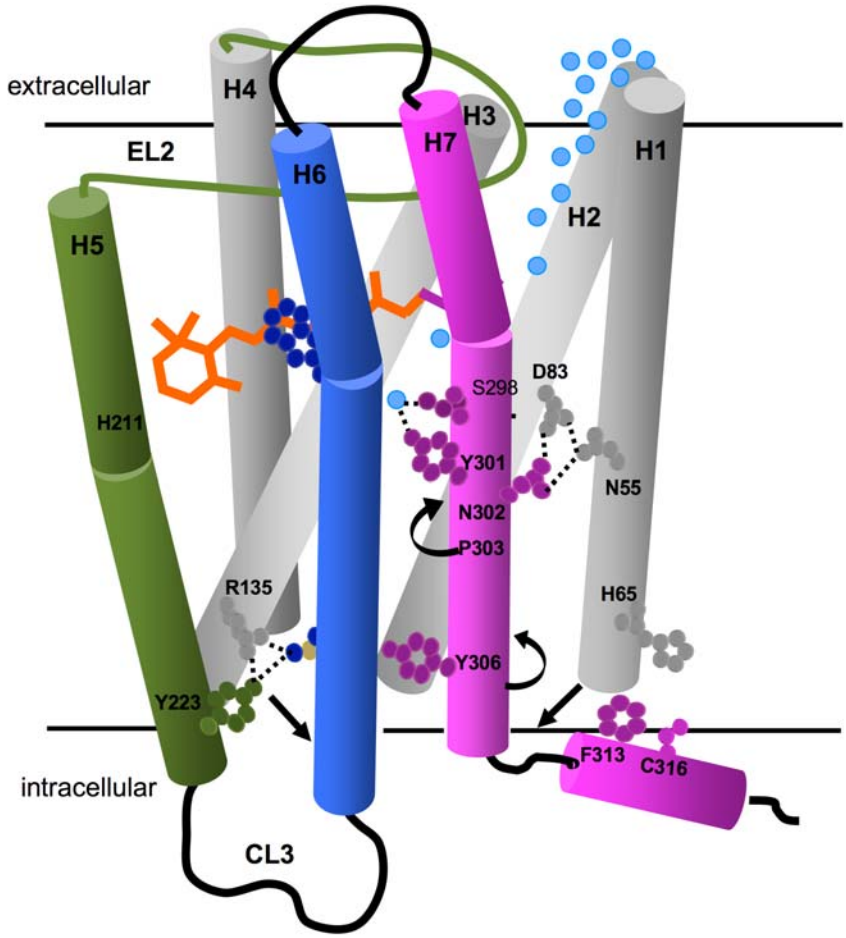


**Meta $II_b$**

**Figure 8.2C:** A cartoon representation of changes in rhodopsin upon retinal isomerization and SB deprotonation: H1-H4 core remains stable. Movement of Trp265 and H7 leads to a rearrangement of the hydrogen bonding network involving NPxxY on H7. Disruption of the hydrogen bonding interactions with Trp265 and Met257 allows the cytoplasmic side of H6 to move outwards. This disrupts the ionic lock between Arg135 (H3) and Glu247 (H6). And a new interaction is established between Tyr223 (H5) and Arg135 (H3) and Met257 (H6). Asn302 on H7 rotates toward H2 and is more strongly hydrogen bonded to Asp83 in meta II. The combined effect of Asn302 rotation and motion of the extracellular part of H7 helps in straightening the helix from its distorted $3_{10}$ conformation near Asn302. The motion of H7 is coupled to a motion of H8 that lead to the disruption of the packing interactions between Tyr306 (H7)–Phe313 (H8) and His65 (H1)-Cys316(H8).

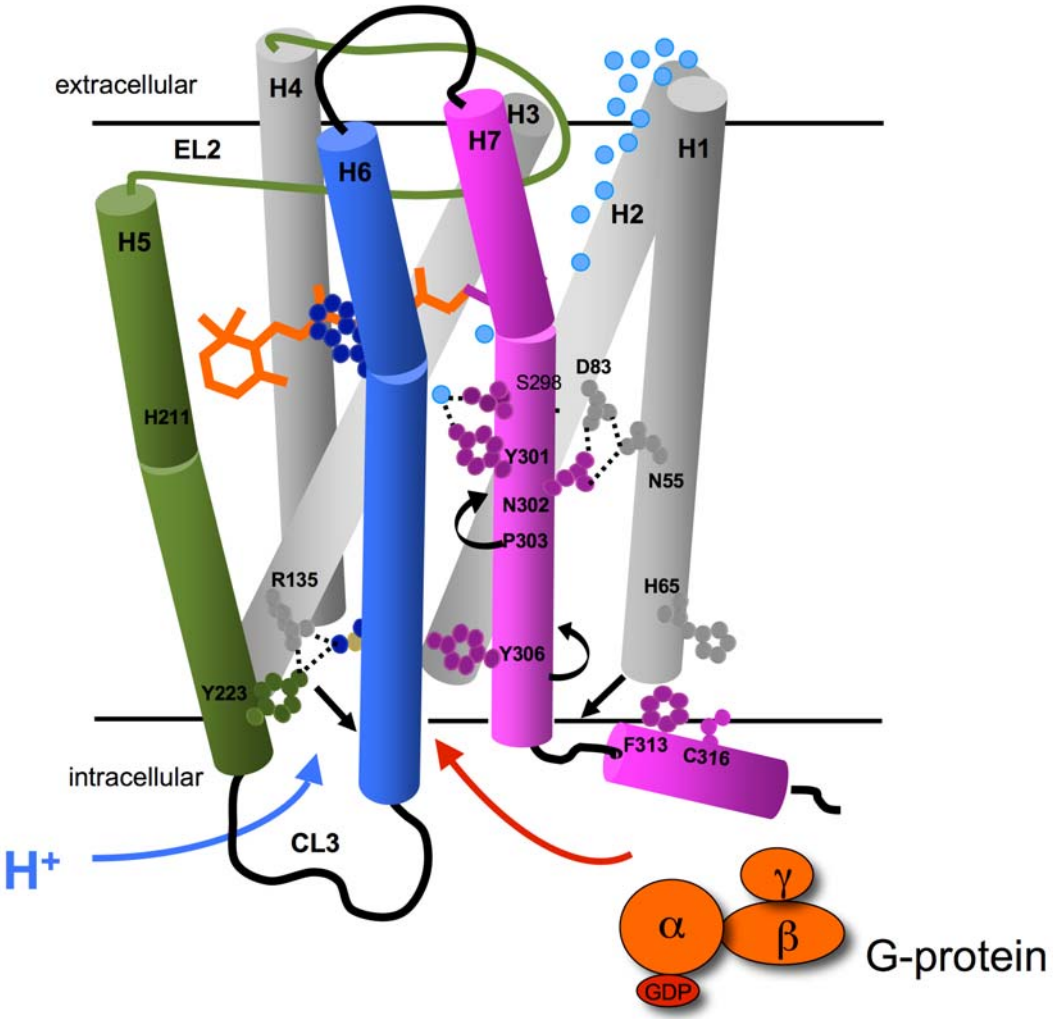


**Meta $II_bH^+$**

**Figure 8.2D:** A cartoon representation of changes in rhodopsin upon retinal isomerization and SB deprotonation: H1-H4 core remains stable. The receptor after undergoing all the structural rearrangements mentioned above is in an active conformation that enable uptake of a proton, from the surrounding, most likely by Glu134 on H3 and it facilitates binding and activation of the G-protein (orange), transducin.

We propose that EL2 motion and SB deprotonation are coupled to the motion of H5 and are needed for the retinal, H7 and H8 to shift into their active positions. The movement of H8 is also consistent with our NMR data where we observed a loss of a 2D DARR NMR contact between $^{13}C\varepsilon_1$-His65 (H1) and $^{13}C\beta$-Cys316 (H8) in meta II (data shown in Chapter 7) indicating a movement of H8 away from the cytoplasmic end of H1 (see Fig. 8.2C) and other biophysical studies [62,293,305,306].

The hydrogen bonding network involving Asp83 couples the retinal binding site to the cytoplasmic end of H7 and H8 through the highly conserved NPxxY motif on H7 (see Fig. 7.1B) [62]. This hydrogen bonding network transmits the steric and electrostatic rearrangements from the retinal binding site to the cytoplasmic side of rhodopsin essential for modulating the interactions of the receptor with the G-protein transducin. All the structural changes and rearrangements mentioned above can be visualized in the schematic cartoon model of rhodopsin activation presented in Fig. 8.2.

Together these results provide a new working model for how structural changes in the retinal upon absorption of a photon are involved in receptor activation and are coupled to structural changes in several functional microdomains described previously in the introduction (Section 1.3.3) [26,310]. The location of the retinal and structural reorganization of the protein upon activation provide a blue print for understanding the action of agonists and antagonists in the large family of class A GPCRs.

# Bibliography


1. Ballesteros, J.A. & Weinstein, H. Integrated methods for the construction of three dimensional models and computational probing of structure-function relations in G-protein coupled receptors. *Methods Neurosci.* 25, 366-428 (1995).
2. Bockaert, J. & Pin, J.P. Molecular tinkering of G protein-coupled receptors: an evolutionary success. *EMBO J.* 18, 1723-1729 (1999).
3. Gether, U. Uncovering molecular mechanisms involved in activation of G protein-coupled receptors. *Endocr. Rev.* 21, 90-113 (2000).
4. Overington, J.P., Al-Lazikani, B. & Hopkins, A.L. Opinion - How many drug targets are there? *Nat. Rev. Drug Discov.* 5, 993-996 (2006).
5. Rovati, G.E., Capra, V. & Neubig, R.R. The highly conserved DRY motif of class A G protein-coupled receptors: Beyond the ground state. *Mol. Pharmacol.* 71, 959-964 (2007).
6. Kolakowski, L.F. Gcrdb - a G-protein-coupled receptor database. *Recept. Channels* 2, 1-7 (1994).
7. Horn, F. et al. GPCRDB: an information system for G protein-coupled receptors. *Nucleic Acids Res.* 26, 275-279 (1998).
8. Probst, W.C., Snyder, L.A., Schuster, D.I., Brosius, J. & Sealfon, S.C. Sequence alignment of the G-protein coupled receptor superfamily. *DNA Cell Biol.* 11, 1-20 (1992).
9. Heck, M. & Hofmann, K.P. Maximal rate and nucleotide dependence of rhodopsin-catalyzed transducin activation - Initial rate analysis based on a double displacement mechanism. *J. Biol. Chem.* 276, 10000-10009 (2001).

10. Krupnick, J.G. & Benovic, J.L. The role of receptor kinases and arrestins in G protein-coupled receptor regulation. *Annu. Rev. Pharmacol. Toxicol.* 38, 289-319 (1998).
11. Lefkowitz, R.J. G protein-coupled receptors. III. New roles for receptor kinases and beta-arrestins in receptor signaling and desensitization. *J. Biol. Chem.* 273, 18677-18680 (1998).
12. Daaka, Y. et al. Essential role for G protein-coupled receptor endocytosis in the activation of mitogen-activated protein kinase. *J. Biol. Chem.* 273, 685-688 (1998).
13. Fredriksson, R. & Schiöth, H.B. The repertoire of G-protein-coupled receptors in fully sequenced genomes. *Mol. Pharmacol.* 67, 1414-1425 (2005).
14. Palczewski, K. G protein-coupled receptor rhodopsin. *Annu. Rev. Biochem.* 75, 743-767 (2006).
15. Fredriksson, R., Lagerström, M.C., Lundin, L.G. & Schiöth, H.B. The G-protein-coupled receptors in the human genome form five main families. Phylogenetic analysis, paralogon groups, and fingerprints. *Mol. Pharmacol.* 63, 1256-1272 (2003).
16. Mirzadegan, T., Benko, G., Filipek, S. & Palczewski, K. Sequence analyses of G-protein-coupled receptors: Similarities to rhodopsin. *Biochemistry* 42, 2759-2767 (2003).
17. Ji, T.H., Grossmann, M. & Ji, I. G protein-coupled receptors. I. Diversity of receptor-ligand interactions. *J. Biol. Chem.* 273, 17299-17302 (1998).
18. Farrens, D.L., Altenbach, C., Yang, K., Hubbell, W.L. & Khorana, H.G. Requirement of rigid-body motion of transmembrane helices for light activation of rhodopsin. *Science* 274, 768-770 (1996).
19. Gether, U. et al. Agonists induce conformational changes in transmembrane domains III and VI of the $\beta_2$ adrenoceptor. *EMBO J.* 16, 6737-6747 (1997).

20. Ghanouni, P., Steenhuis, J.J., Farrens, D.L. & Kobilka, B.K. Agonist-induced conformational changes in the G-protein-coupling domain of the $\beta_2$ adrenergic receptor. *Proc. Natl. Acad. Sci. U.S.A.* 98, 5997-6002 (2001).

21. Yao, X.J. et al. Coupling ligand structure to specific conformational switches in the $\beta_2$-adrenoceptor. *Nature Chemical Biology* 2, 417-422 (2006).

22. Sheikh, S.P. et al. Similar structures and shared switch mechanisms of the $\beta_2$-adrenoceptor and the parathyroid hormone receptor - Zn(II) bridges between helices III and VI block activation. *J. Biol. Chem.* 274, 17033-17041 (1999).

23. Elling, C.E. et al. Metal ion site engineering indicates a global toggle switch model for seven-transmembrane receptor activation. *J. Biol. Chem.* 281, 17337-17346 (2006).

24. Han, S.J. et al. Identification of an agonist-induced conformational change occurring adjacent to the ligand-binding pocket of the M-3 muscarinic acetylcholine receptor. *J. Biol. Chem.* 280, 34849-34858 (2005).

25. Eilers, M., Hornak, V., Smith, S.O. & Konopka, J.B. Comparison of class A and D G protein-coupled receptors: Common features in structure and activation. *Biochemistry* 44, 8959 -8975 (2005).

26. Ballesteros, J. et al. Functional microdomains in G-protein-coupled receptors - the conserved arginine-cage motif in the gonadotropin-releasing hormone receptor. *J. Biol. Chem.* 273, 10445-10453 (1998).

27. Bownds, D. Site of attachment of retinal in rhodopsin. *Nature* 216, 1178-1181 (1967).

28. Wald, G. Carotenoids and the visual cycle. *J. Gen. Physiol.* 19, 351-371 (1935).

29. Kühn, H. Light-regulated and GTP-regulated interaction of GTPase and other proteins with bovine photoreceptor-membranes. *Nature* 283, 587-589 (1980).

30. Kühne, W. On the stable colours of the retina. *J. Physiol. (Lond.)* 1, 109-212 (1878).

31. Okada, T. et al. The retinal conformation and its environment in rhodopsin in light of a new 2.2 Å crystal structure. *J. Mol. Biol.* 342, 571-583 (2004).

32. Hubbard, R. & Kropf, A. The action of light on rhodopsin. *Proc. Natl. Acad. Sci. U.S.A.* 44, 130-139 (1958).

33. Menon, S.T., Han, M. & Sakmar, T.P. Rhodopsin: Structural basis of molecular physiology. *Physiol. Rev.* 81, 1659-1688 (2001).

34. Hubbell, W.L., Altenbach, C., Hubbell, C.M. & Khorana, H.G. Rhodopsin structure, dynamics, and activation: A perspective from crystallography, site-directed spin labeling, sulfhydryl reactivity, and disulfide cross-linking. *Adv. Protein Chem.* 63, 243-290 (2003).

35. Schoenlein, R.W., Peteanu, L.A., Mathies, R.A. & Shank, C.V. The first step in vision: femtosecond isomerization of rhodopsin. *Science* 254, 412-415 (1991).

36. Fisher, M.M. & Weiss, K. Laser photolysis of retinal and its protonated and unprotonated normal-butylamine Schiff-base. *Photochem. Photobiol.* 20, 423-432 (1974).

37. Kim, J.E., Tauber, M.J. & Mathies, R.A. Wavelength dependent cis-trans isomerization in vision. *Biochemistry* 40, 13774-13778 (2001).

38. Hamm, H.E. & Gilchrist, A. Heterotrimeric G proteins. *Curr. Opin. Cell Biol.* 8, 189-196 (1996).

39. Sakmar, T.P., Menon, S.T., Marin, E.P. & Awad, E.S. Rhodopsin: Insights from recent structural studies. *Annu. Rev. Biophys. Biomol. Struct.* 31, 443-484 (2002).

40. Baylor, D.A. Photoreceptor Signals and Vision. *Invest. Ophthalmol. Vis. Sci.* 28, 34-49 (1987).

41. Richard, E.A. & Lisman, J.E. Rhodopsin inactivation is a modulated process in *Limulus* photoreceptors. *Nature* 356, 336-338 (1992).

42. Lefkowitz, R.J. et al. G-protein-coupled receptors: regulatory role of receptor kinases and arrestin proteins. *Cold Spring Harb. Symp. Quant. Biol.* 57, 127-133 (1992).

43. Premont, R.T., Inglese, J. & Lefkowitz, R.J. Protein kinases that phosphorylate activated G protein-coupled receptors. *FASEB J.* 9, 175-182 (1995).

44. Graykeller, M.P., Detwiler, P.B., Benovic, J.L. & Gurevich, V.V. Arrestin with a single amino acid substitution quenches light-activated rhodopsin in a phosphorylation-independent fashion. *Biochemistry* 36, 7058-7063 (1997).

45. Vuong, T.M. & Chabre, M. Deactivation kinetics of the transduction cascade of vision. *Proc. Natl. Acad. Sci. U.S.A.* 88, 9813-9817 (1991).

46. Otto-Bruc, A., Antonny, B., Vuong, T.M., Chardin, P. & Chabre, M. Interaction between the retinal cyclic GMP phosphodiesterase inhibitor and transducin. Kinetics and affinity studies. *Biochemistry* 32, 8636-8645 (1993).

47. Hargrave, P.A. et al. The Structure of Bovine Rhodopsin. *Biophys. Struct. Mech.* 9, 235-244 (1983).

48. Nathans, J. & Hogness, D.S. Isolation, sequence analysis, and intron-exon arrangement of the gene encoding bovine rhodopsin. *Cell* 34, 807-814 (1983).

49. Palczewski, K. et al. Crystal structure of rhodopsin: A G protein-coupled receptor. *Science* 289, 739-745 (2000).

50. Li, J., Edwards, P.C., Burghammer, M., Villa, C. & Schertler, G.F.X. Structure of bovine rhodopsin in a trigonal crystal form. *J. Mol. Biol.* 343, 1409-38 (2004).

51. Warne, T. et al. Structure of a $\beta_1$-adrenergic G-protein-coupled receptor. *Nature* 454, 486-491 (2008).

52. Cherezov, V. et al. High-resolution crystal structure of an engineered human $\beta_2$-adrenergic G protein-coupled receptor. *Science* 318, 1258-1265 (2007).

53. Murakami, M. & Kouyama, T. Crystal structure of squid rhodopsin. *Nature* 453, 363-367 (2008).

54. Sakmar, T.P., Franke, R.R. & Khorana, H.G. Glutamic acid-113 serves as the retinylidene Schiff base counterion in bovine rhodopsin. *Proc. Natl. Acad. Sci. U.S.A.* 86, 8309-8313 (1989).

55. Nathans, J. Determinants of visual pigment absorbance: identification of the retinylidene Schiff's base counterion in bovine rhodopsin. *Biochemistry* 29, 9746-9752 (1990).

56. Robinson, P.R., Cohen, G.B., Zhukovsky, E.A. & Oprian, D.D. Constitutively active mutants of rhodopsin. *Neuron* 9, 719-725 (1992).

57. Fu, D., Ballesteros, J.A., Weinstein, H., Chen, J. & Javitch, J.A. Residues in the seventh membrane-spanning segment of the dopamine D2 receptor accessible in the binding-site crevice. *Biochemistry* 35, 11278-11285 (1996).

58. Wess, J., Gdula, D. & Brann, M.R. Site-directed mutagenesis of the m3 muscarinic receptor: Identification of a series of threonine and tyrosine residues involved in agonist but not antagonist binding. *EMBO J.* 10, 3729-3734 (1991).

59. Roth, B.L., Shoham, M., Choudhary, M.S. & Khan, N. Identification of conserved aromatic residues essential for agonist binding and second messenger production at 5-hydroxytryptamine(2A) receptors. *Mol. Pharmacol.* 52, 259-266 (1997).

60. Rao, V.R. & Oprian, D.D. Activating mutations of rhodopsin and other G protein-coupled receptors. *Annu. Rev. Biophys. Biomol. Struct.* 25, 287-314 (1996).

61. Baldwin, J.M. The probable arrangement of the helices in G protein-coupled receptors. *EMBO J.* 12, 1693-1703 (1993).

62. Lehmann, N., Alexiev, U. & Fahmy, K. Linkage between the intramembrane H-bond network around aspartic acid 83 and the cytosolic environment of helix 8 in photoactivated rhodopsin. *J. Mol. Biol.* 366, 1129-1141 (2007).

63. Fahmy, K. et al. Protonation states of membrane-embedded carboxylic acid groups in rhodopsin and metarhodopsin II: A Fourier-transform infrared spectroscopy study of site-directed mutants. *Proc. Natl. Acad. Sci. U.S.A.* 90, 10206-10210 (1993).

64. Rath, P., DeCaluwe, L.L., Bovee-Geurts, P.H., Degrip, W.J. & Rothschild, K.J. Fourier transform infrared difference spectroscopy of rhodopsin mutants: light activation of rhodopsin causes hydrogen-bonding change in residue aspartic acid-83 during meta II formation. *Biochemistry* 32, 10277-10282 (1993).

65. Crocker, E. et al. Location of Trp265 in metarhodopsin II: Implications for the activation mechanism of the visual receptor rhodopsin. *J. Mol. Biol.* 357, 163-172 (2006).

66. Lin, S.W. & Sakmar, T.P. Specific tryptophan UV-absorbance changes are probes of the transition of rhodopsin to its active state. *Biochemistry* 35, 11149-11159 (1996).

67. Vogel, R. et al. Functional role of the "Ionic Lock" - An interhelical hydrogen-bond network in family a heptahelical receptors. *J. Mol. Biol.* 380, 648-655 (2008).

68. Park, J.H., Scheerer, P., Hofmann, K.P., Choe, H.W. & Ernst, O.P. Crystal structure of the ligand-free G-protein-coupled receptor opsin. *Nature* 454, 183-187 (2008).

69. Okada, T. & Nakamichi, H. X-ray crystallography of rhodopsin. *Phase Transit.* 77, 21-29 (2004).

70. Kaushal, S., Ridge, K.D. & Khorana, H.G. Structure and function in rhodopsin: the role of asparagine-linked glycosylation. *Proc. Natl. Acad. Sci. U.S.A.* 91, 4024-4028 (1994).

71. Karnik, S.S. & Khorana, H.G. Assembly of functional rhodopsin requires a disulfide bond between cysteine residues 110 and 187. *J. Biol. Chem.* 265, 17520-17524 (1990).

72. Hwa, J., Klein-Seetharaman, J. & Khorana, H.G. Structure and function in rhodopsin: Mass spectrometric identification of the abnormal intradiscal disulfide bond in misfolded retinitis pigmentosa mutants. *Proc. Natl. Acad. Sci. U.S.A.* 98, 4872-4876 (2001).

73. Franke, R.R., Sakmar, T.P., Graham, R.M. & Khorana, H.G. Structure and function in rhodopsin. Studies of the interaction between the rhodopsin cytoplasmic domain and transducin. *J. Biol. Chem.* 267, 14767-14774 (1992).

74. Janz, J.M. & Farrens, D.L. Rhodopsin activation exposes a key hydrophobic binding site for the transducin α-subunit C terminus. *J. Biol. Chem.* 279, 29767-29773 (2004).

75. Yang, K., Farrens, D.L., Hubbell, W.L. & Khorana, H.G. Structure and function in rhodopsin. Single cysteine substitution mutants in the cytoplasmic interhelical

E-F loop region show position-specific effects in transducin activation. *Biochemistry* 35, 12464-12469 (1996).

76. Marin, E.P. et al. The amino terminus of the fourth cytoplasmic loop of rhodopsin modulates rhodopsin-transducin interaction. *J. Biol. Chem.* 275, 1930-1936 (2000).
77. Weiss, E.R., Osawa, S., Shi, W. & Dickerson, C.D. Effects of carboxyl-terminal truncation on the stability and G protein-coupling activity of bovine rhodopsin. *Biochemistry* 33, 7587-7593 (1994).
78. Ballesteros, J.A. et al. Activation of the $\beta_2$-adrenergic receptor involves disruption of an ionic lock between the cytoplasmic ends of transmembrane segments 3 and 6. *J. Biol. Chem.* 276, 29171-29177 (2001).
79. Liu, W., Eilers, M., Patel, A.B. & Smith, S.O. Helix packing moments reveal diversity and conservation in membrane protein structure. *J. Mol. Biol.* 337, 713-729 (2004).
80. Eilers, M., Patel, A.B., Liu, W. & Smith, S.O. Comparison of helix interactions in membrane and soluble α-bundle proteins. *Biophys. J.* 82, 2720-2736 (2002).
81. Chelikani, P. et al. Role of group-conserved residues in the helical core of $\beta_2$-adrenergic receptor. *Proc. Natl. Acad. Sci. U.S.A.* 104, 7027-7032 (2007).
82. Okada, T., Takeda, K. & Kouyama, T. Highly selective separation of rhodopsin from bovine rod outer segment membranes using combination of bivalent cation and alkyl(thio)glucoside. *Photochem. Photobiol.* 67, 495-499 (1998).
83. Okada, T. et al. X-ray diffraction analysis of three-dimensional crystals of bovine rhodopsin obtained from mixed micelles. *J. Struct. Biol.* 130, 73-80 (2000).
84. Oprian, D.D., Molday, R.S., Kaufman, R.J. & Khorana, H.G. Expression of a synthetic bovine rhodopsin gene in monkey kidney cells. *Proc. Natl. Acad. Sci. U.S.A.* 84, 8874-8878 (1987).
85. Jansen, J.J.M., Mulder, W.R., De Caluwe, G.L.J., Vlak, J.M. & De Grip, W.J. In vitro expression of bovine opsin using recombinant baculovirus: the role of

glutamic acid (134) in opsin biosynthesis and glycosylation. *Biochim. Biophys. Acta* 1089, 68-76 (1991).

86. Sheikh, S.P., Zvyaga, T.A., Lichtarge, O., Sakmar, T.P. & Bourne, H.R. Rhodopsin activation blocked by metal-ion-binding sites linking transmembrane helices C and F. *Nature* 383, 347-350 (1996).
87. Struthers, M., Yu, H.B. & Oprian, D.D. G protein-coupled receptor activation: Analysis of a highly constrained, "straitjacketed" rhodopsin. *Biochemistry* 39, 7938-7942 (2000).
88. Altenbach, C., Kusnetzow, A.K., Ernst, O.P., Hofmann, K.P. & Hubbell, W.L. High-resolution distance mapping in rhodopsin reveals the pattern of helix movement due to activation. *Proc. Natl. Acad. Sci. U.S.A.* 105, 7439-7444 (2008).
89. Nakamichi, H. & Okada, T. Local peptide movement in the photoreaction intermediate of rhodopsin. *Proc. Natl. Acad. Sci. U.S.A.* 103, 12729-12734 (2006).
90. Nakamichi, H. & Okada, T. Crystallographic analysis of primary visual photochemistry. *Angew. Chem. Int. Ed. Engl.* 45, 4270-4273 (2006).
91. Zhukovsky, E.A., Robinson, P.R. & Oprian, D.D. Transducin activation by rhodopsin without a covalent bond to the 11-cis-retinal chromophore. *Science* 251, 558-560 (1991).
92. Han, M., Smith, S.O. & Sakmar, T.P. Constitutive activation of opsin by mutation of methionine 257 on transmembrane helix 6. *Biochemistry* 37, 8253-8261 (1998).
93. Reeves, P.J., Kim, J.M. & Khorana, H.G. Structure and function in rhodopsin: A tetracycline-inducible system in stable mammalian cell lines for high-level expression of opsin mutants. *Proc. Natl. Acad. Sci. U.S.A.* 99, 13413-13418 (2002).
94. Reeves, P.J., Thurmond, R.L. & Khorana, H.G. Structure and function in rhodopsin: High level expression of a synthetic bovine opsin gene and its mutants

in stable mammalian cell lines. *Proc. Natl. Acad. Sci. U.S.A.* 93, 11487-11492 (1996).

95. Dulbecco, R. & Freeman, G. Plaque production by the polyoma virus. *Virology* 8, 396-397 (1959).

96. Eilers, M., Reeves, P.J., Ying, W.W., Khorana, H.G. & Smith, S.O. Magic angle spinning NMR of the protonated retinylidene schiff base nitrogen in rhodopsin: Expression of $^{15}$N-lysine and $^{13}$C-glycine labeled opsin in a stable cell line. *Proc. Natl. Acad. Sci. U.S.A.* 96, 487-492 (1999).

97. Eilers, M., Ying, W.W., Reeves, P.J., Khorana, H.G. & Smith, S.O. Magic angle spinning nuclear magnetic resonance of isotopically labeled rhodopsin. *Meth. Enzymol.* 343, 212-222 (2002).

98. Lugtenburg, J. The synthesis of $^{13}$C-labeled retinals. *Pure Appl. Chem.* 57, 753-762 (1985).

99. Liu, R.S.H. & Asato, A.E. Synthesis and photochemistry of stereoisomers of retinal. *Meth. Enzymol.* 88, 506-516 (1982).

100. Patel, A.B. et al. Coupling of retinal isomerization to the activation of rhodopsin. *Proc. Natl. Acad. Sci. U.S.A.* 101, 10048-10053 (2004).

101. Mayo, K.H., Daragan, V.A., Idiyatullin, D. & Nesmelova, I. Peptide internal motions on nanosecond time scale derived from direct fitting of $^{13}$C and $^{15}$N NMR spectral density functions. *J. Magn. Reson.* 146, 188-195 (2000).

102. Larsson, G., Martinez, G., Schleucher, J. & Wijmenga, S.S. Detection of nano-second internal motion and determination of overall tumbling times independent of the time scale of internal motion in proteins from NMR relaxation data. *J. Biomol. NMR* 27, 291-312 (2003).

103. Tycko, R. Biomolecular solid state NMR: Advances in structural methodology and applications to peptide and protein fibrils. *Annu. Rev. Phys. Chem.* 52, 575-606 (2001).

104. Mehring, M. & Waugh, J.S. Magic-angle NMR experiments in solids. *Phys. Rev., B* 5, 3459-3471 (1972).

105. Levitt, M.H. *Spin Dynamics*, 543-546 (John Wiley & Sons, Ltd, Chichester, 2001).

106. Smith, S.O. & Griffin, R.G. High-resolution solid-state NMR of proteins. *Annu. Rev. Phys. Chem.* 39, 511-535 (1988).

107. Lowe, I.J. Free Induction Decays of Rotating Solids. *Phys. Rev. Lett.* 2, 285-287 (1959).

108. Andrew, E.R., Bradbury, A. & Eades, R.G. Nuclear magnetic resonance spectra from a crystal rotated at high speed. *Nature* 182, 1659 (1958).

109. Schaefer, J. & Stejskal, E.O. Carbon-13 nuclear magnetic resonance of polymers spinning at the magic angle. *J. Am. Chem. Soc.* 98, 1031-1032 (1976).

110. Maricq, M.M. & Waugh, J.S. NMR in rotating solids. *J. Chem. Phys.* 70, 3300-3316 (1979).

111. Bennett, A.E., Rienstra, C.M., Auger, M., Lakshmi, K.V. & Griffin, R.G. Heteronuclear decoupling in rotating solids. *J. Chem. Phys.* 103, 6951-6958 (1995).

112. Fung, B.M., Khitrin, A.K. & Ermolaev, K. An improved broadband decoupling sequence for liquid crystals and solids. *J. Magn. Reson.* 142, 97-101 (2000).

113. Hartmann, S.R. & Hahn, E.L. Nuclear double resonance in the rotating frame. *Phys. Rev.* 128, 2042-2053 (1962).

114. Pines, A., Gibby, M.G. & Waugh, J.S. Proton-enhanced NMR of dilute spins in solids. *J. Chem. Phys.* 59, 569-590 (1973).

115. Peersen, O.B., Wu, X. & Smith, S.O. Enhancement of CP-MAS signals by variable amplitude cross polarization. Compensation for inhomogeneous B1 fields. *J. Magn. Reson.* 106, 127-131 (1994).

116. Raleigh, D.P., Levitt, M.H. & Griffin, R.G. Rotational resonance in solid state NMR. *Chem. Phys. Lett.* 146, 71-76 (1988).

117. Gullion, T. & Schaefer, J. Detection of weak heteronuclear dipolar coupling by rotational-echo double-resonance NMR. in *Advances in Magnetic Resonance, Vol. 13; Conference on "High Resolution NMR in Solids", January 19-21, 1989*

(ed. Warren, W.S.) 57-84 (Academic Press, Inc., San Diego, California, USA; London, England, UK, 1989).

118. Bennett, A.E. et al. Homonuclear radio frequency-driven recoupling in rotating solids. *J. Chem. Phys.* 108, 9463-9479 (1998).

119. Sodickson, D.K., Levitt, M.H., Vega, S. & Griffin, R.G. Broad-band dipolar recoupling in the nuclear-magnetic-resonance of rotating solids. *J. Chem. Phys.* 98, 6742-6748 (1993).

120. Takegoshi, K., Nakamura, S. & Terao, T. $^{13}C$-$^{1}H$ dipolar-assisted rotational resonance in magic-angle spinning NMR. *Chem. Phys. Lett.* 344, 631-637 (2001).

121. Castellani, F. et al. Structure of a protein determined by solid-state magic-angle-spinning NMR spectroscopy. *Nature* 420, 98-102 (2002).

122. Crocker, E. et al. Dipolar assisted rotational resonance NMR of tryptophan and tyrosine in rhodopsin. *J. Biomol. NMR* 29, 11-20 (2004).

123. Cavanagh, J., Fairbrother, W.J., Palmer, A.G. & Skelton, N.J. *Protein NMR Spectroscopy*, (Academic Press, San Diego, 1996).

124. Ernst, R.R., Bodenhausen, G. & Wokaun, A. *Principles of Nuclear Magnetic Resonance in One and Two Dimensions*, (Clarendon Press, Oxford, 1987).

125. Metz, G., Wu, X. & Smith, S.O. Ramped-amplitude cross polarization in magic angle spinning NMR. *J. Magn. Reson. A.* 110, 219-227 (1994).

126. Heck, M. et al. Signaling states of rhodopsin: Formation of the storage form, metarhodopsin III, from active metarhodopsin II. *J. Biol. Chem.* 278, 3162-3169 (2003).

127. Salgado, G.F.J. et al. Deuterium NMR structure of retinal in the ground state of rhodopsin. *Biochemistry* 43, 12819-12828 (2004).

128. Lau, P.W., Grossfield, A., Feller, S.E., Pitman, M.C. & Brown, M.F. Dynamic structure of retinylidene ligand of rhodopsin probed by molecular simulations. *J. Mol. Biol.* 372, 906-917 (2007).

129. Han, M., Groesbeek, M., Smith, S.O. & Sakmar, T.P. Role of the C9 methyl group in rhodopsin activation: Characterization of mutant opsins with the artificial chromophore 11-cis-9-demethylretinal. *Biochemistry* 37, 538-45 (1998).

130. Beck, M., Siebert, F. & Sakmar, T.P. Evidence for the specific interaction of a lipid molecule with rhodopsin which is altered in the transition to the active state metarhodopsin II. *FEBS Lett.* 436, 304-308 (1998).

131. Arnis, S. & Hofmann, K.P. Two different forms of metarhodopsin II: Schiff base deprotonation precedes proton uptake and signaling state. *Proc. Natl. Acad. Sci. U.S.A.* 90, 7849-7853 (1993).

132. Lamola, A.A., Yamane, T. & Zipp, A. Metarhodopsin I <-> Metarhodopsin II Equilibrium - Effects of Detergents and Pressure. *Exp. Eye Res.* 18, 19-27 (1974).

133. Parkes, J.H. & Liebman, P.A. Temperature and pH dependence of the metarhodopsin I-metarhodopsin II kinetics and equilibria in bovine rod disk membrane suspensions. *Biochemistry* 23, 5054-5061 (1984).

134. Thorgeirsson, T.E., Lewis, J.W., Wallace-Williams, S.E. & Kliger, D.S. Effects of temperature on rhodopsin photointermediates from lumirhodopsin to metarhodopsin-Ii. *Biochemistry* 32, 13861-13872 (1993).

135. Kusnetzow, A.K., Altenbach, C. & Hubbell, W.L. Conformational states and dynamics of rhodopsin in micelles and bilayers. *Biochemistry* 45, 5538-5550 (2006).

136. Szundi, I., Lewis, J.W. & Kliger, D.S. Effect of digitonin on the rhodopsin meta I-meta II equilibrium. *Photochem. Photobiol.* 81, 866-873 (2005).

137. Matsumoto, H. & Yoshizawa, T. Recognition of opsin to longitudinal length of retinal isomers in formation of rhodopsin. *Vision Res.* 18, 607-609 (1978).

138. Vogel, R. et al. Agonists and partial agonists of rhodopsin: Retinal polyene methylation affects receptor activation. *Biochemistry* 45, 1640-1652 (2006).

139. Vogel, R., Siebert, F., Lüdeke, S., Hirshfeld, A. & Sheves, M. Agonists and partial agonists of rhodopsin: Retinals with ring modifications. *Biochemistry* 44, 11684-11699 (2005).

140. Hubbard, R. & Wald, G. Cis-trans isomers of vitamin A and retinene in the rhodopsin system. *J. Gen. Physiol.* 36, 269-315 (1952).

141. Elling, C.E., Thirstrup, K., Holst, B. & Schwartz, T.W. Conversion of agonist site to metal-ion chelator site in the $\beta_2$-adrenergic receptor. *Proc. Natl. Acad. Sci. U.S.A.* 96, 12322-12327 (1999).

142. Cooper, A. Energy uptake in the first step of visual excitation. *Nature* 282, 531-533 (1979).

143. Smith, S.O., Courtin, J., de Groot, H., Gebhard, R. & Lugtenburg, J. 13C magic-angle spinning NMR studies of bathorhodopsin, the primary photoproduct of rhodopsin. *Biochemistry* 30, 7409-7415 (1991).

144. Palings, I., van den Berg, E.M.M., Lugtenburg, J. & Mathies, R.A. Complete assignment of the hydrogen out-of-plane wagging vibrations of bathorhodopsin: chromophore structure and energy storage in the primary photoproduct of vision. *Biochemistry* 28, 1498-1507 (1989).

145. Eyring, G., Curry, B., Broek, A., Lugtenburg, J. & Mathies, R. Assignment and interpretation of hydrogen out-of-plane vibrations in the resonance Raman spectra of rhodopsin and bathorhodopsin. *Biochemistry* 21, 384-393 (1982).

146. Ruprecht, J.J., Mielke, T., Vogel, R., Villa, C. & Schertler, G.F.X. Electron crystallography reveals the structure of metarhodopsin I. *EMBO J.* 23, 3609-3620 (2004).

147. Emeis, D., Kuhn, H., Reichert, J. & Hofmann, K.P. Complex-formation between metarhodopsin-II and GTP-binding protein in bovine photoreceptor-membranes leads to a shift of the photoproduct equilibrium. *FEBS Lett.* 143, 29-34 (1982).

148. Okada, T., Ernst, O.P., Palczewski, K. & Hofmann, K.P. Activation of rhodopsin: new insights from structural and biochemical studies. *Trends Biochem. Sci.* 26, 318-324 (2001).

149. Shichida, Y. & Imai, H. Visual pigment: G-protein-coupled receptor for light signals. *Cell. Mol. Life. Sci.* 54, 1299-1315 (1998).

150. Wang, Q., Schoenlein, R.W., Peteanu, L.A., Mathies, R.A. & Shank, C.V. Vibrationally coherent photochemistry in the femtosecond primary event of vision. *Science* 266, 422-424 (1994).

151. Lewis, J.W. & Kliger, D.S. Absorption spectroscopy in studies of visual pigments: Spectral and kinetic characterization of intermediates. *Meth. Enzymol.* 315, 164-178 (2000).

152. Cooper, A. & Converse, C.A. Energetics of primary processes in visual excitation: photocalorimetry of rhodopsin in rod outer segment membranes. *Biochemistry* 15, 2970-2978 (1976).

153. Longstaff, C., Calhoon, R.D. & Rando, R.R. Deprotonation of the Schiff base of rhodopsin is obligate in the activation of the G-protein. *Proc. Natl. Acad. Sci. U.S.A.* 83, 4209-4213 (1986).

154. Kim, J.M. et al. Structural origins of constitutive activation in rhodopsin: Role of the K296/E113 salt bridge. *Proc. Natl. Acad. Sci. U.S.A.* 101, 12508-12513 (2004).

155. Matthews, R.G., Hubbard, R., Brown, P.K. & Wald, G. Tautomeric forms of metarhodopsin. *J. Gen. Physiol.* 47, 215-240 (1963).

156. Fahmy, K., Sakmar, T.P. & Siebert, F. Transducin-dependent protonation of glutamic acid 134 in rhodopsin. *Biochemistry* 39, 10607-10612 (2000).

157. Kim, J.M., Altenbach, C., Thurmond, R.L., Khorana, H.G. & Hubbell, W.L. Structure and function in rhodopsin: Rhodopsin mutants with a neutral amino acid at E134 have a partially activated conformation in the dark state. *Proc. Natl. Acad. Sci. U.S.A.* 94, 14273-14278 (1997).

158. Knierim, B., Hofmann, K.P., Ernst, O.P. & Hubbell, W.L. Sequence of late molecular events in the activation of rhodopsin. *Proc. Natl. Acad. Sci. U.S.A.* 104, 20290-20295 (2007).

159. Melia, T.J., Cowan, C.W., Angleson, J.K. & Wensel, T.G. A comparison of the efficiency of G protein activation by ligand-free and light-activated forms of rhodopsin. *Biophys. J.* 73, 3182-3191 (1997).

160. Vogel, R. & Siebert, F. Conformations of the active and inactive states of opsin. *J. Biol. Chem.* 276, 38487-38493 (2001).

161. Vogel, R. et al. Deactivation of rhodopsin in the transition from the signaling state Meta II to Meta III involves a thermal isomerization of the retinal chromophore C=N double bond. *Biochemistry* 42, 9863-9874 (2003).

162. Bartl, F.J., Ritter, E. & Hofmann, K.P. Signaling states of rhodopsin - Absorption of light in active metarhodopsin II generates an all-trans-retinal bound inactive state. *J. Biol. Chem.* 276, 30161-30166 (2001).

163. Vogel, R., Siebert, F., Zhang, X.Y., Fan, G.B. & Sheves, M. Formation of Meta III during the Decay of Activated Rhodopsin Proceeds via Meta I and Not via Meta II. *Biochemistry* 43, 9457 -9466 (2004).

164. Zimmermann, K., Ritter, E., Bartl, F.J., Hofmann, K.P. & Heck, M. Interaction with transducin depletes metarhodopsin III: A regulated retinal storage in visual signal transduction? *J. Biol. Chem.* 279, 48112-48119 (2004).

165. Zhukovsky, E.A. & Oprian, D.D. Effect of carboxylic acid side chains on the absorption maximum of visual pigments. *Science* 246, 928-930 (1989).

166. Blatz, P.E., Mohler, J.H. & Navangul, H.V. Anion-induced wavelength regulation of absorption maxima of Schiff bases of retinal. *Biochemistry* 11, 848-855 (1972).

167. Albeck, A., Livnah, N., Gottlieb, H. & Sheves, M. 13C NMR studies of model compounds for bacteriorhodopsin: Factors affecting the retinal chromophore chemical shifts and absorption maximum. *J. Am. Chem. Soc.* 114, 2400-2411 (1992).

168. Honig, B., Greenberg, A.D., Dinur, U. & Ebrey, T.G. Visual-pigment spectra: implications of the protonation of the retinal Schiff base. *Biochemistry* 15, 4593-4599 (1976).

169. Yoshizawa, T. & Wald, G. Pre-lumirhodopsin and the bleaching of visual pigments. *Nature* 197, 1279-1286 (1963).

170. Blatz, P.E. & Liebman, P.A. Wavelength regulation in visual pigments. *Exp. Eye Res.* 17, 573-580 (1973).

171. Korenstein, R., Muszkat, K.A. & Sharafy-Ozeri.S. Photochromism and thermochromism through partial torsion about an essential double bond. Structure of the B colored isomers of bianthrones *J. Am. Chem. Soc.* 95, 6177-6181 (1973).

172. Kochendoerfer, G.G., Lin, S.W., Sakmar, T.P. & Mathies, R.A. How color visual pigments are tuned. *Trends Biochem. Sci.* 24, 300-305 (1999).

173. Lin, S.W. et al. Mechanisms of spectral tuning in blue cone visual pigments - Visible and raman spectroscopy of blue-shifted rhodopsin mutants. *J. Biol. Chem.* 273, 24583-24591 (1998).

174. Sekharan, S., Sugihara, M. & Buss, V. Origin of spectral tuning in rhodopsin - It is not the binding pocket. *Angew. Chem. Int. Ed. Engl.* 46, 269-271 (2007).

175. Steinberg, G., Ottolenghi, M. & Sheves, M. pKa of the protonated Schiff base of bovine rhodopsin: A study with artificial pigments. *Biophys. J.* 64, 1499-1502 (1993).

176. Baylor, D.A., Lamb, T.D. & Yau, K.W. The membrane current of single rod outer segments. *J. Physiol. (Lond.)* 288, 589-611 (1979).

177. Birge, R.R. & Barlow, R.B. On the molecular origins of thermal noise in vertebrate and invertebrate photoreceptors

. *Biophys. Chem.* 55, 115-126 (1995).

178. Kukura, P., McCamant, D.W., Yoon, S., Wandschneider, D.B. & Mathies, R.A. Structural observation of the primary isomerization in vision with femtosecond-stimulated Raman. *Science* 310, 1006-1009 (2005).

179. Pan, D.H. & Mathies, R.A. Chromophore structure in lumirhodopsin and metarhodopsin I by time-resolved resonance Raman microchip spectroscopy. *Biochemistry* 40, 7929-7936 (2001).

180. Palings, I. et al. Assignment of fingerprint vibrations in the resonance Raman spectra of rhodopsin, isorhodopsin, and bathorhodopsin: implications for chromophore structure and environment. *Biochemistry* 26, 2544-2556 (1987).

181. Siebert, F. Application of FTIR spectroscopy to the investigation of dark structures and photoreactions of visual pigments. *Israel J. Chem.* 35, 309-323 (1995).

182. Kochendoerfer, G.G., Verdegem, P.J.E., van der Hoef, I., Lugtenburg, J. & Mathies, R.A. Retinal analog study of the role of steric interactions in the excited state isomerisation dynamics of rhodopsin. *Biochemistry* 35, 16230-16240 (1996).

183. Struts, A.V. et al. Structural analysis and dynamics of retinal chromophore in dark and metal states of rhodopsin from $^{2}$H NMR of aligned membranes. *J. Mol. Biol.* 372, 50-66 (2007).

184. Feng, X. et al. Determination of a molecular torsional angle in the metarhodopsin-I photointermediate of rhodopsin by double-quantum solid-state NMR. *J. Biomol. NMR* 16, 1-8 (2000).

185. Salom, D. et al. Crystal structure of a photoactivated deprotonated intermediate of rhodopsin. *Proc. Natl. Acad. Sci. U.S.A.* 103, 16123-16128 (2006).

186. Luca, S. et al. The conformation of neurotensin bound to its G protein-coupled receptor. *Proc. Natl. Acad. Sci. U.S.A.* 100, 10706-10711 (2003).

187. Ratnala, V.R.P. et al. Solid-state NMR evidence for a protonation switch in the binding pocket of the H1 receptor upon binding of the agonist histamine. *J. Am. Chem. Soc.* 129, 867-872 (2007).

188. Harbison, G.S. et al. Solid-state $^{13}$C NMR detection of a perturbed 6-s-trans chromophore in bacteriorhodopsin. *Biochemistry* 24, 6955-6962 (1985).

189. Smith, S.O. et al. Solid-state NMR studies of the mechanism of the opsin shift in the visual pigment rhodopsin. *Biochemistry* 29, 8158-8164 (1990).

190. Smith, S.O. et al. Low-temperature solid-state $^{13}$C NMR studies of the retinal chromophore in rhodopsin. *Biochemistry* 26, 1606-1611 (1987).

191. Verhoeven, M.A. et al. Ultra-high-field MAS NMR assay of a multispin labeled ligand bound to its G-protein receptor target in the natural membrane environment: Electronic structure of the retinylidene chromophore in rhodopsin. *Biochemistry* 40, 3282-3288 (2001).

192. Creemers, A.F.L. et al. $^{1}H$ and $^{13}C$ MAS NMR evidence for pronounced ligand-protein interactions involving the ionone ring of the retinylidene chromophore in rhodopsin. *Proc. Natl. Acad. Sci. U.S.A.* 99, 9101-9106 (2002).

193. Hu, J.G. et al. Early and late M intermediates in the bacteriorhodopsin photocycle - a solid-state NMR study. *Biochemistry* 37, 8088-8096 (1998).

194. Harbison, G.S., Herzfeld, J. & Griffin, R.G. Solid-state nitrogen-15 nuclear magnetic resonance study of the Schiff base in bacteriorhodopsin. *Biochemistry* 22, 1-4 (1983).

195. Shriver, J.W., Mateescu, G.D. & Abrahamson, E.W. A proton and carbon-13 nuclear magnetic resonance spectroscopy study of the conformation of a protonated 11-cis-retinal Schiff base. *Biochemistry* 18, 4785-4792 (1979).

196. Han, M., DeDecker, B.S. & Smith, S.O. Localization of the retinal protonated Schiff base counterion in rhodopsin. *Biophys. J.* 65, 899-906 (1993).

197. Lüdeke, S. et al. The role of Glu181 in the photoactivation of rhodopsin. *J. Mol. Biol.* 353, 345-356 (2005).

198. Shriver, J., Abrahamson, E.W. & Mateescu, G.D. The structure of visual pigments. I. Carbon-13 nuclear magnetic resonance spectroscopy of N-all-trans-retinylidenepropylimine and its protonated species. *J. Am. Chem. Soc.* 98, 2407-2409 (1976).

199. Farrens, D.L. & Khorana, H.G. Structure and function in rhodopsin. Measurement of the rate of metarhodopsin II decay by fluorescence spectroscopy. *J. Biol. Chem.* 270, 5073-5076 (1995).

200. Wald, G. & Brown, P.K. The molar extinction of rhodopsin. *J. Gen. Physiol.* 37, 189-200 (1953).

201. Harbison, G.S. et al. Dark-adapted bacteriorhodopsin contains 13-cis, 15-syn and all-trans, 15-anti retinal Schiff bases. *Proc. Natl. Acad. Sci. U.S.A.* 81, 1706-1709 (1984).

202. Bagley, K.A. et al. Fourier-transform infrared difference spectroscopy of rhodopsin and its photoproducts at low temperature. *Biochemistry* 24, 6055-6071 (1985).

203. Okada, T. et al. Functional role of internal water molecules in rhodopsin revealed by x-ray crystallography. *Proc. Natl. Acad. Sci. U.S.A.* 99, 5982-5987 (2002).

204. Farrar, M.R. et al. Solid state NMR study of [ε-13C]Lys-bacteriorhodopsin: Schiff base photoisomerization. *Biophys. J.* 65, 310-315 (1993).

205. Honig, B., Hudson, B., Sykes, B.D. & Karplus, M. Ring orientation in β-ionone and retinals. *Proc. Natl. Acad. Sci. U.S.A.* 68, 1289-1293 (1971).

206. Spooner, P.J.R. et al. Relative orientation between the β-ionone ring and the polyene chain for the chromophore of rhodopsin in native membranes. *Biochemistry* 41, 7549-7555 (2002).

207. Giessner-Prettre, C. & Pullman, B. Intermolecular nuclear shielding due to the aromatic amino acids of proteins and to porphyrins. *J. Theor. Biol.* 31, 287 (1971).

208. Du Vernet, R. & Boekelheide, V. Nuclear Magnetic-Resonance Spectroscopy - Ring-Current Effects on C-13 Chemical-Shifts. *Proc. Natl. Acad. Sci. U.S.A.* 71, 2961-2964 (1974).

209. Terstegen, F. & Buss, V. Geometries and interconversion pathways of free and protonated β-ionone Schiff bases. An ab initio study of photoreceptor chromophore model compounds. *Chem. Phys.* 225, 163-171 (1997).

210. Terstegen, F., Carter, E.A. & Buss, V. Interconversion pathways of the protonated β-ionone Schiff base: An ab initio molecular dynamics study. *Int. J. Quantum Chem.* 75, 141-145 (1999).

211. Samson, M. et al. The second extracellular loop of CCR5 is the major determinant of ligand specificity. *J. Biol. Chem.* 272, 24934-24941 (1997).

212. Shi, L. & Javitch, J.A. The second extracellular loop of the dopamine D-2 receptor lines the binding-site crevice. *Proc. Natl. Acad. Sci. U.S.A.* 101, 440-445 (2004).

213. Klco, J.M., Wiegand, C.B., Narzinski, K. & Baranski, T.J. Essential role for the second extracellular loop in C5a receptor activation. *Nat. Struct. Mol. Biol.* 12, 320-326 (2005).

214. Scarselli, M., Li, B., Kim, S.K. & Wess, J. Multiple residues in the second extracellular loop are critical for M-3 muscarinic acetylcholine receptor activation. *J. Biol. Chem.* 282, 7385-7396 (2007).

215. Terakita, A., Yamashita, T. & Shichida, Y. Highly conserved glutamic acid in the extracellular IV-V loop in rhodopsins acts as the counterion in retinochrome, a member of the rhodopsin family. *Proc. Natl. Acad. Sci. U.S.A.* 97, 14263-14267 (2000).

216. Wang, Z.Y., Asenjo, A.B. & Oprian, D.D. Identification of the chloride-binding site in the human red and green color vision pigments. *Biochemistry* 32, 2125-2130 (1993).

217. Han, M. & Smith, S.O. NMR constraints on the location of the retinal chromophore in rhodopsin and bathorhodopsin. *Biochemistry* 34, 1425-1432 (1995).

218. Sakmar, T.P., Franke, R.R. & Khorana, H.G. The role of the retinylidene Schiff base counterion in rhodopsin in determining wavelength absorbance and Schiff base pKa. *Proc. Natl. Acad. Sci. U.S.A.* 88, 3079-3083 (1991).

219. Cohen, G.B., Oprian, D.D. & Robinson, P.R. Mechanism of activation and inactivation of opsin: Role of Glu113 and Lys296. *Biochemistry* 31, 12592-12601 (1992).

220. Rader, A.J. et al. Identification of core amino acids stabilizing rhodopsin. *Proc. Natl. Acad. Sci. U.S.A.* 101, 7246-7251 (2004).

221. Janz, J.M., Fay, J.F. & Farrens, D.L. Stability of dark state rhodopsin is mediated by a conserved ion pair in intradiscal loop E-2. *J. Biol. Chem.* 278, 16982-16991 (2003).

222. Doi, T., Molday, R.S. & Khorana, H.G. Role of the intradiscal domain in rhodopsin assembly and function. *Proc. Natl. Acad. Sci. U.S.A.* 87, 4991-4995 (1990).

223. Holst, B. & Schwartz, T.W. Molecular mechanism of agonism and inverse agonism in the melanocortin receptors - $Zn^{2+}$ as a structural and functional probe. *Ann. N. Y. Acad. Sci.* 994, 1-11 (2003).

224. Sharma, D. & Rajarathnam, K. $^{13}C$ NMR chemical shifts can predict disulfide bond formation. *J. Biomol. NMR* 18, 165-171 (2000).

225. Herzfeld, J. et al. Solid-state $^{13}C$ NMR study of tyrosine protonation in dark-adapted bacteriorhodopsin. *Biochemistry* 29, 5567-5574 (1990).

226. DeLange, F. et al. Tyrosine structural changes detected during the photoactivation of rhodopsin. *J. Biol. Chem.* 273, 23735-23739 (1998).

227. Patel, A.B. et al. Changes in interhelical hydrogen bonding upon rhodopsin activation. *J. Mol. Biol.* 347, 803-812 (2005).

228. Yan, E.C.Y. et al. Function of extracellular loop 2 in rhodopsin: Glutamic acid 181 modulates stability and absorption wavelength of metarhodopsin II. *Biochemistry* 41, 3620-3627 (2002).

229. Janz, J.M. & Farrens, D.L. Role of the retinal hydrogen bond network in rhodopsin Schiff base stability and hydrolysis. *J. Biol. Chem.* 279, 55886-55894 (2004).

230. Furutani, Y., Shichida, Y. & Kandori, H. Structural changes of water molecules during the photoactivation processes in bovine rhodopsin. *Biochemistry* 42, 9619-9625 (2003).

231. Davidson, F.F., Loewen, P.C. & Khorana, H.G. Structure and function in rhodopsin: Replacement by alanine of cysteine residues 110 and 187, components of a conserved disulfide bond in rhodopsin, affects the light-activated metarhodopsin II state. *Proc. Natl. Acad. Sci. U.S.A.* 91, 4029-4033 (1994).

232. Goodwin, J.A., Hulme, E.C., Langmead, C.J. & Tehan, B.G. Roof and floor of the muscarinic binding pocket: Variations in the binding modes of orthosteric ligands. *Mol. Pharmacol.* 72, 1484-1496 (2007).

233. Javitch, J.A., Fu, D. & Chen, J. Residues in the fifth membrane-spanning segment of the dopamine D2 receptor exposed in the binding-site crevice. *Biochemistry* 34, 16433-16439 (1995).

234. Yan, E.C.Y. et al. Photointermediates of the rhodopsin S186A mutant as a probe of the hydrogen-bond network in the chromophore pocket and the mechanism of counterion switch. *J. Phys. Chem. C* 111, 8843-8848 (2007).

235. Olah, M.E., Jacobson, K.A. & Stiles, G.L. Role of the 2nd extracellular loop of adenosine receptors in agonist and antagonist binding - Analysis of Chimeric $A_1/A_3$-adenosine receptors. *J. Biol. Chem.* 269, 24692-24698 (1994).

236. Wurch, T., Colpaert, F.C. & Pauwels, P.J. Chimeric receptor analysis of the ketanserin binding site in the human 5-hydroxytryptamine$_{1D}$ receptor: Importance of the second extracellular loop and fifth transmembrane domain in antagonist binding. *Mol. Pharmacol.* 54, 1088-1096 (1998).

237. Conner, M. et al. Systematic analysis of the entire second extracellular loop of the V-1a vasopressin receptor - Key residues, conserved throughout a G-protein-coupled receptor family, identified. *J. Biol. Chem.* 282, 17405-17412 (2007).

238. Pfleger, K.D.G., Pawson, A.J. & Millar, R.P. Changes to gonadotropin-releasing hormone (GnRH) receptor extracellular loops differentially affect GnRH analog binding and activation: Evidence for distinct ligand-stabilized receptor conformations. *Endocrinology* 149, 3118-3129 (2008).

239. Madabushi, S. et al. Evolutionary trace of G protein-coupled receptors reveals clusters of residues that determine global and class-specific functions. *J. Biol. Chem.* 279, 8126-8132 (2004).

240. Holst, B., Elling, C.E. & Schwartz, T.W. Partial agonism through a zinc-ion switch constructed between transmembrane domains III and VII in the tachykinin NK1 receptor. *Mol. Pharmacol.* 58, 263-270 (2000).

241. Martinez-Gimeno, M. et al. Three novel mutations (P215L, T289P, and 3811-2 A->G) in the rhodopsin gene in autosomal dominant retinitis pigmentosa in Spanish families. *Hum. Mutat.* 16, 95-96 (2000).

242. Schwartz, T.W., Frimurer, T.M., Holst, B., Rosenkilde, M.M. & Elling, C.E. Molecular mechanism of 7TM receptor activation - A global toggle switch model. *Annu. Rev. Pharmacol. Toxicol.* 46, 481-519 (2006).

243. McAllister, S.D. et al. Structural mimicry in class A G protein-coupled receptor rotamer toggle switches - The importance of the F3.36(201)/W6.48(357) interaction in cannabinoid CB1 receptor activation. *J. Biol. Chem.* 279, 48024-48037 (2004).

244. Borhan, B., Souto, M.L., Imai, H., Shichida, Y. & Nakanishi, K. Movement of retinal along the visual transduction path. *Science* 288, 2209-2212 (2000).

245. Meng, E.C. & Bourne, H.R. Receptor activation: What does the rhodopsin structure tell us? *Trends Pharmacol. Sci.* 22, 587-593 (2001).

246. Spooner, P.J.R. et al. The ring of the rhodopsin chromophore in a hydrophobic activation switch within the binding pocket. *J. Mol. Biol.* 343, 719-730 (2004).

247. Schmidt-Rohr, K. & Spiess, H.W. *Multidimensional Solid-State NMR and Polymers*, (Academic Press, London, 1994).

248. Baldus, M. & Meier, B.H. Broadband polarization transfer under magic-angle spinning: Application to total through-space-correlation NMR spectroscopy. *J. Magn. Reson.* 128, 172-193 (1997).

249. Ramachandran, R., Ladizhansky, V., Bajaj, V.S. & Griffin, R.G. $^{13}C$-$^{13}C$ rotational resonance width distance measurements in uniformly $^{13}C$-labeled peptides. *J. Am. Chem. Soc.* 125, 15623-15629 (2003).

250. Schreiber, M., Sugihara, M., Okada, T. & Buss, V. Quantum mechanical studies on the crystallographic model of bathorhodopsin. *Angew. Chem. Int. Ed. Engl.* 45, 4274-4277 (2006).

251. Röhrig, U.F., Guidoni, L. & Rothlisberger, U. Early steps of the intramolecular signal transduction in rhodopsin explored by molecular dynamics simulations. *Biochemistry* 41, 10799-10809 (2002).

252. Altenbach, C. et al. Structural features and light-dependent changes in the cytoplasmic interhelical E-F loop region of rhodopsin: a site-directed spin-labeling study. *Biochemistry* 35, 12470-12478 (1996).

253. Getmanova, E. et al. NMR spectroscopy of phosphorylated wild-type rhodopsin: Mobility of the phosphorylated C-terminus of rhodopsin in the dark and upon light activation. *Biochemistry* 43, 1126-1133 (2004).

254. Patel, A.B. Ph.D., Stony Brook University (2004).

255. Gibson, N.J. & Brown, M.F. Lipid headgroup and acyl chain composition modulate the MI-MII equilibrium of rhodopsin in recombinant membranes. *Biochemistry* 32, 2438-2454 (1993).

256. Imai, H. et al. Single amino acid residue as a functional determinant of rod and cone visual pigments. *Proc. Natl. Acad. Sci. U.S.A.* 94, 2322-2326 (1997).

257. Jäger, F. et al. Interactions of the β-ionone ring with the protein in the visual pigment rhodopsin control the activation mechanism. An FTIR and fluorescence study on artificial vertebrate rhodopsins. *Biochemistry* 33, 7389-7397 (1994).

258. Bartl, F.J. et al. Partial agonism in a G protein-coupled receptor: Role of the retinal ring structure in rhodopsin activation. *J. Biol. Chem.* 280, 34259-34267 (2005).

259. Liapakis, G. et al. The forgotten serine - A critical role for Ser-203(5.42) in ligand binding to and activation of the $\beta_2$-adrenergic receptor. *J. Biol. Chem.* 275, 37779-37788 (2000).

260. Strader, C.D., Candelore, M.R., Hill, W.S., Sigal, I.S. & Dixon, R.A.F. Identification of two serine residues involved in agonist activation of the β-adrenergic receptor. *J. Biol. Chem.* 264, 13572-13578 (1989).

261. Marjamäki, A. et al. Chloroethylclonidine binds irreversibly to exposed cysteines in the fifth membrane-spanning domain of the human $\alpha_{2A}$-adrenergic receptor. *Mol. Pharmacol.* 53, 370-376 (1998).

262. Shapiro, D.A., Kristiansen, K., Kroeze, W.K. & Roth, B.L. Differential modes of agonist binding to 5-Hydroxytryptamine$_{2A}$ serotonin receptors revealed by mutation and molecular modeling of conserved residues in transmembrane region 5. *Mol. Pharmacol.* 58, 877-886 (2000).

263. Elling, C.E., Nielsen, S.M. & Schwartz, T.W. Conversion of antagonist-binding site to metal-ion site in the tachykinin NK-1 receptor. *Nature* 374, 74-77 (1995).

264. Thirstrup, K., Elling, C.E., Hjorth, S.A. & Schwartz, T.W. Construction of a high affinity zinc switch in the κ-opioid receptor. *J. Biol. Chem.* 271, 7875-7878 (1996).

265. Rosenkilde, M.M., Lucibello, M., Holst, B. & Schwartz, T.W. Natural agonist enhancing bis-His zinc-site in transmembrane segment V of the tachykinin $NK_3$ receptor. *FEBS Lett.* 439, 35-40 (1998).

266. Ballesteros, J.A., Shi, L. & Javitch, J.A. Structural mimicry in G protein-coupled receptors: Implications of the high-resolution structure of rhodopsin for structure-function analysis of rhodopsin-like receptors. *Mol. Pharmacol.* 60, 1-19 (2001).

267. Javitch, J.A., Fu, D.Y., Liapakis, G. & Chen, J.Y. Constitutive activation of the $\beta_2$ adrenergic receptor alters the orientation of its sixth membrane-spanning segment. *J. Biol. Chem.* 272, 18546-18549 (1997).

268. Baranski, T.J. et al. C5a receptor activation - Genetic identification of critical residues in four transmembrane helices. *J. Biol. Chem.* 274, 15757-15765 (1999).

269. Govaerts, C. et al. Activation of CCR5 by chemokines involves an aromatic cluster between transmembrane helices 2 and 3. *J. Biol. Chem.* 278, 1892-1903 (2003).

270. Luo, X., Zhang, D. & Weinstein, H. Ligand-induced domain motion in the activation mechanism of a G-protein-coupled receptor. *Protein Eng.* 7, 1441-1448 (1994).

271. Sansom, M.S.P. & Weinstein, H. Hinges, swivels and switches: The role of prolines in signalling via transmembrane α-helices. *Trends Pharmacol. Sci.* 21, 445-451 (2000).

272. Shi, L. et al. $\beta_2$ adrenergic receptor activation - Modulation of the proline kink in transmembrane 6 by a rotamer toggle switch. *J. Biol. Chem.* 277, 40989-40996 (2002).

273. Javitch, J.A., Ballesteros, J.A., Weinstein, H. & Chen, J.Y. A cluster of aromatic residues in the sixth membrane-spanning segment of the dopamine D2 receptor is accessible in the binding-site crevice. *Biochemistry* 37, 998-1006 (1998).

274. Heitz, F. et al. Site-directed mutagenesis of the putative human muscarinic M-2 receptor binding site. *Eur. J. Pharmacol.* 380, 183-195 (1999).

275. Shi, L. & Javitch, J.A. The binding site of aminergic G protein-coupled receptors: The transmembrane segments and second extracellular loop. *Annu. Rev. Pharmacol. Toxicol.* 42, 437-467 (2002).

276. Gerber, B.O., Meng, E.C., Dotsch, V., Baranski, T.J. & Bourne, H.R. An activation switch in the ligand binding pocket of the C5a receptor. *J. Biol. Chem.* 276, 3394-3400 (2001).

277. Blanpain, C. et al. The core domain of chemokines binds CCR5 extracellular domains while their amino terminus interacts with the transmembrane helix bundle. *J. Biol. Chem.* 278, 5179-5187 (2003).

278. Chan, T., Lee, M. & Sakmar, T.P. Introduction of Hydroxyl-Bearing Amino-Acids Causes Bathochromic Spectral Shifts in Rhodopsin - Amino-Acid Substitutions Responsible for Red-Green Color Pigment Spectral Tuning. *J. Biol. Chem.* 267, 9478-9480 (1992).

279. Han, M., Lin, S.W., Minkova, M., Smith, S.O. & Sakmar, T.P. Functional interaction of transmembrane helices 3 and 6 in rhodopsin - Replacement of phenylalanine 261 by alanine causes reversion of phenotype of a glycine 121 replacement mutant. *J. Biol. Chem.* 271, 32337-32342 (1996).

280. Nakayama, T.A. & Khorana, H.G. Mapping of the amino acids in membrane-embedded helices that interact with the retinal chromophore in bovine rhodopsin. *J. Biol. Chem.* 266, 4269-4275 (1991).

281. Högger, P., Shockley, M.S., Lameh, J. & Sadée, W. Activating and inactivating mutations in N-terminal and C-terminal I3 loop junctions of muscarinic acetylcholine Hm1 receptors. *J. Biol. Chem.* 270, 7405-7410 (1995).

282. Shapiro, D.A., Kristiansen, K., Weiner, D.M., Kroeze, W.K. & Roth, B.L. Evidence for a model of agonist-induced activation of 5-hydroxytryptamine 2A serotonin receptors that involves the disruption of a strong ionic interaction between helices 3 and 6. *J. Biol. Chem.* 277, 11441-11449 (2002).

283. Han, M., Lin, S.W., Smith, S.O. & Sakmar, T.P. The effects of amino acid replacements of glycine 121 on transmembrane helix 3 of rhodopsin. *J. Biol. Chem.* 271, 32330-32336 (1996).

284. Zhou, W. et al. A reciprocal mutation supports helix 2 and helix 7 proximity in the gonadotropin-releasing hormone receptor. *Mol. Pharmacol.* 45, 165-170 (1994).

285. Sealfon, S.C. et al. Related contribution of specific helix 2 and 7 residues to conformational activation of the serotonin 5-$HT_{2A}$ receptor. *J. Biol. Chem.* 270, 16683-16688 (1995).

286. Donnelly, D. et al. Conserved polar residues in the transmembrane domain of the human tachykinin NK2 receptor: functional roles and structural implications. *Biochem. J.* 339, 55-61 (1999).

287. Petkova, A.T. et al. Tryptophan interactions in bacteriorhodopsin: A heteronuclear solid-state NMR study. *Biochemistry* 41, 2429-2437 (2002).

288. Chabre, M. & Breton, J. Orientation of aromatic residues in rhodopsin. Rotation of one tryptophan upon the meta I to meta II transition after illumination. *Photochem. Photobiol.* 30, 295-299 (1979).

289. Dunham, T.D. & Farrens, D.L. Conformational changes in rhodopsin - Movement of helix F detected by site-specific chemical labeling and fluorescence spectroscopy. *J. Biol. Chem.* 274, 1683-1690 (1999).

290. Scheerer, P. et al. Crystal structure of opsin in its G-protein-interacting conformation. *Nature* 455, 497-502 (2008).

291. Ganter, U.M., Schmid, E.D., Perez-Sala, D., Rando, R.R. & Siebert, F. Removal of the 9-methyl group of retinal inhibits signal transduction in the visual process. A Fourier transform infrared and biochemical investigation. *Biochemistry* 28, 5954-5962 (1989).

292. Fritze, O. et al. Role of the conserved NPxxY(x)(5,6)F motif in the rhodopsin ground state and during activation. *Proc. Natl. Acad. Sci. U.S.A.* 100, 2290-2295 (2003).

293. Altenbach, C., Klein-Seetharaman, J., Cai, K.W., Khorana, H.G. & Hubbell, W.L. Structure and function in rhodopsin: Mapping light-dependent changes in distance between residue 316 in helix 8 and residues in the sequence 60-75, covering the cytoplasmic end of helices TM1 and TM2 and their connection loop CL1. *Biochemistry* 40, 15493-15500 (2001).

294. Cohen, G.B., Yang, T., Robinson, P.R. & Oprian, D.D. Constitutive activation of opsin: Influence of charge at position 134 and size at position 296. *Biochemistry* 32, 6111-6115 (1993).

295. Dryja, T.P., Berson, E.L., Rao, V.R. & Oprian, D.D. Heterozygous missense mutation in the rhodopsin gene as a cause of congenital stationary night blindness. *Nat. Genet.* 4, 280-283 (1993).

296. Jin, S.N., Cornwall, M.C. & Oprian, D.D. Opsin activation as a cause of congenital night blindness. *Nat. Neurosci.* 6, 731-735 (2003).

297. Yan, E.C.Y. et al. Retinal counterion switch in the photoactivation of the G protein-coupled receptor rhodopsin. *Proc. Natl. Acad. Sci. U.S.A.* 100, 9262-9267 (2003).

298. Govardhan, C.P. & Oprian, D.D. Active site-directed inactivation of constitutively active mutants of rhodopsin. *J. Biol. Chem.* 269, 6524-6527 (1994).

299. Fahmy, K. & Sakmar, T.P. Regulation of the rhodopsin-transducin interaction by a highly conserved carboxylic acid group. *Biochemistry* 32, 7229-7236 (1993).

300. Arnis, S., Fahmy, K., Hofmann, K.P. & Sakmar, T.P. A conserved carboxylic acid group mediates light-dependent proton uptake and signaling by rhodopsin. *J. Biol. Chem.* 269, 23879-23881 (1994).

301. Lewis, J.W., Szundi, I., Kazmi, M.A., Sakmar, T.P. & Kliger, D.S. Proton movement and photointermediate kinetics in rhodopsin mutants. *Biochemistry* 45, 5430 -5439 (2006).

302. Ramon, E. et al. Critical role of electrostatic interactions of amino acids at the cytoplasmic region of helices 3 and 6 in rhodopsin conformational properties and activation. *J. Biol. Chem.* 282, 14272-14282 (2007).

303. Perlman, J.H. et al. Interactions between conserved residues in transmembrane helices 1, 2, and 7 of the thyrotropin-releasing hormone receptor. *J. Biol. Chem.* 272, 11937-11942 (1997).

304. Prioleau, C., Visiers, I., Ebersole, B.J., Weinstein, H. & Sealfon, S.C. Conserved helix 7 tyrosine acts as a multistate conformational switch in the 5HT2C receptor - Identification of a novel "locked-on" phenotype and double revertant mutations. *J. Biol. Chem.* 277, 36577-36584 (2002).

305. Altenbach, C., Cai, K.W., Klein-Seetharaman, J., Khorana, F.G. & Hubbell, W.L. Structure and function in rhodopsin: Mapping light-dependent changes in distance between residue 65 in helix TM1 and residues in the sequence 306-319 at the cytoplasmic end of helix TM7 and in helix H8. *Biochemistry* 40, 15483-15492 (2001).

306. Krishna, A.G., Menon, S.T., Terry, T.J. & Sakmar, T.P. Evidence that helix 8 of rhodopsin acts as a membrane-dependent conformational switch. *Biochemistry* 41, 8298-8309 (2002).

307. Mukhopadhyay, S., Cowsik, S.M., Lynn, A.M., Welsh, W.J. & Howlett, A.C. Regulation of $G_i$ by the $CB_1$ cannabinoid receptor C-terminal juxtamembrane region: Structural requirements determined by peptide analysis. *Biochemistry* 38, 3447-3455 (1999).

308. Mukhopadhyay, S., McIntosh, H.H., Houston, D.B. & Howlett, A.C. The CB1 cannabinoid receptor juxtamembrane C-terminal peptide confers activation to specific G proteins in brain. *Mol. Pharmacol.* 57, 162-170 (2000).

309. Schertler, G.F.X. Structure of rhodopsin and the metarhodopsin I photointermediate. *Curr. Opin. Struct. Biol.* 15, 408-415 (2005).

310. Flanagan, C.A. et al. The functional microdomain in transmembrane helices 2 and 7 regulates expression, activation, and coupling pathways of the gonadotropin-releasing hormone receptor. *J. Biol. Chem.* 274, 28880-28886 (1999).

311. Case, D.A. et al. The Amber biomolecular simulation programs. *J. Comput. Chem.* 26, 1668-1688 (2005).

312. Sugihara, M., Hufen, J. & Buss, V. Origin and consequences of steric strain in the rhodopsin binding pocket. *Biochemistry* 45, 801-810 (2006).

313. Gascón, J.A. & Batista, V.S. QM/MM study of energy storage and molecular rearrangements due to the primary event in vision. *Biophys. J.* 87, 2931-2941 (2004).

314. Schoenlein, R.W., Peteanu, L.A., Wang, Q., Mathies, R.A. & Shank, C.V. Femtosecond dynamics of cis-trans isomerization in a visual pigment analog - isorhodopsin. *J. Phys. Chem.* 97, 12087-12092 (1993).

315. Liu, R.S.H. & Hammond, G.S. Reflection on medium effects on photochemical reactivity. *Acc. Chem. Res.* 38, 396-403 (2005).

316. Wang, Q. et al. Femtosecond spectroscopy of a 13-demethylrhodopsin visual pigment analogue: The role of nonbonded interactions in the isomerization process. *J. Phys. Chem.* 100, 17388-17394 (1996).

317. Gärtner, W. & Ternieden, S. Influence of a steric hindrance in the chromophore of rhodopsin on the quantum yield of the primary photochemistry. *J. Photochem. Photobiol. B* 33, 83-86 (1996).

318. Han, M. & Smith, S.O. High-resolution structural studies of the retinal--Glu113 interaction in rhodopsin. *Biophys. Chem.* 56, 23-29 (1995).

319. Lewis, J.W., Szundi, I., Kazmi, M.A., Sakmar, T.P. & Kliger, D.S. Time-resolved photointermediate changes in rhodopsin glutamic acid 181 mutants. *Biochemistry* 43, 12614-12621 (2004).

# Appendix

## *A.1 Molecular dynamics simulations of rhodopsin*

Restrained molecular dynamics (MD) simulations were performed using the SANDER module of the molecular modeling package AMBER8 [311] to obtain an atomistic model of meta II starting from the high resolution (2.2 Å) crystal structure of rhodopsin [31]. The simulation system consisted of rhodopsin embedded in a layer of octane molecules serving as a membrane mimetic environment with the cytoplasmic and extracellular (or intradiscal) domains solvated by water. The overall setup was similar to that described by Röhrig *et al*. [251]. Retinal is *isomerized* from 11-*cis* to all-*trans* by applying a torsional restraint (50 kcal/mol/Å) on the retinal C10-C11-C12-C13 dihedral angle.

Structural constraints provided by solid-state NMR measurements of the metarhodopsin II intermediate are combined with molecular dynamics simulations to help visualize the pathway for light activation of rhodopsin. Since the time scale for the formation of the metarhodopsin II intermediate (> 1 ms) is beyond that readily accessible by molecular dynamics, we use NMR distance restraints from $^{13}C$ dipolar recoupling measurements to guide the simulations. The simulations yield a working model for how retinal isomerization and thermal relaxation are coupled to receptor activation.

NMR distance restraints listed in Table 1 are used to guide the MD simulations such that the final state satisfies the meta II experimental constraints. The distance restraints were obtained from the crosspeak intensities observed between $^{13}C$ sites in two

dimensional dipolar assisted rotational resonance (DARR) NMR experiments [120,122]. The intensity of a crosspeak is related to the strength of the dipolar coupling, which in turn is related to the internuclear distance. We typically obtain spectra with a mixing time of 600 msec and correlate the intensity with internuclear distance. Prior to measurements on meta II, we obtain DARR NMR spectra of rhodopsin and compare the crosspeak intensities with through-space $^{13}C\ldots{}^{13}C$ distances obtained from the crystal structure. On the basis of many such comparisons, we categorize strong crosspeaks as corresponding to internuclear distances of ~4 Å or less, moderate crosspeaks as corresponding to distances of up to 5 Å and weak crosspeaks as corresponding to distances of up to 6 Å (Table 1).

### *A.1.1 Retinal isomerization: trajectory of the retinal C20 methyl group*

Fig. A.1A presents a space filling model of the retinal chromophore and amino acids forming retinal binding site based on the crystal structure of rhodopsin [31]. The mesh surface illustrates the shape of the binding site and shows that the retinal C19 methyl group is tightly packed, while there is a cavity extending from the C20 methyl group toward EL2. Part of that cavity is occupied by crystallographic water (Wat2a in the 1L9H rhodopsin structure [203]). In our simulations, isomerization is modeled by applying a strong torsional restraint to the C10-C11=C12-C13 dihedral angle, and the retinal isomerizes with motion of the C20 methyl group in the clockwise direction (viewed from the Schiff base end of the retinal) passing through the cavity seen in Fig. A.1A.

There is a substantial body of data consistent with this trajectory and with the strong influence of the protein in determining the structure and photochemistry of the 11-*cis* retinal. First, the retinal binding site appears to be responsible for inducing conformational distortions that prime the retinal for isomerization in a clockwise direction [251,312,313]. The crystal structure of rhodopsin shows that the C20 methyl group is ~30° out of the plane formed by C12-C13=C14 carbons. Buss and coworkers [312] used a combined quantum mechanics/molecular mechanics approach (DFTB/CHARMM) to

study the origin of the chromophore conformation in rhodopsin. They found that the C10-C11=C12-C13 dihedral angle is negative due interactions of the retinal with the retinal-binding pocket. Specifically, they attribute the non-planar distortion of the chromophore, including the direction of rotation, to the interaction of the Glu113 counterion with the retinal PSB and to the fact that the two ends of the retinal are fixed.

Second, the torsions about the C11=C12 and C12-C13 bonds are required for the extremely fast, selective photoreaction to the 11-*trans* isomer with a high quantum yield [314]. The recent crystal structure of bathorhodopsin [90,250] reveals a clockwise rotation (viewed from the Schiff base end of the retinal). This moves the retinal C12-H proton away from EL2 and the retinal C19 methyl group away from the retinal C10-H proton. Liu *et al.* [315] suggest that steric contact of the retinal C12-H proton with the carbonyl of Cys187 (EL2) helps drive the retinal C12-H group away from the EL2. The large rotation of the C20 methyl group toward EL2 is in agreement with our recent solid-state NMR studies on meta II (explained in Chapter 4) showing that the retinal C20 methyl group gains a contact with Gly114 (H3). It is noteworthy that when the retinal C20 methyl group is removed (i.e. in 13-desmethyl-rhodopsin), the photoreaction is slowed [316] and the quantum yield is reduced [182,317].

Fig. A.1B presents the structure of the retinal binding site highlighting several of the amino acids that influence the trajectory of the retinal C20 methyl group. In this view, Gly114 and Ala117 on TM helix H3 are on the far side of the retinal, Tyr268 (H6) and Trp265 (H6) are on the near side of the retinal, and residues on EL2 (Cys187, Gly188 and Ile189) form a lid above the retinal. Glu181 is also part of EL2 and may contribute to the retinal photochemistry by positioning a negative charge (or partial charge) next to the C12 and lowering the C11=C12 bond order [49,196,318,319]. The conformation of the retinal in the dark state is shown in red, while the conformation immediately following isomerization (20 ps) is shown in orange. In the simulation, the C10-C11=C12-C13

dihedral angle changes from –40° found in the rhodopsin crystal structure to approximately 178.5°

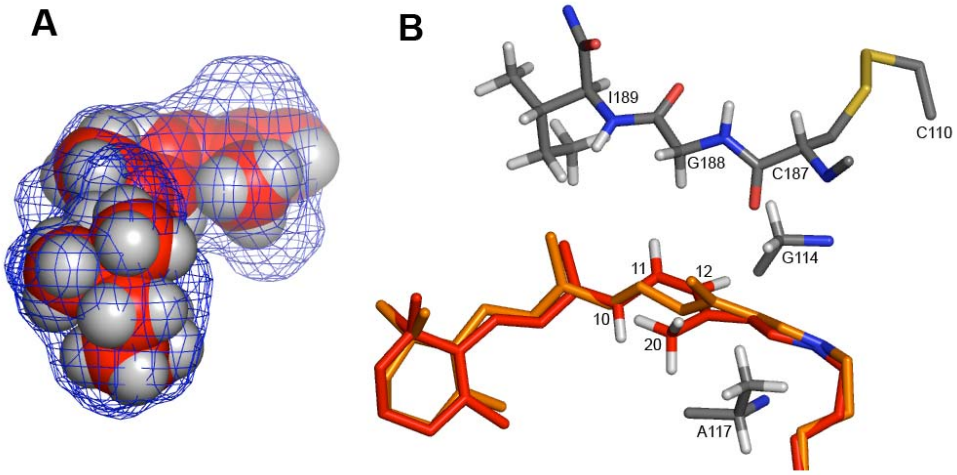


**Figure A.1:** (A) The packing of residues around the retinal chromophore in the crystal structure of rhodopsin is visualized by calculating a cavity surface for the binding site. The shape of this cavity likely determines the motion and placement of the retinal C20 methyl group upon isomerization. A void space above C20 in the direction of the EL2 loop is apparent. The view in this panel is from ionone ring end of the retinal (B) Structure of the retinal binding site highlighting the amino acids that influence the trajectory of the C20 methyl group. Hydrogens on sidechains and retinal C10, C11, C12, C20 are shown.

**Table A.1. Distance restraints for MD simulations from solid-state MAS NMR experiments.**

| # | Retinal β-Ionone Ring - H5 | | Distance (Å) | |
|---|---|---|---|---|
| | | | Meta II | Rho (pdb:1U19) |
| A1 | C6 | 207 Met CE | < 4 | 5.35 |
| A2 | C7 | 207 Met CE | < 4 | 4.9 |
| A3 | C16 | 207 Met CE | < 5 | 3.8 |
| A4 | C17 | 207 Met CE | < 5 | 4.5 |
| A5 | C16 | 207 Met C | < 5 | 4.9 |
| A6 | C16 | 211 His C | < 5 | 4.9 |
| A7 | C16 | 208,212 Phe C*(ring) | < 5 | 4.65-6.2 |
| A8 | C17 | 208,212 Phe C*(ring) | < 5 | 4.2-6.1 |
| A9 | C5 | 207 Met CE | < 5 | 6.7 |
| A10 | C18 | 207 Met CE | < 5 | 7.1 |
| A11 | C5 | 121 Gly CA | > 6 | 5.1 |
| A12 | C18 | 121 Gly CA | > 6 | 3.7 |
| A13 | C5 | 167 Cys CB | > 6 | 8.2 |
| A14 | C6 | 167 Cys CB | > 6 | 8.0 |
| A15 | C7 | 167 Cys CB | > 6 | 7.8 |
| | | **Retinal Polyene Chain - Protein** | | |
| B1 | C20 | 114 Gly CA | < 6 | 7.2 |
| B2 | C20 | 188 Gly CA | > 6 | 6.2 |
| B3 | C12 | 114 Gly CA | > 6 | 4.6 |
| B4 | C12 | 188 Gly CA | > 6 | 4.3 |
| B5 | C12 | 268 Tyr CZ | < 5 | 4.9 |
| B6 | C14 | 268 Tyr CZ | < 5 | 6.0 |
| B7 | C20 | 268 Tyr CZ | < 5 | 4.2 |
| B8 | C12 | 191 Tyr CZ | > 6 | 7.5 |
| B9 | C14 | 191 Tyr CZ | > 6 | 9.2 |
| B10 | C20 | 191 Tyr CZ | > 6 | 8.0 |
| B11 | C12 | 178 Tyr CZ | > 6 | 7.2 |
| B12 | C14 | 178 Tyr CZ | > 6 | 9.1 |
| B13 | C20 | 178 Tyr CZ | > 6 | 9.7 |
| B14 | C12 | 192 Tyr CZ | > 6 | 10.5 |
| B15 | C14 | 192 Tyr CZ | > 6 | 11.2 |
| B16 | C20 | 192 Tyr CZ | > 6 | 10.8 |
| B17 | C19 | 268Tyr $CZ^{100}$ | > 6 | 4.3 |
| B18 | C19 | 191 Tyr $CZ^{100}$ | > 6 | 4.7 |
| B19 | C19 | 118 Thr C* | < 5 | 4.5-6.4 |

| | | | | |
|---|---|---|---|---|
| B20 | C14 | 186 Ser CB[100] | > 6 | 4.5 |
| B21 | C15 | 186 Ser CB[100] | > 6 | 4.05 |
| B22 | C19 | 188 Gly CA[100] | > 6 | 4.6 |
| B23 | C9 | 189 Ile C*[&] | > 6 | 3.55-6.0 |
| B24 | C12 | 187 Cys C=O[&] | > 6 | 4.2 |
| B25 | C20 | 187 Cys C=O[&] | > 6 | 6.2 |
| B26 | C12 | 188 Gly C=O[&] | > 6 | 5.6 |
| B27 | C20 | 188 Gly C=O[&] | > 6 | 7.5 |
| | | **Retinal - Trp265** | | |
| C1 | C19 | 265 Trp CE3,CZ3,CH2[65] | < 5 | 6.0-10.0 |
| C2 | 121 Gly CA | 265 Trp CE3,CZ3,CH2[65] | > 6 | 3.7-5.9 |
| C3 | C20 | 265 Trp Ring[65] | > 6 | 3.9-8.3 |
| C4 | C18 | 265 Trp Ring | > 6 | 3.65-5.1 |
| C5 | C5 | 265 Trp Ring | > 6 | 3.7-5.3 |
| | | **Protein-Protein** | | |
| D1 | 167 Cys CB | 211 His CE | > 4 & < 6 | 3.9 |
| D2 | 167 Cys CB | 207 Met CE | < 5 | 7.8 |
| D3 | 167 Cys CB | 206 Tyr CZ | > 5 & < 6 | 5.3 |
| D4 | 207 Met CE | 211 His CE | < 5 | 9.7 |
| D5 | 163 Met CE | 211 His CE | < 5 | 4.01 |
| D6 | 211 His CE | 206 Tyr CZ | < 5 (same) | 4.4 |
| D7 | 288 Met CE | 268 Tyr CZ[&] | < 5 | 3.9 |
| D8 | 288 Met CE | 191 Tyr CZ[&] | < 5 | 5.2 |
| D9 | 288 Met CE | 192 Tyr CZ[&] | > 6 | 5.65 |
| D10 | 86 Met CE | 120 Gly CA[65] | < 5 (same) | 4.2 |
| D11 | 114 Gly CA | 178 Tyr CZ[&] | > 6 | 4.5 |
| D12 | 296 Lys CE | 44 Met CE[&] | > 5 & < 6 | 4.7 |
| D13 | 298 Ser CB | 86 Met CE[&] | > 5 & < 6 | 4.8 |
| D14 | 298 Ser CB | 301 Tyr CZ[&] | < 4 | 4.9 |
| D15 | 264 Cys CB | 301 Tyr CZ[&] | < 5 (same) | 4.8 |
| D16 | 316 Cys CB | 65 His CE1[&] | > 6 | 3.55 |
| D17 | 160 Thr (CA/CB) | 126/161 Trp (ring) [&] | < 5 | (4.7-8.9)/(4.8-8.7) |

* All carbons of the amino acid.
[&] Unpublished results.

## *A.2 Hydrogen bonding interaction in the second extracellular loop 2 (EL2)*

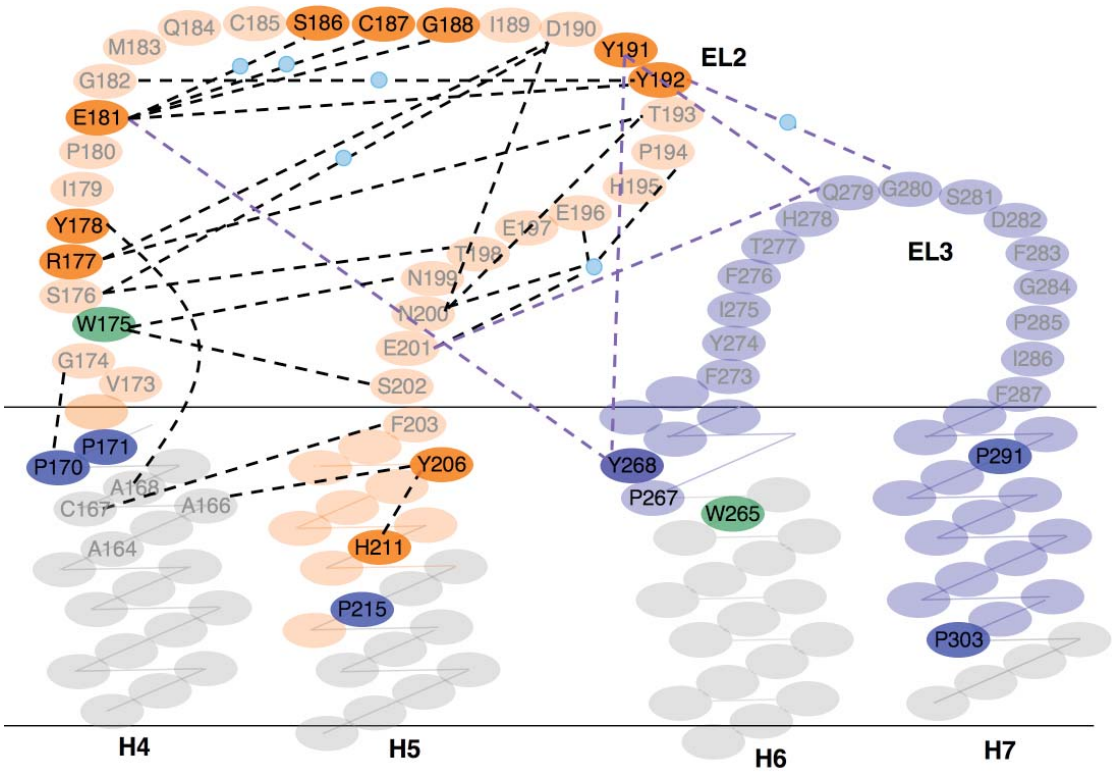


**Figure A.2. A 2D schematic of the rhodopsin sequence highlighting the two helix-loop-helix (HLH) segments:** H4 (Pro171)-EL2-H5(Pro215) presented in orange and H6(Pro267)-EL3-H7(Pro291) presented in blue. The dotted lines present the potential hydrogen bonding interactions between residues within EL2 (black), between EL2 and H4/H5 (black) and between EL2 and the H6(Pro267)-EL3-H7(Pro291) segment (purple) in rhodopsin. The potential hydrogen bonding pairs were identified on the basis of the O…O, N…O and N…N distances in crystal structures of rhodopsin [31,50]. A number of these hydrogen-bonding interactions are mediated through water molecules (blue filled circles) bound to the loops and helices near the extracellular end of rhodopsin. The figure

highlights the fact that EL2 is well structured and has multiple interactions with the extracellular ends of H4 and H5 forming a tightly coupled unit in rhodopsin. On activation, we observe a rearrangement of this hydrogen bonding network based on our $^{13}C$ NMR chemical shift data for residues highlighted in dark orange. Residues highlighted in dark green are the conserved trptophans in rhodopsin. Trp175 on H4 is highly conserved among rhodopsin like GPCRs. Trp265 on H6 is highly conserved across the family of class a GPCRs.

Many of the interactions between EL2 and the extracellular ends of H5, H6 and H7 change in meta II. Glu181 is hydrogen bonded to Tyr192 (EL2) and Tyr268 (H6) in rhodopsin. Our NMR studies on the E181Q mutant have shown that the hydrogen bonding network involving Glu181, Tyr191, Tyr192 and Tyr268 remains intact, although it undergoes a rearrangement in meta II (see Chapter 4). The backbone carbonyl of Ala166 (H4) is hydrogen bonded to the Cζ-OH of Tyr206 (H5). We show Tyr206 becomes more weakly hydrogen-bonded in meta II consistent with loss of this H-bond. The carbonyl of Cys167 is not hydrogen bonded, but packs against Phe203 on H5 [50]. We have shown there is a change in the H4-H5 interface in the region of Cys167 (see chapter 5) Specifically, we observe a new Cys167-Met207 crosspeak in the 2D DARR NMR spectrum of meta II consistent with a shorter internuclear distance and displacement of Phe203. The carbonyl of Ala168 (H4) is hydrogen bonded to the Cζ-OH of Tyr178 (EL2). Although the Y178F difference spectrum does not change, the position of Tyr178 (relative to Gly114 on H3) must change since in meta II since we lose the Tyr178-Gly114 crosspeak observed in rhodopsin (see Chapter 4). It is important to note that many of these changes are not reflected in the crystal structure of opsin [68]. For example, in the opsin structure Tyr178 is within 4.5 Å of Gly114 and remains hydrogen bonded to the backbone carbonyl of Ala168. Glu181 does not hydrogen bond to any of the tyrosines on EL2 or H6 (i.e. Tyr178, Tyr191, Tyr192 or Tyr268). Rather Glu181 directly interacts with Ser186 and Gly188. Met288 is within 5.0 Å of Tyr191, but is ~8.3 Å from Tyr268.

## *A.3 Assignment of $^{13}C\alpha$-glycine chemical shifts*

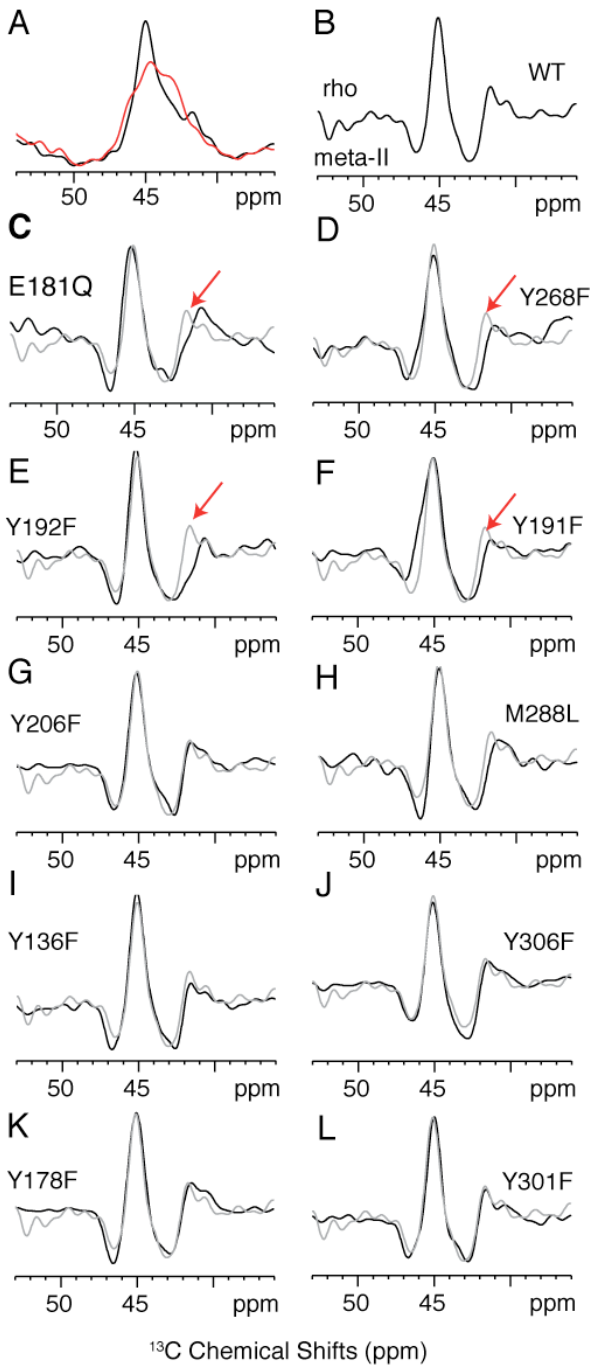

**Figure A.3.1. D $^{13}$C CP-MAS NMR spectra of rhodopsin and meta II labeled with $^{13}$Cα-glycine.** (a) Overlap of the $^{13}$C 1D CP-MAS NMR spectra of the $^{13}$Cα-glycine resonance in rhodopsin (black) and meta II (red). (b) Wild type difference spectra between rhodopsin and meta II. The difference spectrum exhibits 2-3 positive (rhodopsin) and 2 negative (meta II) peaks. In rhodopsin, the resonances at 42.0 ppm and 45.5 ppm are assigned to Gly188 on EL2 and Gly114 on H3, respectively. The chemical shifts are in agreement with the secondary structure for Gly114 and Gly188. (c) - (l) Difference spectra of rhodopsin mutants labeled with $^{13}$Cα-glycine. The Gly188 resonance at 42.0 ppm is dramatically influenced in the E181Q, Y191, Y192F, and Y268F mutants. The difference spectra of the remaining rhodopsin mutants labeled with $^{13}$Cα-glycine closely resemble the wild type difference spectrum. The difference spectrum in gray corresponds to wild type rhodopsin.

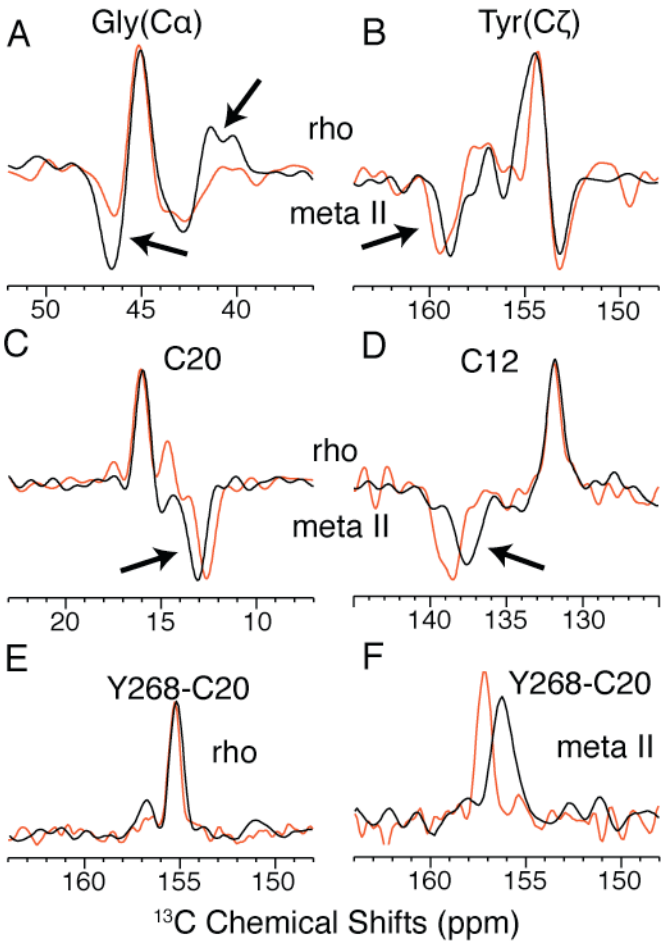


**Figure A.3.2. 1D and 2D $^{13}$C NMR of the G188A mutant of rhodopsin.** 1D $^{13}$C NMR difference spectra between the G188A mutant in rhodopsin and meta II in the region of (a) $^{13}$Cα-glycine, (b) $^{13}$Cζ-tyrosine, (c) $^{13}$C20 retinal and (d) $^{13}$C12-retinal. The mutant difference spectra (orange) are overlapped with the respective difference spectra collected on wild-type rhodopsin (black). (a) Loss of the positive peak at 42.0 ppm in the mutant difference spectrum as compared to the difference spectrum of wild-type rhodopsin allows the assignment of this resonance to Gly188 in rhodopsin. (b) The negative peak at 159.3 ppm corresponding to Tyr191 on EL2 shifts downfield in the mutant difference spectrum indicating that mutation of Gly188 affects the chemical shift of the nearby Tyr191 residue on EL2. In (c) and (d) the positive $^{13}$C20 and $^{13}$C12 resonances in the

G188A mutant overlap perfectly with their respective resonances in wild-type rhodopsin. However, in meta II of the G188A mutant, the $^{13}$C20 resonance is shifted upfield and the $^{13}$C12 resonance is shifted downfield as compared to wild-type rhodopsin. (e) and (f) Rows from the 2D DARR NMR spectra showing crosspeaks between $^{13}$Cζ-Tyr268 and the retinal $^{13}$C20 methyl group in rhodopsin and meta II, respectively. The orange and black spectra correspond to the G188A mutant and wild-type protein, respectively. (e) The $^{13}$Cζ-Tyr268 chemical shift remains the same in the G188A mutant and wild-type rhodopsin. (f) On conversion to meta II, the $^{13}$Cζ-Tyr268 resonance shifts downfield in the meta II spectrum of the G188A mutant as compared to wild-type meta II. These data show that the G188A mutation influences the $^{13}$C chemical shifts of at least two tyrosine residues, Tyr191 (EL2) and Tyr268 (H6), and the C12 and C20 retinal carbons in meta II.

## *A.4 Assignment of the $^{13}$Cζ-Tyr206 chemical shift*

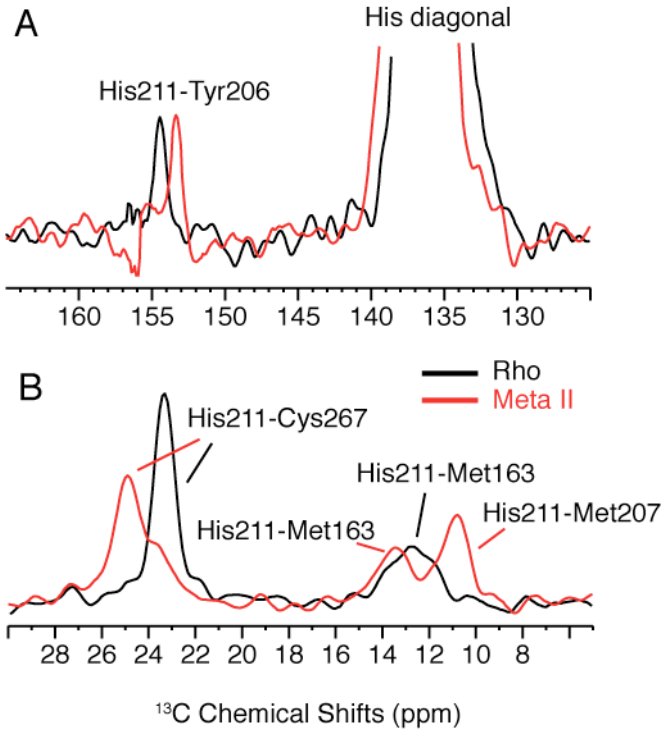


**Figure A.4. Assignment of the resonance at 153.6 ppm in meta II to $^{13}$Cζ-Tyr206.** (a) 2D DARR NMR spectra of rhodopsin (black) and meta II (red) using rhodoposin labeled at $^{13}$Cζ-tyrosine, $^{13}$Cβ -cysteine and $^{13}$Cε1-histidine. In the crystal structure of rhodopsin [31], Tyr206(Cζ) is the only tyrosine within 5.5 Å of His211(Cε1); the next closest tyrosine is 12.1 Å away. In rhodopsin, we observe a strong crosspeak between $^{13}$Cε1-His211 at 136.9 ppm and $^{13}$Cζ-Tyr206 on H5 at 154.8 ppm. Upon conversion to meta II, the crosspeak shifts to 137.5 ppm for $^{13}$Cε1-His211 and 153.6 ppm for $^{13}$Cζ-Tyr206. The chemical shifts for the $^{13}$Cε1-His211 in rhodopsin and meta II were verified by mutating His211 to alanine [227]. $^{13}$Cε1-His211 has a unique chemical shift as compared to other histidines because it is the only histidine located within the transmembrane helices. The other histidines are located in the loops and exhibit a broad resonance at ~130.0 ppm. (b) Rearrangement of H5 as a result of retinal isomerization and motion

upon conversion to meta II. Rows from 2D DARR NMR spectra taken through the diagonal of $^{13}$Cε1-His211 in rhodopsin (black) at 136.9 ppm and meta II (red) at 137.5 ppm. In rhodopsin, we observe crosspeaks with $^{13}$Cβ-Cys167 at 23.7 ppm and $^{13}$Cε-Met163 at 13.0 ppm on H4. In meta II, crosspeaks with $^{13}$Cβ-Cys167 are observed at 25.3 ppm, and with Met207 at 13.8 ppm and Met163 at 11.2 ppm. On conversion to meta II, the His211-Cys167 contact weakens, whereas the His211 side chain packs closer to the Met207 side chain on H5.

## *A.5 Difference spectra for different selectively $^{13}C$ labeled amino acids in rhodopsin*

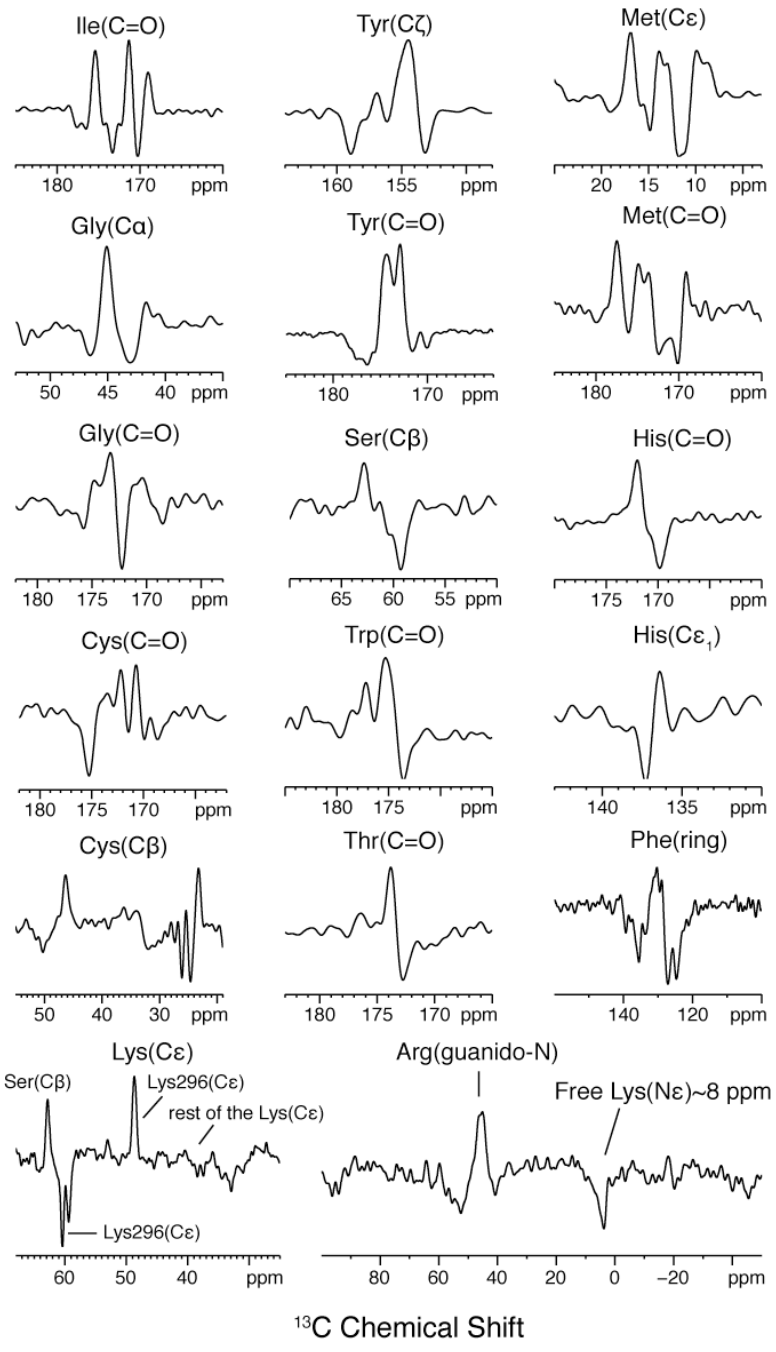

**Figure A.5: Difference spectra between rhodopsin and meta II for a number of selectively $^{13}C$ labeled amino acids.** Positive peaks correspond to rhodopsin and negative peaks correspond to meta II. The peaks in the difference spectra provide information on amino acids that change their chemical environment (e.g. protonation states and hydrogen bonding strengths) upon conversion from rhodopsin to meta II and therefore gives us useful insight on the structural rearrangement of the protein on activation.

*$^{13}C\zeta$-tyrosine difference spectra between mutant and WT receptor states*

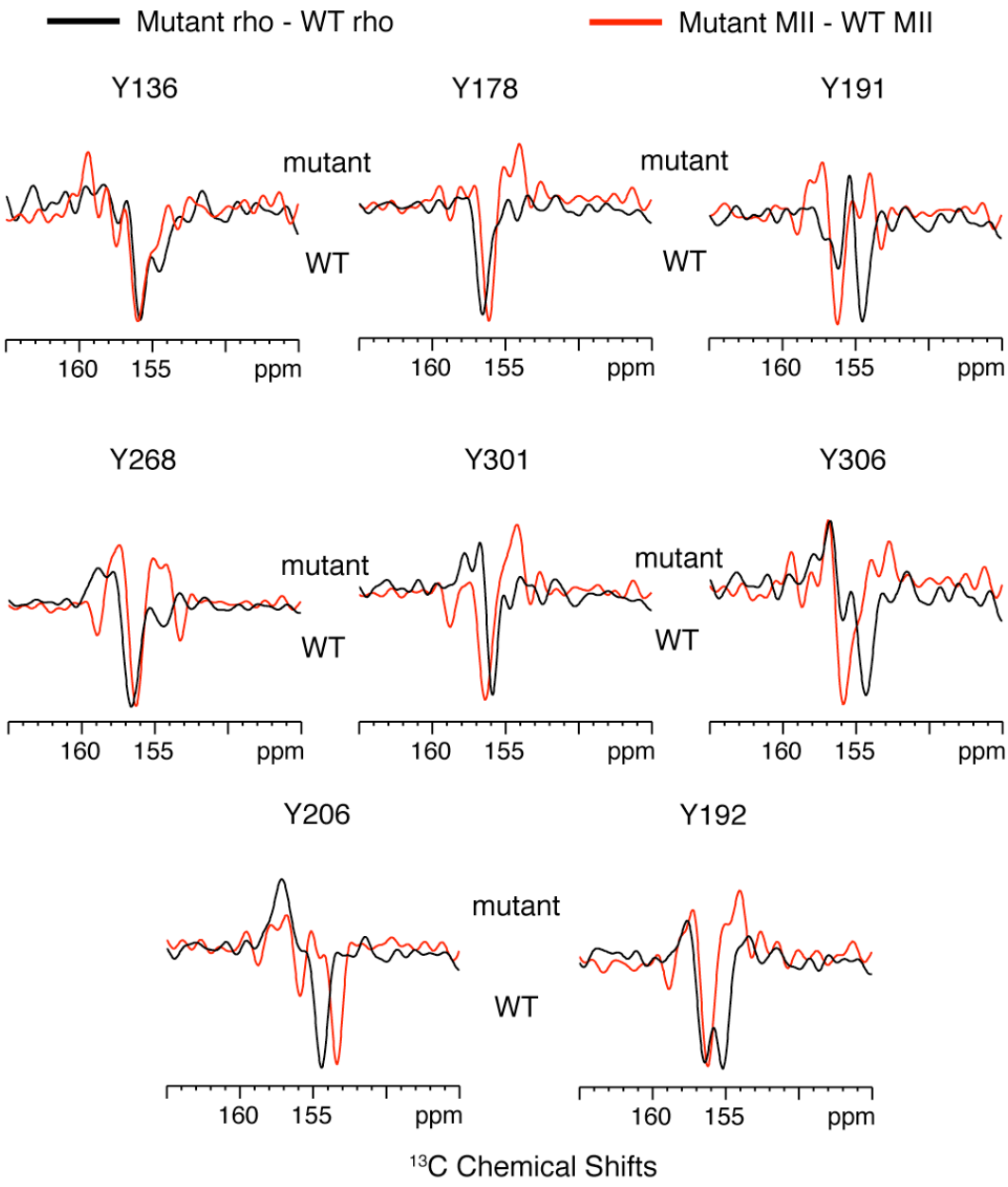

**Figure A.6: $^{13}C\zeta$-tyrosine difference spectra between mutant rhodopsin/meta II and WT rhodopsin/meta II.** The positive peaks correspond to mutant receptor states (rhodopsin/meta II) and negative peaks correspond to WT receptor states (rhodopsin/meta II). The largest negative peak in the difference spectra for both rhodopsin (black) and meta II (red) most likely corresponds to the resonance peak of the tyrosine residue mutated. Below I have tabulated the chemical shifts obtained for various tyrosine residues in rhodopsin and meta II.

| Tyrosine | Rhodopsin (ppm) | Meta II (ppm) |
|---|---|---|
| Y136 | 156.2 | 156.4 |
| Y178 | 156.9 | 156.5 |
| Y191 | 154.9 | 156.6 |
| Y268 | 156.7 | 157.0 |
| Y301 | 156.3 | 156.8 |
| Y306 | 154.7 | 156.3 |
| Y192 | 156.8/155.6 | 156.6 |
| Y206 | 154.8 | 153.8 |

**Note:** All the chemicals shifts here are referenced to $^{13}$C1-Gly at 176.46 ppm.